

M. S. Gregory

THE ANALYSIS OF STRUCTURES

with particular reference to  
Elastic Instability of Frames

by

F. van der Woude B.E. (Hons.), Grad. I.E. Aust.

A thesis submitted for the degree of  
Doctor of Philosophy, in the  
Faculty of Engineering,  
University of Tasmania, Hobart.

[Examiner:

Professor N.W. Murray  
civil engineering dept.

Monash University

Victoria.]



- December 1967 -



(i)

CONTENTS

	Page
PREFACE	iii
SUMMARY	vii
CHAPTER ONE - ELASTIC INSTABILITY OF FRAMES	
1.1 Introduction	1
1.2 The pin-ended column	2
1.3 The practical column	4
1.4 Design techniques	5
1.5 Design of frames	7
1.6 Elastic instability of frames	8
1.7 Review of existing methods for the determination of elastic buckling loads	10
1.8 The buckling of a simple frame	17
1.9 The practical frame; experimental methods	29
1.10 The practical frame; predicted behaviour	32
1.11 Concluding remarks	38
References	41
CHAPTER TWO - ENERGY METHODS	
2.1 Introduction	43
2.2 The two types of energy	43
2.3 Energy analysis of a string model	44
2.4 A strain energy method applied to beams	51
2.5 Strain energy analysis of statically indeterminate frames	59
2.6 Iterative solution	60
2.7 Proof of linear combinations method	65
2.8 Physical interpretation	67
2.9 Numerical example	68
2.10 Concluding remarks	70
References	71
CHAPTER THREE - A NEW METHOD FOR CALCULATING BUCKLING MODES AND LOADS OF FRAMES	
3.1 Introduction	72
3.2 Development of method	72
3.3 General analysis	74
3.4 Upper and lower bounds	79
3.5 Physical interpretation of the linearized stiffness approach	82
3.6 Computational procedures	83

(ii)

CONTENTS (Cont'd.)

	Page
3.7 Two-bay Warren truss	87
3.8 Roof truss buckling in its plane	90
3.9 Two-storey rectangular portal frame	97
3.10 Tetrahedral frame	99
3.11 Lateral buckling of through-bridges	106
3.12 Two-bay Warren truss through-bridge	108
3.13 Eight-bay through-truss bridge	116
3.14 Concluding remarks	126
References	127
CHAPTER FOUR - THE BEHAVIOUR OF OVERBRACED FRAMES	
4.1 Introduction	129
4.2 Review	130
4.3 Statical indeterminacy of frames	132
4.4 The use of complementary energy in the analysis of overbraced frames	135
4.5 The bending shortening of pin-ended members	138
4.6 The behaviour of pin-jointed overbraced frames	140
4.7 The measured behaviour of rigidly-jointed overbraced frames	152
4.8 Elastic buckling loads of rigidly-jointed overbraced frames	157
4.9 Overbraced frames with one degree of statical indeterminacy	165
4.10 Examples of interaction curves	166
4.11 The behaviour of initially crooked overbraced frames	173
4.12 The analysis of initially crooked overbraced frames	175
4.13 A worked example	179
4.14 The effect of prestrain	183
4.15 Concluding remarks	184
References	185
APPENDIX Stability functions series	187

PREFACE

Broadly speaking, an engineer's constant aim is the creation of something which serves mankind. In order to achieve his aim the engineer has to tackle numerous problems arising between the time of conception and the final bringing into service of the product. To this end it is convenient to picture the process as divided into three stages. The first stage is to recognise the existence of the real problem, with its multitude of complexities and details, all at varying levels of importance. The real problem is always too difficult to handle directly, and as an aid to thinking, great simplifications are made. The simplified problem may be called the physical model, in which only the more important aspects of the real problem are defined. The setting up of a physical model requires skill, judgement and, in most cases, experience with similar situations. It follows that the first physical model may at times be subject to subsequent variations and revisions. Finally, a mathematical model is formulated; this model attempts to describe, by means of mathematical equations, the behaviour of the physical model. For example, if the real problem is one of structural design, the unknowns in the final equations are usually design parameters such as stress, deflection, beam depth and so on. Thus the solution of the equations defines the behaviour of the physical model in terms of design parameters, but the degree to which these apply to the real problem depends on how well the physical model represents the real structure. Final design is achieved only after many cycles of appraisal, modifications to the physical model, refinements, re-evaluation, and so on.

The above philosophy is generally applicable, indeed it is believed to be the only successful method of problem solving in any field, especially in engineering.

This thesis is concerned with the problem of the behaviour of framed structures. Throughout the work, emphasis is placed on the geometry of the deformations of the frame. Although it is often not appreciated, the geometric approach has dominated throughout the history of structural engineering development. The reason for this is obvious, because once the deformations of a structure are known, other quantities like stresses, strains, bending moments and so on, are easily calculated. Another reason is that deformations, unlike forces (the alternative to a geometric approach is a force approach), can be pictured and drawn to scale or sketched. Such a picture is readily obtained from experiments and one is always pleasantly surprised at how much information can be drawn from but the simplest measurements of deformations. The author has experienced most success from simply constructed, light and flexible models which, apart from being inexpensive, are easily deformed by hand, and the deformed



models are quickly sketched or traced. Frequently a wire or cardboard model may be used in order to gain a preliminary understanding of the deformations.

Once a picture of the deformations of a structure has been formed in one's mind, the formulation of physical and mathematical models follows naturally. For example, in general all the members of a frame <sup>bend</sup> in two directions, twist, and stretch or shorten, but quite often only one of these types of deformation is important. The physical model describing this type of behaviour is obvious. Nevertheless one must not lose sight of other possible deformations; these may need to be introduced as subsequent refinements. A good example of when the first physical model must be changed, is provided by the class of frames in which the member stretchings (or shortenings) are the primary deformations. Such frames are liable to instability, that is the deformed frame with its members remaining straight is not always stable, and the frame buckles under certain combinations of loading. When it does, then of course the bending deformations become most important, and the physical model must be modified to include these deformations as well as the member stretchings and shortenings.

Instability of frames is one of the main topics of this thesis. Undoubtedly most of the ideas about instability are based on the work of the great mathematician Leonhard Euler, in the eighteenth century. It was Euler who first established a buckling condition for a simple uniform pin-ended column. These ideas have gradually been expanded to embrace a much wider field of structures such as buckling of frames, plates, shells, beam webs, and so on. However, it should not be forgotten that Euler's analysis is only a mathematical model of a much simplified physical model of a real column, and there is a danger of using the results of such an analysis in situations where it is no longer valid, even as a first approximation. Euler type buckling is defined by a bifurcation, or a number of bifurcations, on the load-deformation diagram for the structure; at each of these forks on the diagram the structure deforms according to a consistent pattern, and under constant loading it suddenly deflects into some other pattern called the buckling mode; the corresponding loads are called the buckling or critical loads. This type of buckling is in fact a reasonable description of the behaviour of isolated columns and statically determinate frames, but in most other structures there exist influences which do not permit them to deflect under constant load, and their buckling behaviour cannot therefore be of the Euler type. Examples of this different buckling behaviour are shells and redundant frames; the latter are examined in this thesis. Generally speaking, Euler type buckling is the exception rather than the rule.

In addition, there is the question of the practical significance of the existence of some unstable state. In practice a structure always exhibits deformations other than those which are considered in the physical model. Among these are the deformations which arise when the structure buckles, and their importance usually increases as the structure is subjected to greater primary deformations. When the additional deformations are included in the analysis, the calculated load carrying capacity of the structure is greatly affected, and may be far less than the buckling load predicted if they are ignored.

Unfortunately, some of the above considerations are frequently neglected in current literature. Thus, although the problem of structural behaviour has been intensively investigated, there remains an untold number of questions. The author hopes that the work to follow herein may provide a useful attempt to pose important practical questions, and give a guide as to how they may be answered, and hence promote a clearer understanding of the behaviour of structures, which is urgently needed by structural designers.

In conformity with the definition of an engineer's aim, as given earlier, the aim of this thesis is to investigate the problem of the behaviour of framed structures, with particular reference to elastic instability. Design is continually kept in mind as being the end product of this research, and wherever possible, design procedures are suggested. Some of these may not be unique, nor have they been proved in practice, but the author believes that the principles are soundly based on a reasonable understanding of structural behaviour.

\*

\*

\*

ACKNOWLEDGEMENTS

In a work of this kind it is impossible to acknowledge each and every person who at some time or other has been involved in its fulfilment. I hereby thank everyone concerned, and in particular I wish to express my deep appreciation of the helpful advice and stimulus received from the following persons:

Professor A.R. Oliver, Professor of civil and mechanical engineering at the University of Tasmania;

Dr. M.S. Gregory, Reader in civil and mechanical engineering at the University of Tasmania, and supervisor of this research;

the late Professor W. Merchant of the Manchester college of science and technology, England;

emeritus Professor J.J. Koch of Delft, Holland.

Thanks are also due to Miss A. Clark for the care with which she prepared this manuscript.

\*

\*

\*

The work described in this thesis was carried out during the period March 1963 to December 1967, in the department of civil and mechanical engineering at the university of Tasmania, Hobart, Australia.

I hereby declare that, except as stated herein, this thesis contains no material which has been accepted for the award of any degree or diploma in any university, and that, to the best of my knowledge or belief, this thesis contains no copy or paraphrase of material previously published or written by another person, except where due reference is made in the text of this thesis.

*F. Van der Woude.*

F. Van der Woude.

SUMMARY

CHAPTER ONE begins with a preliminary examination of the problem of instability of frames. This is followed by a brief description of the development of instability studies, starting with Euler's analysis of a pin-ended column and culminating with the now classical matrix analysis of rigidly jointed frames. A simple frame is analyzed in order to show that the various methods of analysis all have the same physical and mathematical models but employ different methods of handling the mathematics. Experimental methods are discussed, and the chapter concludes with the formulation of a mathematical model suitable for the prediction of frame behaviour. This model can be used to obtain an estimate of the load carrying of a frame, and hence it provides a useful design procedure.

CHAPTER TWO deals with the application of energy methods in structural analysis. The two types, complementary energy and strain energy, are introduced by means of a simple example and it is clearly shown that they are equivalent to geometric and statical considerations respectively. These ideas are extended and applied to some common beam problems, for which rapid approximate solutions are found. It is then shown that the classical matrix method of structural analysis, using joint displacements as unknowns, is equivalent to a strain energy approach, and this naturally leads to a **powerful** approximate method of solution. The method is applied to the analysis of a two-bay eight-storey building frame, and the results are compared with a computer solution.

CHAPTER THREE proposes a new method for the determination of buckling modes and loads of rigidly jointed frames. The method is based on a strain energy analysis, and it is identified as a linearization of the usual stiffness matrix approach. This leads to a useful iterative numerical scheme. Proofs are given of upper and lower bound theorems, and the method is applied to a number of frames, including a few in three dimensions. Most of these analyses are checked by experimental measurements.

CHAPTER FOUR extends the work into the analysis of redundant frames. The complementary energy method is proposed as the most convenient way of deriving the compatibility equations relating the member shortenings. A mathematical model is developed for the evaluation of the shortening of bent pin-ended members. The problem of buckling of redundant frames is introduced by means of an analysis of a simple pin-jointed frame, and some useful ideas are brought to light. The following section presents some

of the results of experimental work on the behaviour of redundant frames with rigid joints. It is shown that the buckling behaviour is not of the Euler type. An earlier definition of instability is therefore closely re-examined, and this leads to a new formulation of the problem. A general stability criterion is set up mathematically and applied to some simple singly-redundant frames, and the results are compared with measurements. In conclusion a method for predicting the behaviour of initially crooked redundant frames is developed and applied to a trivial example.

NOTATION

Symbols are defined when they first appear in the text. The general notation used is as follows:

A	cross sectional area
C	complementary energy
E	Young's modulus
f(or $\sigma$ )	stress
G	torsion modulus
I	second moment of area (or unit matrix)
J	polar second moment of area
$\tilde{a}$	stiffness matrix
$l$	member length
M	bending moment
P	axial force in a member
Q	Euler load of pin-ended member
$r = \sqrt{I/A}$	radius of gyration
U	strain energy
W	applied load
X	generalized force
x	generalized displacement (or coordinate)
y(or z)	deflection
$\Delta$	member shortening (also sway)
$\epsilon$	strain
$\phi$	curvature
$\lambda$	latent root
$\theta, \omega$	rotation
$\sim$	superscript to denote a matrix or vector.

## CHAPTER ONE

### ELASTIC INSTABILITY OF FRAMES

#### 1.1 INTRODUCTION

Instability of structures is a subject which has received a considerable amount of attention, originating with Euler's analysis of the buckling of a pin-ended column. The classical approach developed by Euler also forms the foundation of the analysis of instability of structures. A structure is said to be in stable equilibrium when small changes in loading are accompanied by correspondingly small changes in the deformations. On the other hand, instability is associated with a state of unstable equilibrium when small changes in loading produce large changes in the deformations ultimately resulting in failure of the structure. Mathematically this definition of instability can be written as

$$\partial x / \partial X = \infty \quad (1.1)$$

where  $x$  is a generalized displacement and  $X$  is the corresponding generalized force. Inversely this becomes

$$\partial X / \partial x = 0 \quad (1.2)$$

and this formal definition of instability is adopted in the work to follow; in practice it is easier to use than the former, which exhibits the difficulties of manipulating infinities.

Broadly speaking failure of a structure by instability may be separated into two distinct classes. Firstly there is the failure brought about by large scale yielding of parts of the structure. When this occurs these parts continue to deform under constant or nearly constant load and may be thought of as hinges. As more hinges form the structure eventually becomes a mechanism and collapses as such, the load at which this occurs is known as the collapse load; the analysis of this type of instability is a complete study in its own right.

Secondly, large deformations may take place in the elastic range of the material, if at some stage the structure can no longer support its loads due to its decreasing stiffness as the loads are increased. This type of instability is usually referred to as elastic buckling.

So far the term 'structure' has been employed in its general sense, embracing frames, plates and shells, single machine elements and so on. This thesis is mainly concerned with instability of frames and in particular with the problems of elastic buckling of frames.

Essentially this problem is the same as that posed by Euler, and in order to obtain a clear understanding of what is involved, the fundamental ideas are recapitulated in the following sections. The treatment given in these sections is found in most textbooks on structural analysis but is included here for the sake of completeness.

## 1.2 THE PIN-ENDED COLUMN

Consider a pin-ended column AB initially straight, compressed by an axial force  $P$  as shown in figure 1.1. We ask ourselves if there exists

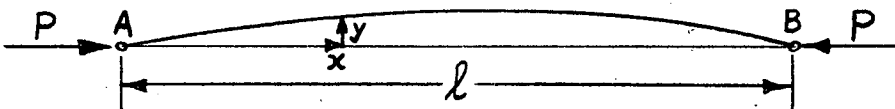


figure 1.1 - pin-ended column

an equilibrium configuration other than the straight form. Supposing there is, let  $y = f(x)$  describe this configuration. Then the bending moment at the point  $(x, y)$  on the deflected centre line of the column is given by

$$M = - Py \quad (1.3)$$

anticlockwise moments being considered positive. If the deflections  $y$  are small compared with the length of the column, the curvature is approximately given by

$$\phi = d^2y/dx^2 \quad (1.4)$$

According to the usual assumptions in linear theory of bending of beams, the bending moment is related to the curvature by the expression

$$M = EI \phi \quad (1.5)$$

Thus equation (1.3) becomes

$$EI(d^2y/dx^2) + Py = 0 \quad (1.6)$$

The solution of this differential equation is

$$y = a \sin kx + b \cos kx ; k^2 = P/EI \quad (1.7)$$



Use of the boundary conditions of zero end deflections reduces this to

$$y = a_n \sin k_n x \quad (1.8)$$

where  $k_n = n\pi/l$  ;  $n = 1, 2, 3, \dots$

or  $y = 0$  everywhere, this solution being trivial. It is seen that a deflected equilibrium configuration is possible only for certain discrete values of  $P$  given by

$$P_n = n^2 \pi^2 EI / l^2 \quad (1.9)$$

and the corresponding deflected shapes are of sinusoidal form

$$y_n = a_n \sin(n\pi x/l) \quad (1.10)$$

where  $a_n$  is undefined as to magnitude, although it is restricted by the approximate expression for the curvature and by the condition of linearity implied in equation (1.5).  $P_n$  is called the  $n$ th. buckling load of the column and  $y_n$  is called the corresponding buckling mode.

This problem was first solved by Euler some two hundred years ago and is still used today as the basis of all elastic instability studies relating to frames. When  $n = 1$  we have what is called the fundamental buckling condition, and  $P_1 = \pi^2 EI / l^2 = Q$  is commonly known as the Euler load, this being the smallest load at which the pin-ended column has an equilibrium configuration other than the straight form. For values of  $P$  less than  $Q$  the column is in equilibrium only in the straight form, at  $P = Q$  the column is in neutral equilibrium, and at values of  $P$  greater than  $Q$  the column is in unstable equilibrium. The behaviour of this mathematical model of the column is indicated graphically in figure (1.2) by two straight lines.

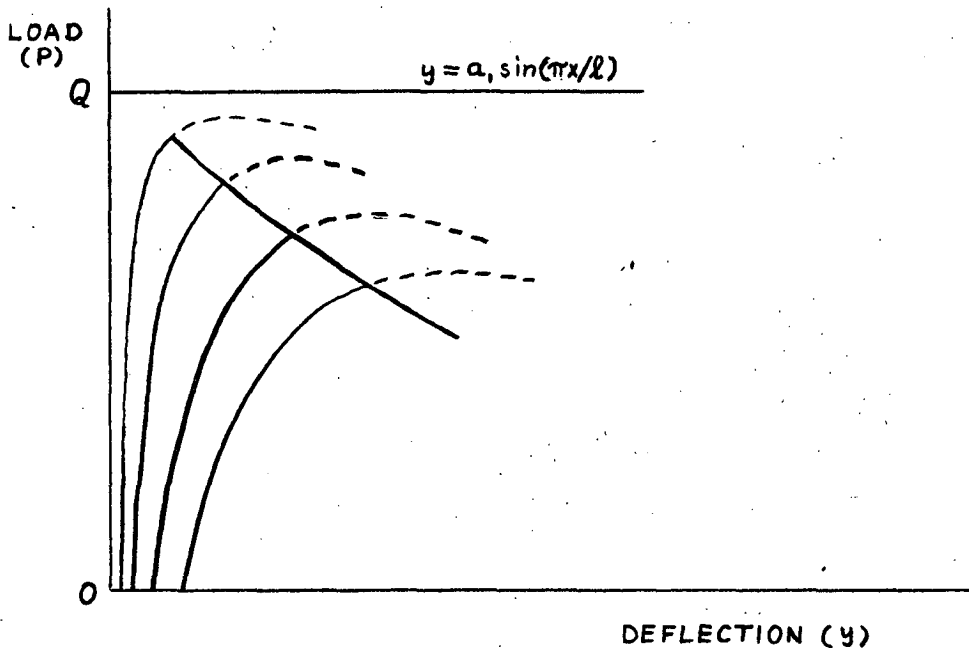


figure 1.2 - load deformation diagram

The buckling loads and modes for columns with other end conditions can be obtained by similar analyses, and in general it is possible to put the fundamental buckling load in the form

$$P_1 = \pi^2 EI (el)^2 \quad (1.11)$$

where  $(el)$  is called the effective length of the column, that is the length of a pin-ended column having the same buckling load as the column under question.

### 1.3 THE PRACTICAL COLUMN

Euler's analysis, as set out in the previous section, is idealized in the sense that it implies perfect straightness of the column, ends completely free to rotate, purely axial load (that is no eccentricity), uniformity of cross-section and homogeneity of the material. In practice such conditions are never realized, and the lack of these conditions is broadly classified under the heading of initial imperfections. As a consequence of initial imperfections, a column under test will begin to deflect as soon as a load is applied and Euler's analysis is therefore no longer a reasonable representation of the behaviour of a practical column. The mathematical analysis can be improved to take into account some initial imperfections such as eccentricity of loading, initial curvature and the effects of end moments, and experiments have shown that for a large class of columns the behaviour under load can be fairly well predicted. If the ends of the column are pinned, (that is free to rotate,) it can be shown that as the ratio  $P/Q$  approaches unity the behaviour of an imperfect column is asymptotic to Euler's theory. This has led to the very useful experimental technique known as the Southwell plot, which is discussed in more detail in section (1.9). The Euler load is generally not reached in tests, unless there are some external restraints, since as the deflections tend to become large the strain in parts of the column exceeds the yield value. How closely the Euler load can be approached depends on the magnitude of the imperfections. Despite the fact that the Euler load may not be reached in practice, it is and remains a useful result. The behaviour of a column under test is shown superimposed on the Euler mathematical model in figure (1.2). The various curves are for different magnitudes of initial crookedness and the post-yield regions are indicated by broken curves. The maximum load which the column can carry is usually not much greater than the load to cause first yield.

#### 1.4 DESIGN TECHNIQUES

The estimation of allowable loads on columns can be done in several ways but only the more commonly used techniques are described here.

(a) Euler stress formula

The Euler stress,  $f_E$  is defined as

$$f_E = Q/A = \pi^2 EI / Al^2 = \pi^2 E / (l/r)^2 \quad (1.12)$$

which is the direct axial stress at which the column buckles. It is also known as the critical stress. Expression (1.12) is shown graphically by the continuous curve in figure (1.3). The non-linearity of the stress

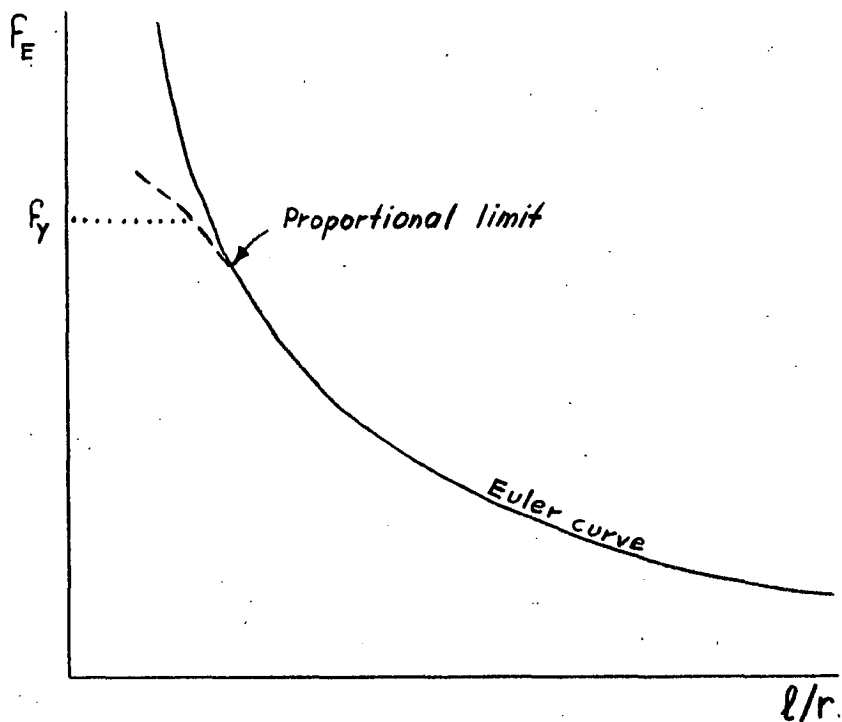


figure 1.3 - critical stress curve

strain relation after the proportional limit reduces the critical stress, and the dashed curve gives the critical stress beyond this point. For design purposes the increase in critical stress above the yield stress is generally ignored, and the dotted line is used. For a given  $l/r$ , ratio the critical stress is read from the graph, and the allowable average stress is obtained by dividing the critical stress by a suitable factor of safety, which is taken either constant or a function of the  $l/r$  ratio. The major difficulty with this design method appears to be the selection of a factor of safety. This is because the behaviour of a column in practice is quite different from that predicted by the Euler theory. To overcome this difficulty a large factor of safety is used.

(b) Design based on initial imperfections

In this design technique the effects of initial imperfections are all replaced by a single initial curvature pattern. The function representing this pattern does not affect the calculations to any significant extent, and for simplicity a sine curve is generally used, that is the initial shape of the column is defined by

$$y_0 = a_0 \sin(\pi x/l) \quad (1.13)$$

If  $y$  is the shape of the column when it carried an axial load  $P$ , then equations (1.3) and (1.4) still hold, but the bending moment-curvature relation is changed to

$$M = EI(\phi - \phi_0') \quad (1.14)$$

where  $\phi_0$  is the initial curvature. The differential equation is solved in the usual way, and the maximum extreme fibre stress occurring at the centre of the column is readily found to be

$$f_{\max} = (P/A)[1 + A a_0 / (1 - P/Q) Z] \quad (1.15)$$

where  $A$  is the cross sectional area and  $Z$  is the section modulus. Equating this to the yield stress, we obtain the well known Perry formula

$$f' = P'/A = \frac{1}{2}[f_y + (n+1)f_E] - \frac{1}{2}\sqrt{[f_y + (n+1)f_E]^2 - 4 f_y f_E} \quad (1.16)$$

where  $P'$  is the load which will just cause first yield  $f_y$  in the extreme fibres, and  $f_E$  is the Euler stress as defined above. The quantity  $n$  is a measure of the magnitude of the imperfections and is defined by

$$n = a_0 v/r^2 \quad (1.17)$$

where  $v$  is the distance from the neutral axis to the extreme fibres, and  $r$  is the radius of gyration.  $n$  is usually specified as some fraction of the  $l/r$  ratio, which is meant to allow for small inherent eccentricities as well as initial curvature. The allowable average stress is obtained by dividing  $f'$  by a factor of safety.

(c) Empirical Formulas

A third design technique is by the use of purely empirical formulas. These are of the form

- (i) the Rankine formula,  $f = a / [1 + b(l/r)^2]$
- (ii) the Johnson parabolic formula,  $f = a - b(l/r)^2$
- (iii) the straight line formula,  $f = a - b(l/r)$

In all cases  $f$  is the allowable average axial stress, and the constants  $a$  and  $b$  are chosen to fit experimental results. A factor of safety is also incorporated in these formulas. The use of these formulas is generally restricted to certain ranges of the  $l/r$  ratio.

\*

\*

\*

There are of course numerous arguments for or against the use of any particular design technique. Present day design codes differ in opinion, but with sensibly chosen numerical values in the relevant formulas there is probably little difference in the end result, irrespective of which technique is used. It must be borne in mind that all the design formulas mentioned are in reality empirical, as each involves the selection of a factor of safety or other quantity, and these are obtained only by experiment and by experience of what has been proved to be safe. This is the basis of all design codes.

If the column has end conditions other than pinned, the length  $l$  in the design formulas is replaced by the effective length.

### 1.5 DESIGN OF FRAMES

So far the discussion of design methods has been restricted to isolated columns whose effective lengths are known or can be readily estimated. In the design of compression members of frames these design formulas are still applicable, provided the effective lengths of these members can be found. Since the end conditions are generally not known beforehand some difficulty arises, and this is the real problem in frame design. Design codes usually give a table of effective lengths for compression members with various end connections, but, although these are reliable, the designs are probably overconservative since attention is focussed on individual members. If the frame has weak joints it is close to being pin-jointed, and the design of compression members on an

individual basis should be adequate. However, most frames have rigid or nearly rigid joints, so that lateral deflections in any member affect the whole frame. The magnitude of the deflections depends on the stiffnesses of the joints, which in turn depends on the conditions in the neighbouring members, and so on. Thus the concept of a buckling member is no longer useful, and the stability of the whole frame must be investigated and used in design, together with an overall factor of safety.

Although it is possible to calculate the elastic buckling loads of frames, and hence the effective lengths, more numerical computation is required than is generally warranted for routine design office work, and therefore most frames are designed using empirical information from design codes. Here again the only justification seems to be the satisfactory performance of past designs. The designer is also faced with the question of economy; that is, the additional cost of non-standard member sizes, which may have to be used, could well exceed the savings on the "more efficient" design.

The problem of frame design is discussed again in section (1.11), together with the author's proposal for improved design techniques.

## 1.6 ELASTIC INSTABILITY OF FRAMES

As for the pin-ended column, the basic problem of elastic instability of frames is to find those loads, or combination of loads, for which the frame has an equilibrium configuration other than that in which all members remain straight. If the frame has pinned joints, the buckling load would be the smallest load at which one of the members carries its Euler load, for then this member buckles on its own and cannot sustain an increase in load, thereby effectively rendering the frame a mechanism. If the frame is  $m$ -fold statically indeterminate with respect to the axial forces in its members, then in general  $(m + 1)$  members must carry the Euler load when the frame buckles. For the time being, only statically determinate frames are considered; the buckling of redundant frames is treated in chapter four. The buckling mode in the statically determinate case is defined simply by the deflected shape of the buckled member, that is a half sine wave.

In practice the joints of a frame are nearly rigid, and the analysis of elastic instability becomes more difficult as the whole frame must be taken into account. Drastic simplifications are necessary to get

a manageable mathematical model. These are common to all methods of attack and are described here in order to keep in mind the limitations of the analyses. For simplicity, only plane frames buckling in their plane are considered, but the arguments are readily extended into three dimensions.

The first simplifying step is to replace the real frame by a physical model of the same dimensions, having its members perfectly straight initially, the centrelines of the members lie in one plane and intersect at the joints, the joints are perfectly rigid, and loads are applied at the joints only and in the plane of the frame. It is also customary to neglect secondary bending moments arising from changes in the geometry of the frame due to the changes in the axial lengths of the members. The bending moments resulting from lateral deformation of the members are called primary bending moments. It is clear that the simplified model of the frame can be loaded so that the members remain straight. To define buckling of the physical model, the concept of an initial disturbance is useful. Suppose the frame is given a disturbance, exciting lateral deformations in the plane of the frame; if there is no other load on the frame it remains in stable equilibrium, and the deflected shape can be calculated by standard methods of analysis. If the disturbance is applied when the frame carries some load, additional bending moments arise as a result of the axial forces in the members, and hence the deflections are increased, giving increased bending moments and so on. Equilibrium may be stable or unstable depending on the magnitude of the primary load. Obviously if this is small, equilibrium is stable but at some discrete values of the primary load the additional deflections due to the axial forces in the members are just larger than those caused by the disturbance acting alone, and then the final deformations are undefined and the frame is said to buckle. Although the magnitude of the deformations is undefined, the frame assumes a definite shape, called the buckling mode. In general there exist several buckling modes, each associated with a different value of the primary load. In this definition of buckling it has been assumed that although the deformations are undefined as to magnitude, they are sufficiently small not to cause yielding, and that the usual small deflection theory is applicable.

The basic problem of elastic instability is therefore the determination of loadings on the physical model for which an infinitesimal disturbance is sufficient to excite buckling. In actual frames, disturbances need not be introduced as the crookedness of the members,

eccentricity of loads and many other factors cause the members to deflect as soon as load is applied, in the same way as the pin-ended column in section (1.3). The behaviour of practical frames is discussed in more detail in sections (1.9) and (1.10).

Several methods of solution are available; the more commonly used approaches are summarized in the following section, in a sequence designed to bring out the ideas leading up to the new method developed by the author in chapter three of this thesis.

## 1.7 REVIEW OF EXISTING METHODS FOR THE DETERMINATION OF ELASTIC BUCKLING LOADS

### (a) Moment distribution convergence as a stability criterion

This method is due to Hoff (reference 1), and is the result of the impact of the Hardy-Cross moment distribution method on structural analysis. A disturbing moment is applied at one joint of the frame, and the frame's response is determined by moment distribution. Hoff originally used the Berry functions ( $\alpha, \beta$ ), tabulated by Niles and Newell (reference 2), to calculate the stiffness and carry over factors of the members, but more recently these have been tabulated directly by Livesley and Chandler (reference 3). At loads below the critical, the moment distribution process converges, whereas at loads above the critical value the process diverges. The convergence of the moment distribution process is therefore a useful criterion of stability. If only a single disturbance is used, it is necessary to ensure that it does in fact excite a component of the buckling mode under consideration. In actual problems it is likely that the designer will want to take into account the initial curvatures in the members, lateral loading of the members and other effects, so that a disturbing moment is not needed to induce primary bending. This is perhaps the main advantage of the Hoff method in that the primary bending moments and a check on the stability are obtained by one computational process, although the nearness of the buckling load will in general not be established unless these calculations are repeated for other load values.

On the other hand there are several major disadvantages to this method. Firstly, in some cases it is difficult to establish whether the distribution process is converging or diverging. This can partly be overcome by changing the order of balancing the joints. Secondly, even if the buckling load is sandwiched closely, the method does not give the associated buckling mode directly, this must be computed separately. Thirdly, it is not possible to draw a graph to determine the buckling load



by extrapolation or interpolation. Finally, the Hoff method involves a considerable amount of numerical labour, as in any practical frame it takes a long time for a disturbance at one joint to be distributed throughout the frame, and even longer for the carry-overs to return to that joint.

Gregory (reference 4) has shown that the amount of computation is considerably reduced by applying disturbing moments at all the joints rather than at only one joint. This is particularly so if the correct buckling mode can be pictured, for then the disturbances can be given the correct signs and ratios so as to excite the required buckling mode; model observations are almost always necessary to provide this picture. It is seen that this technique is very similar to that of taking into account the initial curvatures of the members. If the initial curvatures are chosen, on the basis of model tests or otherwise, to closely represent the final buckling mode, then the final bending moments will be very reliable for design purposes, and convergence (or divergence) of the distribution process should be rapid.

(b) Stiffness method

Merchant (reference 5) developed a method which determines the moment  $M$  required at a particular joint of the frame to produce a given rotation  $\theta$  at that joint. The stiffness  $K$ , defined by

$$M = K \theta \quad (1.18)$$

is calculated for a number of load values, and the lowest buckling load is that for which the stiffness first becomes zero. Although moment distribution is used in the numerical work, this method has the advantage of giving a graph such as in figure (1.4), and most of the difficulties mentioned in part (a) of this section do not exist, because we are now searching for a zero rather than an infinity. Nevertheless, several distribution processes must be carried out to establish the form of the graph. There exist methods of estimating the lowest buckling load by extrapolation from but a few points on the curve at relatively low loads at which the inherent difficulties of moment distribution are not so pronounced; these techniques are a valuable aid in obtaining a reliable estimate of the buckling load. As in the Hoff method, the buckling mode must be computed separately.

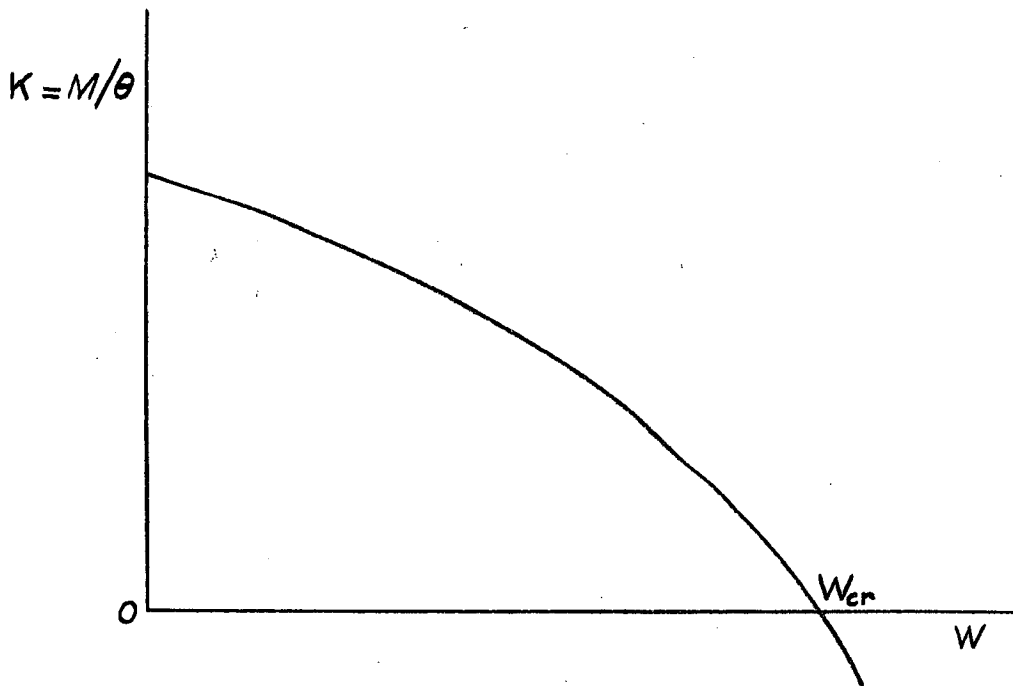


figure 1.4 - stiffness graph

(c) Matrix methods

With the advent of electronic digital computers, matrix formulation of problems in structural analysis and related fields has become increasingly popular. Matrix methods are particularly suited to the problem of the determination of elastic buckling loads and modes of framed structures.

When the matrix of the equations relating member end moments to the corresponding end slopes is set up, the mathematical criterion for buckling is that the determinant of coefficients of  $M$  or  $\theta$  vanishes. Essentially this is a generalization of Merchant's stiffness method; all the joints are rotated and the requirements of joint equilibrium give the joint moments necessary to produce these rotations. The stiffness  $s$  and carry over factor  $c$ , as tabulated by Livesley and Chandler, (see also appendix A) relate the end moments to the end slopes by the equations

$$\begin{aligned} M_{AB} &= k(s\theta_A + sc\theta_B) \\ M_{BA} &= k(sc\theta_A + s\theta_B) \end{aligned} \tag{1.19}$$

where  $k = EI/l$ , and the first subscript denotes the end under consideration. For a plane frame consisting of say  $n$  joints, equations such as (1.19) are written down for each member, and the moments applied at the joints are obtained

by summation of the end moments of members connected at the respective joints. For example if members 1, 2, and 3 intersect at the  $r$ th. joint of the frame and this joint is rotated through a small angle  $\theta_r$ , as shown in figure (1.5), then the member end moments are

$$\begin{aligned} M_{r1} &= k_1(s_1\theta_r + s_1c_1\theta_1) \\ M_{r2} &= k_2(s_2\theta_r + s_2c_2\theta_2) \\ M_{r3} &= k_3(s_3\theta_r + s_3c_3\theta_3) \end{aligned} \quad (1.20)$$

where  $\theta_1, \theta_2, \theta_3$  are the rotations at the far ends of the respective members. For equilibrium of the joint an external moment  $M_r$  is required,

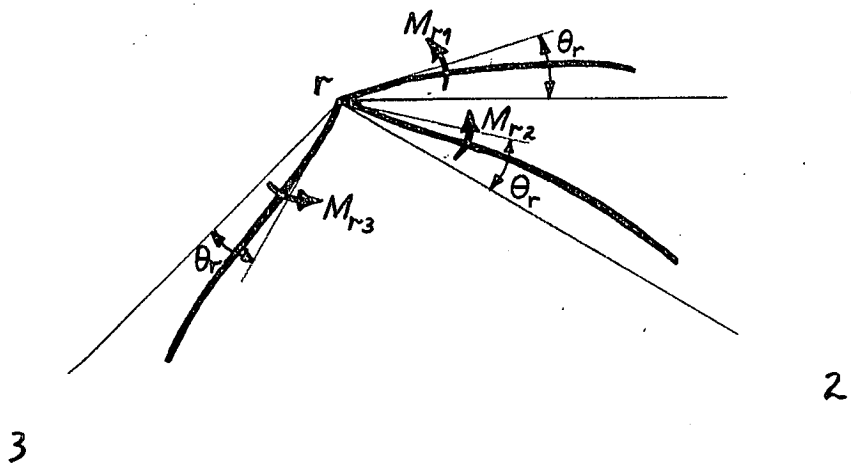


figure 1.5 - Group of members at a joint

given by

$$M_r = M_{r1} + M_{r2} + M_{r3} \quad (1.21)$$

which, after the substitution of equations (1.20), becomes of the form

$$M_r = a_{rr}\theta_r + a_{r1}\theta_1 + a_{r2}\theta_2 + a_{r3}\theta_3 \quad (1.22)$$

where the coefficients  $a$  depend on the  $k$  values of each member and upon the stability functions,  $s$  and  $sc$  of the members. Equations such as this are written for each joint, so that in general the following system of equations is obtained

$$\tilde{M} = \tilde{K} \cdot \tilde{\theta} \quad (1.23)$$

where  $\tilde{K}$  is a symmetric matrix, called the stiffness matrix, the elements of which are a function of the stability functions of some or of all the members of the frame,  $\tilde{M}$  is the vector defining the joint moments, and  $\tilde{\theta}$  is the vector defining the corresponding joint rotations.

In general the mathematical model of the frame is undisturbed, so that  $\tilde{M}$  is a null vector, and equation (1.23) becomes

$$\tilde{K} \cdot \tilde{\theta} = \tilde{0} \quad (1.24)$$

A non-trivial solution exists only if the determinant of  $\tilde{K}$ , that is  $|\tilde{K}|$ , is identically zero and then the rotations are undefined in magnitude, but they bear a definite ratio to each other.

Thus, mathematically speaking, the problem has been reduced to the determination of those load values for which  $|\tilde{K}|$  vanishes, and this is perhaps the most powerful method for the estimation of buckling loads and modes of framed structures. Here again several mathematical techniques are available, but it suffices to describe only the more commonly used methods of solution.

(i) Evaluation of the determinant

The classical approach in this case is the obvious one, that is to evaluate the determinant at a number of load values. The buckling loads are then found graphically and the associated modes are calculated by setting an arbitrary rotation equal to unity and solving the equations for the remaining unknowns. For frames of any complexity the order of the determinant becomes high, and this method is apt to become very tedious as well as inaccurate due to accumulating errors in the evaluation of the determinant.

(ii) Latent roots of the stiffness matrix

Gregory (reference 6) has shown that equation (1.23) is conveniently solved by the extraction of latent roots and latent vectors of the matrix  $\tilde{K}$ . A latent root,  $\lambda$ , of  $\tilde{K}$  is defined as

$$\lambda = M_i / \theta_i \quad ; \quad i = 1, 2, \dots, n \quad (1.25)$$

From this definition it is seen that  $\lambda$  represents a kind of generalised overall stiffness of the frame. Substitution of equation (1.25) into (1.23) yields

$$(\tilde{K} - \lambda \tilde{I}) \cdot \tilde{\theta} = \tilde{0} \quad (1.26)$$

where  $\tilde{I}$  is the unit matrix. That is, the matrix  $\tilde{K}$  is modified by subtracting  $\lambda$  from each of the elements on the leading diagonal. As before, a non-trivial solution exists only if the determinant  $|\tilde{K} - \lambda\tilde{I}|$  is identically zero, which is the condition used to calculate  $\lambda$ . In general there exist  $n$  latent roots for a given  $(n \times n)$  symmetric matrix, each associated with a different latent vector.

At any of the buckling loads of the frame the determinant  $|\tilde{K}|$  itself vanishes, and the righthandside of equation (1.23) is zero, so that one of the latent roots of the matrix  $\tilde{K}$  also vanishes. It can be shown that at loads smaller than the lowest buckling load all the latent roots are positive, whence it follows that the lowest buckling load is that for which the smallest latent root first becomes zero, and the associated buckling mode is the corresponding latent vector. The largest latent root of a matrix is readily extracted by a standard intensification process (see for example reference 7), and Gregory shows that this can be used to find the smallest latent root by what he calls a "parallel shift" of the latent roots, which is analogous to a transfer of origin. That is, if  $\lambda^1$  is the largest latent root of the matrix  $(\tilde{K} - g\tilde{I})$ , then the smallest latent root of  $\tilde{K}$ ,  $\lambda_1$  is given by

$$\lambda_1 = \lambda^1 + g \quad * \quad (1.27)$$

and the lowest buckling load is found by graphing  $\lambda_1$  against load to determine its first zero.

The most important feature of Gregory's method is that the parallel shift does not change the latent vectors of  $\tilde{K}$ ; hence the latent vector associated with the largest latent root of  $(\tilde{K} - g\tilde{I})$  at the lowest buckling load is in fact the corresponding buckling mode. A further advantage of this method is that convergence of the intensification process is greatly enhanced by starting with a trial vector close to the buckling mode, and this can be obtained from tests on crude models of the frame, often a cardboard model is sufficient.

Although it may seem that the extraction of two latent roots is required, the labour involved is but a little more than that of extracting one, because only a rough estimate of  $g$  is required; it is necessary only to ensure that the shift is numerically larger than the mean of  $\lambda_1$  and  $g$ .

---

\*  $g$  is the magnitude of the "shift" which is equal to the largest latent root of  $\tilde{K}$ .

(iii) McMinn's method

McMinn (reference 8) calculates the lowest buckling load from the applied matrix  $\tilde{Q}$  defined by

$$\tilde{Q} = \tilde{B}\tilde{D}^{-1} - \tilde{I} \quad (1.28)$$

where  $\tilde{B}\tilde{D}^{-1}$  is the matrix obtained from  $\tilde{K}$  by dividing each column by its element on the leading diagonal, and the elements on the leading diagonal are zero. The lowest buckling load in this case is the load at which the largest latent root of  $\tilde{Q}$  equals -2. Although McMinn's modification of the stiffness matrix requires less work than Gregory's parallel shift, it suffers the disadvantage that the latent vector of  $\tilde{Q}$  corresponding to its largest latent root is not simply related to the buckling mode; the mode must be computed separately. This also necessitates the use of an unguided choice for the first trial vector in the intensification process.

(d) Energy methods

Rayleigh (reference 9) first conceived the idea of using assumed deflection curves in a strain energy integral, and minimizing this integral to calculate what he calls the "disposable parameters" involved in defining the curves. This method of approximate solution is used to solve a wide variety of problems; for example the buckling load of a pin-ended column may be calculated to any degree of accuracy by continually improving the assumption for the deflected shape (see for example reference 10).

The Rayleigh method is readily extended to the stability analysis of frames. The buckled shape of each member is guessed, its strain energy is evaluated, and the results are summed to obtain the total strain energy of the frame. The strain energy of a single member,  $U$  is defined by (see chapter two)

$$U = \int_0^l \int_0^\phi M d\phi dx - \int_0^\Delta P d\Delta - \int_0^{\theta_A} M_{AB} d\theta_A - \int_0^{\theta_B} M_{BA} d\theta_B \quad (1.29)$$

where  $\Delta$  is the axial shortening due to bending and is given by

$$\Delta = \frac{1}{2} \int_0^l (dy/dx)^2 dx \quad (1.30)$$

In the case of a linear moment curvature relation, the first term in equation (1.29) becomes

$$\int_0^l \int_0^\phi M d\phi dx = \int_0^l \int_0^\phi EI \phi d\phi dx = \frac{1}{2} \int_0^l EI \phi^2 dx = \frac{1}{2} \int_0^l EI (d^2y/dx^2)^2 dx \quad (1.31)$$

If the loaded but undeflected state is chosen as energy reference datum, then under the assumption already made that  $P$  remains unaltered by the lateral deformations, the second term becomes

$$-\int_0^{\Delta} P d\Delta = -\frac{1}{2}P \int_0^{\ell} (dy/dx)^2 dx \quad (1.32)$$

For the whole frame, the total strain energy is

$$U = \sum_{\text{members}}^{\text{all}} \left\{ \frac{1}{2} \int_0^{\ell} EI (d^2y/dx^2)^2 dx - \frac{1}{2} P \int_0^{\ell} (dy/dx)^2 dx - \int_0^{\theta_A} M_{AB} d\theta_A - \int_0^{\theta_B} M_{BA} d\theta_B \right\} \quad (1.33)$$

It is seen that the first term in this summation represents the internal strain energy of bending for the whole frame. The second term is the work done by the external loads on the frame, and it is readily shown that

$$\sum_{\text{members}}^{\text{all}} \left\{ \frac{1}{2} P \int_0^{\ell} (dy/dx)^2 dx \right\} = \sum_i \left\{ \int_0^{\delta_i} W_i d\delta_i \right\} \quad (1.34)$$

where  $\delta_i$  is the deflection of the load  $W_i$ , and the summation extends over all the applied loads. Similarly, the summation involving the member end moments is equivalent to

$$\sum_j \left\{ \int_0^{\theta_j} M_j d\theta_j \right\} \quad (1.35)$$

which is the work done by the joint moments  $M_j$  by rotating the joints through the small angles  $\theta_j$ , the summation extending over all the joints. In the general analysis of the idealized mathematical model, the joints are undisturbed, and this term therefore vanishes. It remains then to specify the deflected shape of each member in terms of one parameter, or more in the Rayleigh-Ritz method, evaluate the necessary integrals, and minimize expression (1.33) with respect to the disposable parameters. This leads to a system of linear equations, and hence to the usual criterion that the determinant of coefficients must vanish for a non-zero solution of the parameters.

## 1.8 THE BUCKLING OF A SIMPLE FRAME

In order to obtain a deeper appreciation of the underlying principles in the analysis of elastic stability of frames, the fundamental buckling load and mode for the equilateral triangular frame shown in figure (1.6) will be calculated by the various methods discussed in the previous section. Although this frame has no practical

application it is one of the simplest to analyse. Figure (1.6a) shows the antisymmetric buckling mode, and figure (1.6b) the symmetric mode,

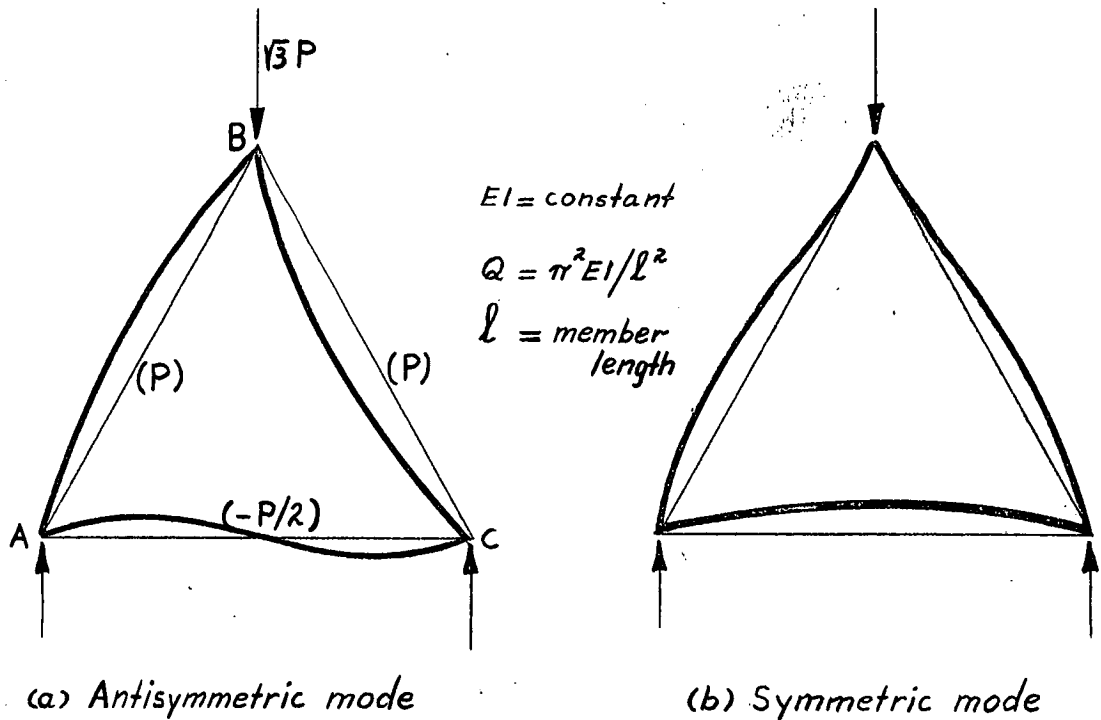


figure 1.6 - Buckling modes of equilateral triangular frame

these being the first two possible buckling modes. The symbols in parentheses at the centres of the members are the axial loads in the members, compression being considered positive. In this problem it is convenient to treat  $P$  as the primary load parameter, and the lowest buckling load is denoted by  $P_{cr}$ .

#### Preliminary analysis

Obviously the compression members  $AB$  and  $BC$  have some restraint against rotation at the ends, so that  $P_{cr}$  must be greater than  $Q$ , the Euler load of the members. Also, in the case of symmetric buckling, these members are equivalent to columns built-in at  $B$ , and partially restrained at  $A$  and  $C$ . If  $A$  and  $C$  were free to rotate, the buckling load would be  $2.05Q$ , which is therefore a lower bound for symmetric buckling. For the anti-symmetric mode,  $M_{BA} = M_{BC} = 0$ , (since  $M_{BA} = M_{BC}$  from antisymmetry, and their sum is zero for equilibrium at joint  $B$ ), so that the members  $AB$  and  $BC$  are equivalent to columns pinned at  $B$ , and having partial rotational restraint at  $A$  and  $C$ . Thus  $P_{cr}$  must be less than  $2.05Q$  in the antisymmetric mode.



This preliminary analysis establishes that the fundamental buckling mode is antisymmetrical, and that  $P_{cr}$  lies between  $Q$  and  $2.05Q$ .

(a) Solution by the moment distribution convergence criterion

Figure (1.7) shows the distribution and carry-over factors of the members, at the primary load  $P = Q$ . A disturbing moment of 100 units is applied at joint B, and the distribution process is carried out in the table alongside figure (1.7), only half the calculations being

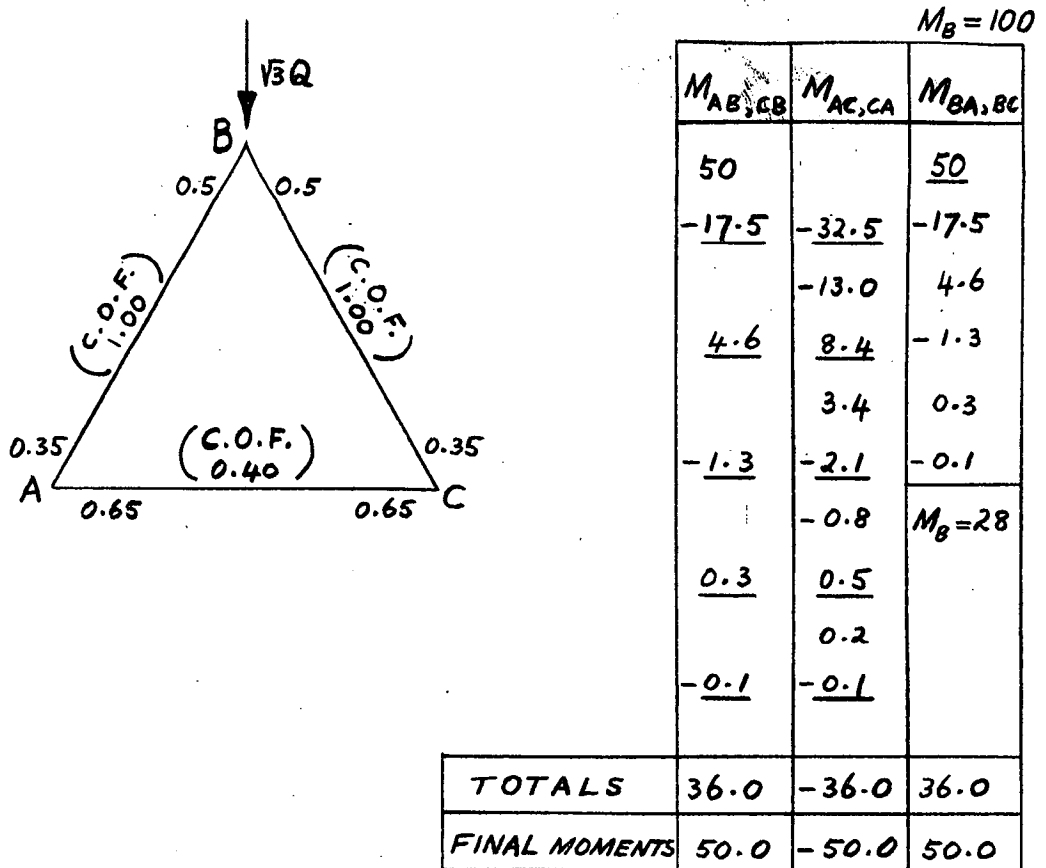
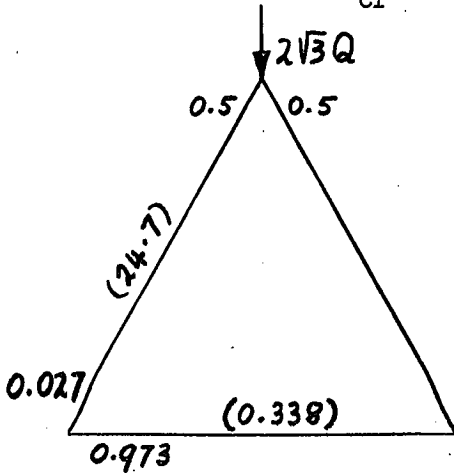


figure 1.7 - distribution and carry-over factors

shown as they are antisymmetrical. It is seen that after joint A is balanced, and therefore also joint C, there is an out of balance moment of 28 units at joint B, and since this is less than the original disturbing moment of 100 units, the process is converging, so that  $P_{cr}$  has not been exceeded, as was to be expected from the preliminary analysis. The out of balance moment of 28 units, when redistributed, obviously gives identical calculations decreased by the ratio  $28/100$ , so that the final bending moments are easily obtained as the sum of an infinite geometric progression. At this load the balancing of joints A and C need not have been completed, as it can be seen after the first cycle that the process is convergent.

The distribution process is repeated for a primary load of  $2Q$  in the following table, and in this case one cycle is sufficient to indicate divergence, so that  $P_{cr}$  has been exceeded.



$M_B = 100$

$M_{AB}$	$M_{AC}$	$M_{BA}$
1235		50
- 33	-1202	-824
	- 394	
11	383	262

Knowing values of  $P$  both above and below  $P_{cr}$ , we can halve the interval between converging and diverging cases, thereby successively reducing the range until the desired accuracy is obtained. It is found, after four more distribution processes, that the buckling load is within the range

$$1.60Q < P_{cr} < 1.65Q$$

and for all practical purposes we can take  $P_{cr} = 1.63Q$ .

As mentioned earlier, the buckling mode is not obtained and must be computed separately. The best way to do this is to work from the bending moments calculated at a load somewhat less than  $P_{cr}$ . At  $P = 1.6Q$  the bending moments are

$$M_{BA} = M_{BC} = 50 \text{ units}$$

$$M_{AB} = -M_{AC} = 1145 \text{ units} = -M_{CA} = M_{CB}$$

The joint rotations are given by the equations

$$(EI/l)\theta_A = \frac{1}{6} [2\beta M_{AB} - \alpha M_{BA}]$$

$$(EI/l)\theta_B = \frac{1}{6} [-\alpha M_{AB} + 2\beta M_{BA}]$$

where  $\alpha, \beta$  are the Berry functions for member AB. Dropping the factor  $(6EI/l)$ , and using the tables in Niles and Newell, we obtain

$$\theta_A = -1040 ; \theta_B = 2470$$

As a check, the calculations for member AC give

$$\theta_A = \theta_C = -1020$$

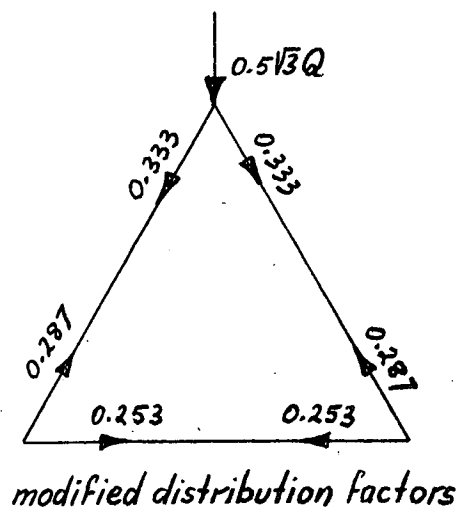
Hence the buckling mode is approximately expressed by the ratio

$$\theta_A : \theta_B : \theta_C = -0.376 : 1 : -0.376$$

It can be seen that for a frame having several joints, considerable extra computation is needed to obtain the buckling mode. In this particular problem convergence or divergence is readily detected, but in more difficult frames this is not always the case, and it is usually necessary to perform additional tests such as altering the order of balancing the joints. This is especially important if the fundamental mode is not known. For example, if equal and opposite disturbing moments are applied to joints A and C of the equilateral triangular frame, the symmetric mode is excited, and if the distribution is kept symmetrical it will be found to be convergent at loads greater than  $1.63Q$ . Altering the order of balancing in this case reveals divergence, indicating that the fundamental buckling load has been exceeded.

(b) Solution by Merchant's stiffness method

In this method joint B is rotated a unit amount, and its stiffness calculated, that is the moment at that joint. This is most easily carried out in the form of a relaxation table. Since individual member end moments are not of interest, it is convenient to use the so called modified distribution factors, that is if an external moment  $M$  is applied at a joint, then the moments required at neighbouring joints to prevent their rotation are found by multiplying  $M$  by the appropriate modified distribution factors. These are shown alongside the relaxation table below. The first line in the table gives the moment required at



RELAXATION TABLE			
Operation	$M_A$	$M_B$	$M_C$
$\theta_B = 1$		6.59	
distribution	2.19		2.19
balance	-2.19		-2.19
dist.	-0.56	-1.26	-0.56
bal.	0.56		0.56
dist.	0.14	0.32	0.14
bal.	-0.14		-0.14
dist.	-0.04	-0.08	-0.04
bal.	0.04		0.04
dist.	0.01	0.02	0.01
Final joint moments	0.01	5.59	0.01

joint B to produce a unit rotation there. This is distributed in line (2), and at this stage  $\theta_B = 1$  ;  $\theta_A = \theta_C = 0$ . The moments at A and C are then balanced by equal and opposite external moments there, which in turn must be distributed, resulting in unbalance of A and C. These are again balanced and distributed, and so on until the out of balance moments are sufficiently small. Equations (1.19) are used to calculate the end moments, and the primary load is arbitrarily taken as  $0.5Q$ . To the accuracy shown, the joint stiffness at  $P = 0.5Q$  is 5.59. Similar calculations at other load values give the stiffness plot shown in figure (1.8). From the graph, the buckling load is obtained as

$$P_{cr} = 1.63Q$$

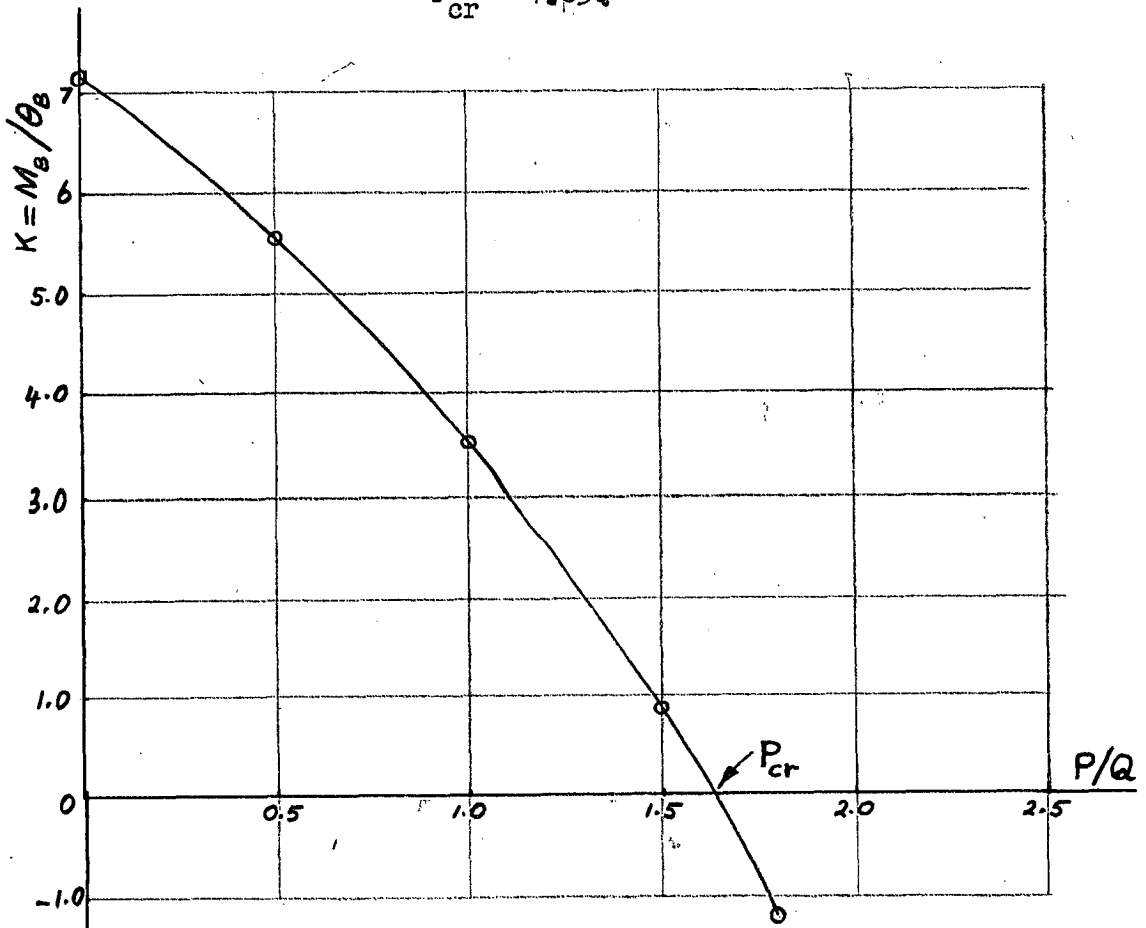


figure 1.8 - Stiffness for equilateral triangular frame

which agrees with the value calculated before. The buckling mode in this case is also simple to calculate if it is remembered that the balancing of a joint implies a rotation there given by

$$\theta = \delta M / \sum s$$

where  $\delta M$  is the moment to be balanced, and  $\sum s$  is the sum of the member stiffnesses at that joint. In this operation the other joints are prevented

from rotation, and the moments to do this are calculated using the modified distribution factors. At  $P = 1.63Q$  the sum of the balancing moments applied to joint A (and joint C) amounts to  $-2.38$  units, and the sum of the stiffness of the members at A is  $6.13$ , so that

$$\theta_A = \theta_C = -0.388$$

Thus the buckling mode is given by

$$\theta_A : \theta_B : \theta_C = -0.388 : 1 : -0.388$$

This is probably more accurate than that obtained by Hoff's method, in which the rotations can be calculated only at a load less than critical.

In most problems the stiffness graph need not be plotted completely, as the lowest buckling load can be estimated fairly accurately by extrapolation. For example, linear extrapolation from the two points  $P = 0.5Q$  and  $P = 1.0Q$  gives  $P_{cr} \approx 1.93Q$ . From the form of the graph it readily follows that  $P_{cr}$  must in fact be less than this, and the calculation of a negative stiffness at  $P = 1.8Q$  confirms this. Linear extrapolation between  $1.0Q$  and  $1.8Q$  gives a lower bound, that is  $P_{cr} > 1.58Q$ . Once three points on the graph have been found a much better estimate of  $P_{cr}$  can be found by quadratic extrapolation, that is by drawing a parabola through the points. For the three points  $0.5Q$ ,  $1.0Q$  and  $1.8Q$  this gives  $P_{cr} \approx 1.61Q$ , which is seen to be only 1% different from the exact value.

### (c) Solution by matrix methods

Denoting the stiffness and carry over factors of the compression members by  $s$  and  $c$  respectively, and those for the tension member by  $s'$  and  $c'$ , the end moments are determined from equations (1.19), and summation at the joints gives the stiffness matrix as

$$\tilde{K} = \begin{bmatrix} (s + s') & sc & s'c' \\ sc & 2s & sc \\ s'c' & sc & (s+s') \end{bmatrix} \quad (1.36)$$

where the stability functions can be found in Livesley and Chandler's tables (reference 3) as functions of the  $P/Q$  ratio of the members.

### (i) Zeros of determinant

The determinant of most easily evaluated by setting up the matrix numerically, and expanding according to the rule of Sarrus for

third-order determinants. Figure (1.9) shows the plot of the value of the determinant,  $D$  against the load  $P$ , a wide range being covered as a matter of interest. It is seen that the determinant vanishes at  $P = 1.63Q$  and at

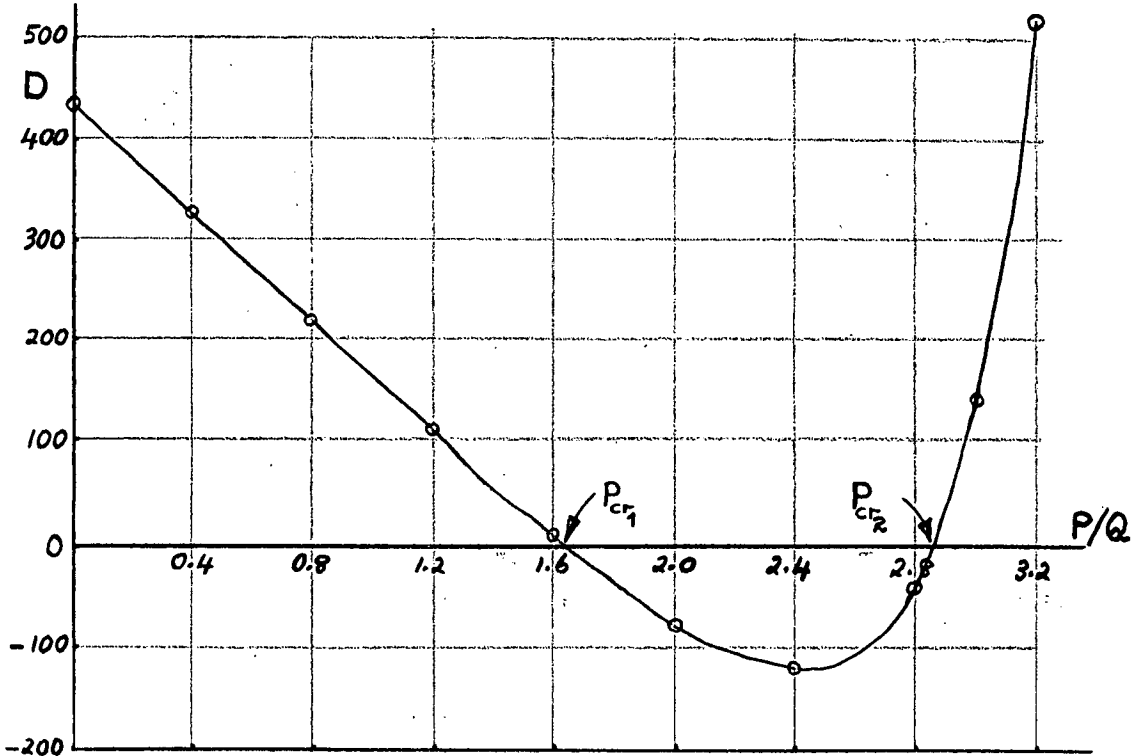


figure 1.9 - Value of determinant for equilateral triangular frame

$P = 2.87Q$ , which are the buckling loads for the antisymmetric and symmetric modes respectively. To calculate the buckling modes corresponding to these loads it is necessary to solve the stiffness equations. At  $P = 1.63Q$  these equations are

$$6.13\theta_A + 3.01\theta_B + 1.78\theta_C = 0$$

$$3.01\theta_A + 2.30\theta_B + 3.01\theta_C = 0$$

$$1.78\theta_A + 3.01\theta_B + 6.13\theta_C = 0$$

If  $\theta_B$  is put equal to unity, the solution of the equations is

$$\theta_A = \theta_C = -0.382$$

which defines the buckling mode corresponding to  $P_{cr} = 1.63Q$ .

At  $P = 2.87Q$  the equations are

$$1.67\theta_A + 6.27\theta_B + 1.68\theta_C = 0$$

$$6.27\theta_A - 7.89\theta_B + 6.27\theta_C = 0$$

$$1.68\theta_A + 6.27\theta_B + 1.67\theta_C = 0$$

In this case it is found that if  $\theta_B$  is equated to unity, the solution is undefined. This is because the determinant of any two of the equations is in fact zero, which in turn means that the original third order determinant can be factorized, one factor giving the antisymmetric mode, and the other factor giving the symmetric mode. The symmetric mode has  $\theta_B = 0$ , and the solution of the above equations then becomes  $\theta_A = -\theta_C$ , which defines this mode completely.

(ii) Latent roots of the stiffness matrix

The latent roots of the matrix  $\tilde{K}$  are calculated from the condition that the determinant of the matrix  $(\tilde{K} - \lambda \tilde{I})$  vanishes. From equations (1.36) it follows that for the frame under consideration, this condition is

$$\begin{vmatrix} (s + s' - \lambda) & sc & s'c' \\ sc & (2s - \lambda) & sc \\ s'c' & sc & (s + s' - \lambda) \end{vmatrix} = 0 \quad (1.37)$$

Generally only the smallest latent root is of interest, and this can be found by Gregory's parallel shift method. However, in this case it is easy to determine all the latent roots by expanding the above determinant and solving the resulting cubic equation. Figure (1.10) shows

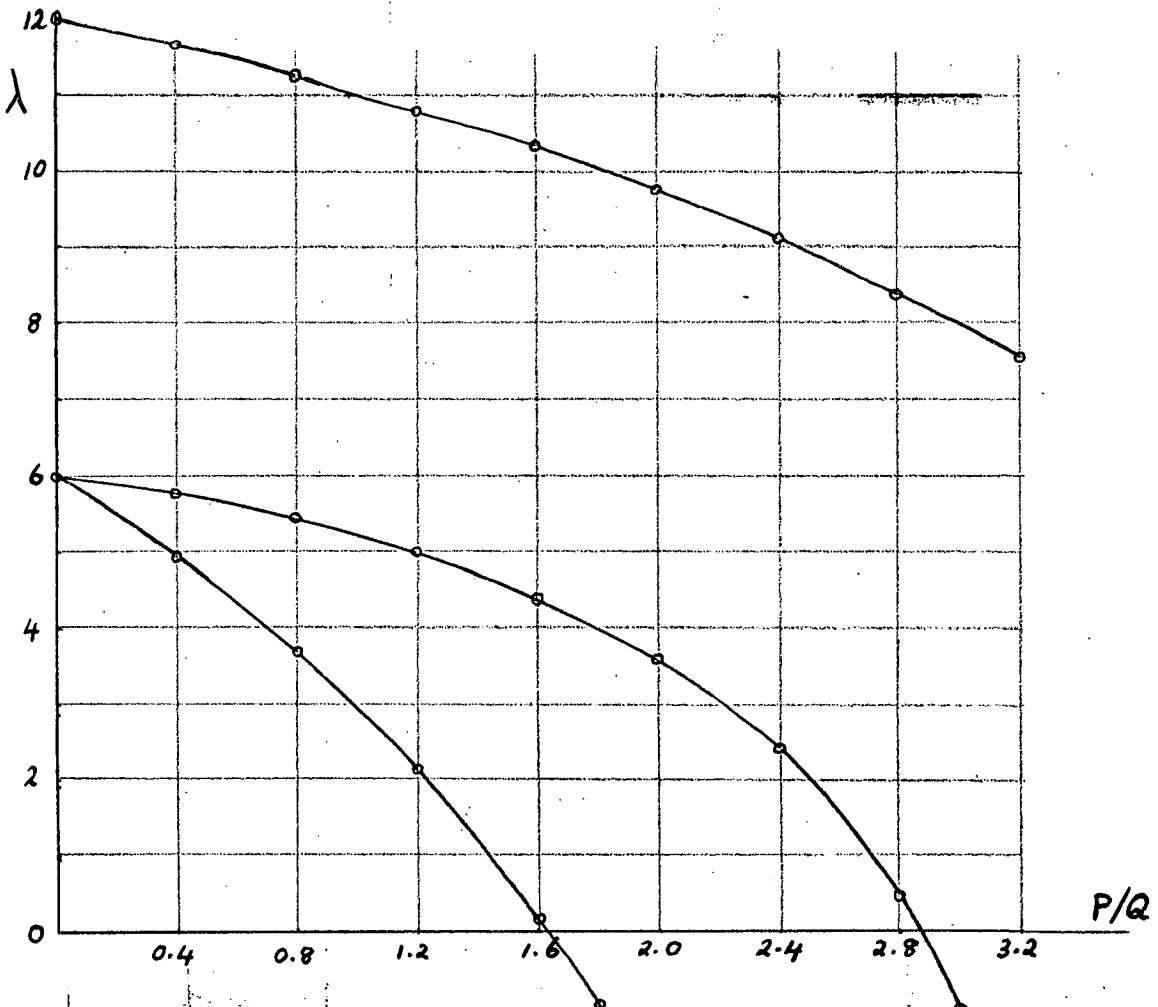


figure 1.10 - Latent roots of equilateral triangular frame

the latent roots plotted against load. It is seen that one of the roots vanishes at  $P = 1.63Q$  and one at  $P = 2.87Q$ , the first two buckling loads. The latent vectors corresponding to these loads are respectively

$$\theta_A : \theta_B : \theta_C = -0.385 : 1 : -0.385$$

and

$$\theta_A : \theta_B : \theta_C = 1 : 0 : -1$$

which represent the two modes shown in figure (1.6). These results agree with those obtained previously.

### (iii) McMinn's Method

At  $P = 0$  the stiffness matrix is

$$\tilde{K} = \begin{bmatrix} 7.09 & 2.47 & 1.86 \\ 2.47 & 4.93 & 2.47 \\ 1.86 & 2.47 & 7.09 \end{bmatrix}$$

Dividing each column by its element on the leading diagonal, and replacing the leading diagonal elements by zero, the matrix  $BD^{-1}$  is obtained as

$$\tilde{BD}^{-1} = \begin{bmatrix} 0 & 0.501 & 0.262 \\ 0.348 & 0 & 0.348 \\ 0.262 & 0.501 & 0 \end{bmatrix}$$

and hence the allied matrix  $Q$  becomes

$$\tilde{Q} = \tilde{BD}^{-1} - \tilde{I} = \begin{bmatrix} -1 & 0.501 & 0.262 \\ 0.348 & -1 & 0.348 \\ 0.262 & 0.501 & -1 \end{bmatrix}$$

A standard process for extracting the largest latent root is given in reference 7. With  $(1, 1, 1)$  as a starting vector, six iterations give the vector

$$u_6 = (-0.678, 1, -0.678)$$

and the estimate of the largest latent root at this stage is  $-1.468$ .

Two more steps give

$$u_7 = (-0.681, 1, -0.681)$$

$$u_8 = (-0.680, 1, -0.680)$$

Thus, to slide rule accuracy, the process has converged, and since the largest latent root is numerically less than two, the buckling load has



not been exceeded. Similar calculations at  $P = 1.5Q$  and  $1.8Q$  are sufficient to give a reasonable plot, from which the buckling load is obtained as

$$P_{cr} = 1.63Q$$

and the latent vector corresponding to this load is

$$(1, -0.975, 1)$$

which is seen to bear no simple relation to the buckling mode.

#### (d) Solution to Rayleigh's method

The specification of the functional form for the assumed deflected shape is quite arbitrary, and in this case, polynomials are convenient. The simplest polynomials which can be fitted are

$$y = 4 y_0 [(x/l) - (x/l)^2] \quad \text{for members AB and BC}$$

$$\text{and} \quad y = 4 y_0 [(x/l) - 2(x/l)^2] \quad \text{for member AC, } (0 \leq (x/l) \leq \frac{1}{2}) \quad (1.38)$$

These shapes correspond to the <sup>anti</sup>symmetric mode, and satisfy the boundary conditions of zero deflection at the joints, and also of compatibility of slopes at the joints. The disposable parameter,  $y_0$  is the central deflection of the compression members.

The total strain energy of the frame is evaluated according to equation (1.33), and the condition for its minimum is expressed by the equation

$$\partial U / \partial y_0 = 384 y_0 EI / l^3 - 8 y_0 P / l = 0$$

whence, either (i)  $y_0 = 0$ ; that is the trivial solution, or (ii)  $P = 48(EI/l^2)$ ; in which case  $y_0$  is undefined. The latter solution is thus an estimate of the buckling load for the anti-symmetric mode, and it can be shown (see for example reference 10) that this estimate is an upper bound, so that  $P_{cr} < 48EI/l^2$ . This is about three times the correct value, and the error is attributed to the inadequacy of the assumed shapes. As can be seen from equations (1.38), these assumed curves imply a constant curvature, and hence a constant bending moment, along the members, and obviously the joints are not in equilibrium moment-wise. A better shape would be

$$\begin{aligned} y &= y_0 \sin(\pi x/l) && \text{for AB and BC} \\ y &= \frac{1}{2} y_0 \sin(2\pi x/l) && \text{for AC} \end{aligned} \quad (1.39)$$

These curves satisfy equilibrium at the joints, but in this case all member end moments are zero, which is also unrealistic. The estimate of the buckling load, obtained from minimum strain energy, is  $39.5 (EI/l^2)$ , which is little better than the previous estimate.

The simplest polynomials which satisfy equilibrium at the joints, as well as compatibility of slopes and deflections, are

$$\begin{aligned} y &= (16y_0/9)[(x/l) + 3(x/l)^2 - 7(x/l)^3 + 3(x/l)^4] && \text{for AB and BC} \\ y &= (16y_0/9)[(x/l) - 3(x/l)^2 + 2(x/l)^3] && \text{for AC, } (0 \leq (x/l) \leq \frac{1}{2}) \end{aligned} \quad (1.40)$$

Minimum strain energy gives an upper bound for the buckling load,

$$P_{cr} < 16.6 EI/l^2 = 1.68Q$$

which is seen to be only about 3% high. Better estimates can be found by satisfying boundary conditions in higher derivatives, but the gain in accuracy is offset by the increase in the amount of computation.

\*

\*

\*

From the example just studied it is evident that all methods for the determination of buckling loads and modes are basically similar, the only differences being in the approach to the numerical computation. Hoff's method, using moment distribution, is in fact the relaxation solution of the flexibility matrix, that is the set of simultaneous equations in the member end moments. At the buckling load the determinant of coefficients vanishes, so that the solution is undefined for even the smallest disturbance, which means that the process must diverge at the buckling load.

Merchant's method overcomes this by putting an arbitrary joint rotation equal to unity, and by keeping this constant, the successive distribution of out of balance joint moments yields a finite solution, and the moment at the disturbed joint becomes zero at the buckling load. The distribution process is readily seen to be equivalent to the relaxation solution for the remaining joint rotations in equations (1.23).

The latent root method, as developed by Gregory, is a logical extension of Merchant's method. All the joints are rotated simultaneously, and the latent root solution is essentially a linear combination of elementary

Merchant type solutions, the "unit" rotation being adjusted to make the stiffness at all joints the same.

McMinn's method defies a physical explanation although undoubtedly this exists.

Energy methods are generally approximate solutions, and the physical interpretation as given in most texts, leaves much to be desired. It is shown in the following chapter that energy methods are merely alternative devices for setting up equations of statics (strain energy) or geometry (complementary energy), and these equations are exact or approximate, depending on the nature of the simplifications which are necessarily made.

As well as the methods mentioned above, various authors have proposed alternative solutions, notably Bolton, Waters, Allen (references 11, 12, 13 respectively.) Some authors suggest replacing the frame, or parts thereof, by groups of members, with various simplifying assumptions for the end conditions, such as pinned ends or fixed ends. This is of course the simplification of an already simplified mathematical model of the real frame which can be a dangerous practice for obvious reasons.

Irrespective of which method of analysis is finally decided upon, difficulties of one kind or another are bound to arise. Generally speaking it is a question of convenience of numerical solution and the ability to apply engineering judgment and intuition, keeping in mind firstly that engineers require quick reliable answers rather than accurate results, and secondly that the analysis of this mathematical model is but the first step in the assessment of the performance of a frame.

#### 1.9 THE PRACTICAL FRAME; EXPERIMENTAL METHODS

The concept of buckling of the simplified mathematical model, as set out in the previous sections, is defined by means of an initial disturbance. In actual frames these disturbances need not necessarily be introduced, as the initial imperfections such as initial curvatures, eccentricity of loads and many other factors are sufficient to excite lateral deformations as soon as load is applied. In fact the behaviour is very similar to that of a pin ended column with initial curvature. Assuming that the initial crookedness of the isolated pin-ended column can be expressed as a linear combination of the buckling modes, that is as the Fourier series

$$y_0 = \sum_{n=1}^{\infty} a_n \sin(n\pi x/l) , \quad (1.41)$$

then the differential equation of equilibrium (1.6) is modified to

$$EI(d^2y/dx^2 - d^2y_0/dx^2) + Py = 0 \quad (1.42)$$

The solution of equation (1.42) gives the deflected shape under load as

$$y = \sum_{n=1}^{\infty} \frac{a_n \sin(n\pi x/l)}{1 - P/n^2Q} \quad (1.43)$$

Thus each component of the initial crookedness pattern is magnified by the ratio  $1/(1-P/n^2Q)$ . As  $P$  approaches  $Q$  the first term dominates, and the deflected shape is closely approximated by the first term, that is

$$y \approx a_1 \sin(\pi x/l)/(1-P/Q) \quad (1.44)$$

The central deflection is given by

$$\delta_c = a_1/(1-P/Q)$$

where  $a_1$  is the initial central crookedness. This expression is shown graphically in figure (1.11a). The deflection is a hyperbolic function of the load  $P$ , running away to infinity as  $P$  approaches  $Q$ . Southwell

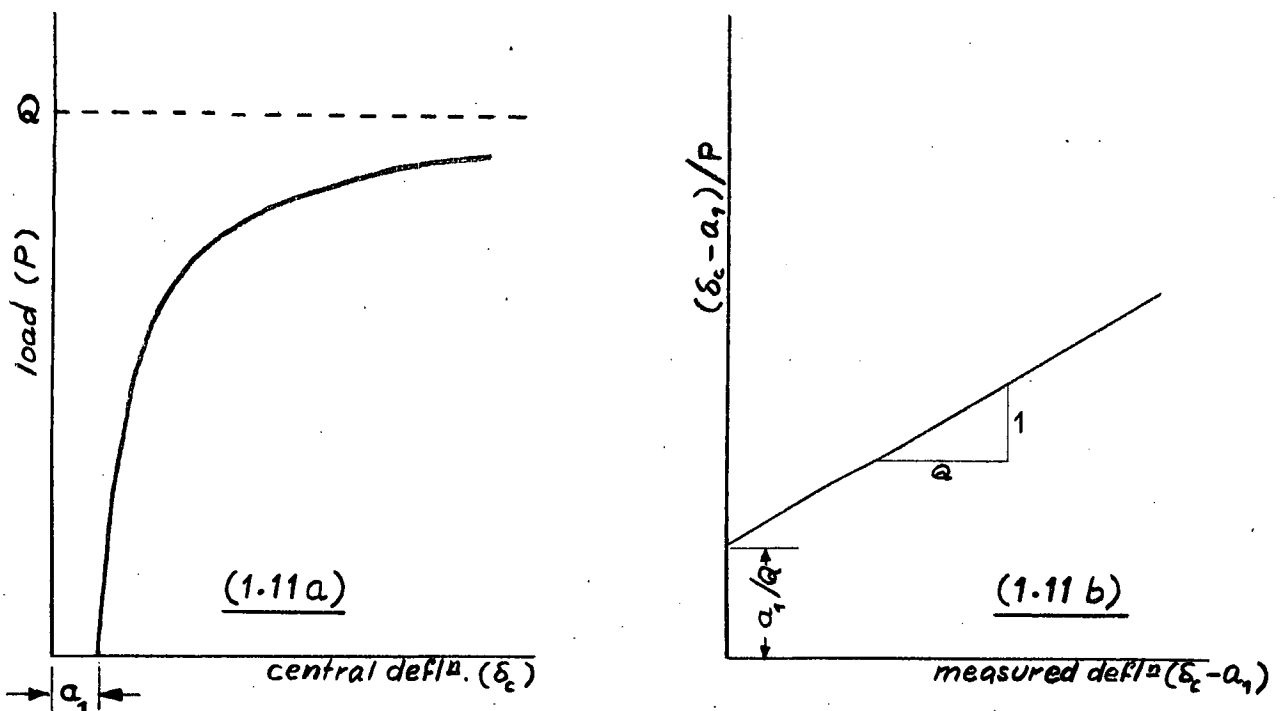


figure (1.11) - Southwell Plot

(reference 14) first recognised this as a valuable tool for the experimental determination of the buckling loads of columns. In a test, the measured

deflection is  $(\delta_c - a_1)$ , which shifts the hyperbola to pass through the origin. The plot of  $(\delta_c - a_1)/P$  against  $(\delta_c - a_1)$  is then a straight line of slope  $1/Q$  and intercept  $a_1/Q$ , as shown in figure (1.11b). This graph is commonly known as the Southwell plot on deflection.

The Southwell plot has been widely used for the experimental determination of the elastic buckling loads of frames, and it works equally well for rotations, curvatures or indeed any deformation parameter which can be expressed in the form of equation (1.44). Gregory (reference 15) shows that it is convenient to use measured strains, and justifies the general use of the Southwell plot on the basis of numerous tests, some of which are verified analytically. A rigorous mathematical proof of the Southwell plot on plane or space frames has since been given by Ariaratnam (reference 16). In general, if  $y_0$  represents the initial crookedness of the frame, then this can be expressed as a linear combination of the  $n$  buckling modes  $y_1, y_2, \dots, y_n$ . That is

$$y_0 = \sum_{i=1}^n a_i y_i \quad (1.45)$$

If  $\lambda$  is used to denote a generalized load parameter, and  $\lambda_1, \lambda_2, \dots, \lambda_n$  are the critical values of  $\lambda$ , then the frame deflections  $y$ , under load  $\lambda$ , are given by

$$y = \sum_{i=1}^n a_i y_i / (1 - \lambda / \lambda_i) \quad (1.46)$$

That is each component is magnified by the ratio  $1/(1 - \lambda / \lambda_i)$  in the same way as the pin-ended column. Also, as  $\lambda$  approaches the first buckling load,  $\lambda_1$  say, the first term dominates, and a linear Southwell plot is obtained. Expression (1.46) can be differentiated, whence it is seen that the same expression also applies to rotations and curvatures.

Gregory also suggests the possibility of using the Southwell plot equation as a design formula, by equating the maximum strain to the yield strain, giving an equation similar to the Perry formula for the pin-ended column. This method is a definite improvement on the design of frames by individual members using the pin-ended column formulas with guessed effective lengths. However, as Gregory points out, "a great deal of experimental work is required to determine, systematize and tabulate the variation of  $\phi$  (a crookedness parameter) and  $A_{cr}$  (the critical action causing elastic buckling) for many types of structures".

### 1.10 THE PRACTICAL FRAME: PREDICTED BEHAVIOUR

The behaviour of a practical frame, and its load carrying capacity depend to a great extent on the magnitude of the initial imperfections, and to a lesser extent on the functional form of these imperfections. In most instances the load carrying capacity is considerably less than the calculated lowest buckling load, so that the latter loses its importance somewhat. The designer ultimately wants to know how much load his frame can safely carry, and thus a satisfactory prediction of frame behaviour becomes increasingly important.

In this section an attempt is made to develop a simplified mathematical model to predict the behaviour of an initially crooked frame under load. The treatment given is that of the author. Attention is focussed primarily on the joint rotations; once these are known, the deflected shape of every member can be plotted, and curvatures, strains, bending moments and stresses are directly inferred. The functional form of the initial crookedness pattern is chosen to resemble the fundamental buckling mode, and sinusoidal curves are used for simplicity. Single member equations are derived in the following paragraph, and the equations for the whole frame are obtained by summation.

Consider an initially crooked member deformed by an axial force  $P$  and end moments  $M_{AB}$ ,  $M_{BA}$  as shown in figure (1.12). Assume that the initial crookedness can be expressed as a linear combination of the buckling modes,

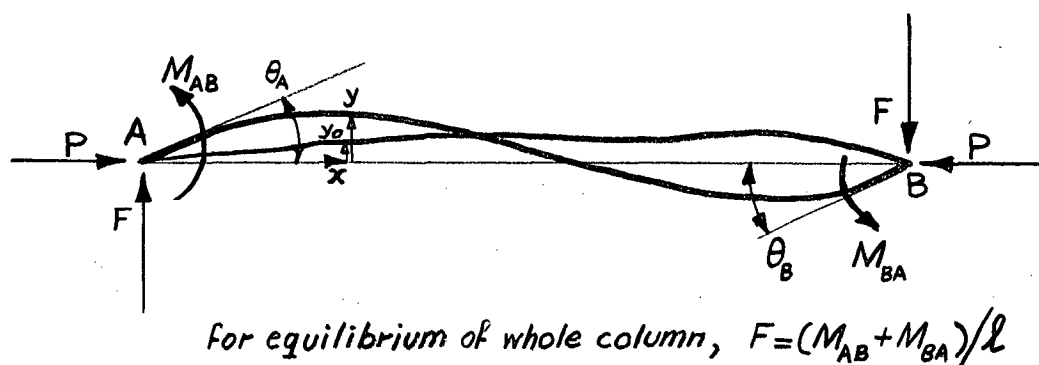


figure 1.12

which, in this case, is the infinite Fourier series

$$y_0 = \sum_{n=1}^{\infty} a_n \sin(n\pi x/l) \quad (1.47)$$

The deflected shape under load  $P$  is given by the function  $y = f(x)$ , yet to be determined. The bending moment at the point  $(x, y)$  on the centreline of the deflected column,  $M$  is given by

$$M = -M_{AB}[1-(x/l)] + M_{BA}(x/l) - Py \quad (1.48)$$

and for linearly elastic material behaviour we have

$$M = EI(d^2y/dx^2 - d^2y_0/dx^2) \quad (1.49)$$

The solution of the resulting differential equation is

$$y = A \cos(\sqrt{\rho} \pi x/l) + B \sin(\sqrt{\rho} \pi x/l) - (M_{AB}/P)(1-x/l) + M_{BA}(x/l) + \sum_{n=1}^{\infty} a_n \sin(n \pi x/l) / (1-P/n^2 Q) \quad (1.50)$$

where the constants  $A$  and  $B$  are determined from the boundary conditions that the deflection at the ends is zero, and the slopes are  $\theta_A, \theta_B$  respectively at  $A$  and  $B$ . This gives, after some manipulation,

$$A = M_{AB}/P$$

$$B = -A \cot 2\alpha - (M_{BA}/P) \operatorname{cosec} 2\alpha ; \alpha = \frac{1}{2} \pi \sqrt{\rho} ; \rho = P/Q$$

$$M_{AB} = (EI/l)(s\theta'_A + sc\theta'_B) \quad (1.51)$$

$$M_{BA} = (EI/l)(sc\theta'_A + s\theta'_B)$$

where

$$\theta'_A = \theta_A - \sum_{n=1}^{\infty} n \pi a_n / l(1-P/n^2 Q) ; \theta'_B = \theta_B - \sum_{n=1}^{\infty} (-1)^n n \pi a_n / l(1-P/n^2 Q) \quad (1.52)$$

It is seen that the expressions for the end moments are of the same form as for the initially straight column (see equations 1.19), the rotations being modified to include the effect of the initial curvature. At first sight it appears that the deflections are infinite at  $P = Q$ , but this is not so; the terms in  $a_1$ , that is  $n = 1$ , are

$$(s - sc)/(1-P/Q) \quad (1.53)$$

and the limit of this expression as  $P \rightarrow Q$  can be shown to be  $\pi^2/4$ . The summations in expressions (1.52) represent the initial end slopes corresponding to the various Fourier terms in (1.47), but magnified by the ratios  $n/(1-P/n^2 Q)$ .

In the analysis of a whole frame it is convenient to choose the Fourier coefficients in such a way that there is no initial lack of fit of angle between members at a joint, and that the initial joint

rotations are in the same ratio as at buckling. Two coefficients per member suffice for this, and the magnitude of the imperfections can be chosen as the average measured value for the frame, or as an arbitrary fraction of the member lengths. Alternatively, the initial imperfections need not be in exactly the same ratio as at buckling, but can be chosen to resemble the buckling mode. Once the initial crookedness pattern has been formulated the member end moments can be found from equations (1.51), and summation at the joints gives the joint moments. In general there are no applied joint moments, and the following matrix equation is obtained

$$\tilde{K} \cdot \tilde{\theta} = \tilde{\theta}_0 \quad (1.54)$$

where  $\tilde{K}$  is the symmetric stiffness matrix which is identical to that for a frame with no crookedness,  $\tilde{\theta}$  is the vector defining the joint rotations under load, and  $\tilde{\theta}_0$  is the vector defining the initial joint rotations, each component of which is magnified by the ratios appearing in equations (1.52). Equation (1.54) is solved for the joint rotations at various load values.

As an example, the behaviour of the equilateral triangular frame shown in figure (1.6) is predicted. The crookedness pattern chosen is that shown in figure (1.13), and the coefficients  $a_1$ ,  $a_2$ ,  $a_3$  are to be determined

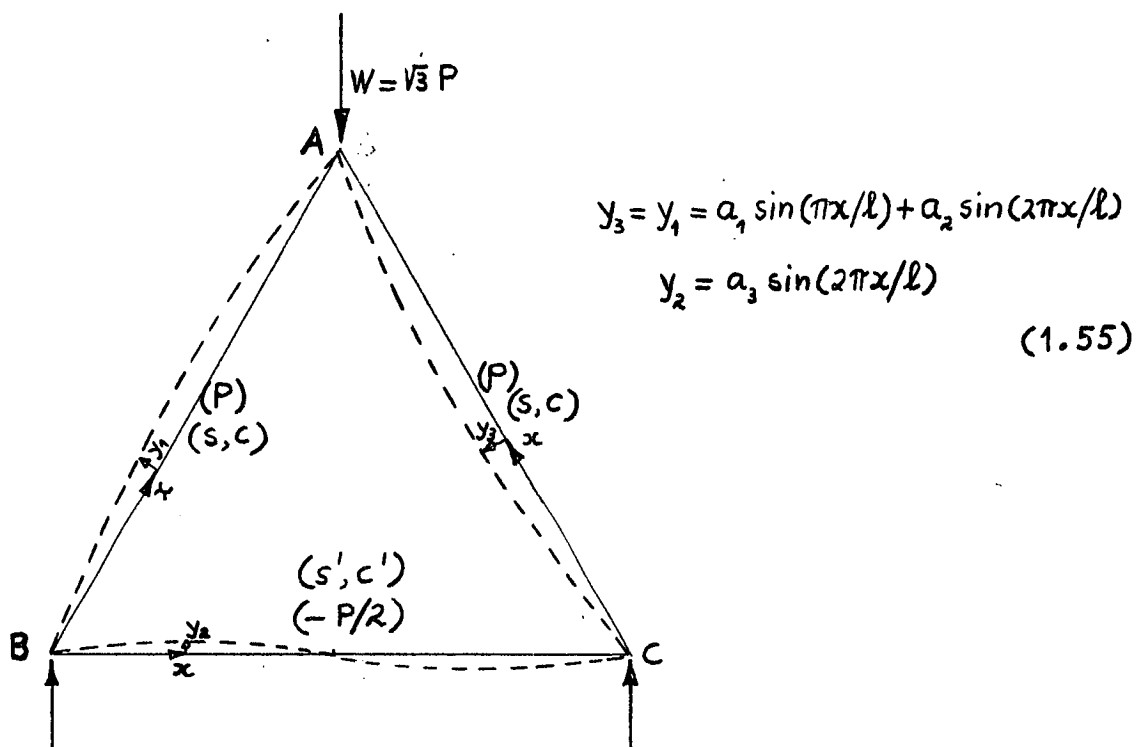


figure 1.13 - Crooked triangle



so that the initial joint rotations are in the same ratio as at buckling, that is

$$\begin{aligned}(\pi/l)(a_1 + 2a_2) &= -0.385\theta_0 \\(\pi/l)(2a_3) &= -0.385\theta_0 \\(\pi/l)(-a_1 + 2a_2) &= 1.00\theta_0\end{aligned}\tag{1.56}$$

Solution of these equations gives the Fourier coefficients as

$$\begin{aligned}\pi a_1/l &= -0.693\theta_0 \\2\pi a_2/l &= 0.308\theta_0 \\2\pi a_3/l &= -0.385\theta_0\end{aligned}\tag{1.57}$$

where  $\theta_0$  is the initial rotation at joint B.

When the frame carries a load  $W$  the member end moments are given by

$$\begin{aligned}M_{AB} &= k[s\theta'_A + sc\theta'_B] ; M_{BA} = k[sc\theta'_A + s\theta'_B] \\M_{AC} &= k[s'\theta''_A + s'c'\theta'_C] ; M_{CA} = k[s'c'\theta''_A + s'\theta'_C] \\M_{BC} &= k[s\theta'_B + sc\theta''_C] ; M_{CB} = k[sc\theta'_B + s\theta''_C]\end{aligned}\tag{1.58}$$

where

$$\begin{aligned}\theta'_A &= \theta_A - (\pi a_1/l)/(1-\rho) - (2\pi a_2/l)/(1-\rho/4) \\\theta''_A &= \theta_A - (2\pi a_3/l)/(1+\rho/8) \\\theta'_B &= \theta_B + (\pi a_1/l)/(1-\rho) - (2\pi a_2/l)/(1-\rho/4) \\\theta'_C &= \theta_C - (2\pi a_3/l)/(1+\rho/8) \\\theta''_C &= \theta_C - (\pi a_1/l)/(1-\rho) - (2\pi a_2/l)/(1-\rho/4) \\\rho &= Wl^2/\sqrt{3}\pi^2EI\end{aligned}\tag{1.59}$$

The values of  $a_1$ ,  $a_2$ ,  $a_3$  are given by equations (1.57). The end moments are summed at joints to obtain the joint moments, which are equated to zero and the resulting linear simultaneous equations are solved for the joint rotations; these results are plotted non-dimensionally in figure (1.14a) against the load parameter  $\rho$ . Superimposed on these graphs are the results obtained with a crookedness pattern of a half-sine wave in the compression members and a full sine wave in the tension member, that is

$$\begin{aligned}y_1 &= a_1 \sin(\pi x/l) \\y_2 &= a_2 \sin(2\pi x/l) ,\end{aligned}\tag{1.60}$$

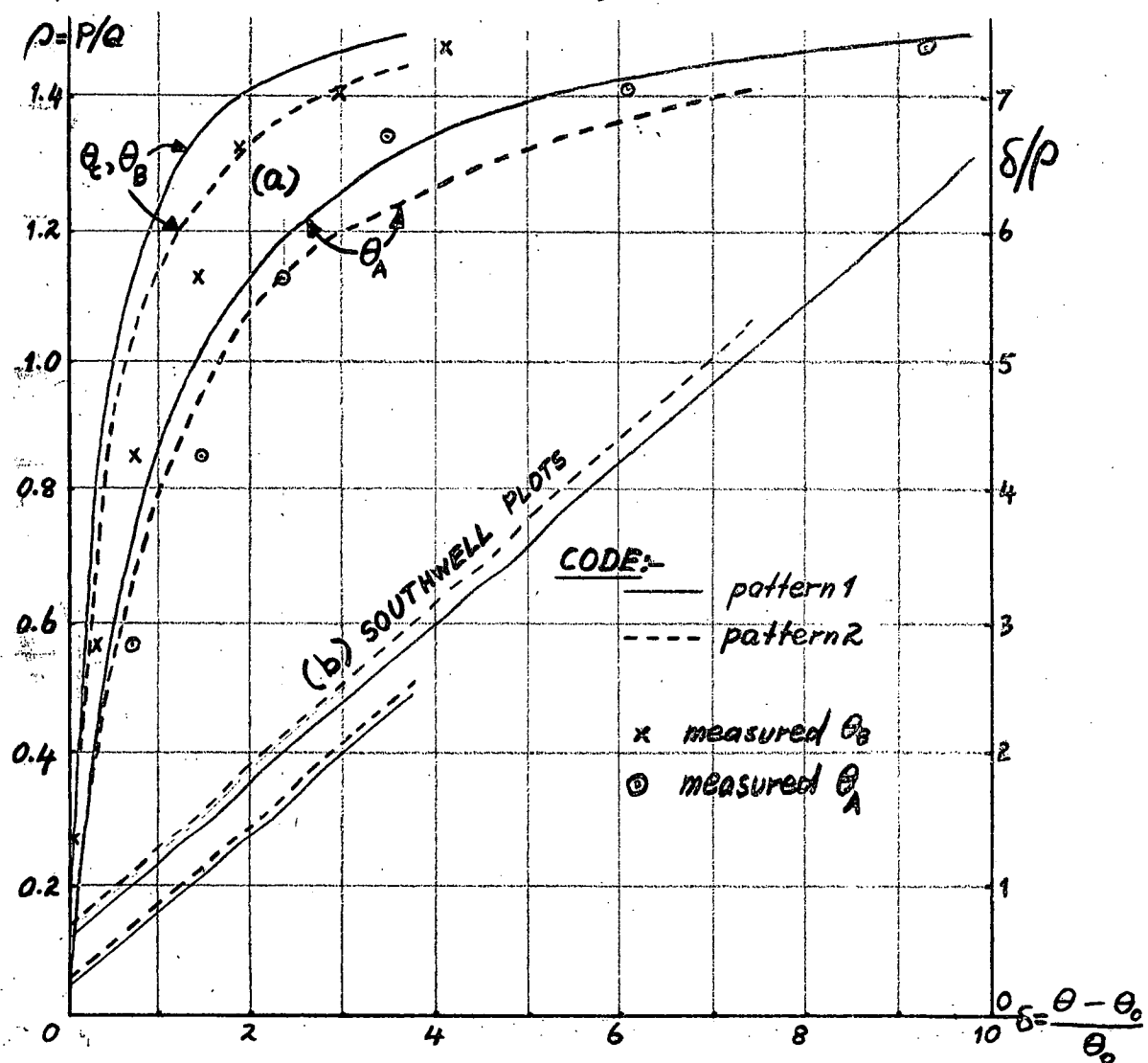


figure 1.14 - Calculated behaviour

with  $a_1 = 2a_2 = (1/\pi)\theta_0$  (referred to as pattern 2). As can be seen, the rotations in this case run away more rapidly than with the initial crookedness pattern 1; this is because the average crookedness is greater. The Southwell plots for the two sets of results are shown in figure (1.14b). These are almost linear, but show a slight tendency to a higher buckling mode at low loads indicating that the crookedness patterns contain a small portion of second and higher mode components. The two plots do not differ significantly from parallel, and from the inverse slopes the buckling load is obtained as

$$P_{cr} = 1.64$$

which is in excellent agreement with the result obtained in section (1.8). The intercepts give the first mode components of the initial rotations as

$$(\theta_A)_0 = 0.97\theta_0$$

$$(\theta_B)_0 = 0.36\theta_0$$

for pattern 1, and

$$(\theta_A)_0 = 1.13\theta_0$$

$$(\theta_B)_0 = 0.46\theta_0$$

for pattern 2

Comparing these values with the initial rotations, it follows that the first pattern was predominantly first mode, whereas for the second pattern there is little agreement. It must be remembered that these results are not very reliable because the intercepts are relatively small.

Figure (1.15) shows the measured behaviour of the rotations in a test on a model made from  $\frac{1}{2}$  in. x  $\frac{1}{8}$  in. mild steel strips 10.1 in. long. The central crookedness in the compression members was estimated to be  $\frac{1}{64}$  in. The flexural rigidity was determined by measurement of

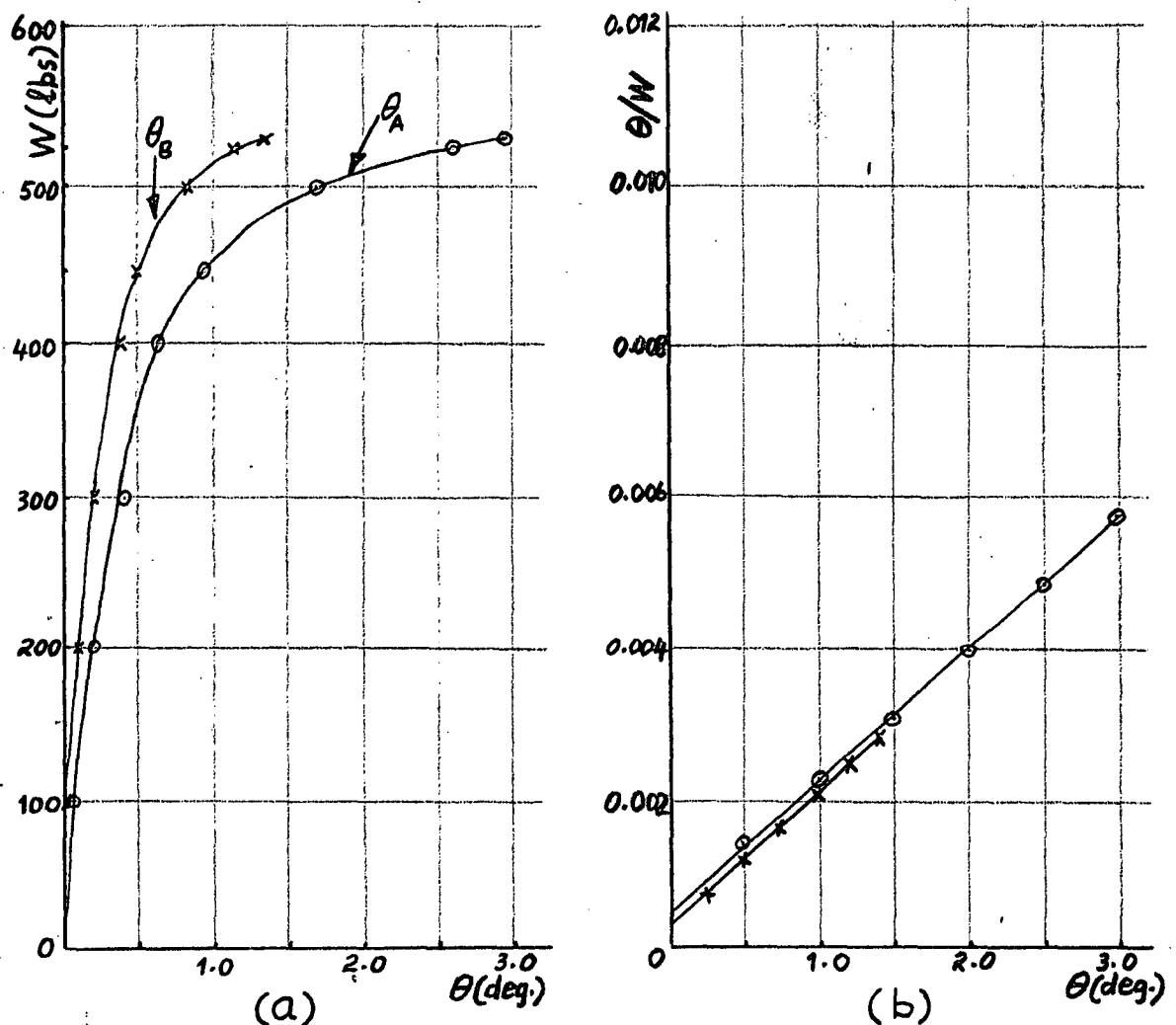


figure 1.15 - measured behaviour

deflections of a simply supported beam with central load, giving  $EI = 2220 \text{ lbs. in}^2$ ; the calculated buckling load is 605 lbs. Rotations were measured by shining a beam of light on to mirrors glued to the joints and observing the movement of the image on a scale. The Southwell plots on the measured rotations are shown in figure (1.15b), and are seen to be nearly linear indicating a buckling mode of 575 lbs. which is about 5% lower than the calculated value. From the intercepts of the Southwell plots the first mode components of the initial rotations are

$$(\theta_A)_0 = 0.29 \text{ degrees}$$

$$(\theta_B)_0 = 0.17 \text{ degrees}$$

which are comparable with the measured central crookedness of 1/64 in. and a half sine wave pattern giving

$$(\theta_A)_0 = -(\theta_B)_0 = 0.28 \text{ degrees.}$$

With this value for  $\theta_0$ , the measured behaviour is compared non-dimensionally with the calculated behaviour in figure (1.14), which indicates reasonable agreement. It must be borne in mind that the above comparisons are rather superficial, as there is no rigorous basis for the choice of  $\theta_0$  to plot rotations in terms of  $\theta_0$ ; that is, any of the curves could be arbitrarily scaled horizontally. However the Southwell plots and the load carrying capacity are governed primarily by the upper limits of the curves, and these are asymptotic to the horizontal, so that any scaling has a relatively small effect on the load to produce a given deformation.

It is also interesting to plot the variation of the ratio  $\theta_B/\theta_A$  against load. This is shown ~~in~~ in figure (1.16)\* for both crookedness patterns, and superimposed on these is the measured plot. As is to be expected, the predicted ratio  $\theta_B/\theta_A$  stays nearly constant at 0.385, the initial rotations being in the same ratio as at buckling. For crookedness pattern (2), consisting of a half sine wave in the compression members and a full sine wave in the tension member, the ratio varies almost linearly with load, but this linearity seems to be of little practical value, and it is most likely a coincidence. The measured variation is rather erratic at first, mainly because small errors in reading cause relatively large changes in the ratio. However, at loads approaching buckling, the ratio of the rotations tends to the value of 0.385 given by the calculated buckling mode.

#### 1.11 CONCLUDING REMARKS

From the example studied in the previous section it is seen that the method of calculating the deformations of a loaded initially crooked frame can also be used to estimate the elastic buckling loads of frames, by means of a Southwell plot on calculated rotations. This technique was first introduced by Lundquist (reference 17), who used moment distribution to calculate the rotation of some joint. However, the behaviour of a real frame is such that the buckling load is never reached in practice, so that the buckling load of a frame is not as

---

\* see p. 42 for figure (1.16).

important in this context as say, the load to cause first yield. These loads may differ widely, depending on the overall slenderness of the frame. Most frames have low slenderness ratios,  $l/r$  in the vicinity of 100, and the load to cause first yield plays a dominant role. The yield load depends on the magnitude of the deformations, which in turn depend mainly on the magnitude of the initial imperfections. For this reason it is a pity that in the literature so much attention has been paid to the evaluation of buckling loads, and that buckling modes are usually treated as secondary. It is the author's opinion that the buckling mode is of primary interest, since once this is known an analysis such as in the previous section is readily performed, and from this the engineer can extract the necessary information for design.

However, as mentioned in section (1.5), a detailed analysis of the stability of a frame and of its behaviour under working loads for design purposes may not be warranted from the point of view of cost.

If the frame is of minor importance or of the "one-off type", it would certainly be designed on the individual member basis, but if the frame is major, or if there is to be a large number of them, a more detailed investigation should be carried out, and this will probably reward itself. Such a design can be based on the techniques described in the previous section, and the author suggests the following steps:

- (a) Design the frame on the basis of buckling of individual members, using code recommended effective length ratios, crookedness parameter, and a permissible stress formula such as Perry-Robertson.
- (b) Estimate, by one of the methods outlined in section (1.7), the fundamental buckling load and mode of the preliminary design.
- (c) Impose an unfavourable crookedness pattern, for example a pattern resembling the fundamental buckling mode, and determine the behaviour of the frame up to say, first yield. This appears to be the most difficult step at this stage as there is insufficient data on which to base the selection of an overall crookedness parameter to describe the imperfections of the frame. However, resort can always be made to single column data.
- (d) Calculate the factor of safety against yield. A refinement of this step is to calculate the factor of safety against total collapse, but this involves an analysis of the behaviour of the frame in the elasto-plastic region. This region is not easy to handle, and since the reserve of strength above first yield is usually small, the additional computation is not considered worthwhile, except for stiff frames.

(e) Modify the preliminary design, by comparing the calculated factor of safety and the design factor of safety. Again, the latter may have to be chosen from single column data and recommendations.

Steps (b), to (c) are then repeated until satisfactory agreement is obtained. Alternatively, the preliminary design can be modified after step (b). From the buckling load and mode of the preliminary design, the effective lengths of the members are easily calculated, and these can then be used to obtain the modified member sizes.

A design along these lines is by no means to be classified as a better design, but it is felt that it is on a more realistic basis; that is, more attention is paid to the behaviour of the frame as a whole rather than the behaviour of individual members. In this context the technique described is merely the next step in frame design.

Finally, it must be stressed again that the mathematical models presented in this chapter describe only approximately the frame behaviour. Drastic simplifications were made to formulate them, and among the effects not taken into account are non-linearity, large deformations, secondary bending moments, initial stresses and yielding. All these affect the behaviour of the frame, and the mathematical model needs to be considerably refined to include these effects. At present such a complete study would be too difficult, and since the additional effects are generally small, a knowledge of the buckling load and mode, together with a measure of the overall crookedness of a frame, provides a reasonable picture of the frame behaviour.

#### ADDITIONAL NOTES FOR CHAPTER ONE

Section 1.4: The numerical figures in the Perry formula are due to Professor Andrew Robertson who, as a result of exhaustive tests, showed that the Perry formula works well for pin-ended columns for an average value of  $n$  of  $0.001 \text{ l/r}$ , and he suggested the lower limit of  $0.003 \text{ l/r}$  for design purposes. These figures, together with a factor of safety of 2.36, were subsequently recommended by the steel structures research committee (reference 18).

Sections 1.6, 1.7: The history of the development of stability analysis for frames has been well set out by Bleich (reference 19), and a large part of these sections is based on his book.

Lundquist appears to have been the first person to use moment distribution in stability analyses by what is now called "Lundquist's series criterion". In essence this method is the same as the moment distribution convergence criterion. Hoff proved, by a consideration of the total potential energy of the system, that convergence of the moment distribution is a necessary and sufficient condition for stability.

#### REFERENCES

1. N.J. Hoff, "The Analysis of Structures", Wiley (1956); p 294f
2. A.S. Niles and J.S. Newell, "Airplane Structures" vol, 2, Wiley (1948); pp 72, 107
3. R.K. Livesley and D.B. Chandler, "Stability Functions for Structural Frameworks", Manchester University Press (1956)
4. M.S. Gregory, "The Buckling of Structures" Ph.D. Thesis, University of Tasmania (1960); p 32
5. W. Merchant, "The Failure Load of Rigid Jointed Frameworks as influenced by Stability", The Structural Engineer (July 1954).
6. M.S. Gregory, "Elastic Instability", Spon (1966).
7. S.J. McMin, "Matrices for Structural Analysis", Spon (1962).
8. S.J. McMin, "The Determination of Critical Loads of Plane Frames", The Structural Engineer (July 1961).
9. J.W.S. Rayleigh, "The Theory of Sound" vol I, Dover (1945); see, for example p. 112.
10. G. Temple and W.G. Bickley, "Rayleigh's Principle", O.U.P. (1933); p 95f
11. A. Bolton, "A Quick Approximation to the Critical Load of Rigidly Jointed Frames", The Structural Engineer (March 1955).
12. H. Waters, "Direct Approximation to the Critical Loads of Rigidly Jointed Plane Structures", Civil Engineering and Public Works Review (February 1964).
13. H.N. Allen, "The Estimation of the Critical Loads of Certain Frameworks", The Structural Engineer (April 1957).
14. R.V. Southwell, "On the Analysis of Experimental Observations on Problems of Elastic Stability", Proc. Roy. Soc. A135, 601 (1932)
15. M.S. Gregory, "The Use of Measured Strains to obtain Critical Loads", Civil Engineering and Public Works Review (Jan. 1960).
16. S.T. Ariaratnam, "The Southwell Method for Predicting Critical Loads of Elastic Structures", Quarterly Jnl. of Mech. and App. Maths. vol XIV (1961); p 137
17. E.E. Lundquist, "Stability of Structural Members under Axial Load", N.A.C.A. Tech. note No. 617 (Oct. 1937).

18. A.J.S. Pippard and J.F. Baker, "The Analysis of Engineering Structures", Edward Arnold & Co. (1936).
19. F. Bleich, "Buckling Strength of Metal Structures", McGraw-Hill Book Company Inc. (1952); p 193f.

Additional references not specifically quoted:

- (a) E.E. Lundquist, "Principles of Moment Distribution applied to Stability of Structural Members", Proc. 5th International Congress of Applied Mechanics (1938). "A Method for Estimating the Critical Buckling Load for Structural Members", N.A.C.A. Tech. note No. 717 (July 1939)
- (b) N.J. Hoff, "Stable and Unstable Equilibrium of Plane Frameworks", Journal of the Aeronautical Sciences, vol 8 (1940- 1941) . "Stress Analysis of Aircraft Frameworks", Jnl. Roy. Aer. Soc. vol. 45 (1941). "The Proportioning of Aircraft Frameworks", Journal of the Aeronautical Sciences, vol 8 (1940-1941).
- (c) L.H. Donnell, "The Problem of Elastic Stability", Part I of a symposium "Survey of problems of thin-walled structures" of the Aeronautics Division of the A.S.C.E., (June 1932).
- (d) M.S. Gregory, "Framed Structures: the Instability Problem", Proc. I.C.E. (London) Vol 35 pp 451-473; Nov. 1966.

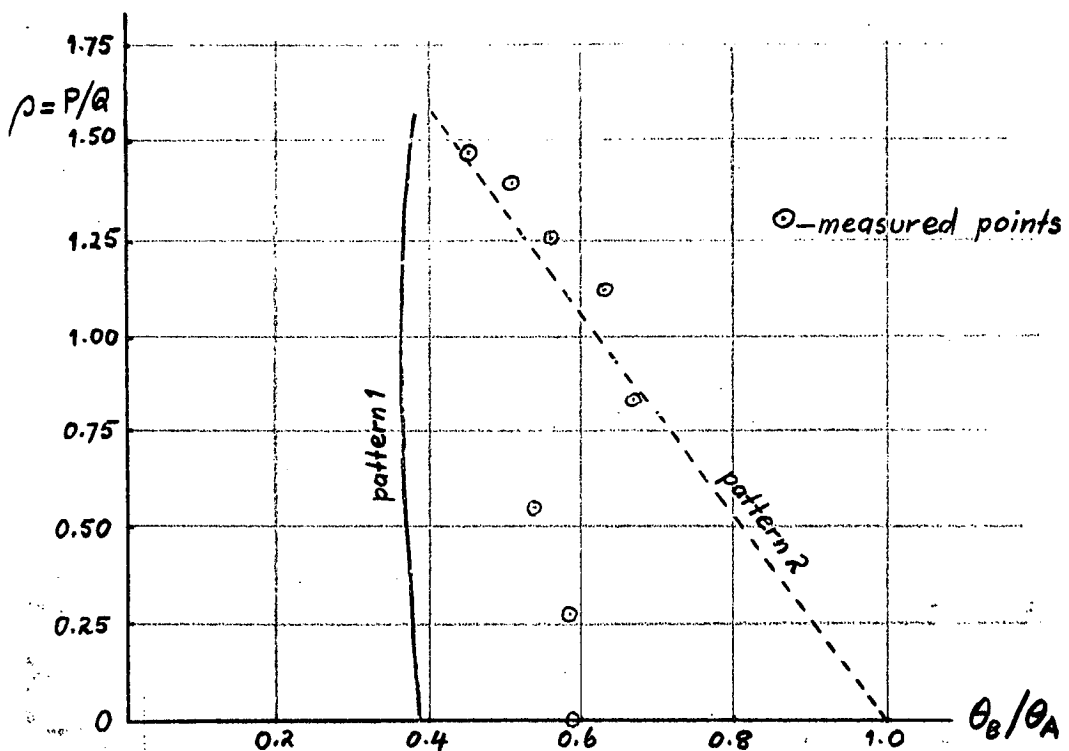


figure 1.16 - Variation of  $\theta_B/\theta_A$



## CHAPTER TWO

### ENERGY METHODS

#### 2.1 INTRODUCTION

Energy methods have provided a useful tool for solving certain problems in structural analysis and related fields. Their use dates back to the days of Castigliano (1873), who developed what is now known as the principle of least work, for the analysis of statically indeterminate frameworks. Since then the use of energy principles has covered a wider field, and has been considerably consolidated.

This chapter begins with a close examination of the fundamental ideas behind energy methods generally, in order to obtain a better appreciation of their use and limitations. These elementary principles are demonstrated with the aid of a simple inelastic string model loaded with deadweights, and it is shown that the two distinct energy approaches, strain energy and complementary energy, are merely alternative techniques for deriving equations of statics and equations of geometrical compatibility respectively. Once this is established, more difficult problems can be attacked, continually keeping in mind the limitation of the equivalence just mentioned.

Energy methods give no information not obtainable directly, either from statical or compatibility considerations, but their power lies in the ease with which approximate solutions can be found. In this chapter approximate solutions are derived for some standard beam problems, leading up to an iterative solution of large frames, such as, for example, multi-bay, multi-storey building frames.

#### 2.2 THE TWO TYPES OF ENERGY

Consider a force  $P$  which moves through a distance  $\delta$  in the direction of the force; the variation of  $P$  with  $\delta$  is shown graphically in figure (2.1). The strain energy,  $U$  is defined as the area under the curve, that is

$$U = \int_0^{\delta} P \, d\delta \quad (2.1)$$

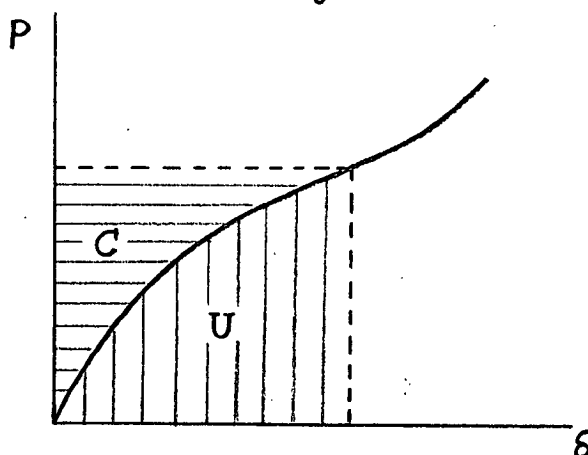


figure 2.1

whereas the complementary energy is defined as the area to the left of the curve, that is

$$C = \int_0^P \delta dP \quad (2.2)$$

These areas are shown shaded in the figure. The relation between the force  $P$  and its displacement  $\delta$  can be quite arbitrary, and the energies exist so long as the integrations can be performed.

In the reverse process we define the existence of the two energy functions  $U$  and  $C$ , and by differentiation we see that

$$dU/d\delta = P \quad (2.3)$$

$$dC/dP = \delta \quad (2.4)$$

That is, differentiation of strain (complementary) energy with respect to the displacement (force) gives the corresponding force (displacement). In other words there exists a duality between the two processes. The same principle applies to any "generalized force" or "action" and its corresponding "generalized displacement", for example moment-rotation, stress-strain.

From figure (2.1) it is readily seen that for a linear relation between the force  $P$  and its displacement  $\delta$ , the strain and complementary energies are equal, and can be interchanged at will. This has caused some confusion in the past.

In the case of a system of generalized forces, the separate energies of the individual forces are summed over the whole system, and differentiation of the total strain energy with respect to some generalized displacement gives the corresponding generalized force, or vice-versa when complementary energy is used. However, in these cases it becomes necessary to define the dependence or otherwise of the forces and displacements involved in the energy integral, as will be demonstrated in the following section.

### 2.3 ENERGY ANALYSIS OF A STRING MODEL

In order to examine the basic principles underlying the use of energy methods in structural analysis, consider the system shown in figure (2.2). This particular problem is treated by Southwell (reference 1), who bases his analysis on small deflection theory, but it is shown here that this restriction is not necessary. Essentially the system consists of a vertical string  $ABC$  supporting a weight  $W$ . This string is displaced by a horizontal string  $BD$ , passed over a pulley to support another weight  $w$ . As the displacements vary, the latter string departs from its horizontal position, but in the experimental work carried out on this model the string was always kept horizontal by means of a slip knot at  $B$ .

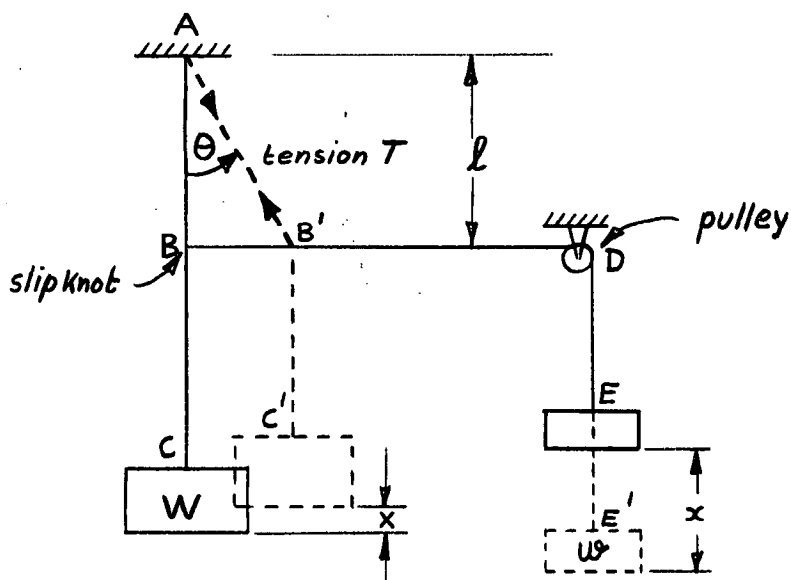


figure 2.2 - inelastic string model

For simplicity in the analysis of this system, the string is assumed to be inelastic; under these conditions the displaced shape is wholly defined in terms of a single parameter, either  $x$ , the vertical displacement of weight  $w$ , or  $X$ , the vertical displacement of the weight  $W$ , or  $\theta$ , the inclination of the initially vertical string  $AB$ .

(a) Analysis by statics

Let  $T$  be the tension in part  $AB'$  of the displaced string. Then for equilibrium of the slip knot, we have

$$\sum H = 0 = -T \sin \theta + w \quad (2.5)$$

$$\sum V = 0 = -T \cos \theta + W \quad (2.6)$$

The solution of these equations for the angle  $\theta$  is obviously

$$\tan \theta = w/W \quad (2.7)$$

The displacement of the weight  $w$ ,  $x$  is given by

$$x = l \tan \theta = (l/W)w \quad (2.8)$$

Alternatively, the unknown tension  $T$  can be eliminated directly by examining the equilibrium of the displaced string  $AB'C'$ . For the resultant moment about  $A$ , of all the forces acting on this string, to be zero, we must have

$$\sum M = 0 = -Wx + wl \quad (2.9)$$

which gives the same result as before. If the weight  $W$ , supported by the vertical string  $ABC$ , is kept constant, then it follows that the displacement of the weight  $w$ ,  $x$  is linearly related to  $w$ , and it is seen from the above analysis that this linearity is independent of the magnitude of the displacement, provided that the string  $BD$  is kept horizontal. Southwell analyses the system by treating the vertical string as being displaced by horizontal forces applied at fixed points along the string, in which case the vertical distance varies, so that the linear relation between  $x$  and  $w$  holds only for small displacements.

(b) Strain energy analysis

For the purpose of this analysis, consider firstly the potential energy of the weights  $W$  and  $w$ , and define the total strain energy as

$$U = \int_0^X W dX + \int_0^x w dx \quad (2.10)$$

There is no need in this problem to make a distinction between internal and external strain energy, so long as the displacements  $X$  and  $x$  are measured in the same direction as their corresponding forces  $W$  and  $w$ . For small variations

$\delta X$ ,  $\delta x$  of the displacements from their equilibrium values, the variation in total strain energy is

$$\delta U = W(\delta X) + w(\delta x) \quad (2.11)$$

with the restriction that the variations are to be carried out subject to the requirements of geometrical compatibility of the variations of displacements. From figure (2.3) it is seen that these requirements are

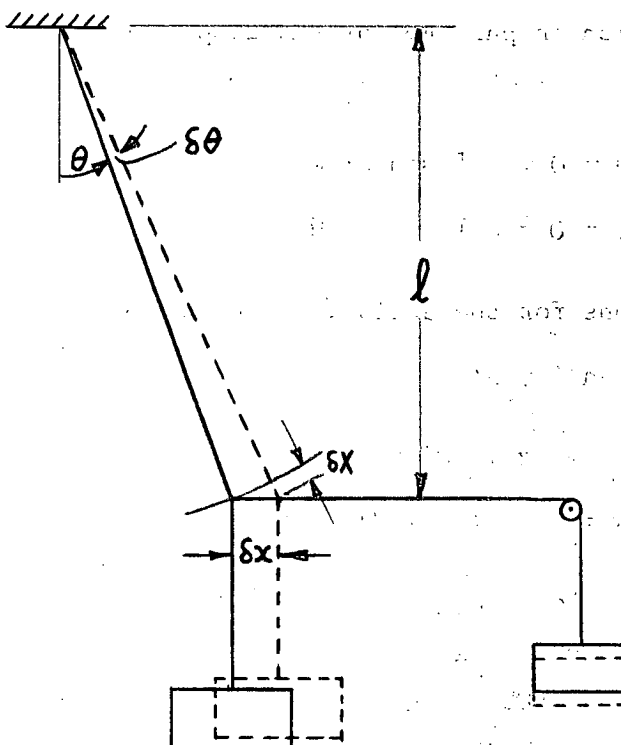


figure 2.3

$$\delta x = l \sec^2 \theta (\delta \theta) \quad ; \quad \delta X = - l \sec \theta \tan \theta (\delta \theta) \quad (2.12)$$

the minus sign arises because  $\delta X$  is opposite in direction to that of its corresponding force  $W$ . Alternatively we may write

$$\delta X = -(\delta x) \sin \theta \quad (2.13)$$

By equation (2.11), the variation in strain energy in terms of  $x$  is

$$\delta U = - W(\delta x) \sin \theta + w(\delta x) \quad (2.14)$$

In the limit as  $\delta x$  approaches zero, this can be written

$$\partial U / \partial x = - W \sin \theta + w \quad (2.15)$$

[A complete derivative could be used in this case, because the strain energy can be expressed in terms of one parameter  $x$ , the single degree of freedom of the system]. For the strain energy to be a minimum, its derivative vanishes, that is

$$- W \sin \theta + w = 0 \quad (2.16)$$

Following the argument in section (2.2) of this chapter, this equation should represent the equation of equilibrium in the direction of differentiation, in this case in the horizontal direction. Comparison with the exact equation (2.5), shows that the equivalence is valid only if  $T = W$ , which is approximately true for small displacements. Similar expressions can be derived by differentiation along different paths; for example, the variation in strain energy in terms of  $\delta \theta$  is obtained from equations (2.11) and (2.12) as

$$\delta U = - W l \sec \theta \tan \theta (\delta \theta) + w l \sec^2 \theta (\delta \theta) \quad (2.17)$$

whence we obtain, in the limit

$$\partial U / \partial \theta = - W l \sec \theta \tan \theta + w l \sec^2 \theta \quad (2.18)$$

When equated to zero, this leads to an approximate equation of equilibrium comparable to the moment equation (2.9) of the exact analysis. In this case the degree of approximation is found to be  $\sin \theta \approx \tan \theta$ , which is valid for small displacements. It is also interesting to derive the results from the 'conservation of energy' equation. In this example the work done by the variable weight  $w$  as it moves down a distance  $x$  is  $\frac{1}{2}wx$ , and the energy required to raise the constant weight  $W$  through a height  $X$  is  $WX$ , and the displacements are given by

$$x = l \tan \theta \quad ; \quad X = l(\sec \theta - 1) \quad (2.19)$$

Conservation of energy requires

$$\frac{1}{2}wl \tan \theta = Wl(\sec \theta - 1) \quad (2.20)$$

This equation, when solved for the angle  $\theta$ , reduces to

$$\tan (\theta/2) = \frac{1}{2}(w/W) \quad \text{or} \quad \tan \theta = (w/W)[1 + \frac{1}{4}(w/W)^2] \quad (2.21)$$

Again this is a correct result when the displacements are small, but for large displacements this expression differs from those obtained from minimum strain energy equations.

In all the above arguments the discrepancies are obvious; no account has been taken of the work done in sliding the knot to keep the string BD horizontal. In order to improve the strain energy analysis, this work should be included, and we are thus led to consider the following strain energy expression

$$U = \int_0^x WdX + \int_0^x wdx + \int_0^t Tdt \quad (2.22)$$

where  $t$  is the displacement corresponding to the tension  $T$  in the inclined string. With this definition it is convenient to visualise the system as three forces concurrent at the point B, as shown in figure (2.4a). The equations of equilibrium relating these three forces can be derived from minimum strain

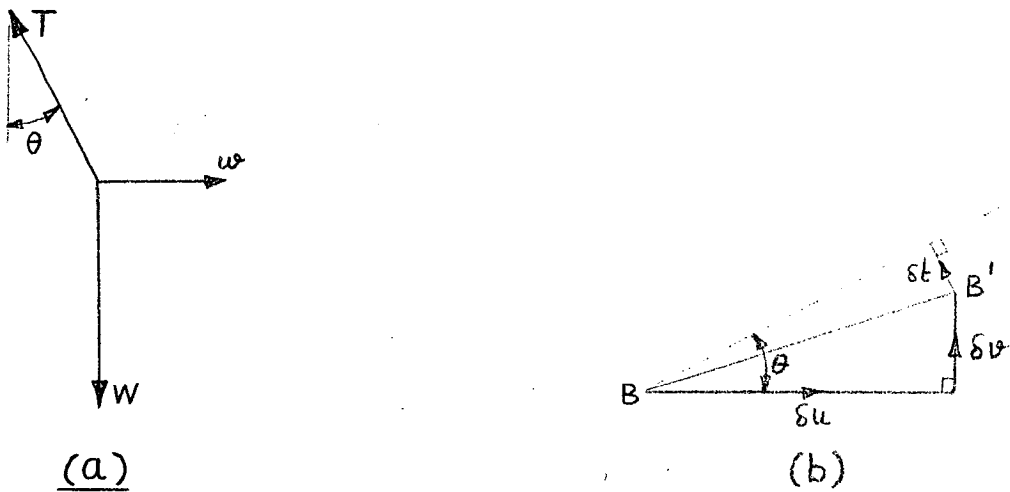


figure 2.4

energy equations, provided that variations in the strain energy are carried out subject to the restricting equations of geometrical compatibility. Since B is a point in a plane it has two degrees of freedom of movement, so that a small displacement of B from its equilibrium position can be expressed in terms of two independent parameters, such as  $\delta u$  and  $\delta v$  shown in figure (2.4b).

The variations in the displacements  $x$ ,  $X$  and  $t$  of the respective forces  $w$ ,  $W$  and  $T$  are obtained from this figure as

$$\delta x = \delta u \quad ; \quad \delta X = -\delta v \quad ; \quad \delta t = -(\delta u) \sin \theta + (\delta v) \cos \theta \quad (2.23)$$

The variation in strain energy is

$$\delta U = W(\delta X) + w(\delta x) + T(\delta t) \quad (2.24)$$

Substitution of the restricting equations (2.23) gives

$$\delta U = -W(\delta v) + w(\delta u) - T \sin \theta (\delta u) + T \cos \theta (\delta v) \quad (2.25)$$

From this expression the equation of equilibrium in any direction can be obtained by suitably choosing  $\delta u$  and  $\delta v$ , and passing to the limit to get derivatives of  $U$ , which are then equated to zero. For example, if  $\delta v$  is put zero we obtain

$$\partial U / \partial u = w - T \sin \theta = 0 \quad (2.26)$$

which is the correct equation of equilibrium in the horizontal direction. Similarly, to derive the equation of equilibrium in the direction of the force  $T$ , we impose a displacement in that direction by putting

$$\delta u = -(\delta t) \sin \theta \quad ; \quad \delta v = (\delta t) \cos \theta \quad (2.27)$$

This gives

$$\partial U / \partial t = -w \sin \theta - W \cos \theta + T \sin^2 \theta + T \cos^2 \theta = 0$$

which is seen to be the correct equation of equilibrium in the direction of the inclined string.

This method of strain energy of forces acting at a point always yields correct equations of equilibrium. However, the problem as posed required that the string BD remained horizontal. One way to visualize this in the above mathematical model is by first allowing B to rise, and then returning it to its original horizontal level by moving the point of support A in the direction of the inclined string AB. It is seen that the system has thus been made conservative. Stilwell (reference 2) proposes an alternative conservative system by introducing a small pulley at the knot, and applying a moment to the pulley to keep the string horizontal; the work done on the pulley as it rotates is included in the strain energy expression.

### (c) Complementary energy analysis

With reference to figure (2.4), the complementary energy is defined as

$$C = \int_0^w X dW + \int_0^w x dw + \int_0^T t dT \quad (2.28)$$

Variations in complementary energy are to be carried out subject to the restricting equations of equilibrium. In this case there are three forces  $w$ ,  $W$  and  $T$ , of which  $w$  and  $W$  are independent; that is, a change in either does not affect the other. The third force  $T$  is not independent, but is related to  $w$  and  $W$  by the equations of equilibrium, and the complementary energy is to be differentiated subject to these restrictions. Taking, for example, the derivative with respect to the variable weight  $w$ , we find

$$\partial C / \partial w = x + X(\partial W / \partial w) + t(\partial T / \partial w) \quad (2.29)$$

Since  $w$  and  $W$  are independent,  $\partial W / \partial w = 0$ , and from equation (2.5) we find

$$\partial T / \partial w = \operatorname{cosec} \theta \quad (2.30)$$

whence we obtain

$$\partial C / \partial w = x + t \operatorname{cosec} \theta = 0 \quad (2.31)$$

or

$$t = -x \sin \theta \quad (2.32)$$

This is seen to be the correct equation of geometrical compatibility of the displacements. In the same manner we find

$$t = -X \cos \theta \quad (2.33)$$

which is also a correct result. Figure (2.5) shows the displacements  $x$ ,  $X$  and  $t$ , the arrows indicating their positive directions, which are those of the corresponding forces.

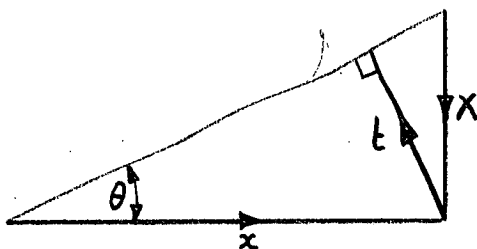


figure 2.5

\* \* \* \* \*

Although the treatment given in this section is rather brief, the following important principles emerge clearly:



- (i) Variations in strain energy, carried out subject to the requirements of geometrical compatibility, when equated to zero, are equivalent to equations of equilibrium.
- (ii) Variations in complementary energy, carried out subject to the requirements of statical equilibrium, when equated to zero, are equivalent to equations of geometrical compatibility.

Care must be taken in both cases to define the independent parameters, and also to ensure the inclusion of those terms in the relevant energy expressions, which are to appear in the equations of equilibrium (or compatibility) to be derived from these expressions. In some problems erroneous results can be obtained from what appear to be valid energy expressions. A good example of this has been given by Oliver (reference 3), where the complementary energy method applied to the pin-ended column gives the shortening twice its correct value. In general the only way to ensure the validity of an energy expression is to identify the equation of equilibrium (strain energy), or of compatibility (complementary energy), which it replaces.

#### 2.4 A STRAIN ENERGY METHOD APPLIED TO BEAMS

In this section the basic ideas, developed on an inelastic string model, are extended to include elastic problems, such as bending of beams. The usual small deflection theory of beams neglects the effect of shear on the deflections; the same simplification is made in this section in evaluating the strain energy of deformed beams. Consider a small element of length  $ds$  of the beam, as shown in figure 2.6. The

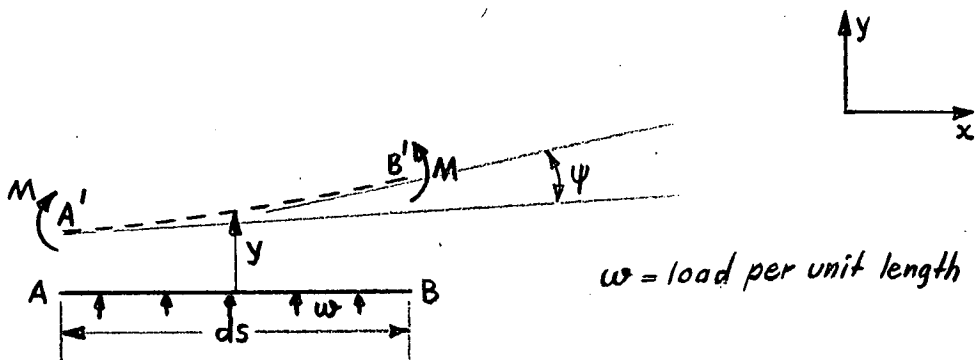


figure 2.6 - beam element

load on the beam is assumed to be expressible as

$$w = f(x) \quad (2.34)$$

where  $x$  measures the position along the beam, and the positive direction of the load  $w$  is the same as the direction of the deflection, which in this case is taken according to the usual cartesian coordinate system. With this sign convention, bending moments are taken as positive when they produce a positive curvature, that is when  $d^2y/dx^2 > 0$ . After bending, the element AB takes up the new position A'B', and if axial load and shear are neglected, the total strain energy of the element is given by

$$dU = \int_0^\psi M d\psi - \int_0^y w ds \quad (2.35)$$

where  $\psi$  is the angle through which the bending moment  $M$  rotates, that is is the change in slope over the length  $ds$  of the beam. In the inelastic string problem there was no need to define internal and external strain energies as separate quantities. However, in the present treatment this distinction must be made; thus, in the above expression for the total strain energy, the first term represents the internal strain energy, that is the energy required to deform the element  $ds$ , while the second term is the work done by the load  $w$ , herein called the external strain energy. In terms of the curvature  $\phi$  of the element, we have

$$\psi = \phi ds \quad (2.36)$$

whence it follows that

$$dU = \int_0^\phi M d\phi ds - \int_0^y w dy ds \quad (2.37)$$

Integration over the whole beam gives the total strain energy as

$$U = \int_0^l \left( \int_0^\phi M d\phi - \int_0^y w dy \right) ds \quad (2.38)$$

where  $l$  denotes the length of the beam. In the case of a linear moment-curvature relation defined by

$$M = EI\phi \quad , \quad (2.39)$$

together with the usual approximation for the curvature,  $\phi = d^2y/dx^2$ , this expression reduces to

$$U = \int_0^l \left[ \frac{1}{2} EI (d^2y/dx^2)^2 - \int_0^y w dy \right] ds \quad (2.40)$$

It is interesting to apply the calculus of variations to this strain energy expression in order to establish its validity. Assuming  $y = y(x)$  is the correct deformed shape of the beam in its equilibrium position, consider another shape close to this. That is, define a variation in the deformed shape such that

$$y + \delta y = y + \alpha \eta \quad (2.41)$$

where  $\eta$  is a function similar to  $y$ , and  $\alpha$  is a parameter which can be made as small as desired. Using equation (2.40), the variation in strain

energy is given by

$$U + \delta U = \int_0^l \left[ \frac{1}{2} EI (d^2 y / dx^2 + \alpha d^2 \eta / dx^2)^2 - \int_0^{y+\alpha\eta} w dy \right] ds \quad (2.42)$$

Expanding this expression, and neglecting the term in  $\alpha^2$ , it is found that

$$\delta U = \int_0^l [\alpha EI (d^2 y / dx^2) (d^2 \eta / dx^2) - \alpha w \eta] ds \quad (2.43)$$

The first term, when integrated twice by parts, reduces to

$$\int_0^l \alpha EI (d^4 y / dx^4) ds = [\alpha EI \eta (d^3 y / dx^3)]_0^l + [\alpha EI (d\eta / dx) (d^2 y / dx^2)]_0^l \quad (2.44)$$

The two expressions to be evaluated at the limits of integration, 0 and l, can be made to vanish by suitably restricting the type of variation as defined by  $\eta$ . When the variation is chosen so that the deformed shape  $(y + \alpha \eta)$ , and its first derivative, are correct at the boundary, then  $\eta$  and  $(d\eta / dx)$  both vanish at the boundaries, and we are left with

$$\delta U = \alpha \int_0^l [EI (d^4 y / dx^4) - w] ds \quad (2.45)$$

In the limit, as  $\alpha$  tends to zero, this can be written as

$$\partial U / \partial \alpha = \int_0^l \eta [EI (d^4 y / dx^4) - w] ds \quad (2.46)$$

For the total strain energy to be a minimum, this expression must vanish. The only way in which this can be achieved for all possible types of variations (provided  $\eta$  and its first derivative are zero at the boundaries), is for the expression in brackets to be zero at every point along the beam. That is, the strain energy is minimum when

$$EI (d^4 y / dx^4) - w = 0 \quad (2.47)$$

which is seen to be a valid equation of equilibrium, identical to that usually developed from elementary principles in small deflection theory.

When the load consists of one or more point loads, the double integral expression for the work done by the loads is replaced by the summation of integrals

$$\sum_{\text{loads}} \left[ \int_0^{y_i} W_i dy_i \right] \quad (2.48)$$

where  $y_i$  denotes the deflection of the load  $W_i$ , and the summation is applied over all the loads.

Having established the validity of the above strain energy expression, it may be used to solve beam problems, keeping in mind of course that the solution is of necessity limited to the same extent as the usual small deflection theory. One of the powers of energy methods is the ease

with which approximate solutions can be found, and this is demonstrated by analysing the deflected shapes of some simple beam problems commonly encountered.

(a) Simply supported beam

(i) Central concentrated load

Consider a simply supported beam of uniform cross section  $EI$ , span  $l$ , carrying a concentrated load  $W$  at the centre of the span. Obviously the deflected shape is symmetrical about the centre of the span, so that any approximate function to be used in the strain energy should at least satisfy this requirement. In the variational treatment given above, it was stated that the approximate function and its first derivative should be "correct" at the boundaries, that is at the simply supported ends in this problem. However, returning to equation (2.44), it is seen that the expressions at the limits of integration also involve a term  $EI(d^2y/dx^2)$ , which is the bending moment at the ends. At a simply supported, or at a free end, this is zero, so that  $(d\eta/dx)$  need not be zero there.

The simplest approximate shape would be

$$y = a_1 \sin(\pi x/l) \quad (2.49)$$

with the origin at one of the simple supports. The parameter  $a_1$  is the deflection at the centre, and is to be chosen to make the total strain energy a minimum. The total strain energy is evaluated from equation (2.40) as

$$U = \frac{1}{4}a_1^2 \pi^4 EI/l^3 - \int_0^l W da_1 \quad (2.50)$$

Minimizing this with respect to  $a_1$ , we find

$$\partial U / \partial a_1 = 0 = \frac{1}{2} a_1 \pi^4 EI/l^3 - W \quad (2.51)$$

This expression gives as an estimate for the central deflection

$$a_1 = 2Wl^3/\pi^4 EI \quad (2.52)$$

which differs by only about 2% from the more exact result of  $Wl^3/48EI$ .

Thus in this case minimum energy gives the maximum deflection sufficiently accurate for practical purposes. The correct deflected shape is given by

$$y = a_1 [3(x/l) - 4(x/l)^3] \quad ; \quad 0 \leq x \leq l/2 \quad (2.53)$$

Using this in the strain energy equation, we naturally find the correct value for  $a_1$ . The approximate and exact functions are compared graphically in figure (2.7), and are seen to be very little different. Up to about  $1/3$  span the approximate deflection is greater than the exact function, and

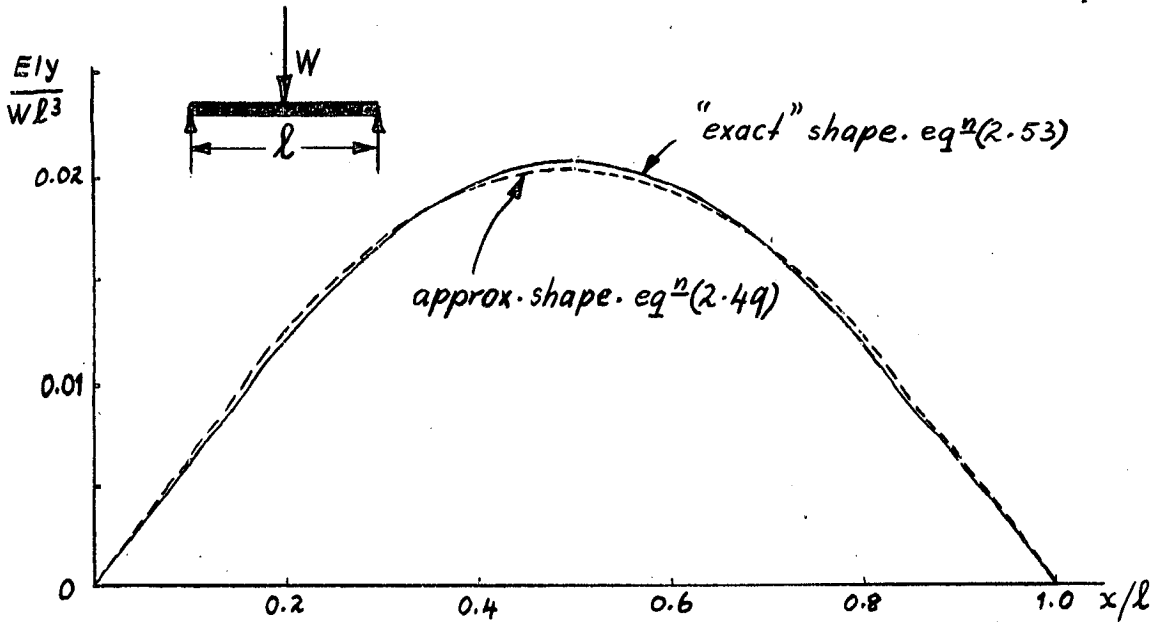


figure 2.7 - Deflected shape of a simply supported beam

in the middle third of the span the deflection is underestimated. The largest difference occurs at the centre.

Although the deflected shape is a good fit, the slope is less so, and the curvature is even worse, so that the approximate function is not reliable for the purpose of calculating bending moments. This is due to the inherent loss of accuracy caused by differentiation. The maximum bending moment at the centre, as obtained from equations (2.49) and (2.52), is  $0.020Wl$ ; compared with the accurate result of  $Wl/4$ , this represents a difference of some 25%.

(ii) Uniformly distributed load

The same approximate function for the deflected shape, when used for the beam with a uniformly distributed load  $w$  per unit length, gives results which are even more accurate than in the concentrated central load case. The central deflection is obtained as

$$a_1 = 4wl^4/\pi^5 EI \quad (2.54)$$

which differs by only about 0.2% from the more accurate result. The maximum bending moment, calculated from the approximate shape, is  $0.129w l^2$ , which is only about 3% different from the correct value.

(iii) Non-symmetric cases

When the beam is not symmetrically loaded, the symmetric half sine wave can still be used as an approximate expression for the deflected shape, but the results are generally no longer sufficiently accurate. In this case the assumed shape must be improved, and the

function which lends itself most easily to the evaluation of strain energy is the Fourier series, and two terms usually give sufficient accuracy. Taking for example the case of a simply supported beam carrying a concentrated load  $W$  at a quarter span, we can assume a deflected shape given by

$$y = a_1 \sin(\pi x/l) + a_2 \sin(2\pi x/l) \quad (2.55)$$

The total strain energy corresponding to this shape is

$$U = (\pi^4 EI/l^3) (\frac{1}{4} a_1^2 + 4a_2^2) - \int_0^l W d\delta \quad (2.56)$$

where  $\delta$  is the deflection under the load, and is expressed in terms of the parameters  $a_1$  and  $a_2$  as

$$\delta = a_1/\sqrt{2} + a_2 \quad (2.57)$$

Minimization of the strain energy with respect to these parameters gives the two equations

$$\begin{aligned} \partial U/\partial a_1 &= \frac{1}{2} \pi^4 EI a_1 / l^3 - W/\sqrt{2} = 0 \\ \partial U/\partial a_2 &= 8 \pi^4 EI a_2 / l^3 - W = 0 \end{aligned} \quad (2.58)$$

Using the values of  $a_1$  and  $a_2$ , as determined from these equations, in the assumed shape, the deflection under the load is found to be

$$\delta = 9Wl^3/8 \pi^4 EI \quad (2.59)$$

which differs by about 1½% from the exact value. The maximum deflection occurs at a distance 0.451 from the support nearest the load, (compared with 0.441 computed by the exact method) and is  $Wl^3/68.0EI$  which is 1% greater than the exact value.

From the above few simple examples it becomes evident that strain energy affords a quick and reliable method of computing beam deflections. The agreement with more exact theory in general depends on how well the approximate function for the deflected shape fits the problem. Usually sufficient accuracy can be achieved with a function which satisfies only the geometric boundary conditions, that is those relating to deflection and slope only. However, in some problems this is not enough, and boundary conditions in bending moments, must also be satisfied. In the simply supported beam problems these conditions are automatically fulfilled when using a Fourier sine series, since this has zero curvature, and hence bending moment, at the boundaries. When the simply supported beam is deformed by the action of moments applied at its ends, the Fourier sine series gives poor results as is seen in the next example.

(iv) End moments

Consider the simply supported beam deformed by end moments  $M_A, M_B$ , and let the end slopes be  $\theta_A, \theta_B$  respectively. Proceeding in the same manner as in the previous example we find

$$U = (\pi^4 EI / l^3) (\frac{1}{4} a_1^2 + 4a_2^2) - \int_0^{\theta_A} M_A d\theta_A - \int_0^{\theta_B} M_B d\theta_B \quad (2.60)$$

where

$$\theta_A = (\pi/l)(a_1 + 2a_2) \quad ; \quad \theta_B = (\pi/l)(-a_1 + 2a_2) \quad (2.61)$$

Minimization of the strain energy with respect to the parameters  $a_1$  and  $a_2$ , and subject to the restricting equations of geometry gives

$$\partial U / \partial a_1 = \frac{1}{2} \pi^4 EI a_1 / l^3 - \pi M_A / l + \pi M_B / l = 0 \quad (2.62)$$

$$\partial U / \partial a_2 = 8 \pi^4 EI a_2 / l^3 - 2 \pi M_A / l - 2 \pi M_B / l = 0$$

Substitution of  $a_1, a_2$ , as obtained from these equations, in equations (2.61), gives the solution in familiar form

$$\begin{aligned} \theta_A &= (1/2 \pi^2 EI) (5M_A - 3M_B) \\ \theta_B &= (1/2 \pi^2 EI) (-3M_A + 5M_B) \end{aligned} \quad (2.63)$$

whereas the exact solution is

$$\begin{aligned} \theta_A &= (1/6 EI) (2M_A - M_B) \\ \theta_B &= (1/6 EI) (-M_A + 2M_B) \end{aligned} \quad (2.64)$$

The coefficients in these two solutions differ by about 24% and 9% respectively, based on the accurate solution. The reason for the large discrepancies is, as explained above, due to the fact that the approximate shape has zero curvature at the ends, whereas the exact function has curvatures equal to  $-M_A/EI$  and  $M_B/EI$  respectively.

(b) Cantilever beam

An approximate function for the deflected shape of a cantilever, which fits the boundary conditions up to and including the second derivative, is

$$y = a_1 [1 - \cos(\pi x / 2l)] \quad (2.65)$$

with the origin taken at the built-in end. When used in the strain energy method this function gives satisfactory solutions for the concentrated load at the free end, and for the uniformly distributed load. If necessary, a second term,  $a_2 [1 - \cos(3\pi x / 2l)]$ , can be added to the above function to gain more accuracy.

(c) Beam built-in at both ends

A satisfactory approximate function for the deflected shape of a built-in beam is

$$y = a_1 [1 - \cos(2\pi x/l)] \quad (2.66)$$

which is symmetric about the centre of the beam. For non-symmetric cases, a second term,  $a_2 [\cos(\pi x/l) - \cos(3\pi x/l)]$ , must be added.

(d) Propped cantilever

The simplest approximate function for the deflected shape of a propped cantilever, satisfying the boundary conditions up to and including the second derivative, is the single parameter function

$$y = a_1 [\cos(\pi x/2l) - \cos(3\pi x/2l)] \quad (2.67)$$

and this gives satisfactory results for the loadings commonly encountered. An additional term of the form,  $a_2 [\cos(5\pi x/2l) - \cos(7\pi x/2l)]$ , will give more accurate results.

\* \* \* \* \*

From the above simple examples it is seen that quite reasonable estimates of the deflections can be obtained with the use of only one parameter in the guessed function defining the deflected shape. However in more complicated problems a one parameter energy solution often does not give sufficient accuracy, and it therefore becomes necessary to choose approximate functions for the deflected shape involving several parameters. These parameters are then determined so as to make the total strain energy a minimum, which is equivalent to satisfying all the equilibrium requirements "on the average". In this section Fourier series were used, because the integrals involved in the strain energy function are then easily evaluated. The results thus obtained were generally close to those obtained from the usual small deflection theory. Exact results could be found by using an infinite series, or the correct deflected shape if this is known. Once this has been established it is no longer necessary to evaluate the strain energy integral, as the minimum strain energy equations can be set up directly from equilibrium considerations, as is shown in the following section.



## 2.5 STRAIN ENERGY ANALYSIS OF STATICALLY INDETERMINATE FRAMES

In this section it is shown that the analysis of statically indeterminate frameworks can conveniently be carried out using minimum strain energy principles. It is not a separate method of analysis, but merely an alternative technique for the derivation of the equations of equilibrium, which can equally well be set up directly.

Following the classical method of analysis, attention is focussed on the deformations of the joints of the frame, and the loadings on the frame members are replaced by "fixed end moments" (see for example reference 4.) Thus the first problem is to determine the end moments which, in combination with the actual loading, produce no joint rotations. These end moments are then relaxed and the resulting rotations are the same as those produced by the loading itself.

In order to solve the above problem by means of strain energy principles, consider the beam shown in figure (2.8). Let  $\theta_A$ ,  $\theta_B$  be the end rotations, and  $M_A$ ,  $M_B$  be the respective end moments to produce these

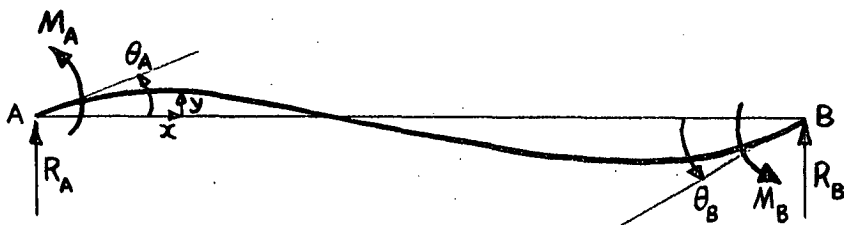
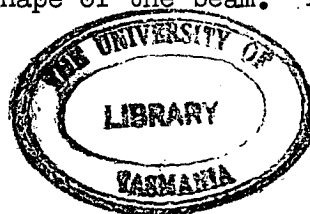


figure 2.8

rotations, both quantities being measured in the anticlockwise sense. From elementary beam theory, the deflected shape of the beam is known to be a polynomial function, and the function

$$y = 1\theta_A[(x/l) - 2(x/l)^2 + (x/l)^3] + 1\theta_B[-(x/l)^2 + (x/l)^3] \quad (2.68)$$

satisfies the geometric boundary conditions of the problem, that is those relating to deflections and slopes. Having defined the shape in terms of the two end rotations, we can proceed in the usual manner, and minimize the total strain energy with respect to the free parameters. This case is the same as that in part 2.4(a) (iv) above, except for the difference in the functions describing the deflected shape of the beam. The equations of minimum strain energy are



$$\partial U / \partial \theta_A = (EI/l)(4\theta_A + 2\theta_B) - M_A = 0 \quad (2.69)$$

$$\partial U / \partial \theta_B = (EI/l)(2\theta_A + 4\theta_B) - M_B = 0$$

and these are seen to be the exact relationships, as was to be expected, since the exact shape was used in the strain energy function.

When analyzing a frame by the above method, the deflected shape of the whole frame must be specified, and this is done by using an expression such as (2.68) for each beam element in terms of its end rotations. If the joints of the frame can be assumed rigid then the end rotations are equal to the joint rotations, and thus the total number of parameters involved is equal to the number of joints in the frame. Since energies are additive, the minimum strain energy equations for the whole frame are obtained by adding equations such as (2.69), and there is thus no need to evaluate the strain energy. Also, because the functions for the deflected shapes are exact, the solution of the final linear algebraic equations is also exact.

So far only joint rotation has been considered, but the ideas are easily generalized to take into account joint translations. Also, no account has been taken of axial load effects which is customary and reasonable provided the axial loads are small compared with the buckling loads of the members treated as pin-ended columns.

## 2.6 ITERATIVE SOLUTION

The method of analysis outlined in the previous section is known as the deformation method. The final equations represent the conditions of equilibrium of the joints, in terms of the generalised joint displacements. As always, if the correct deflected shape is used to evaluate the strain energy, the equations derived from minimum strain energy principles are exact equations of equilibrium, and it would therefore seem that there is no advantage to be gained. Indeed this is so; one would derive the equations directly, and an exact solution of these equations is theoretically possible. However, even with the present high speed electronic computers there is a limit to the number of equations which can be handled; this limit depends on the size of the machine. The same applies if computations are to be done by hand. Should this be the case, then the engineer is once more faced with the problem of developing alternative numerical techniques in order to obtain a satisfactory solution. Here again energy methods can provide an answer. The iterative solution presented in this section is that of the author, and is believed to be new.

Suppose that by some device one can obtain approximate values for some of the unknown generalized displacements, or approximate ratios for a group of unknowns in the analysis of a frame. If the exact values were known, there would be no problem, as any of the equations could be used to solve for the remaining unknowns, but if the values are approximate, then different solutions are obtained depending on which equations are used. Naturally the "best average" is sought, and strain energy principles, being an averaging process, can be used advantageously. The method is most easily understood by way of a simple example; a general proof follows readily.

Consider the two storey rectangular portal frame shown in figure (2.9). The dimensions, loads and stiffnesses are of no significance,

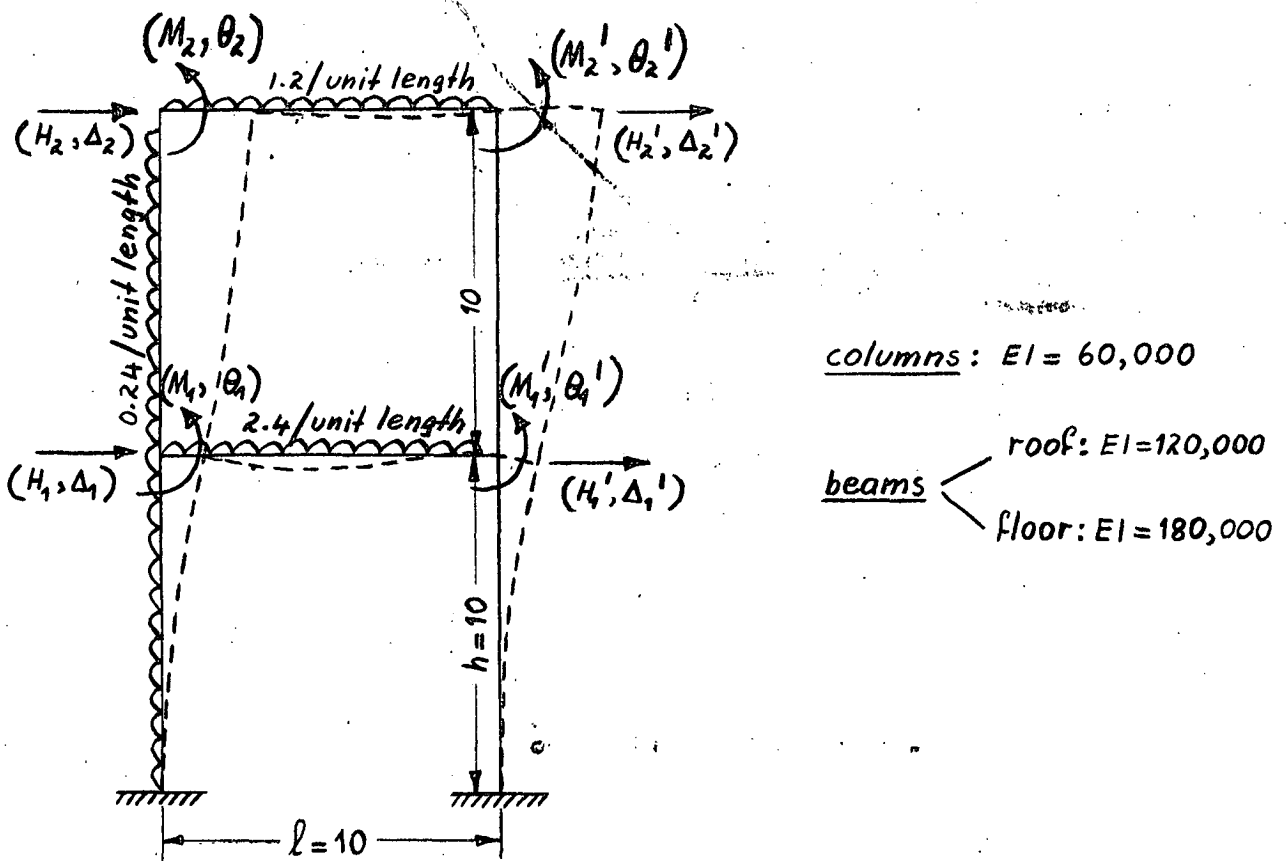


figure 2.9 - Portal frame

and are non-dimensional for convenience. The deflected frame is sketched in exaggerated scale, and the generalized joint displacements together with their generalized joint forces are written enclosed in parentheses; their positive directions are indicated by arrows. If axial load effects are neglected, and if deformations small, then  $\Delta'_1 = \Delta_1$  ;  $\Delta'_2 = \Delta_2$ .

The equations of equilibrium are readily set up, and in matrix form they are

$$(60) \begin{bmatrix} 48 & -24 & 0 & -60 & 0 & -60 \\ -24 & 24 & 60 & 60 & 60 & 60 \\ 0 & 60 & 2000 & 200 & 600 & 0 \\ -60 & 60 & 200 & 1200 & 0 & 400 \\ 0 & 60 & 600 & 0 & 2000 & 200 \\ -60 & 60 & 0 & 400 & 200 & 1200 \end{bmatrix} \begin{bmatrix} \Delta_1 \\ \Delta_2 \\ \theta_1 \\ \theta_2 \\ \theta'_1 \\ \theta'_2 \end{bmatrix} = \begin{bmatrix} H_1 \\ H_2 \\ M_1 \\ M_2 \\ M'_1 \\ M'_2 \end{bmatrix} = \begin{bmatrix} 2.4 \\ 1.2 \\ -20 \\ -8 \\ 20 \\ 10 \end{bmatrix} \quad (2.70)$$

where the factor (60) represents the term  $(EI/1001)$ . The generalized joint forces are obtained by adding algebraically the member fixed end moments and reactions, and negating the results. Using strain energy, the exact shape of each member is specified in terms of its end sways and rotations, its strain energy evaluated, and the total minimized. In this problem the parameters involved are the two sways and four rotations. The equations of minimum total strain energy are the same as (2.70), the first being  $\partial U / \partial \Delta_1 = 0$ , the second  $\partial U / \partial \Delta_2 = 0$ , and so on. There are only six equations in this problem, and their solution is readily found by hand computation.

To obtain an approximate solution it is necessary to guess the magnitude of some of the unknowns. This is not easily done, but approximate ratios can be determined from the sketch of the deflected shape of the portal frame. As a very crude approximation, we have

$$\begin{aligned} \Delta_2 &\approx 2\Delta_1 \\ \theta_2 &\approx \theta_1 \\ \theta'_2 &\approx \theta'_1 \end{aligned} \quad (2.71)$$

To use the six equations for obtaining the "best" solution for the three unknowns  $\Delta_1$ ,  $\theta_1$ ,  $\theta'_1$ , we take linear combinations to reduce the number of equations to three. The correct combinations are those with the ratios the same as in equations (2.71), that is  $(E_1 + 2E_2)$ ,  $(E_3 + E_4)$ ,  $(E_5 + E_6)$ , where  $E_i$  refers to the  $i$ th equation. Justification for this is given in the following section. In matrix form these combinations are

$$(60) \begin{bmatrix} 48 & 180 & 180 \\ 180 & 3600 & 1000 \\ 180 & 1000 & 3600 \end{bmatrix} \begin{bmatrix} \Delta_1 \\ \theta_1 \\ \theta'_1 \end{bmatrix} = \begin{bmatrix} 4.80 \\ -28.0 \\ 30.0 \end{bmatrix} \quad (2.72)$$

These equations are readily solved, giving

$$\begin{aligned}\Delta_1 &= 0.00232 \\ \theta_1 &= -0.000272 \\ \theta'_1 &= 0.0000987\end{aligned}\tag{2.73}$$

To complete the solution, approximate values for the remaining three unknowns  $\Delta_2$ ,  $\theta_2$ ,  $\theta'_2$  must be found. This could be done by using the guessed ratios, but better values are obtained from the original equations of equilibrium (2.70), using the computed values of

$\Delta_1$ ,  $\theta_1$ ,  $\theta'_1$  as a partial solution. A satisfactory procedure is to solve the equations of equilibrium of those generalized joint forces related to the generalized joint displacements still to be determined. In this problem, after substituting equations (2.73) in the second, fourth and last of equations (2.70), and solving the resulting three equations for the remaining three unknowns, we find

$$\begin{aligned}\Delta_2 &= 0.00375 \\ \theta_2 &= -0.0001735 \\ \theta'_2 &= 0.000109\end{aligned}\tag{2.74}$$

Thus equations (2.73) and (2.74) together constitute an approximate solution for the joint rotations and sways of the two storey portal frame. The solution was derived from minimum strain energy principles, using guessed ratios to reduce to final number of equations of equilibrium.

Since the guessed ratios are only rough approximations, the above solution must be improved. Clearly an iterative scheme can be set up; from the first solution new ratios can be calculated, and the number of equations of equilibrium reduced to three as before, and so on. This gives as a second solution for the portal frame deformations

$$\begin{aligned}\Delta_1 &= 0.00294 \\ \Delta_2 &= 0.00447 \\ \theta_1 &= -0.000313 \\ \theta_2 &= -0.000170 \\ \theta'_1 &= 0.000\overset{0997}{\cancel{997}} \\ \theta'_2 &= 0.000102\end{aligned}\tag{2.75}$$

The differences between this solution and the previous solution are not great, and a third iteration gives results which differ only slightly. The results of the iterative solution presented above are summarized in table (2.1), in which all values have been multiplied by a factor of  $10^4$ .

Def.	Approximate solutions			exact solution
	1 <sup>st</sup>	2 <sup>nd</sup>	3 <sup>rd</sup>	
$\Delta_1$	23.2	29.4	30.0	30.0
$\Delta_2$	37.5	44.7	45.3	44.9
$\theta_1$	-2.72	-3.13	-3.18	-3.20
$\theta_2$	-1.74	-1.70	-1.68	-1.66
$\theta'_1$	0.987	0.997	1.08	1.18
$\theta'_2$	1.09	1.02	1.00	1.00

Table 2.1

As can be seen, satisfactory agreement is obtained with the second approximation, that is, after one iteration. A final check on the accuracy of the solution is to calculate the generalized joint forces corresponding to the generalized joint displacements as calculated.

These are

$$\begin{aligned}
 H_1 &= 2.35 \text{ (compared with 2.40 in the original equation)} \\
 H_2 &= 1.202 \text{ (1.20)} \\
 M_1 &= -20.0 \text{ (-20.00)} \\
 M_2 &= -8.03 \text{ (-8.00)} \\
 M_1 &= 18.98 \text{ (20.00)} \\
 M_2 &= 9.97 \text{ (10.00)}
 \end{aligned}
 \tag{2.76}$$

which are within 5%, or less, of the applied forces and moments, so that the solution is satisfactory for practical purposes.

\* \* \* \* \*

The advantage of the above approximate method for a solution of the deformations of the portal frame, is little or nothing. In this example a more accurate solution of the equations can be easily obtained by direct methods. However, as the number of equations increases, the method becomes more feasible. Attention is focussed throughout on the deformations, and frequently reasonable predictions as to the magnitude

of some of these can be made, for example with the aid of inexpensive flexible models. With this information available, fairly accurate results can be obtained, which, although approximate, are of considerable use. Furthermore, it is always possible to iterate towards a better solution. It is felt that convergence of the iterative scheme outlined above is inherent in structural problems, but a formal proof is lacking.

## 2.7 PROOF OF LINEAR COMBINATIONS METHOD

The procedure for finding successive approximate solutions for the deformations by taking linear combinations of the equations of equilibrium, is readily generalized. With the usual simplifications, the deflected shape of any member can be specified in terms of its end displacements and rotations. In problems such as those in the previous section the exact shape of the deflected member is used, and hence the strain energy is also exact. The number of parameters equals the number of joint displacements and rotations, and the total strain energy,  $U$  can be expressed as

$$U = f(x_1, x_2, \dots, x_n) \quad (2.77)$$

where  $x_1, x_2, \dots, x_n$  are the  $n$  generalized joint displacements. The values of these parameters which satisfy the conditions of equilibrium are the same as those which make the total strain energy a minimum. For convenience, put

$$\partial U / \partial x_i = E_i = 0 \quad (2.78)$$

that is the equation of equilibrium corresponding to the  $i$ th generalized displacement  $x_i$ . Suppose that a group of the unknown parameters are expressed in terms of a single parameter, that is

$$x_i = r_i X \quad ; \quad i = 1, 2, \dots, m \quad (2.79)$$

where the first  $m$  are chosen for argument's sake only. The coefficients  $r_i$  are either known, or can be estimated approximately from, for example, a model test. After making the relevant substitutions in the strain energy expression, minimization is carried out with respect to the remaining parameters  $x_i$  ( $i = m + 1, m + 2, \dots, n$ ), and the parameter  $X$  defining the first  $m$  parameters. The equations of minimum total strain energy are the same as equations (2.78) in which the relations (2.79) have been substituted, except that the derivative of  $U$  with

respect to  $X$  becomes

$$\partial U / \partial X = \sum_{i=1}^m (\partial U / \partial x_i) (\partial x_i / \partial X) = \sum_{i=1}^m r_i E_i \quad (2.80)$$

This is seen to be a linear combination of the equations of equilibrium in the generalized forces corresponding to the generalized displacements in the group  $x_i = r_i X$ , with the coefficients  $r_i$  as "weighting factors" in the combination. From this it follows that the approximate solution emphasizes the more important generalized displacements, and for this reason it is better not to attempt to guess these, but rather those which are small in magnitude.

The above argument has been presented on the basis of grouping some generalized displacement in terms of a single parameter  $X$ , using numerical values for the coefficients  $r_i$ ; an extension of the argument to cater for several groups, each having its own parameter and coefficients, follows readily, and formal proof is not necessary.

The use of numerical values for the coefficients enables the number of equations to be reduced, and a solution to be found. However, this solution is only approximate, unless the correct values of the coefficients are used. In order to improve the solution new coefficients must be determined. Several processes suggest themselves; in the first place consider the procedure of the previous section, that is, the generalized displacements which were originally guessed, are calculated from those equations of equilibrium in their corresponding generalized forces. This follows immediately from differentiation of the total strain energy with respect to the coefficients  $r_i$ . Although this method is simple and justifiable, it suffers from the disadvantage that the number of equations to be solved could be almost as large as the original number. A way out of this difficulty is to treat only a certain number as unknowns, using the latest values of the remaining generalized displacements in the respective equations. It is not possible to describe all the possible methods, but whichever is used, it must be a step nearer the correct solution as long as the original equations of equilibrium are used, since ultimately the correct generalized displacements are those which satisfy these equations.

In closing, it must be stressed again that the approximate method presented above is subject to the same simplifications as are usually made in structural analysis, so that the solution for the behaviour of the real structure is only as good as the mathematical model. In framework problems the deformations are usually small, and putting  $\Delta'_1$  equal to  $\Delta_1$  in the portal frame of section (2.6) is quite safe. On the other hand, the neglect of axial load effects may be serious, especially if the



columns carry axial loads which are of appreciable magnitude compared with the Euler loads of the equivalent pin-ended columns. Fortunately this can be taken into account by a reduction in the stiffness coefficients of the members, as will be seen in the next chapter of this thesis.

## 2.8 PHYSICAL INTERPRETATION

A physical picture of the linear combinations technique is as follows: the solution for the  $n$  generalised displacements, by means of the equations of equilibrium in the corresponding generalized forces, can be thought of as a point in an  $n$ -dimensional space. By imposing relations between some of the displacements, the solution of the equations becomes restricted, and the point cannot be reached unless the guessed relations happen to be exact. Any number of solutions can be found, depending on which equations are used to calculate the remaining unknowns. This means that there exists a region of solutions rather than a point, and the "best" solution attainable is a point within this region which, in some sense, lies nearest the point representing the exact solution. The approximate solution may satisfy some of the equations of equilibrium or, by using strain energy, it satisfies them all on the average, by virtue of the linear combinations of the solutions. Thus the process can be pictured as choosing that solution, out of all possibilities within the region, which minimizes some function of the distance between it and the point corresponding to the exact solution.

In fact this picture applies to all strain energy processes; for example the pin-ended column, axially loaded, must satisfy at every point the differential equation

$$M + Py = 0 \quad (2.81)$$

which is derived from equilibrium consideration of an element. In this case the solution is a function rather than an  $n$ -dimensional vector, and again if the exact shape of the buckled column is not known, approximate values for the buckling load can be determined from an approximate function  $y$ . Here again, any number of solutions for the buckling load are available depending on where the equation of equilibrium is satisfied. Using the linear combinations technique, the equations of equilibrium are weighted according to their corresponding displacements. Obviously the linear combination in this problem is of functional form, and may be expressed by the integral

$$\int_0^l (M + Py) \cdot y \, dx \quad (2.82)$$

Using the linear moment curvature relation  $M = EI(d^2y/dx^2)$ , we obtain, after integration by parts

$$P \int_0^l y^2 dx - \int_0^l EI(dy/dx)^2 dx \quad (2.83)$$

which is seen to be an alternative form of the strain energy expression.

The more common form,

$$\int_0^l EI(d^2y/dx^2)^2 dx - P \int_0^l (dy/dx)^2 dx \quad (2.84)$$

is obtained by using curvature,  $d^2y/dx^2$ , as the weighting function, rather than the deflection,  $y$ , as was done here. This type of problem, and many others, can be handled in the same manner, and it clearly demonstrates the power of energy methods in obtaining approximate solutions.

It has been shown again that the strain energy method is not separate, but merely an alternative way of deriving the equations of equilibrium, either the correct equations or a linear combination of them. Any linear combination desired is possible and is treated by methods similar to the straightforward Rayleigh method once this fact is recognized.

## 2.9 NUMERICAL EXAMPLE

In order to test the feasibility of the linear combinations technique, the frame shown in figure (2.10) is analyzed. Shown in the

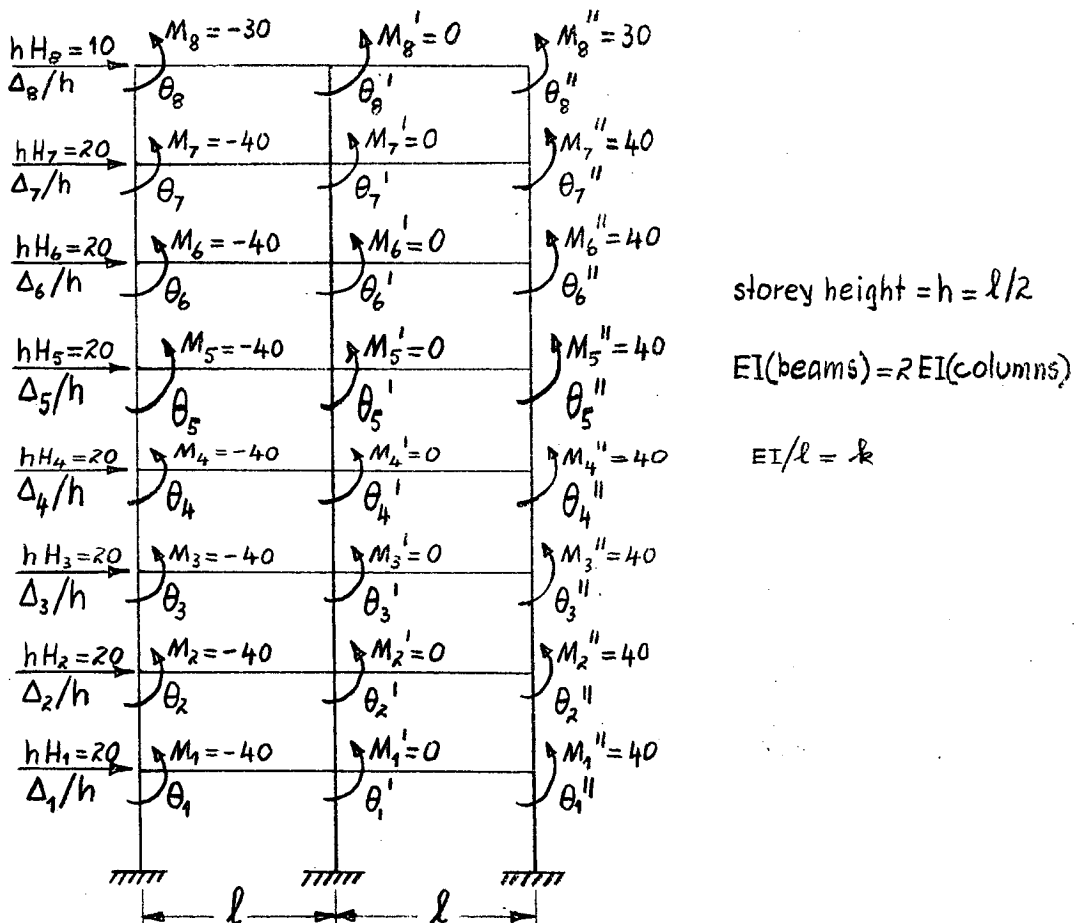


figure 2.10 - Two-bay, eight-storey building frame

same figure are the applied forces and moments, together with the notation for the corresponding generalized displacements. The magnitudes indicated are purely artificial for the sake of this particular problem. Also, sway divided by storey height is used as a generalised displacement, together with the generalized force in the form of horizontal force times storey height. In this problem a convenient grouping of unknowns appears to be

- (a) sways in terms of the single parameter ( $\Delta/h$ )
- (b) rotations in left column in terms of  $\theta$
- (c) " " central " "  $\theta'$
- (d) " " right " "  $\theta''$

As a first estimate of the relative magnitudes of the generalized displacements, the ratios in each group are assumed to increase sinusoidally, from zero at ground level to a maximum at roof level. Using the ratios thus defined the (32 x 32) stiffness matrix is reduced to a (4 x 4) involving the parameters  $\Delta/h, \theta, \theta', \theta''$  whose solution is readily found. Improved ratios are then calculated, a group of eight at the time, using the corresponding equations of equilibrium together with the most recent values for the other 24 unknowns. The calculations are then repeated with the improved ratios.

$\Delta/h$	$-\theta$	$-\theta'$	$\theta''$
40.4 (42.06)	3.57 (3.51)	0.23 (0.21)	2.96 (2.79)
39.8 (41.17)	3.45 (3.41)	0.63 (0.70)	1.27 (1.36)
38.0 (38.99)	4.38 (4.52)	1.25 (1.33)	0.65 (0.51)
34.9 (35.37)	5.24 (5.50)	1.82 (2.00)	-0.25 (-0.50)
30.4 (30.32)	6.09 (6.50)	2.43 (2.67)	-1.10 (-1.50)
24.6 (23.82)	6.96 (7.51)	2.95 (3.32)	-1.93 (-2.48)
16.6 (15.92)	7.59 (8.33)	3.53 (3.96)	-2.72 (-3.48)
7.40 (6.93)	8.81 (9.26)	3.60 (3.89)	-2.91 (-3.40)
0	0	0	0

figure 2.11 - Comparison of exact and approximate solutions.

In this analysis reasonable convergence is obtained after only two iterations. The approximate solution is shown in figure (2.11), together with the results of an exact analysis carried out on the Elliott 503 digital computer; the latter are enclosed in parentheses. As can be seen, the agreement between the two sets of results is reasonably close, taking into account that only two iterations were carried out. Also it is evident that the rotations are greatest at ground level, decreasing gradually towards roof level. This is the direct opposite of the initial guessed form of the ratios, so that considerable improvement could be obtained with a better set of starting values. From the results, member end moments and shears can be calculated, if needed, using equations (2.69).

## 2.10 CONCLUDING REMARKS

In this chapter an attempt has been made to unify energy methods and classical methods of structural analysis. The emphasis has been on strain energy, which is equivalent to the classical deformation method. A solution is derived from equations of equilibrium in terms of the deformations. It has been shown that these equations can be derived from minimum strain energy conditions, using the exact functional form for the deflected structure to evaluate the strain energy. The technique is essentially the same as that known as the Rayleigh-Ritz method in that it uses more than one parameter to define shape; the single parameter method is commonly attributed to Rayleigh. Having identified the validity of the strain energy method, the equations of equilibrium are usually set up directly.

The power of the energy method lies in the ease with which approximate solutions can be found, and in this chapter a frame possessing a relatively large number of degrees of freedom was successfully analysed using the linear combinations technique. This technique has been shown to satisfy certain groups of the equations of equilibrium "on the average", and leads to a reduced stiffness matrix. Convergence towards better approximate solutions is achieved by attempting to satisfy the individual equations of equilibrium, thus leading to improved functions for deriving approximate reduced stiffness matrices. Although the numerical example of the previous section is readily solved on an electronic computer, a foundation has been laid for attacking more complicated frameworks. Three-dimensional frameworks, for example, lead to a large number of equations, and their solution may be out of reach even for machines with large storages. It is felt that some attempt can be made to analyze such frames using the method described in this chapter.

REFERENCES

1. R.V. Southwell, "Theory of Elasticity", O.U.P. 2nd ed. p 20f.
2. R.S. Stilwell, "Structural Stability and the Energy Method",  
Hons. Thesis, Uni. of Tas., (1961).
3. A.R. Oliver "Energy Methods in Structural Analysis",  
Civ. Eng. Trans. I.E. Aust. (March, 1961).
4. T.M. Charlton "Statically Indeterminate Frameworks",  
Longmans (1961).

### CHAPTER THREE

#### A NEW METHOD FOR CALCULATING BUCKLING MODES AND LOADS OF FRAMES

##### 3.1 INTRODUCTION

In chapter one a brief review was given of the various methods available for a determination of buckling modes and loads of frames. Anyone faced with the problem of the design of frames soon becomes aware of the computational difficulties involved in such a stability analysis. It was with this in mind that a simpler approach was sought. The basic problem and customary simplifications are as outlined in section (1.6), and it is shown in this chapter that the Rayleigh-Ritz method of strain energy, using the same parameters as the classical deformation method, leads to a linearized form of the stiffness matrix. The linearized matrix is handled by the usual methods of matrix analysis and is shown to yield an upper bound for the buckling load. If desired, a lower bound can be obtained as well, using a graphical procedure. Successive approximations of the straight line variation of the stiffness matrix quickly yield a reliable estimate of the buckling behaviour. It is shown that considerable computational savings are to be made by using basic geometric data, obtainable from simple inexpensive models, in the standard iterative matrix procedures.

##### 3.2 DEVELOPMENT OF METHOD

It can be seen from section (1.8d) that the buckling load calculated from a single parameter application of the Rayleigh energy method is not reliable. This is so because the functional form, in terms of a single parameter, does not adequately describe the deflected shape of the buckled structure. To improve this situation, the specification of shape must be more flexible, and this can be done by using more parameters. For convenience, parameters which have physical significance are chosen, and these are obviously the frame joint rotations and sway. This has the additional advantage that the conditions of minimum strain energy are readily identified as equations of equilibrium involving the corresponding joint moments or forces. The method is developed on a simple two dimensional example and is generalized in the following section.

Consider again the equilateral triangular frame buckling in its plane. (see figure(1.6) ). The simplest polynomial function describing the shape of any member in terms of its end rotations is

$$y = 1\theta_A[(x/l) - 2(x/l)^2 + (x/l)^3] + 1\theta_B[-(x/l)^2 + (x/l)^3] \quad (3.1)$$

This function satisfies the boundary condition of zero deflection at both ends, and it is known to be the exact shape of a simply supported beam deformed by end moments. Denoting by  $\theta_A$ ,  $\theta_B$ ,  $\theta_C$  the joint rotations of the buckled triangular frame, a function such as (3.1) is fitted to the deflected shape of each member, and the total strain energy is evaluated according to equations (1.33). The following equations of minimum strain energy are obtained

$$\begin{aligned}\partial U / \partial \theta_A &= (EI/l)[(8-2k)\theta_A + (2+k)\theta_B + (2-k)\theta_C] - M_A = 0 \\ \partial U / \partial \theta_B &= (EI/l)[(2+k)\theta_A + (8-8k)\theta_B + (2+k)\theta_C] - M_B = 0 \\ \partial U / \partial \theta_C &= (EI/l)[(2-k)\theta_A + (2+k)\theta_B + (8-2k)\theta_C] - M_C = 0\end{aligned}\quad (3.2)$$

in which  $M_A$ ,  $M_B$ ,  $M_C$  are the applied joint moments, and  $k$  is a load parameter defined by

$$k = Pl^2/30EI \quad (3.3)$$

For the undisturbed structure the joint moments are zero, so that the solution of equations (3.2) for the joint rotations is either the trivial zero solution, or the determinant of coefficients vanishes, in which case the ratios between the joint rotations are defined but the absolute magnitudes are undefined. That is, it is the usual eigenvalue problem; in this case the eigenvalues of  $k$  are measures of the buckling loads, and the eigenvectors represent the modes of buckling as defined by the joint rotations. In this problem there are three eigensolutions, obtained by expansion of the determinant:

$$\begin{aligned}\text{(i)} \quad k_1 &= 0.762 \quad ; \quad \theta_A : \theta_B : \theta_C = -0.342 : 1 : -0.342 \\ \text{(ii)} \quad k_2 &= 4.00 \quad ; \quad \theta_A : \theta_B : \theta_C = 1.00 : 0 : -1.00 \\ \text{(iii)} \quad k_3 &= 5.23 \quad ; \quad \theta_A : \theta_B : \theta_C = 2.34 : 1 : 2.34\end{aligned}\quad (3.4)$$

As can be seen, the first and third represent antisymmetric modes, the latter requiring a reversal of curvature in each member in order to maintain all rotations in the same sense. The second solution corresponds to a symmetric mode. The fundamental mode is the first solution, and equation (3.3) gives the buckling load as

$$P_{cr} = 22.9 EI/l^2 \quad (3.5)$$

which is seen to be about 40% high (see section 1.8). In section (3.4) it is shown that the estimate for the lowest buckling load obtained by this method is of necessity an upper bound, so that equation (3.5) should rather be an inequality, that is

$$P_{cr} < 22.9 EI/l^2 \quad (3.6)$$

Unfortunately the same cannot be said about second and higher modes, except that the exact value of the largest buckling load is never exceeded; that is all the approximate buckling loads lie between the largest and the smallest.

From the work of the previous chapter it follows that equations (3.2) should express the conditions of equilibrium in moments at the joints of the triangular frame. However, when the modes as determined above are used in the original deflection curves and the bending moment diagram drawn from the curvature diagram, it is found that these conditions are not satisfied. It follows that equations (3.2) are not exact, but only approximate, and therefore the guessed deflected shape is not correct. This is due to the effect of axial loads because it is known that the functions are exact for no axial load. However, a structure can be defined with an approximate distribution of stiffness for which the guessed shape coincides with the actual buckled shape and the equations of equilibrium are then satisfied exactly for this new structure.

Merchant (reference 1) has shown that when an approximate shape (which is correct at zero load) is used, the Rayleigh estimate of the buckling load is the same as would be obtained from the intercept on the zero load axis of the tangent to the stiffness curve at zero load. The approximate shape is defined in terms of a single disposable parameter, the same disturbance being used to plot the stiffness curve. As stated by Merchant, this gives unacceptable estimates of the buckling loads due to the sharp curvature of these graphs. Merchant also points out in the same paper that when use is made of a deflected shape which is correct at some load other than zero, a similar relation exists between the Rayleigh estimate of the buckling load and the intersection of the local tangent on the zero load axis. These ideas are generalized below.

### 3.3 GENERAL ANALYSIS

It was shown in the previous section that the minimum strain energy principle leads to a set of approximate equations of equilibrium of the same form as the exact equations which involve the stability functions  $s$  and  $sc$ . In matrix notation the approximate equations are

$$\tilde{K}_E \cdot \tilde{\theta} = \tilde{M}' = \tilde{0} \quad (3.7)$$



where  $\tilde{K}_E$  is the matrix involving elements which vary linearly with load (which will be called "energy coefficients"), and  $\tilde{M}'$  denotes the column vector of "energy moments" which, for the undisturbed structure, becomes the null vector  $\tilde{O}$ .

Since the differential equations of minimum total strain energy are linear, the same results are obtained by summing the  $\partial U / \partial \theta$  equations for all the members. Therefore, for the purpose of this analysis, it will be convenient to isolate any member such as AB from the frame, as in figure (3.1).

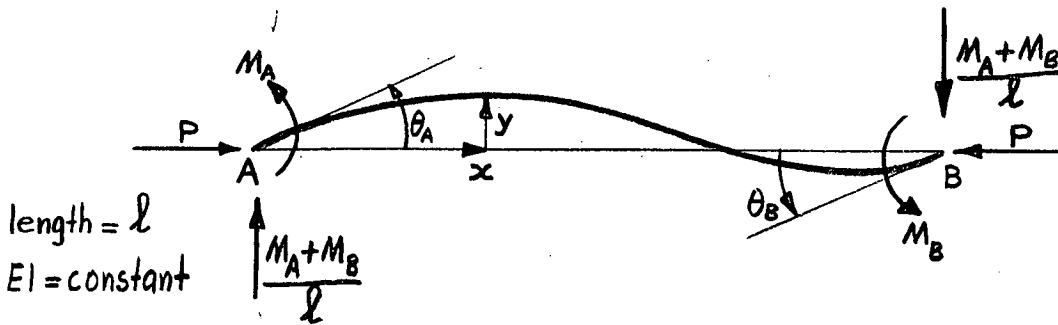


figure 3.1 - Single member under axial load and end moments

Sway is not considered because its effect can be inferred once the method has been established for the simpler case. At zero axial load the shape of the deflected member is as given by equation (3.1). Using this as an approximate shape when the member carries an axial load P, the strain energy is obtained as

$$U = (2EI/l)(\theta_A^2 + \theta_B^2 + \theta_A \theta_B) - (Pl/30)(2\theta_A^2 + 2\theta_B^2 - \theta_A \theta_B) - M_A d_A - M_B d_B \quad (3.8)$$

When this is minimized with respect to the joint rotations  $\theta_A, \theta_B$  we find

$$\partial U / \partial \theta_A = (EI/l)(a_0 \theta_A + b_0 \theta_B) - M_A = 0 \quad (3.9)$$

$$\partial U / \partial \theta_B = (EI/l)(b_0 \theta_A + a_0 \theta_B) - M_B = 0$$

where

$$a_0 = 4 - 2\pi^2 \rho / 15 \quad ; \quad b_0 = 2 + \pi^2 \rho / 30 \quad (3.10)$$

$$\rho = P/Q \quad ; \quad Q = \pi^2 EI / l^2$$

These are seen to be approximate expressions for the end moments, which, in terms of Livesley and Chandler's stability functions, are given by

$$M_A = (EI/l)(s\theta_A + sc\theta_B)$$

$$M_B = (EI/l)(sc\theta_A + s\theta_B) \quad (3.11)$$

Comparison of the coefficients in equations (3.9) and (3.11) reveals that the linear variations  $a_0$  and  $b_0$  are tangent to their counterpart exact functions  $s$  and  $sc$  respectively, the point of tangency being  $\rho = 0$ , for which the assumed shape is exact. This relation was discovered graphically, but may be checked by taking differences of the tabulated functions, or by differentiation. It has been shown by other authors (see for example reference 2) that the Rayleigh method gives an upper bound for the buckling load, or alternatively, the Rayleigh estimate is the buckling load of a stiffer structure, whence it follows that the approximate stiffness must be greater than the exact stiffness. Since the latter is monotonically decreasing, the approximate stiffness curve must be tangent to the exact function.

As regards the accuracy of the straight line approximations, the difference between the tangents and the exact transcendental curves is negligible in the range  $-0.4 < \rho < 0.2$ . The differences at  $\rho = 1$  are about 10% for  $s$  and 6% for  $sc$ , and at higher values of  $\rho$  the differences rapidly increase due to the increasing curvature of the exact functions.

The principle of minimum strain energy thus leads to approximate equations of equilibrium, which are identified as such, and the coefficients in these equations are linear approximations to those in the corresponding exact equations using the stability functions  $s$  and  $sc$ . The approximations are exact at zero load, for which the assumed deflection curve is exact, and furthermore the straight line approximations are tangent to the exact functions.

Obviously the straight line approximations derived above are not accurate enough over the range of axial loads commonly encountered in engineering designs, and improvements must be found to render the method useful. The next step is obvious, that is, use a deflected shape which is correct at some load near the axial load in the member when the frame buckles, and a similar straight line variation is to be expected. It is shown in most textbooks that the exact deflected shape at any axial load is given by

$$y = A \cos(\sqrt{\rho} \pi x/l) + B \sin(\sqrt{\rho} \pi x/l) - (M_A/P)(1 - x/l) + M_B(x/l) \quad (312)$$

where the constants  $A$  and  $B$  are determined from the boundary conditions. The use of this function in the strain energy method involves rather lengthy algebra, and for the purpose of this work it suffices to show how the straight line approximation arises again at one other value of  $\rho$ ; the generality can then be safely inferred. Taking  $\rho = 1$  gives a function which is relatively easy to manipulate, that is

$$y = A \cos(\pi x/l) + B \sin(\pi x/l) - (M_A/P)(1-x/l) + M_B(x/l) \quad (3.13)$$

and use of the boundary conditions in this case gives

$$\begin{aligned} M_A &= M_B = (\pi^2 EI/4l)(\theta_A + \theta_B) \\ A &= (1/4)(\theta_A + \theta_B) \\ B &= (1/2)(\theta_A - \theta_B) \end{aligned} \quad (3.14)$$

Evaluation of the strain energy, and minimization with respect to the rotations  $\theta_A$ ,  $\theta_B$  then leads to the relations

$$\begin{aligned} \partial U / \partial \theta_A &= (EI/l)(a_1 \theta_A + b_1 \theta_B) - M_A = 0 \\ \partial U / \partial \theta_B &= (EI/l)(b_1 \theta_A + a_1 \theta_B) - M_B = 0 \end{aligned} \quad (3.15)$$

where

$$\begin{aligned} a_1 &= (\pi^4/32 + \pi^2/8) - (\pi^4/32 - \pi^2/8)\rho \\ b_1 &= (\pi^4/32 - \pi^2/8) + (3\pi^2/8 - \pi^4/32)\rho \end{aligned}$$

These coefficients can be shown to be tangent at  $\rho = 1$  to the s and sc curves respectively, either by differentiation or by taking differences of the tabulated functions. The two sets of coefficients  $a_0$ ,  $b_0$  and  $a_1$ ,  $b_1$  are compared graphically with the exact functions in figure (3.2), and it is seen that the straight line approximations are sufficiently

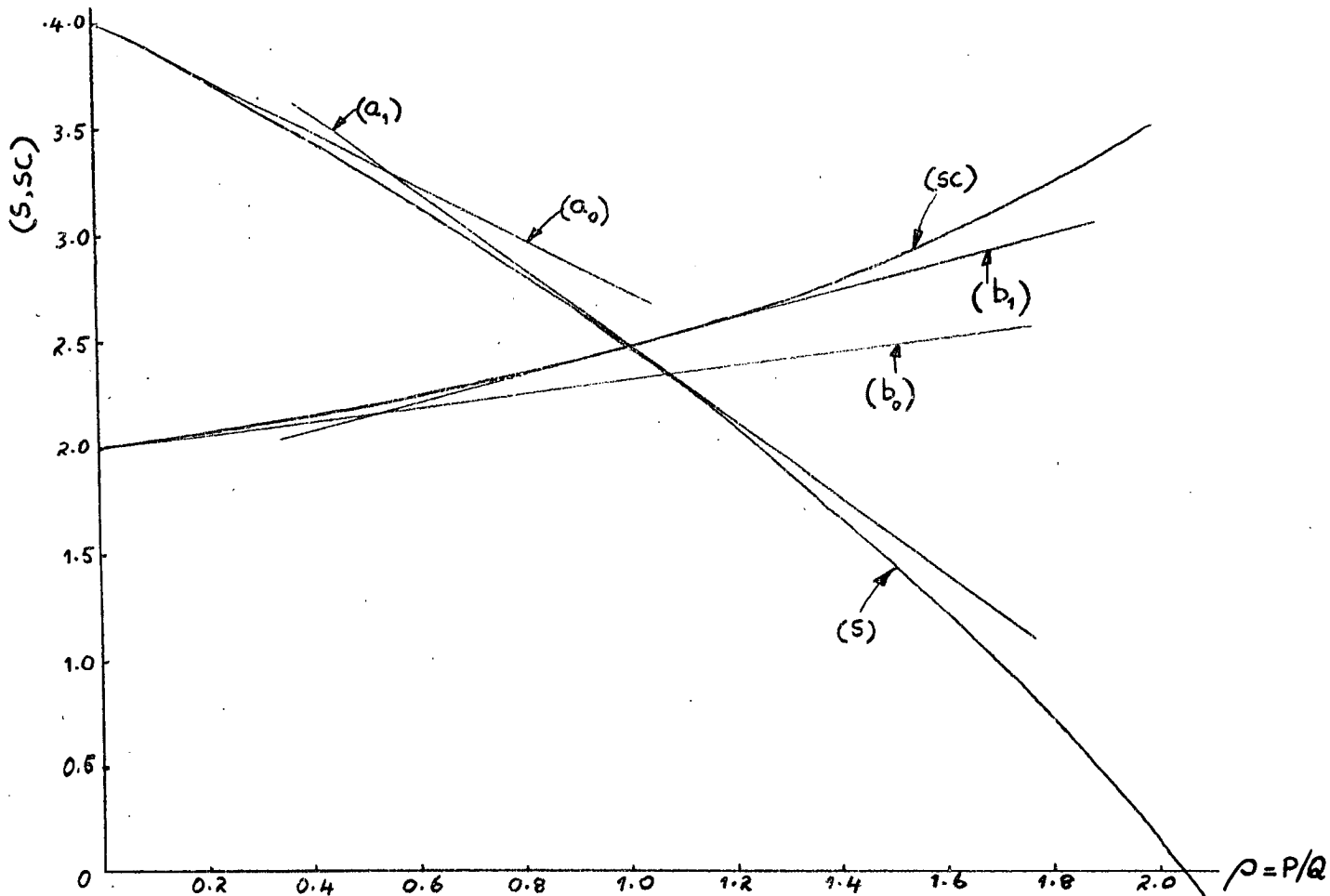


figure 3.2 - Straight line stiffness approximations

accurate, for engineering purposes, within ranges extending considerably on either side of the points of tangency.

It is now possible to generalize the above two particular cases as follows: An approximate deflection curve is chosen by guessing a  $P/Q$  value; this function involves the joint rotations as disposable parameters, and minimization of the strain energy leads to approximate expressions for the end moments in the form

$$\begin{aligned}\partial U / \partial \theta_A &= (EI/l) (a\theta_A + b\theta_B) - M_A = 0 \\ \partial U / \partial \theta_B &= (EI/l) (b\theta_A + a\theta_B) - M_B = 0\end{aligned}\tag{3.17}$$

in which the coefficients  $a$  and  $b$  are linear functions of the axial load, tangent to the exact  $s$  and  $sc$  functions at the guessed value of  $P/Q$ . Alternatively, equations (3.17) give the exact end moments for a member which approximates to the actual member by having a distribution of stiffness causing it to deflect into the assumed shape. If the guessed  $P/Q$  value is close to the correct value, say to within approximately  $\pm 0.2$ , then the difference between the tangents and the exact functions is negligible, and the "energy moments" are sufficiently accurate.

Although the linearization of the stability functions could have been done directly, it is interesting to note that strain energy does just this without modifications, which provides a further example of the way in which energy methods provide an ordering of the calculation.

The general problem of instability of frames can now be formulated in terms of the above mathematical model; that is, equations such as (3.17) are set up for each member, and the end moments summed at the joints. This results in a system of equations of the form

$$\tilde{K}_E \cdot \tilde{\theta} = \tilde{M}' = \tilde{0}\tag{3.18}$$

in which the elements of the matrix  $\tilde{K}_E$  are linear functions of the  $P/Q$  ratios of the members. These equations are known to be approximations to the exact equations, and a solution for the buckling loads and modes is arrived at by setting the determinant of coefficients equal to zero, which corresponds to the undisturbed structure defined earlier. For statically determinate frames the axial load in each member is some fraction of the total load, so that each element of the energy stiffness matrix  $\tilde{K}_E$  is a linear function of the load, and the buckling loads are those values for which the determinant vanishes.

The method just described is a logical development from the generalized stiffness method described in section (1.7 cii), but it shows the distinct advantage of having linearly varying elements in the stiffness matrix. This leads directly to an estimate of the buckling load. The accuracy of the solution can be judged by assessing the relative difference between the calculated buckling load and the initial guess to define shape. If this is poor, the calculated value can be used to define an improved shape and the calculations repeated. Thus the exact values of the buckling load and mode can be approached iteratively.

### 3.4 UPPER AND LOWER BOUNDS

Whenever approximate methods of analysis are used, it is desirable to know whether the results are above or below the values based on a more exact method of computation. It is shown in this section that the buckling loads calculated from the linearized stiffness matrix are upper bounds, that is they are unconservative. A proof of this follows readily in terms of Gregory's latent root plots (reference 3). A typical plot of the smallest latent root is shown in figure (3.3),  $W$  being a generalized load parameter. In general these plots are concave towards the origin. The approximate stiffness matrix, derived from minimum strain energy principles, has elements which vary linearly with load, and the latent root plot for the linearized matrix is superimposed on the exact plot.

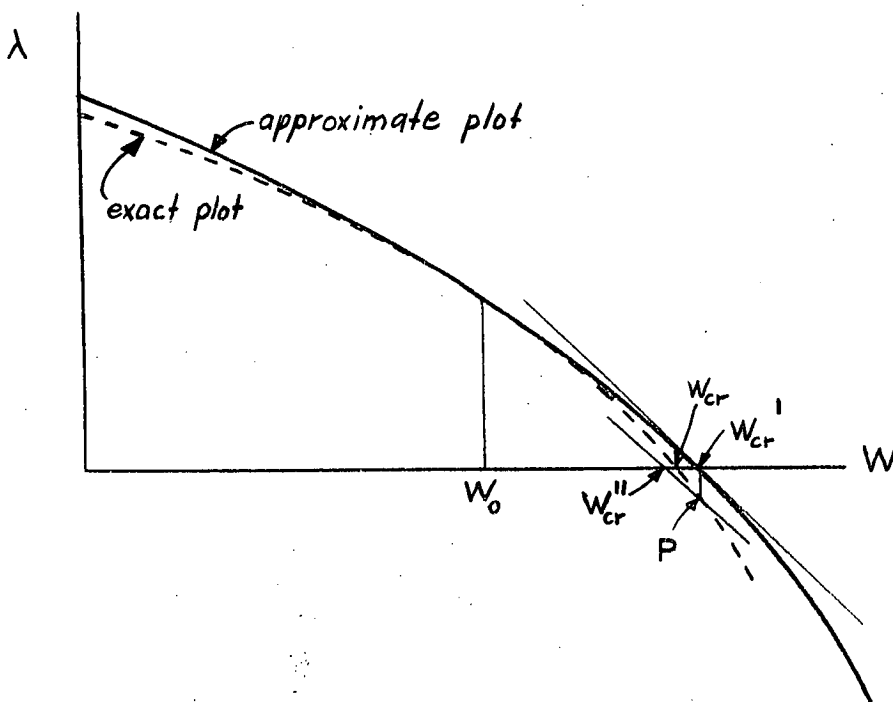


figure 3.3 - Latent root plots

From the tangent property of the individual elements of this matrix it is obvious that the two latent root plots are also tangent at the same value of the load,  $W_0$  say. The exact buckling load,  $W_{cr}$  is found from the intersection of the latent root curve on the load axis, and an approximate value  $W'_{cr}$  is similarly determined. From figure (3.2) it is seen that, whatever the trial value of  $P/Q$ , the linearized stiffness  $s$  of any member is always greater than the exact stiffness. Consequently the overall stiffness of the frame as a whole, of which the latent root is a measure, must also be everywhere greater than the exact stiffness or latent root, whence it follows that the latent root of the linearized matrix vanishes at a higher load than the exact latent root. In other words, linearization of the stiffness matrix yields upper bounds for the buckling load, and this is true irrespective of whether the trial load  $W_0$  is greater than or less than the exact buckling load  $W_{cr}$ . As explained previously,  $W_{cr}$  can be approached iteratively from above by using the calculated upper bound  $W'_{cr}$ , or a value somewhat less than this, as a new trial load in setting up a new linearized stiffness matrix from which a better value of the buckling load can be calculated. This repetitive process generally converges quite quickly, but in some problems it is desirable to have both an upper bound and a lower bound. In such cases the latent root plots provide a simple method. From figure (3.3) it can be seen that the plot corresponding to the linearized matrix is of necessity more nearly linear than the exact plot, so that rather than constructing the entire curve, an estimate of the upper bound is determined from a linear interpolation or extrapolation from two points on the approximate stiffness curve. With one of these points reasonably close to the upper bound, the loss of accuracy is usually small. The point  $P$  on the exact curve is then determined from an analysis of the exact stiffness matrix set up at  $W = W'_{cr}$ .

A lower bound for the buckling load is obtained from the intersection on the load axis of the straight line through  $P$  parallel to the tangent to the approximate curve at  $W'_{cr}$ , or alternatively, parallel to the straight line through the two points used for extrapolation or interpolation.

There are certain possibilities which do not yield true bounds for the buckling load, but if the following rules are observed the method is successful:

- (i) The point of tangency between the approximate and exact curves must lie above the load axis; this restriction can be verified by a few sketches. Mathematically this restriction is  $W_0 < W'_{cr}$ , which is easily satisfied and verified by subsequent calculations.
- (ii) If  $W'_{cr}$  is determined from two points on the approximate curve it must be an overestimate, and this can be achieved by extrapolation from two points both of which are above the load axis. This also ensures that the straight line through these points is flatter than the corresponding portion of the exact curve below the load axis, thereby eliminating the possibility of the value taken to be a lower bound falling above the exact buckling load.

True bounds are always obtained if  $W'_{cr}$  and the slope of the tangent are calculated accurately, provided of course that  $W_0$  is less than  $W'_{cr}$ . However, much labour is saved and little accuracy is lost by the linear extrapolation process.

In some cases it may not be possible to fulfil all the above requirements, but there are several alternative techniques; for example if we interpolate from two points on the approximate latent root curve, the estimate of the upper bound could fall below the exact buckling load. This becomes apparent in the next stage of computation, for the point P then lies above the load axis. The first estimate is then treated as a lower bound and an upper bound is determined by the same procedure as before, as long as it can be ensured that the straight line through P is flatter than the corresponding portion of the exact curve above the load axis.

The validity of these upper and lower bound techniques depends on the latent root curves being monotonically decreasing functions of load, with the approximate curve lying above the exact curve and tangent to it at  $W = W_0$ . It is acceptable from a geometric point of view and has been proved, at least in part, by Merchant (reference 1), using the single joint disturbance as a stiffness criterion.

### 3.5 PHYSICAL INTERPRETATION OF THE LINEARIZED STIFFNESS APPROACH

It has been shown that the buckling loads and modes are determined from a solution of the equations of equilibrium at the joints, namely

$$\tilde{K} \cdot \tilde{x} = \tilde{x} = \lambda \tilde{x} = \tilde{0} \quad (3.19)$$

where  $\tilde{K}$  is the exact stiffness matrix, a function of the load  $W$ , and  $\tilde{x}$  is the column vector defining the joint rotations (or generalized joint displacements) corresponding to the joint moments (or generalized joint forces), represented by the vector  $\tilde{x}$ .

The latent roots  $\lambda$  of the stiffness matrix are defined as the stiffnesses of the frame as a whole when it deforms in a mode given by the latent vectors of  $\tilde{K}$ . The frame first becomes unstable when one of the latent roots, the smallest vanishes; this is the fundamental buckling mode of the mathematical model of the frame, and it represents deformations to which the frame offers least resistance. Each element of the stiffness matrix depends on the stiffness  $s$  and carry over factor  $c$  of some or of all the members of the frame, and these in turn are transcendental functions of the axial loads in the members.

By a strain energy process the elements of the stiffness matrix are replaced by linear functions, and the equations of equilibrium become

$$\tilde{K}_E \cdot \tilde{x}' = \tilde{x}' = \lambda' \tilde{x}' = \tilde{0} \quad (3.20)$$

which are identifiable as approximations to the exact equations. Alternatively, these equations represent exactly the conditions of equilibrium at the joints of an approximate frame, namely one whose members have stiffness varying linearly with axial load. The linearized stiffness is tangent to the exact stiffness at some load,  $W_0$  say, so that the stiffness of the approximate frame as a whole, as represented by the latent roots  $\lambda'$  of  $\tilde{K}_E$ , is also tangent to the stiffness of the actual frame. Because the individual member stiffnesses are greater than the exact stiffnesses, except at  $W = W_0$  where they are equal,  $\lambda'$  is also greater than  $\lambda$ , and therefore vanishes at a higher load, that is the buckling load of the approximate frame is greater than the exact buckling load. Mathematically this is expressed by the inequality

$$W_{cr}' > W_{cr} \quad (3.21)$$



which becomes an equality when  $W_{cr} = W_0$ , for then each equals  $W_{cr}$ .

A lower bound for the buckling load is determined from the condition of zero stiffness of a second approximate frame, in this case one whose members have stiffness varying linearly with axial load, at the same rate as the first, but reduced to give the exact value at  $W = W'_{cr}$  instead of at  $W = W_0$ . By the same argument the smallest latent root of the linearized stiffness matrix for the second approximate frame vanishes at a load less than the exact buckling load, and we can write

$$W'_{cr} < W_{cr} \quad (3.22)$$

which also becomes an equality when the point of tangency between the latent root curves lies on the load axis.

This physical interpretation of the upper and lower bound technique is essentially a comparison method, similar to that of Temple and Bickley (reference 4) for the pin-ended column. An upper bound is obtained by comparison of the actual frame with a mathematical model whose members are stiffer. Its buckling load is therefore greater than that of the actual frame. Similarly, a lower bound is obtained by comparison with a less stiff mathematical model. Since the individual elements of the two linearized matrices are parallel, the curves of their latent roots against load are in general also parallel. The geometrical construction to find a lower bound makes use only of the curve for the stiffer frame and one point on the exact curve, but the essential ideas are the same; it is merely a convenient numerical technique for those cases in which a lower bound is required. As stated before, the upper bound process alone can be used to converge towards the exact buckling load and mode.

### 3.6 COMPUTATIONAL PROCEDURES

Several numerical techniques suggest themselves to calculate the buckling load and mode from the linearized stiffness matrices. Some of these are briefly described in this section, and later applied to examples.

#### (a) Latent root plot

This scheme was used at first as it appears to be the most profitable method of hand computation. The parallel shift method is used to calculate the smallest latent root for a number of load values, and the buckling load is determined graphically as the load

at which the smallest latent root is zero. The chief advantage of the linearized matrix in this method arises from the savings in computation, because the elements of the matrix are readily calculated, in contrast with the exact matrix whose setting up requires a much more extensive use of tables of stability functions. A further advantage is that the approximate latent root curve is more nearly linear, in fact quite often it is linear to sliderule accuracy, so that fewer points suffice to plot the curve. The buckling mode is obtained as the latent vector corresponding to the zero latent root. Convergence of the iterative technique to extract the smallest latent root is speeded up by using trial vectors resembling the buckling mode, and this information can be obtained from simple tests on inexpensive models, usually made of cardboard or wires.

At first one might expect the latent root plot for the linearized stiffness matrix to vary exactly linearly with load. Unfortunately this is so only if the mode, or latent vector, is independent of load, which is generally not the case. However in most problems the variation of mode with load is not severe, so that the approximately calculated latent root does in fact vary more nearly linearly with load than the exact plot.

Another possible feature of the linearized stiffness matrix is that the slope of the latent root plot be related to the latent roots of the matrix of the coefficients of load, but here again this is not the case unless the associated latent vectors of the two matrices are the same. Wittrick (reference 5) has shown that the slope of the plot at any load is given by the expression

$$\partial \lambda / \partial W = \tilde{x}_n^T \cdot \tilde{B} \cdot \tilde{x}_n \quad (3.23)$$

where  $\tilde{x}_n$  is the normalized latent vector,  $\tilde{x}_n^T$  is its transpose, and  $\tilde{B}$  is the matrix of coefficients of load, that is  $\tilde{B} = \partial \tilde{K} / \partial W$ . This is the quickest available method for calculating the slope of the latent root plot, and this, together with the value of the latent root, gives an estimate of the buckling load which is usually only a little above the more accurate upper bound value. The technique can be used repetitively to calculate the upper bound exactly, the process being akin to the Newton method for solving equations of the type  $f(x) = 0$ .

#### (b) Matrix inversion - multiplication

The linearized equations of equilibrium (3.20) can be written in the form

$$(\tilde{A} - W\tilde{B}) \cdot \tilde{x} = \tilde{0} \quad (3.24)$$

in which  $\tilde{A}$ ,  $\tilde{B}$  are symmetric matrices, the elements of  $\tilde{A}$  being the intercept values of the linear approximations, and the elements of  $\tilde{B}$  being the slope values. When both sides of this equation are multiplied by the inverse of  $\tilde{A}$ , denoted by  $\tilde{A}^{-1}$ , and divided by the scalar load parameter  $W$ , we obtain

$$(\tilde{A}^{-1} \cdot \tilde{B} - 1/W \tilde{I}) \cdot \tilde{x} = \tilde{0} \quad (3.25)$$

where  $\tilde{I}$  is the unit matrix. From this it is seen that the latent roots of the matrix  $(\tilde{A}^{-1} \cdot \tilde{B})$  are the reciprocals of the buckling loads, and the smallest buckling load therefore is obtained as the reciprocal of the largest latent root; the buckling modes are the associated latent vectors. A feature of this method is that all the buckling modes and loads are obtained, and the technique is advantageous if an electronic digital computer is available, but matrix inversion and multiplication by hand computation are to be avoided because of the large number of calculations in which there is no physical intuition to guide the human computer.

#### (c) Gravest mode intensification

This method is described by Allen (reference 6), and is frequently used in problems involving linear algebraic equations of the type

$$\tilde{A} \cdot \tilde{x} = W(\tilde{B} \cdot \tilde{x}) \quad (3.26)$$

such as arise also in vibration studies. It is essentially similar to that above; some trial mode, represented by the vector  $\tilde{x}$ , is substituted on the right hand side of equations (3.26) and a new mode is calculated by solving the equations thus obtained. This mode is then used in the original equations again, and another mode is calculated, and so on. The process can be shown to converge towards the fundamental buckling mode. Once the mode has been determined reasonably accurately, it is an easy matter to calculate the buckling load, usually from the so-called Rayleigh quotient, that is

$$W_{cr} = (\tilde{A} \cdot \tilde{x}) \cdot \tilde{x} / (\tilde{B} \cdot \tilde{x}) \cdot \tilde{x} \quad (3.27)$$

This expression is readily identified as a linear combination of all the equations of equilibrium, using the mode  $\tilde{x}$  as the weighting function. It is also the equation of conservation of strain energy. Any errors in the mode increase the value for  $W_{cr}$ , that is, the Rayleigh quotient provides an upper bound.

The rate of convergence to the gravest mode depends on the ratio of the first two buckling loads. Clearly if these two loads are close together, the convergence rate is extremely slow, and the equations need to be solved many times. Since the left hand side always remains the same, the process becomes inefficient, and it seems logical to solve these equations once and for all, which brings us again to the method of matrix inversion.

(d) Iterative method

A further simplification of the equations of equilibrium is affected by linearizing only the elements on the leading diagonal of the stiffness matrix, leaving the off diagonal elements constant at a reasonable load value. After dividing each equation by minus the coefficient of W on the diagonal, it is seen that the buckling loads can be obtained as the latent roots of the resulting matrix. However, frequently some of these are negative so that Gregory's shift method then yields the largest negative buckling load. An alternative procedure, overcoming this difficulty is to rearrange equations (3.24) in the form

$$(\tilde{C} - 1/W \tilde{D}) \cdot \tilde{x} = \tilde{0} \quad (3.28)$$

where  $\tilde{C}$  and  $\tilde{D}$  are the matrices obtained from  $\tilde{A}$  and  $\tilde{B}$  by dividing each equation by W and by the value of the element of  $\tilde{A}$  on the leading diagonal. A trial value for W is then chosen and the off diagonal elements are calculated, after which a new value for W is calculated as the reciprocal of the largest latent root of the resulting matrix. This is then used to modify the off-diagonal elements and the largest latent root is again extracted, and so on until agreement is reached. As before, the buckling mode is the associated latent vector.

If the numerically largest latent root is negative in this method, a shift of the elements on the diagonal must be used in order to obtain the largest positive latent root.

\* \* \* \* \*

Any of the above or other techniques are useful for the solution of equations (3.24). Each has its own merits, but in any particular case the problem should be examined closely before making a decision, keeping in mind the object of the analysis. Although the buckling load calculated from the linearized stiffness matrix is an upper bound, it is usually accurate enough for engineering purposes. The accuracy depends on the initial value chosen to set up the matrix, and often it is not difficult to guess this value to within 25% of the buckling load, and under these conditions the difference between the linearized stability functions and the exact functions is negligible so that the equations need to be set up only once.

Table 3.1 - Linearized stability functions

In order to test the new method for calculating buckling modes and loads, a number of simple frames are analyzed and the results of some are verified experimentally.

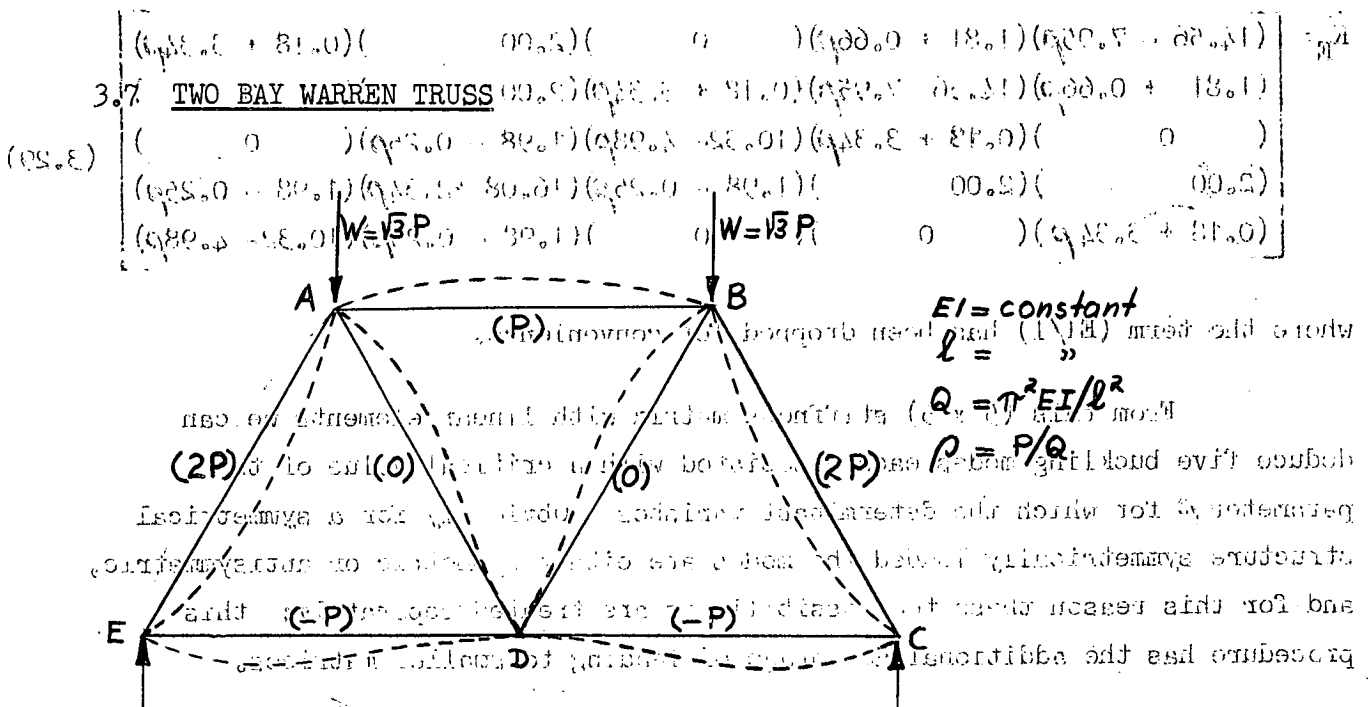


figure 3.4 - Two bay Warren truss buckling in its plane

As a first example, consider the buckling in its plane of the frame shown in figure (3.4). Using  $P = Q$  as a first guess to define an approximate deflected shape for each member, the linearized stability functions are calculated. [These have been calculated on the Elliott 503 computer and tabulated for a range of axial loads, but sufficient accuracy is obtained by taking differences of Livesley's

and Chandler's tables (reference 7)]. The linearized stability functions are shown in table (3.1)

Member	s	sc
AE, BC	$6.28 - 6.14\rho$	$0.18 + 3.34\rho$
AB	$4.28 - 1.81\rho$	$1.81 + 0.657\rho$
AD, BC	4.00	2.00
CD, DE	$4.04 + 1.17\rho$	$1.98 - 0.247\rho$

Example: for member AE  
the stiffness is  
 $s = 6.28 - 3.07 (P/Q)_{AE}$   
 $= 6.28 - 6.14\rho$

Table 3.1 - Linearized stability functions

in which  $\rho$  is a general load parameter for the frame, in this case the P/Q ratio of member AB; the P/Q ratios of the remaining members bear the same ratio to  $\rho$  as do the axial forces since EI and l are the same for all members. The linearized stiffness matrix is set up columnwise, by applying a unit rotation at each joint in turn; this can be done by adding the relevant stability functions shown in the table, and the result is

$$\tilde{K}_E = \begin{bmatrix} (14.56 - 7.95\rho)(1.81 + 0.66\rho)(0)(2.00)(0.18 + 3.34\rho) \\ (1.81 + 0.66\rho)(14.56 - 7.95\rho)(0.18 + 3.34\rho)(2.00)(0) \\ (0)(0.18 + 3.34\rho)(10.32 - 4.98\rho)(1.98 - 0.25\rho)(0) \\ (2.00)(2.00)(1.98 - 0.25\rho)(16.08 + 2.34\rho)(1.98 - 0.25\rho) \\ (0.18 + 3.34\rho)(0)(0)(1.98 - 0.25\rho)(10.32 - 4.98\rho) \end{bmatrix} \quad (3.29)$$

where the term (EI/l) has been dropped for convenience.

From this (5 x 5) stiffness matrix with linear elements we can deduce five buckling modes each associated with a critical value of the parameter  $\rho$  for which the determinant vanishes. Obviously for a symmetrical structure symmetrically loaded the modes are either symmetric or antisymmetric, and for this reason these two possibilities are treated separately; this procedure has the additional advantage of leading to smaller matrices.

(a) Antisymmetric modes

The antisymmetric modes are characterized by the relations

$$\theta_B = \theta_A \quad ; \quad \theta_E = \theta_C \quad (3.30)$$

so that the matrix is reduced to one of third order and we obtain

$$\tilde{K}_E = \begin{bmatrix} (16.37 - 7.29\rho)(0.18 + 3.34\rho)(2.00 \\ (0.18 + 3.34\rho)(10.32 - 4.98\rho)(1.98 - 0.25\rho) \\ (2.00)(1.98 - 0.25\rho)(8.04 + 1.17\rho) \end{bmatrix} \quad (3.31)$$

where the last row has been divided by 2 to preserve symmetry of the matrix.

In this particular case the determinant is readily handled by expansion, and, by equating the resulting cubic polynomial to zero, we obtain the buckling loads as the roots of the equation

$$\rho^3 + 0.19\rho^2 - 32.9\rho + 42.2 = 0 \quad (3.32)$$

The lowest root corresponds to the fundamental antisymmetric buckling mode, and a trial and error solution gives

$$\rho_1 = 1.37 \quad (3.33)$$

which is an upper bound for the first antisymmetric buckling load.

The remaining two roots of the cubic equation are  $\rho_4 = 6.39$ , and

$\rho_5 = -4.83$ ; the last of these represents a mode with the primary loading reversed.

(b) Symmetric modes

These modes satisfy the relations

$$\theta_B = -\theta_A \quad ; \quad \theta_E = -\theta_C \quad ; \quad \theta_D = 0 \quad (3.34)$$

and this information reduces the stiffness matrix to one of second order whose roots, obtained by expansion of the determinant, are

$$\rho_2 = 1.12 \quad \text{and} \quad \rho_3 = 3.72 \quad (3.35)$$

From the above two separate analyses it follows that the fundamental buckling mode of the Warren truss is symmetric, and an upper bound for its buckling load is 1.12. However, the first guess for this parameter was 1.00, and the difference between the tangents and the stability functions is very small over this range of load, so that the above result may be taken as exact to slide rule accuracy.

Substitution of this value in equations (3.29) together with equations (3.34) gives the buckling mode as

$$\theta_A : \theta_B : \theta_C : \theta_D : \theta_E = 1 : -1 : 0.812 : 0 : -0.812 \quad (3.36)$$

and the associated buckling load is

$$W_{cr} = 19.2 EI/l^2 \quad (3.37)$$

### 3.8 ROOF TRUSS BUCKLING IN ITS PLANE

#### (a) Analysis

This particular problem has been solved by various methods (see for example references 8 and 9), and it provides an excellent example of the power of the linearization method used in conjunction with model test information to speed up convergence of iterative latent root extraction techniques. The truss, its loading and joint notation are shown in figure (3.5), and the member properties together

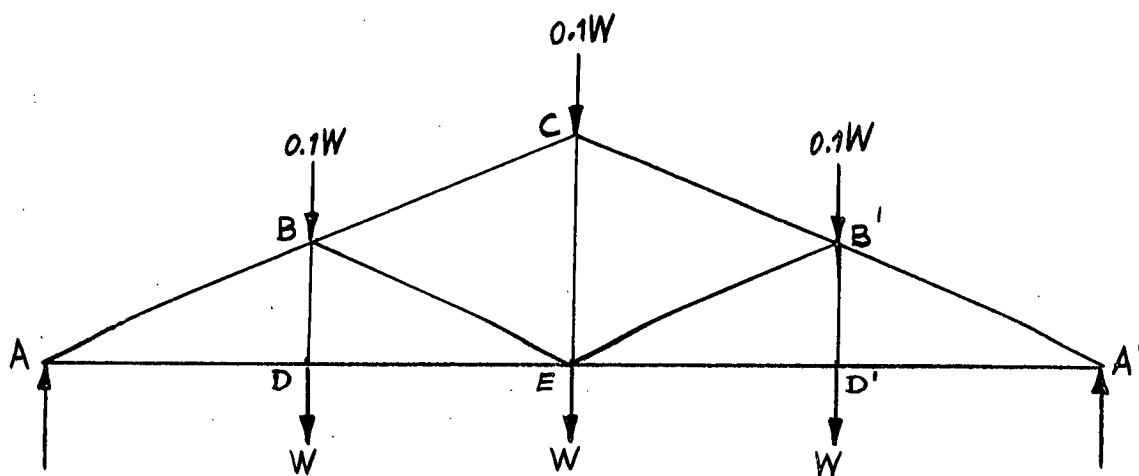


figure 3.5 - Roof truss

with the axial loads are given in table (3.2). Young's modulus is taken as that of mild steel,  $E = 30,000$  k.s.i.

Member	$l$ (in.)	$I$ (in <sup>4</sup> )	$k = EI/l$ (in-kip)	$Q = \pi^2 EI/l^2$ (kip)	$P$ (kip)	$P/Q$
AB, A'B'	129.24	5.20	1207	92.1	4.44W	4.82w
BC, B'C	129.24	5.20	1207	92.1	2.96W	3.21w
AD, A'D'	120.00	4.40	1100	90.5	-4.13W	-4.56w
DE, D'E	120.00	4.40	1100	90.5	-4.13W	-4.56w
BD, B'D'	48.00	0.70	438	90.0	-1.00W	-1.11w
BE, B'E	129.24	1.96	455	34.8	1.48W	4.26w
CE	96.00	0.96	300	30.9	-2.10W	-6.80w

Note  $w = W/100$

Table (3.2) - Data for roof truss



For the purpose of setting up a linearized stiffness matrix, it remains to select a suitable trial load. Normally a reasonable estimate can be made based on engineering judgement; in this case for example a good guess would be the load to make the largest P/Q ratio (in compression) about 1.5. However, in order to demonstrate the upper and lower bound technique, a somewhat poorer value is used. It was pointed out in section (3.3) that the guessing of a P/Q ratio merely defines the deflected shape of a member in terms of its end slopes. In this context it is quite legitimate to use P/Q ratios which do not conform to the primary load analysis, although this is of course desirable in subsequent trials. The linearized stiffness matrix for the roof truss set up with P/Q = 1 in compression members and P/Q = 0 in tension members, is given overleaf.

From model tests it was found that the truss buckles in an antisymmetric mode, and this valuable piece of information is used to reduce the matrix to one of order five, namely

$$\tilde{K}_E \cdot \tilde{x} = \begin{bmatrix} \begin{pmatrix} 9560 \\ -3930w \end{pmatrix} & \begin{pmatrix} 2190 \\ +3830w \end{pmatrix} & \begin{pmatrix} 0 \end{pmatrix} & \begin{pmatrix} 2200 \\ -1650w \end{pmatrix} & \begin{pmatrix} 0 \end{pmatrix} \\ \begin{pmatrix} 2190 \\ +3830w \end{pmatrix} & \begin{pmatrix} 14020 \\ -20400w \end{pmatrix} & \begin{pmatrix} 2190 \\ +2550w \end{pmatrix} & \begin{pmatrix} 876 \\ -160w \end{pmatrix} & \begin{pmatrix} 825 \\ +1270w \end{pmatrix} \\ \begin{pmatrix} 0 \end{pmatrix} & \begin{pmatrix} 2190 \\ +2550w \end{pmatrix} & \begin{pmatrix} 5760 \\ -5680w \end{pmatrix} & \begin{pmatrix} 0 \end{pmatrix} & \begin{pmatrix} 300 \\ -336w \end{pmatrix} \\ \begin{pmatrix} 2200 \\ -1650w \end{pmatrix} & \begin{pmatrix} 876 \\ -160w \end{pmatrix} & \begin{pmatrix} 0 \end{pmatrix} & \begin{pmatrix} 10550 \\ +13840w \end{pmatrix} & \begin{pmatrix} 2200 \\ -1650w \end{pmatrix} \\ \begin{pmatrix} 0 \end{pmatrix} & \begin{pmatrix} 825 \\ +1270w \end{pmatrix} & \begin{pmatrix} 300 \\ -336w \end{pmatrix} & \begin{pmatrix} 2200 \\ -1650w \end{pmatrix} & \begin{pmatrix} 6950 \\ +4430w \end{pmatrix} \end{bmatrix} \begin{bmatrix} \theta_A \\ \theta_B \\ \theta_C \\ \theta_D \\ \theta_E \end{bmatrix} \quad (3.39)$$

and the antisymmetry conditions are expressed by the equations

$$\theta_A' = \theta_A \quad ; \quad \theta_B' = \theta_B \quad ; \quad \theta_D' = \theta_D \quad (3.40)$$

In deriving equations (3.39) from (3.38), and third and fifth rows of the final equations were divided by 2 to preserve symmetry of the matrix.

Before embarking on the numerical solution of these equations it is well to review some of the basic properties of matrices:

- (i) when the leading diagonal of a matrix dominates, that is when every term on the leading diagonal is greater than the sum of the remaining terms in the same row or column, the determinant is positive, and the frame is therefore stable.
- (ii) if any of the terms on the leading diagonal are zero or negative, then the frame is unstable.

These facts are well known (see for example reference 10) and are useful aids in this type of problem especially because the elements are in linearized form, thus enabling quick estimates of both upper and lower bounds, which in turn provide a means of assessing whether or not the first guess to set up the equations was a "good" one. From equations (3.39) it is seen that dominance of the leading diagonal ceases at about  $w = 0.28$  in the second row, and a negative term on the diagonal first appears at  $w = 0.69$ , also in the second row. Thus the determinant vanishes somewhere between these two limits. The middle of the range is  $w = 0.48$ , and this corresponds to P/Q ratios of 2.3, 1.55, 0.24 respectively in the compression members AB, BC, BE; this at once confirms that the first guess was poor, as it was intended to be.

An upper bound for the buckling load is obtained by extrapolation from two points on the latent root curve above the load axis; from the above calculations, the points at  $w = 0.3$  and  $0.4$  should be adequate. The smallest latent roots at these points are extracted by a standard process using Gregory's parallel shift and using crude model measurements as a starting vector, that is

$$\theta_A : \theta_B : \theta_C : \theta_D : \theta_E \approx -0.5 : 1 : -1 : 0.1 : -0.2$$

In both cases slide rule calculations give reasonable convergence (about 5%) after eight iterations, and at that stage a good estimate for the latent root can be obtained by the so-called Rayleigh quotient. The calculations give

$$\begin{aligned} \lambda'_{0.3} &= 1927 ; \quad \tilde{x}'_{0.3} = -0.388 : 0.737 : -1 : 0.019 : -0.113 \\ \lambda'_{0.4} &= 481 ; \quad \tilde{x}'_{0.4} = -0.449 : 0.935 : -1 : 0.008 : -0.131 \end{aligned} \quad (3.41)$$

Extrapolation from these two points gives an upper bound for the buckling load as

$$w'_{cr} = 0.433 \quad \text{or} \quad W'_{cr} = 43.3 \text{ kips.} \quad (3.42)$$

the slope of the straight line through these points being -1446.

The exact stiffness matrix is then set up at this load, and using the same value for the shift, and the vector extrapolated from (3.41) to start the iteration process, convergence is achieved in only four cycles, giving

$$\lambda_{0.433} = -1200 \quad (3.43)$$

This represents the point P on the exact curve in figure (3.3), and the negative sign confirms that the load  $W = 43.3$  kips is an upper bound. From the intersection on the load axis of the line through this point and of slope -1446, we obtain a lower bound of 35.0 kips. Thus finally

$$35.0 < W_{cr} < 43.3 \text{ kips} \quad (3.44)$$

The difference between these two bounds is about 20%, which is reasonable considering the poor guess to set up the linearized stiffness matrix. Also, from several examples solved by this method, it has been found that the mean of the two bounds is usually very close to the exact value for the buckling load, that is

$$W_{cr} \approx 39.2 \text{ kips.} \quad (3.45)$$

This in fact exactly the value quoted by McMinn (reference 9).

Rather than repeating all the calculations with  $W = 39.2$  kips as a new trial load, improved bounds are obtained by calculating one additional point on the exact curve at  $W = 39.2$  kips. From the exact stiffness matrix set up at this load the smallest latent root is calculated as

$$\lambda_{0.392} = -54 \quad (3.46)$$

This is negative so that 39.2 kips is an upper bound. A new lower bound is determined from the intersection on the load axis of the straight line through this point and having the same slope as the line used for extrapolation, i.e. -1446. This gives

$$38.8 < W_{cr} < 39.2 \text{ kips.} \quad (3.47)$$

The difference between these two values is only 1% so that the buckling load can be taken as the mean of the range, that is

$$W_{cr} = 39.0 \text{ kips.} \quad (3.48)$$

The buckling mode is approximately the latent vector of the stiffness matrix set up at  $W = 39.2$ , which is

$$\theta_A : \theta_B : \theta_C : \theta_D : \theta_E = -0.580 : 1 : -0.902 : 0.033 : -0.155 \quad (3.49)$$

and  $\theta_{A'} = \theta_A ; \theta_{B'} = \theta_B ; \theta_{D'} = \theta_D$

(b) Experimental work

A model of the roof truss was made from 16SWG and 18SWG strips of mild steel plate cut to the required width. The spatial dimensions were scaled down by a factor of 12, and the second moments of area by approximately a factor of 400,000. The EI values of the model members were determined from measurement of deflections on simply supported, centrally loaded beams. Since the buckling load depends on the P/Q ratio of the members, the scale factor for the buckling load is given by

$$R = (\pi^2 EI/l^2)_{\text{actual}} / (\pi^2 EI/l^2)_{\text{model}}$$

The values of R for the individual members are shown in table (3.3), from which it is seen that there is considerable variation. Nevertheless

Member	R
AB, A'B'	2860
BC, B'C	2860
AD, A'D'	2810
DE, D'E	2810
BD, B'D'	2340
BE, B'E	2310
CE	2340

Average R = 2630

Table 3.3 - Scale factors

the model is a fair approximation to the actual truss. Also in this scaling down of the roof truss no attention has been paid to the relative  $l/r$  ratios of the members; this could alter appreciably the measured behaviour.

The truss was loaded with deadweights, and the response was measured by means of Huggenberger tensometers, opposing pairs being located on members BC and B'C, and a single instrument on members AB and A'B', lack of space preventing the use of a pair on these members. The location of the gauges was chosen approximately at the points of greatest curvature, judged by eye.

The Huggenberger gauges measure the total strain  $\epsilon$  ; the buckling component of the strain,  $\epsilon'$  is determined from this by allowing for the component due to the axial load, that is

$$\epsilon' = \epsilon \pm P/EA \quad (3.50)$$

where P is the axial load in the member, and A is its area.

The Southwell plot on strains is the graph of  $(\epsilon'/P)$  against  $\epsilon'$ . A typical plot obtained from two opposing tensometers is shown in figures (3.6) and (3.7). The line  $P/EA$  in figure (3.6) nearly bisects the two strain plots, which is a partial check on the proper functioning of the gauges. The average of the tensile and compressive strains was used to derive the Southwell plot. In the

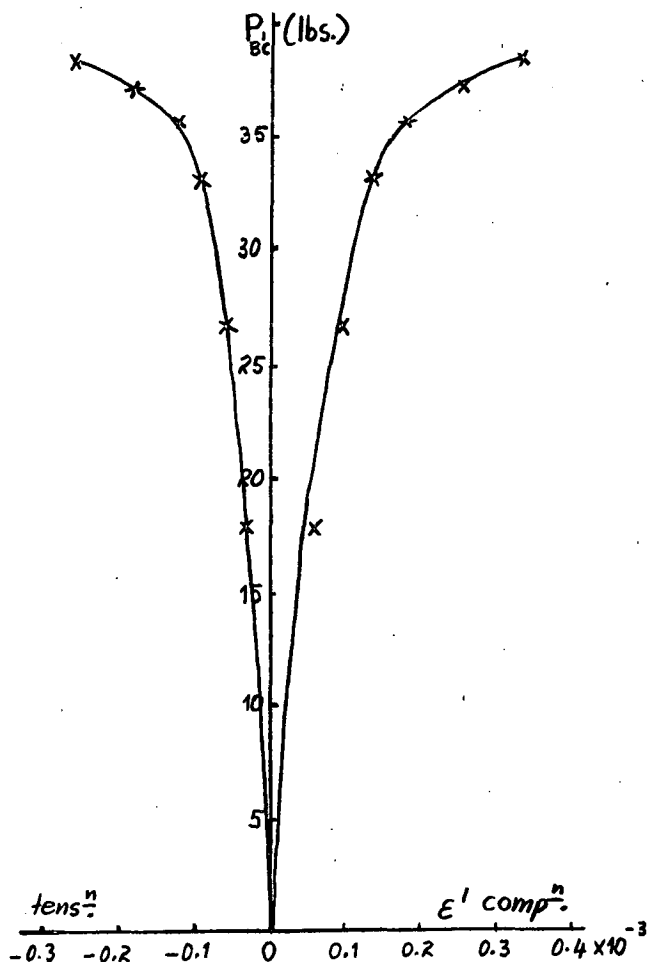


figure 3.6 - Strain in member B'C

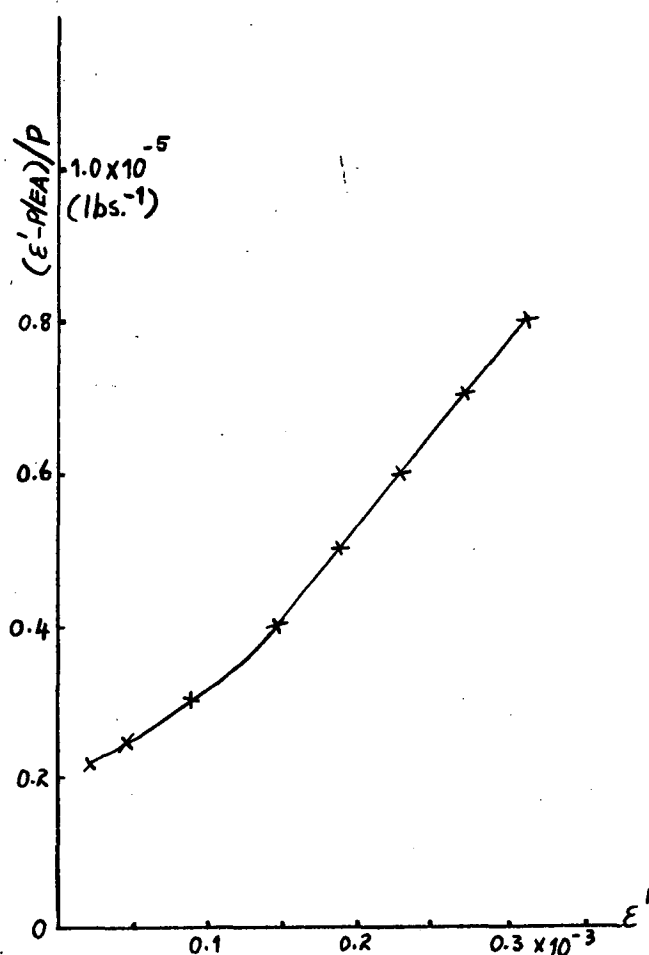


figure 3.7 - Southwell plot

low load region this plot is not linear, which is assumed to be due to initial imperfections of a kind tending to set the frame off in a higher buckling mode. From the linear portion of the Southwell plot the buckling value of the axial load in member B'C is obtained as the inverse slope, and the buckling load for the frame is calculated from this as

$$(W_{cr})_{\text{model}} = 14.6 \text{ lbs.} \quad (3.51)$$

The Southwell plots from the remaining tensometer readings gave the buckling load of the model as 14.9, 13.6, 13.3 lbs., the last two being for the single tensometers on members AB, A'B'.

Taking the mean of these results we have as an estimate of the buckling load of the model

$$(W_{cr})_{\text{model}} = 14.1 \text{ lbs.} \quad (3.52)$$

This value is related to the buckling load of the actual truss by the scale factor of table (3.3) which, for the whole frame, averages to 2630. However, since the behaviour of the frame depends to a greater extent on the stiffness of the compression members, it seems better to take the average value for the compression members only, that is 2680. This gives the buckling load for the actual truss as

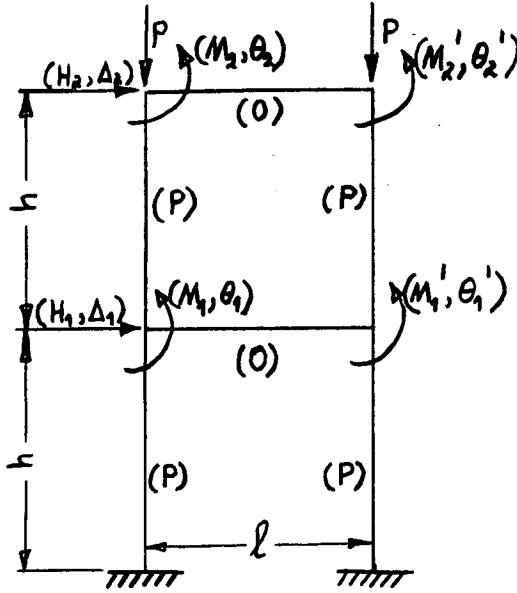
$$W_{cr} = 37.8 \text{ kips.} \quad (3.53)$$

which is in excellent agreement with the predicted value of 39.0 kips.

The model collapsed in the test at a load of just over 13 lbs. Subsequent measurements revealed a severe local thinning of member AB at approximately one quarter of its length from A, and the failure is attributed to this. Nevertheless the load applied covers a sufficient portion of the buckling load to justify the use of Southwell plots.

### 3.9 TWO-STORY RECTANGULAR PORTAL FRAME

As an example involving sidesway, consider the buckling in its plane of the frame shown in figure (3.8). The generalized displacements together with their corresponding generalized forces at the joints are



$EI = \text{constant}$

$h = 1$

Axial loads are shown in parentheses at the centres of the members.

figure 3.8 - Portal frame

included in the figure, six in all.

In problems involving sway, the  $P/Q$  ratio in the members is usually considerably less than unity and a value of 0.5 is a convenient one for setting up the linearized stiffness matrix. Proceeding in the usual way, we obtain the following linear coefficients

$$\begin{pmatrix} 48.2 \\ -48.0\rho \end{pmatrix} \begin{pmatrix} -24.1 \\ +24.0\rho \end{pmatrix} \begin{pmatrix} 0 \end{pmatrix} \begin{pmatrix} -6.02 \\ +1.06\rho \end{pmatrix} \begin{pmatrix} 0 \end{pmatrix} \begin{pmatrix} -6.02 \\ +1.06\rho \end{pmatrix} \\ \begin{pmatrix} -24.1 \\ +24.0\rho \end{pmatrix} \begin{pmatrix} 24.1 \\ -24.0\rho \end{pmatrix} \begin{pmatrix} 6.02 \\ -1.06\rho \end{pmatrix} \begin{pmatrix} 6.02 \\ -1.06\rho \end{pmatrix} \begin{pmatrix} 6.02 \\ -1.06\rho \end{pmatrix} \begin{pmatrix} 6.02 \\ -1.06\rho \end{pmatrix} \\ \begin{pmatrix} 0 \end{pmatrix} \begin{pmatrix} 6.02 \\ -1.06\rho \end{pmatrix} \begin{pmatrix} 12.1 \\ -3.04\rho \end{pmatrix} \begin{pmatrix} 1.97 \\ +0.455\rho \end{pmatrix} \begin{pmatrix} 2.00 \end{pmatrix} \begin{pmatrix} 0 \end{pmatrix} \\ \begin{pmatrix} -6.02 \\ +1.06\rho \end{pmatrix} \begin{pmatrix} 6.02 \\ -1.06\rho \end{pmatrix} \begin{pmatrix} 1.97 \\ +0.455\rho \end{pmatrix} \begin{pmatrix} 8.05 \\ -1.52\rho \end{pmatrix} \begin{pmatrix} 0 \end{pmatrix} \begin{pmatrix} 2.00 \end{pmatrix} \\ \begin{pmatrix} 0 \end{pmatrix} \begin{pmatrix} 6.02 \\ -1.06\rho \end{pmatrix} \begin{pmatrix} 2.00 \end{pmatrix} \begin{pmatrix} 0 \end{pmatrix} \begin{pmatrix} 12.1 \\ -3.04\rho \end{pmatrix} \begin{pmatrix} 1.97 \\ +0.455\rho \end{pmatrix} \\ \begin{pmatrix} -6.02 \\ +1.06\rho \end{pmatrix} \begin{pmatrix} 6.02 \\ -1.06\rho \end{pmatrix} \begin{pmatrix} 0 \end{pmatrix} \begin{pmatrix} 2.00 \end{pmatrix} \begin{pmatrix} 1.97 \\ +0.455\rho \end{pmatrix} \begin{pmatrix} 8.05 \\ -1.52\rho \end{pmatrix} \end{pmatrix} \quad (3.54)$$

Writing this in matrix notation, and equating to zero the disturbing forces, we put this in the form

$$\tilde{A} \cdot \tilde{x} = \tilde{B} \cdot \tilde{x} \quad (3.55)$$

in which  $\tilde{x}$  is the vector of the generalized joint displacements and  $\tilde{A}$  and  $\tilde{B}$  are the component matrices in equations (3.54). The solution of equations (3.55) is contained in the equation

$$(1/\rho) \tilde{x} = (\tilde{A}^{-1} \tilde{B}) \cdot \tilde{x} \quad (3.56)$$

in which  $\tilde{A}^{-1}$  denotes the inverse of the matrix  $\tilde{A}$ . This solution is most easily achieved by Gaussian elimination, details of which are found in most standard textbooks on numerical methods. In this case we obtain

$$(1/\rho) \begin{bmatrix} \Delta_1/1 \\ \Delta_2/1 \\ \theta_1 \\ \theta_2 \\ \theta'_1 \\ \theta'_2 \end{bmatrix} = \begin{bmatrix} 0.949 & 0.357 & -0.014 & 0.026 & -0.014 & 0.026 \\ -0.446 & 2.12 & -0.003 & 0.065 & -0.003 & 0.065 \\ 0.091 & -0.718 & 0.285 & -0.103 & -0.053 & -0.003 \\ 0.709 & -0.820 & -0.144 & 0.204 & 0.040 & -0.078 \\ 0.091 & -0.718 & -0.053 & -0.003 & 0.285 & -0.103 \\ 0.709 & -0.820 & 0.040 & -0.078 & -0.144 & 0.204 \end{bmatrix} \begin{bmatrix} \Delta_1/1 \\ \Delta_2/1 \\ \theta_1 \\ \theta_2 \\ \theta'_1 \\ \theta'_2 \end{bmatrix} \quad (3.57)$$

From physical considerations this matrix should possess a number of reciprocity relations; in this case there are 16, for example the effect of  $\theta_1$  on  $\theta_2$  should be the same as the effect of  $\theta'_1$  on  $\theta'_2$ , and the effect of  $\Delta_1$  on  $\theta_1$  should be the same as  $\Delta_1$  on  $\theta'_1$  and so on. Although these equalities were not obtained due to rounding-off errors, they have been included in equations (3.57) by averaging the differences, which in no case amounted to more than 3%.

The fundamental buckling load is seen to be the reciprocal of the largest latent root of the matrix in (3.57), and the mode is the associated latent vector.

On a crude cardboard model the mode was observed to be antisymmetric, that is

$$\theta'_1 = \theta_1 \quad ; \quad \theta'_2 = \theta_2 \quad (3.58)$$

Using this information, the above (6 x 6) matrix is reduced to the (4 x 4) matrix

$$(1/\rho) \begin{bmatrix} \Delta_1/1 \\ \Delta_2/1 \\ \theta_1 \\ \theta_2 \end{bmatrix} = \begin{bmatrix} 0.949 & 0.357 & -0.028 & 0.052 \\ -0.446 & 2.12 & -0.006 & 0.130 \\ 0.091 & -0.718 & 0.232 & -0.106 \\ 0.709 & -0.820 & -0.104 & 0.126 \end{bmatrix} \begin{bmatrix} \Delta_1/1 \\ \Delta_2/1 \\ \theta_1 \\ \theta_2 \end{bmatrix} \quad (3.59)$$



Rough measurements on the model gave the modal vector approximately as

$$\begin{pmatrix} 0.4 & 1 & -0.5 & -0.3 \end{pmatrix} \quad (3.60)$$

Multiplying this into the matrix (3.59) we obtain the vector

$$1.908 \begin{pmatrix} 0.386 & 1 & -0.402 & -0.274 \end{pmatrix} \quad (3.61)$$

where the factor 1.908 is chosen merely to reduce the largest element of the vector to unity so that the vector can be compared with the previous vector. This factor is also an estimate of the latent root at this stage. Continuing the process, we find in succession the vectors

$$\begin{array}{l} 1.916 \begin{pmatrix} 0.376 & 1 & -0.390 & -0.281 \end{pmatrix} \\ 1.919 \begin{pmatrix} 0.370 & 1 & -0.388 & -0.286 \end{pmatrix} \\ 1.922 \begin{pmatrix} 0.366 & 1 & -0.387 & -0.288 \end{pmatrix} \\ 1.924 \begin{pmatrix} 0.364 & 1 & -0.386 & -0.290 \end{pmatrix} \\ 1.924 \begin{pmatrix} 0.363 & 1 & -0.386 & -0.290 \end{pmatrix} \end{array} \quad (3.62)$$

Thus the process has converged after only six iterations, the fundamental buckling mode being the last vector, and the corresponding buckling load is the reciprocal of the largest latent root, that is

$$\rho_{cr} = 1/1.924 = 0.520 \quad (3.63)$$

As a check on the arithmetic, the above mode is substituted in the equation of conservation of energy, (see equation 3.27) using the matrices  $\tilde{A}$  and  $\tilde{B}$  of equation (3.55), yielding

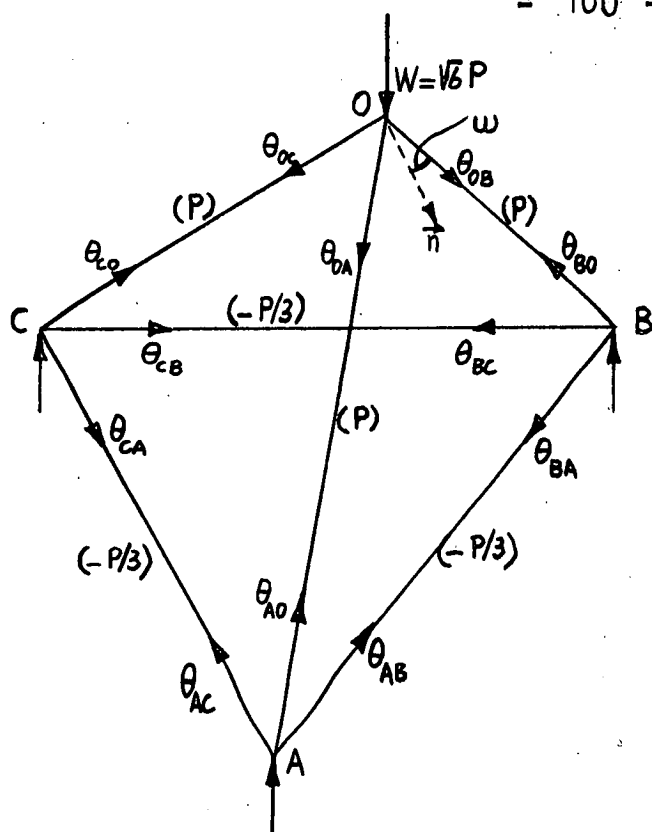
$$\rho_{cr} = 0.521 \quad (3.64)$$

which agrees with the previous value.

It is to be noted that in this example the condition of symmetry could have been fed in at an earlier stage, namely after setting up the complete (6 x 6) stiffness matrix. This reduces it to a (4 x 4) matrix, which would save a considerable amount of arithmetic in deriving the matrix  $(\tilde{A}^{-1} \cdot \tilde{B})$ .

### 3.10 TETRAHEDRAL FRAME

As an introduction to buckling in three dimensions, the stability of the tetrahedral frame of figure (3.9) is investigated. The frame is supported in the horizontal plane ABC, and loaded vertically at the apex O. All members are of equal length  $l$ , and they are of circular cross section, so that the bending stiffness  $EI$  is the same in all directions. The axial forces are shown in parentheses at the member centres.



$EI = \text{constant};$   
 $GJ = \text{constant},$   
 $Q = \frac{2EI}{l^2}$   
 $k = (EI/l); r = GJ/EI$   
 $\vec{n}$  is a vector, co-planar  
 with OAC, and perpendicular  
 to OC.

figure 3.9 - Tetrahedral frame

#### (a) Analysis

The buckling mode of this frame is specified by three rotations at each of the joints; for convenience in setting up the stiffness matrix, the rotations are chosen so that the vectors representing them lie along the axes of the members framing into the joint, the positive directions being away from the joint according to the right hand screw rule. Notation is by means of doubly subscripted variables, the first subscript denotes the joint and the second subscript denotes the direction of the rotation vector.

As the frame deforms, the members twist as well as bend, and the bending is non-planar unless the rotation vectors at opposite ends are co-planar.

The stiffness matrix is most easily set up by applying each of the twelve rotations in turn. The unit rotation vector is resolved into directions along and perpendicular to each of the members meeting at the joint. The former rotation produces equal and opposite end torques  $T_A$ ,  $T_B$ , which are expressed in terms of the twist by means of the relation

$$T = (GJ/l)\phi \quad (3.65)$$

where  $GJ$  is the torsional stiffness, and  $\phi$  is the angle of twist. The rotation vector perpendicular to the member produces bending in the plane perpendicular to that vector, and the bending moments  $M_A$ ,  $M_B$  are determined from the usual relations

$$\begin{aligned}
 M_A &= (EI/l)(s\psi) \\
 M_B &= (EI/l)(sc\psi)
 \end{aligned} \quad (3.66)$$



where  $s$  and  $sc$  are the stability functions, linearized at some trial load, and  $\psi$  is the angle of bending. The end moments and torques are resolved back into the directions of the rotation vectors, and summation gives the moment vectors corresponding to the joint rotations. The angles involved in the resolution of rotations and moments are mostly either  $30^\circ$  or  $60^\circ$ . One other angle is needed, this is the angle between a vector which is perpendicular to one of, and co-planar with, three members making up a plane and the vector along the member not lying in the same plane; e.g. angle  $\omega$  in figure (3.9) between OB and the vector  $\vec{n}$  which lies in the plane OAC and which is perpendicular to OC. The cosine of this angle is  $(\sqrt{3}/6)$ .

It is obvious that the buckling load for this tetrahedral frame must be such as to produce a  $(P/Q)$  ratio somewhere between 1.0 and 2.05 in the compression members. Thus a trial load of  $P = 1.5Q$  ought to be a good one. For this value the linearized stability functions are

$$\begin{aligned} s_{+P} &= 4.86 - 2.27\rho & ; & \quad s_{-P/3} = 4.04 + 0.390\rho \\ sc_{+P} &= 1.366 + 1.006\rho & ; & \quad sc_{-P/3} = 1.980 - 0.082\rho \end{aligned}$$

The following calculations give an indication of how easily the stiffness matrix is set up; for example for a unit rotation  $\theta_{OA}$ , with all other rotations zero, we have

$$\begin{aligned} \phi_{OA} &= 1 & ; & \quad \psi_{OA} = 0 \\ \phi_{OB} &= \phi_{OC} = \frac{1}{2} & ; & \quad \psi_{OB} = \psi_{OC} = \sqrt{3}/2 \end{aligned}$$

The end moments and torques are

$$\begin{aligned} T_{AO} &= T_{OA} = r k \phi_{OA} & ; & \quad m_{OA} = k s_{+P} \psi_{OA}; \quad m_{AO} = k sc_{+P} \psi_{OA} & ; \\ T_{BO} &= T_{OB} = r k \phi_{OB} & ; & \quad m_{OB} = k s_{+P} \psi_{OB}; \quad m_{BO} = k sc_{+P} \psi_{OB} \\ T_{CO} &= T_{OC} = r k \phi_{OC} & ; & \quad m_{OC} = k s_{+P} \psi_{OC}; \quad m_{CO} = k sc_{+P} \psi_{OC} \end{aligned}$$

All other torques and end moments are zero because they involve only rotations which are zero. The joint moments are obtained by summation as follows:

$$\begin{aligned} M_{OA} &= T_{OA} + \frac{1}{2} T_{OB} + \frac{1}{2} T_{OC} + 0 m_{OA} + \sqrt{3}/2 m_{OB} + \sqrt{3}/2 m_{OC} = k(1.50r + 7.29 - 3.41\rho) \\ M_{OB} &= \frac{1}{2} T_{OA} + T_{OB} + \frac{1}{2} T_{OC} + \sqrt{3}/6 m_{OA} + 0 m_{OB} + \sqrt{3}/6 m_{OC} = k(1.25r + 1.22 - 0.568\rho) \\ M_{OC} &= \frac{1}{2} T_{OA} + \frac{1}{2} T_{OB} + T_{OC} + \sqrt{3}/6 m_{OA} + \sqrt{3}/6 m_{OB} + 0 m_{OC} = k(1.25r + 1.22 - 0.568\rho) \\ M_{AO} &= T_{AO} + 0 m_{AO} = k(1.00r) \\ M_{AB} &= \frac{1}{2} T_{AO} + \sqrt{3}/6 m_{AO} = k(0.50r) \\ M_{AC} &= \frac{1}{2} T_{AO} + \sqrt{3}/6 m_{AO} = k(0.50r) \end{aligned} \tag{3.67}$$

$$\begin{aligned}
 M_{BO} &= T_{BO} & &= k(0.50r) \\
 M_{BA} &= \frac{1}{2}T_{BO} + \frac{\sqrt{3}}{2} m_{BO} & &= k(0.25r + 1.02 + 0.754\rho) \\
 M_{BC} &= \frac{1}{2}T_{BO} + \frac{\sqrt{3}}{6} m_{BO} & &= k(0.25r + 0.34 + 0.252\rho) \\
 M_{CO} &= T_{CO} & &= k(0.50r) \quad (3.67 \text{ cont'd.}) \\
 M_{CA} &= \frac{1}{2}T_{CO} + \frac{\sqrt{3}}{2} m_{CO} & &= k(0.25r + 1.02 + 0.754\rho) \\
 M_{CB} &= \frac{1}{2}T_{CO} + \frac{\sqrt{3}}{6} m_{CO} & &= k(0.25r + 0.34 + 0.252\rho)
 \end{aligned}$$

This completes one column of the stiffness matrix. Similar calculations for the remaining rotations give the complete linearized stiffness matrix, which is not shown here for reasons of insufficient space on a single page. Several of the columns of the matrix can be written down by a cyclic interchange of the subscript of the variables in earlier columns, and an interesting point is that there are only eleven different elements, each occurring several times within the matrix.

From tests on a light wire model it was found that the frame buckles symmetrically in the following manner:

$$\begin{aligned}
 \theta_{OA} = \theta_{AO} = 0 \quad ; \quad \theta_{OC} = -\theta_{OB} \quad ; \quad \theta_{CO} = -\theta_{BO} \\
 \theta_{CB} = -\theta_{BC} \quad ; \quad \theta_{CA} = -\theta_{BA} \quad ; \quad \theta_{AC} = -\theta_{AB}
 \end{aligned} \quad (3.68)$$

This information is used to reduce the linearized stiffness matrix to one of fifth order namely:

$$\begin{bmatrix}
 \begin{pmatrix} 6.25 \\ -2.84\rho \end{pmatrix} & \begin{pmatrix} 0.683 \\ +0.502\rho \end{pmatrix} & \begin{pmatrix} 0.335 \end{pmatrix} & \begin{pmatrix} -0.174 \\ -0.252\rho \end{pmatrix} & \begin{pmatrix} -0.857 \\ -0.754\rho \end{pmatrix} \\
 \begin{pmatrix} 0.683 \\ +0.502\rho \end{pmatrix} & \begin{pmatrix} 5.63 \\ -0.842\rho \end{pmatrix} & \begin{pmatrix} -0.328 \\ +0.021\rho \end{pmatrix} & \begin{pmatrix} 0.335 \end{pmatrix} & \begin{pmatrix} -1.328 \\ +0.062\rho \end{pmatrix} \\
 \begin{pmatrix} 0.335 \end{pmatrix} & \begin{pmatrix} -0.328 \\ +0.021\rho \end{pmatrix} & \begin{pmatrix} 5.42 \\ +0.647\rho \end{pmatrix} & \begin{pmatrix} 1.185 \\ +0.118\rho \end{pmatrix} & \begin{pmatrix} 1.513 \\ +0.098\rho \end{pmatrix} \\
 \begin{pmatrix} -0.174 \\ -0.252\rho \end{pmatrix} & \begin{pmatrix} 0.335 \end{pmatrix} & \begin{pmatrix} 1.185 \\ +0.118\rho \end{pmatrix} & \begin{pmatrix} 6.03 \\ -1.348\rho \end{pmatrix} & \begin{pmatrix} 1.715 \\ -0.568\rho \end{pmatrix} \\
 \begin{pmatrix} -0.857 \\ -0.754\rho \end{pmatrix} & \begin{pmatrix} -1.328 \\ +0.062\rho \end{pmatrix} & \begin{pmatrix} 1.513 \\ +0.098\rho \end{pmatrix} & \begin{pmatrix} 1.715 \\ -0.568\rho \end{pmatrix} & \begin{pmatrix} 7.01 \\ -1.410\rho \end{pmatrix}
 \end{bmatrix}
 \begin{bmatrix}
 \theta_{OB} \\
 \theta_{AB} \\
 \theta_{BO} \\
 \theta_{BA} \\
 \theta_{BC}
 \end{bmatrix}
 =
 \begin{bmatrix}
 0 \\
 0 \\
 0 \\
 0 \\
 0
 \end{bmatrix} \quad (3.69)$$

In these equations the measured numerical value of 0.670 for  $r$  has been used, and the factor  $k = EI/l$  has been cancelled. To determine the buckling mode and load these equations are rearranged by dividing each equation by minus  $\rho$  times the constant term of the element on the leading diagonal, giving

$$\begin{bmatrix}
 0.454 & -0.0805 & -0.0536p & 0.0403 & 0.1207 \\
 & -0.1093p & & +0.0278p & +0.1361p \\
 -0.0892 & & -0.0037 & & -0.0110 \\
 -0.1212p & 0.1497 & +0.0582p & -0.0595p & +0.234p \\
 0.0617p & -0.0038 & & -0.0218 & -0.0180 \\
 & +0.0605p & -0.1193 & -0.218p & -0.279p \\
 0.0417 & & -0.0196 & & 0.0942 \\
 +0.0289p & -0.0556p & -0.1966p & 0.224 & -0.284p \\
 0.1076 & -0.0088 & -0.0139 & 0.0810 & \\
 +0.1223p & +0.1892p & -0.216p & -0.244p & 0.201
 \end{bmatrix}
 \begin{bmatrix}
 \theta_{OB} \\
 \theta_{AB} \\
 \theta_{BO} \\
 \theta_{BA} \\
 \theta_{BC}
 \end{bmatrix}
 = p
 \begin{bmatrix}
 \theta_{OB} \\
 \theta_{AB} \\
 \theta_{BO} \\
 \theta_{BA} \\
 \theta_{BC}
 \end{bmatrix}
 \quad (3.70)$$

In these equations,  $p$  is the inverse load parameter,  $(1/\rho)$ , so that the fundamental buckling mode corresponds to the largest value of  $p$  satisfying equations (3.70). This can be determined iteratively as follows: a guessed value of  $p$  is inserted on the left hand side of the equations which are then seen to be a formulation of the usual latent root problems. The largest latent root of the matrix is then extracted by the usual process, and if this does not agree with the guessed value it is used as a new value, and so on until satisfactory agreement is reached.

The stiffness matrix of equations (3.69) was derived for  $\rho = 1.5$ , and this value is also used as a starting point in the above scheme. With  $p = (1/1.5)$ , the matrix on the left side of equations (3.70) becomes:

$$\begin{bmatrix}
 0.454 & -0.1534 & -0.0358 & 0.0588 & 0.212 \\
 -0.1700 & 0.1497 & 0.0351 & -0.0397 & 0.1451 \\
 -0.0412 & 0.0365 & -0.1193 & -0.1672 & -0.204 \\
 0.0610 & -0.0371 & -0.1506 & 0.224 & -0.0951 \\
 0.1891 & 0.1174 & -0.1579 & -0.0817 & 0.201
 \end{bmatrix}
 \quad (3.71)$$

As a starting vector in the largest latent root extraction procedure we use results of rough measurements on the model, that is

$$\begin{pmatrix} 1 & -0.2 & -0.2 & 0.1 & 0.5 \end{pmatrix}$$

and compute in succession the vectors

$$\begin{array}{lll}
 0.604 & \begin{pmatrix} 1 & -0.229 & -0.237 & 0.121 & 0.479 \end{pmatrix} \\
 0.606 & \begin{pmatrix} 1 & -0.243 & -0.230 & 0.143 & 0.462 \end{pmatrix} \\
 0.606 & \begin{pmatrix} 1 & -0.252 & -0.232 & 0.153 & 0.459 \end{pmatrix}
 \end{array}
 \quad (3.72)$$

At this stage the process has already converged satisfactorily, and the largest latent root equals 0.606 which is about 10% below the guessed value 0.667. The new value of  $p$  is substituted in equations (3.70) and the extraction process is continued with the last vector as a starting point. After three iterations it is found that the value of  $p$  is 0.598 which differs only 1.3% from the previous value. However, one more cycle is performed and a further two iterations to extract the largest latent root agree to within 1%. The value of  $p$  obtained is 0.597 so that the buckling load is

$$\rho_{cr} = 1/0.597 = 1.675$$

$$W_{cr} = 40.5 EI/l^2 \quad (3.73)$$

and the buckling mode is given by the ratios

$$\theta_{OB} : \theta_{AB} : \theta_{BO} : \theta_{BA} : \theta_{BC} = 1 : -0.262 : -0.212 : 0.170 : 0.436 \quad (3.74)$$

Although the value of 1.675 for the load parameter is an upper bound, it does not differ significantly from the trial value 1.50; the errors due to the linearization of the stability functions over this range are negligible. As a check on computations, the buckling mode (3.74) is substituted in the equation of conservation of energy using the original matrices  $\tilde{A}$  and  $\tilde{B}$  of equations (3.69); this gives  $\rho_{cr} = 1.660$  which is almost the same as above.

#### (b) Model Tests

A model of the tetrahedral frame was constructed from 1/8 in. diameter bronze welding rods, 17.9 in. long.  $EI$  and  $GJ$  were measured from bending and torsion tests, and verified by vibration tests. The two tests agreed to within 2%, and the average values obtained were

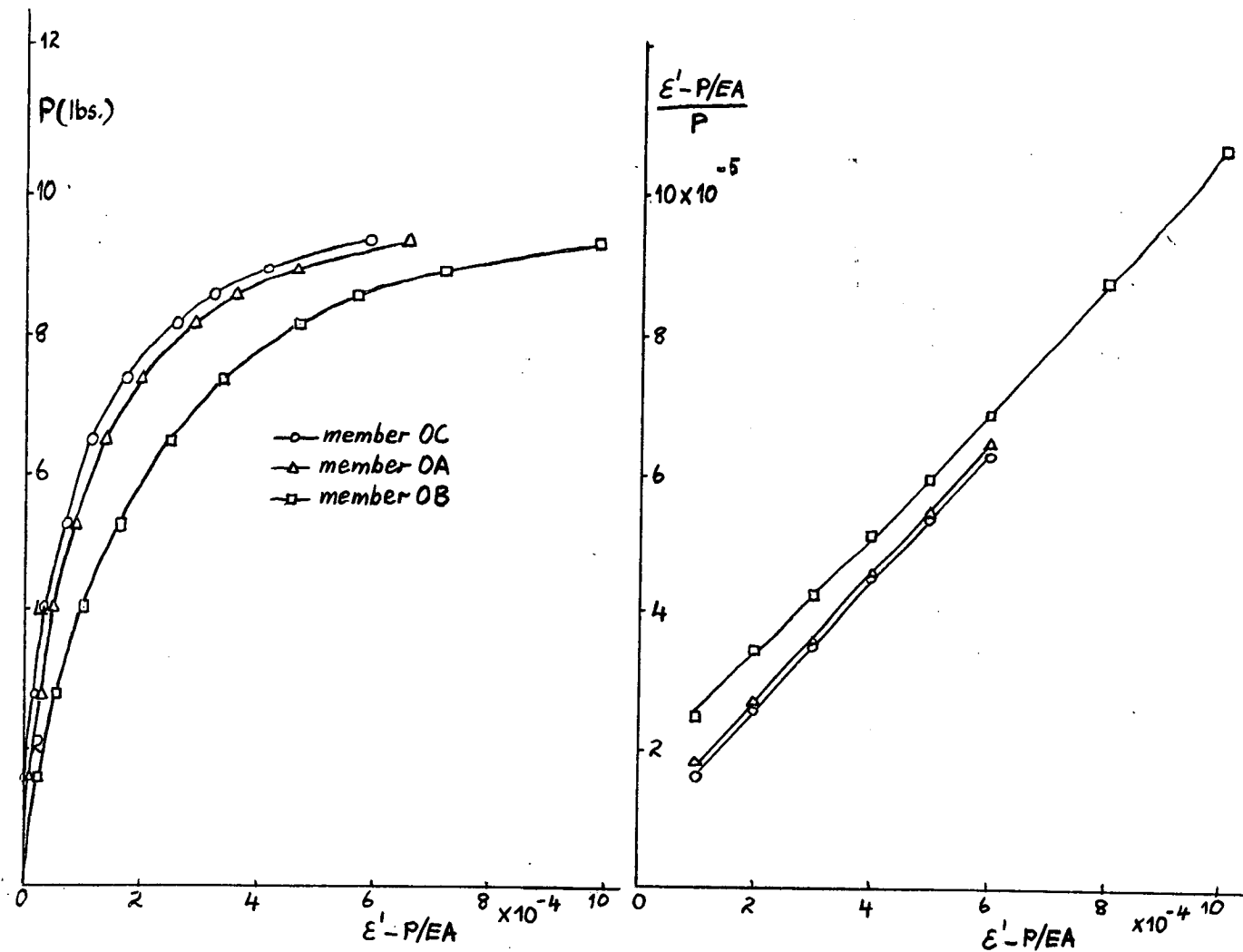
$$EI = 203 \text{ lb.in}^2 ; \quad GJ = 136 \text{ lb.in}^2.$$

giving  $r = GJ/EI = 0.670$ .

Based on simple elastic theory this value corresponds to a Poisson ratio of 0.49 which seems rather high. However, tests on similar rods gave Poisson ratios as high as 0.72 in some instances, which is of course impossible according to theory. Some of these rods were examined under the microscope, and it was found that the outer circular layer, about 0.005 in. thick, exhibited a much finer crystal structure than the body of the material. It is suspected that this layer has a lower stiffness; this would lower  $GJ$  proportionately more than  $EI$ , and hence the high apparent Poisson ratio. A 3/16 in. diameter rod was tested and gave  $EI = 915 \text{ lbs.in}^2$ ,  $GJ = 530 \text{ lb.in}^2$ ; these figures correspond to a

Poisson ratio of 0.72. The rod was then turned down in a lathe to 1/8in. diameter, and this had stiffnesses  $EI = 160 \text{ lb.in}^2$ ,  $GJ = 118 \text{ lb.in}^2$ , which gives a Poisson ratio of 0.36. This test confirms the effect of the weak outer layer on the standard bronze welding rods.

The tetrahedral frame was set up on flexible rubber supports, and Huggenberger tensometers were located approximately at the centres of the compression members, orientated in planes in which the bending was judged by eye to be maximum. The results are shown graphically in figure (3.10) together with the Southwell plots on strains. These are



(a) Strain readings

(b) Southwell plot

close to linear and the buckling load, obtained from the average inverse slopes, is

$$(W_{cr})_{exp} = 26.1 \text{ lbs.}$$

The calculated value of the buckling load is, from equation (3.73) with  $EI = 203 \text{ lb.in}^2$  and  $l = 17.9 \text{ in.}$ ,

$$(W_{cr})_{CALC} = 25.7 \text{ lbs.}$$

The two results are in excellent agreement. Also, the roughly measured mode, used as a starting vector in the calculations, does not differ greatly from calculated mode.

### 3.11 LATERAL BUCKLING OF THROUGH-BRIDGES

Lateral stability of trusses is a subject which has received a considerable amount of attention. One of the earliest attempts at this problem was by Engesser (reference 11), who treats the compression chord of the truss as a uniform bar under axial load  $P$ . Lateral restraint is provided by linear springs spaced at equal intervals along the bar. Assuming that the buckled shape of the bar is a series of half-sine waves of equal length  $v$ , Engesser shows that the buckling load is given by

$$P_{cr} = 2 \sqrt{k EI_c / s} \quad (3.75)$$

where  $EI_c$  is the flexural rigidity of the compression chord,  $k$  is the spring stiffness, and  $s$  is the spring spacing. This formula, although it is based on a crude model, has the merits of simplicity, and it has been shown by Bleich to work well provided the half wave length  $v$  is greater than 1.8 times the spring spacing. In trusses, the lateral restraint is provided by the web members rather than springs, and difficulties arise in assessing the "equivalent spring" stiffness. The web members also provide some rotational restraint and this is not considered in Engesser's mathematical model, nor is the twisting of the compression chord. These deficiencies, together with the fact that the analysis applies only to constant axial load chords, form a serious objection to the use of the simple formula.

Timoshenko (reference 12) provides an improved mathematical model by taking into account the variation in axial load along the compression chord, such as arises when the truss is loaded uniformly. Twisting of the compression chord and rotational restraint of the web members are still neglected, while the lateral restraint is replaced by a continuous elastic foundation. Again, difficulties arise in practice to estimate the 'modulus' of this foundation. An infinite Fourier series is used to define the buckled shape, and the Fourier coefficients are determined from minimum strain energy conditions. Quite reasonable estimates of the buckling load are obtained from only two terms in the series, but the accuracy, depends to a large extent on the accuracy of the calculated equivalent foundation modulus.



More recently, Horne (reference 13) presented an analysis of lateral stability of trusses which considers the truss as a whole unit, rather than just the compression chord as was done by Engesser and Timoshenko. Horne's analysis takes into account lateral bending and twisting of the compression chord and web members, but only twisting of the tension chord; lateral bending of the tension chord is neglected, justifiably, since it is usually small due to the large restraint provided by floorbeams and by the deck. Unfortunately Horne's results apply only to uniform compression chords under uniform axial load, but some modified results are presented for the application to non-uniform cases.

The above methods, and also several others not mentioned, give an approximate solution for the buckling mode and load of trusses. It is difficult to assess their degree of accuracy due to the complicated nature of the simplifications made in deriving the mathematical models; some of the simplifications result in a mathematical model which is stiffer than the actual frame, while others have a weakening effect. Then again, a strain energy analysis usually leads to an upper bound for the buckling load of the mathematical model, but with the uncertainty of whether this is stiffer or weaker than the actual truss, it is not possible to predict whether the results are safe or unsafe.

A more exact analysis must necessarily take into account the interaction between all the members of the truss, together with their stiffness variation with axial load. Livesley (reference 14) developed a general computer programme for the analysis of structures based on the deformation method. This takes into account the above factors and can be used to calculate the buckling load and mode of through truss bridges, although there is a restriction on the number of joints in the frame; the number depends on the storage capacity of the machine available. A similar approach is proposed by Schmidt and Stevens (reference 15), who present a comparison with experimental results and also with an "equivalent elastic line theory" for a six bay Warren truss.

The complete stiffness matrix for this type of structure is generally of high order, and manual computation is out of question. However, by using the linear combinations technique developed in section (2.7) of this thesis, the number of equations is reduced to as few as desired, and by linearizing the elements of the stiffness matrix, the buckling load and mode

are readily estimated with a slide rule or desk calculator as the computing medium. With inexpensive model tests as a guide, the important joint displacements and rotations are singled out, and the remainder are grouped as ratios under one or more parameters. Model tests are also used to advantage in defining simple functions to determine the weighting ratios in the individual groups. In a sense this technique is similar to the simplified analysis of Engesser and Timoshenko, but differs from them in not neglecting the less important deformations of the buckled truss. The buckling load, obtained as a solution of the reduced stiffness matrix, is an upper bound, but with good weighting ratios and a reasonable first guess to linearize the member stiffnesses, the discrepancy should not be large.

### 3.12 TWO-BAY WARREN TRUSS THROUGH-BRIDGE

As an introductory example, the stability of the bridge model shown in figure (3.11) is analyzed. All members are for

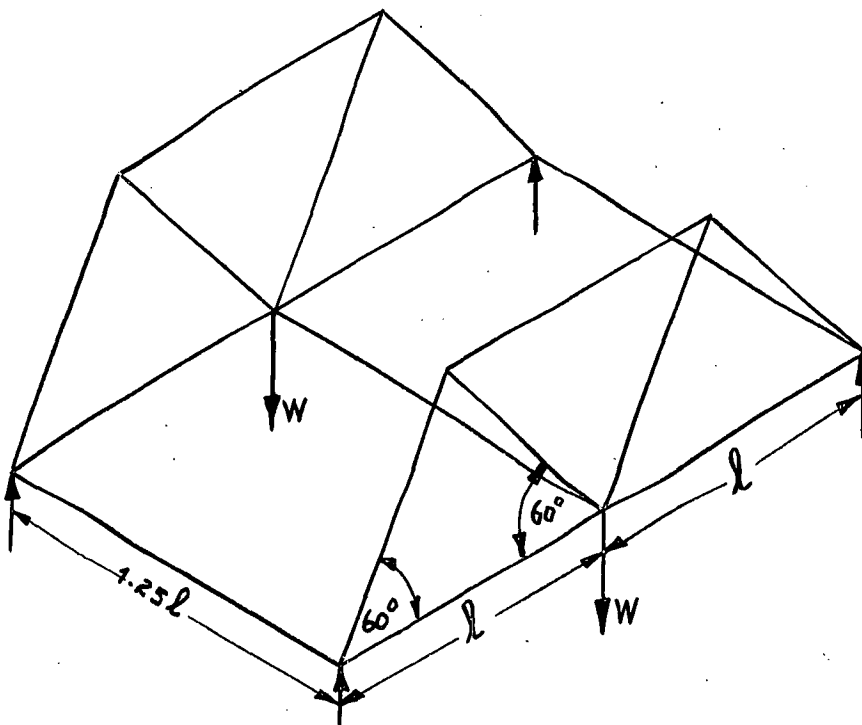


figure 3.11 - Warren truss bridge model

simplicity of the same circular cross section. The bridge is supported at the four lower chord end points, and each truss carries a load  $W$  at the centre of the lower chord and in the plane of the truss.

A rigorous analysis of this frame requires, in order to specify its deformed shape completely, six generalized displacements at each joint, namely three translations and three rotations, giving a total of sixty deformation parameters for the entire frame.

However, some of these can be eliminated and others neglected; from the conditions of support the translations at the four corners of support are zero, in-plane deformations are negligible, and, assuming that the deck is braced, the sideways of lower chord joints are zero. (In the tests conducted on a model the latter condition was achieved by **tying** cotton threads diagonally across the deck). These simplifications are common to most methods of attack on this kind of problem.

(a) Analysis

Even with the above simplifications, there remain a total of twenty-four generalized displacements to describe the buckled shape of the bridge model, namely two rotations at each joint, and a lateral displacement at each upper chord joint. Model observations indicated that the bridge as a whole buckles symmetrically about its longitudinal centreline, and that each truss buckles antisymmetrically out of its plane. It is assumed in the following analysis that this is the fundamental buckling mode, and six parameters are sufficient to describe this mode. These consist of five rotations and one displacement, as shown in figure (3.12) in which the axial forces are also given in parentheses at the centres of the members. Taking  $P = 0.6Q$  as a trial load, where  $Q$  is the Euler load of the truss members,

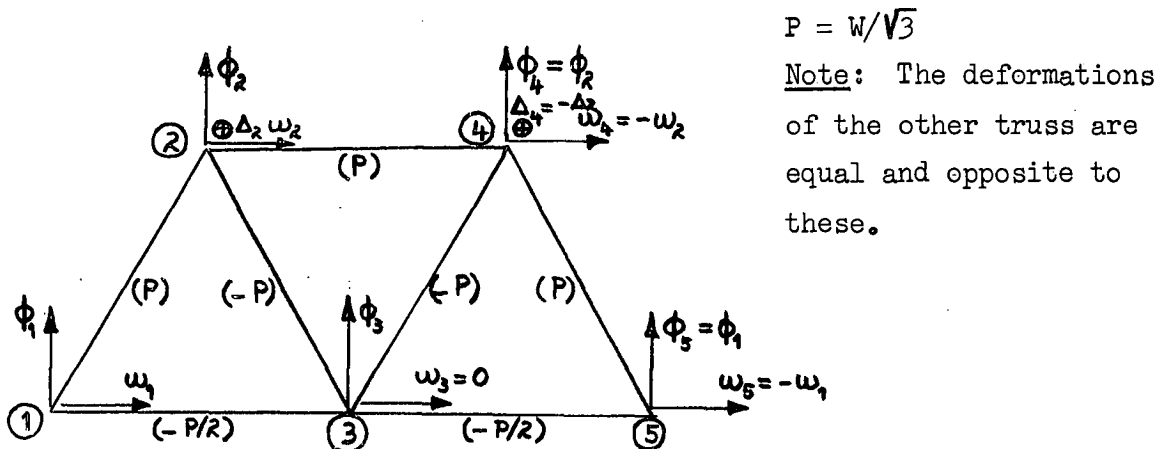


figure 3.12 - Joint rotations and sways

the linearized stiffness matrix is set up in the manner outlined in the previous section. The ratio  $GJ/EI = 0.835$  is used to express torques in terms of  $(EI/l)$ , and after dividing some rows of the matrix by 2, we obtain the symmetric matrix

$$\begin{bmatrix}
 (7.26) & (-1.401) & (-0.139) & (-1.206) & (1.994) & (-0.377) \\
 (-0.220\rho) & (+0.679\rho) & (+0.122\rho) & (-0.211\rho) & (-0.140\rho) & (+0.068\rho) \\
 (-1.401) & (5.70) & (-1.206) & (1.252) & (0) & (0.653) \\
 (+0.679\rho) & (-1.174\rho) & (-0.211\rho) & (+0.366\rho) & (0) & (-0.117\rho) \\
 (-0.139) & (-1.206) & (9.31) & (-0.013) & (-0.133) & (1.574) \\
 (+0.122\rho) & (-0.211\rho) & (-1.186\rho) & (+1.172\rho) & (-0.058\rho) & (-0.146\rho) \\
 (-1.206) & (1.252) & (-0.013) & (8.19) & (1.205) & (1.303) \\
 (-0.211\rho) & (+0.366\rho) & (+1.172\rho) & (-0.310\rho) & (-0.101\rho) & (-0.018\rho) \\
 (1.994) & (0) & (-0.133) & (1.205) & (6.45) & (0.375) \\
 (-0.140\rho) & (0) & (-0.058\rho) & (-0.101\rho) & (+0.894\rho) & (+0.057\rho) \\
 (-0.377) & (0.653) & (1.574) & (1.303) & (0.375) & (0.75341) \\
 (+0.068\rho) & (-0.117\rho) & (-0.146\rho) & (-0.018\rho) & (+0.057\rho) & (-0.38122\rho)
 \end{bmatrix}
 \begin{bmatrix}
 \phi_1 \\
 \omega_1 \\
 \phi_2 \\
 \omega_2 \\
 \phi_3 \\
 \Delta
 \end{bmatrix}
 =
 \begin{bmatrix}
 0 \\
 0 \\
 0 \\
 0 \\
 0 \\
 0
 \end{bmatrix}
 \quad (3.76)$$

In these equations the load parameter  $\rho$  is the P/Q ratio of the compression members. It is anticipated that the buckling mode is dominated by the sway component  $\Delta$ , and for this reason the last element is calculated to five significant figures, which is probably more than is warranted by taking differences of the tabulated stability functions to determine the linear approximations.

In this example the buckling load is determined by Gregory's method; a plot of the smallest latent root against the load parameter is shown in figure (3.13), and this is seen to be linear to within the accuracy of calculations. From the intersection on the load axis the buckling ~~point~~ <sup>load</sup> is obtained as

$$\rho_{cr} = 0.611 \quad (3.77)$$

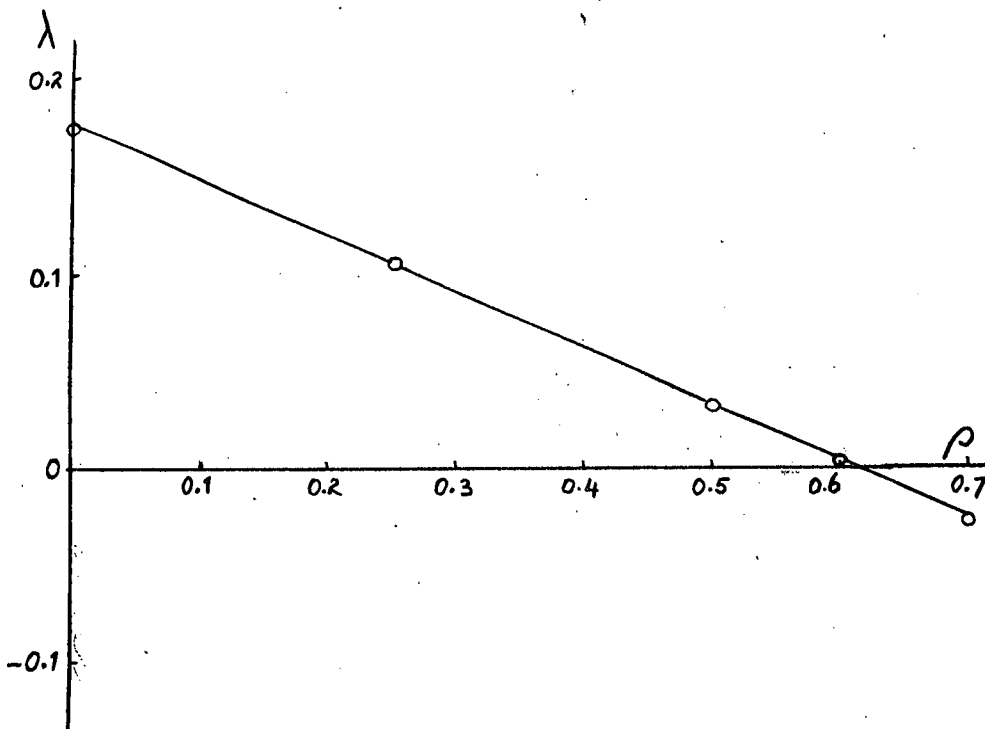


figure 3.13 - Latent root plot for bridge model

which is known to be an upper bound, but seeing that it is close to the trial value of 0.6, it may be taken as exact. In terms of the applied load  $W$  this gives

$$W_{cr} = 10.5 EI/l^2 \quad (3.78)$$

The buckling mode is taken as the latent vector corresponding to the smallest latent root at  $\lambda = 0.6$ , which is

$$\phi_1 : \omega_1 : \phi_2 : \omega_2 : \phi_3 : \Delta_2 = 0.019 : -0.219^{129} : -0.185 : -0.112 : -0.050 : 1 \quad (3.79)$$

### (b) Model tests

A test model of the through bridge was made having 8 in. long truss members and 10 in. floorbeams, all of 1/16 in. diameter bronze welding rods. These light sections were chosen deliberately so that the frame could be deformed easily by hand, and the large deformations observed permitted a qualitative statement to be made regarding the buckling mode which was used in the analysis. Due to the great flexibility of this light frame, measuring equipment such as dial gauges and Huggenberger tensometers are out of question, and sways on the loaded model were measured with a ruler. Since the maximum deflections were of the order of 1 inch this simple method proved to be sufficiently accurate. It was found that the two outward sways were very nearly equal but considerably larger than the inward sways which were also nearly equal. The average values are shown in figure (3.14), together with the Southwell plots. The latter are seen to be linear and parallel to within 1%. From the average slope the buckling load was found to be

$$W_{cr} = 2.14 \text{ lbs.}$$

Measurement with straight edges and a protractor, with the model loaded at 2.05 lbs., gave the buckling mode approximately as

$$\phi_1 : \omega_1 : \phi_2 : \omega_2 : \phi_3 : \Delta_2 \approx 0 : -1/8 : -1/5 : -1/10 : -1/20 : 1$$

which agrees well with the calculated mode.

A similar piece of bronze welding rod, when tested in tension gave the Young's modulus as  $E = 17.4 \times 10^6$  p.s.i., whence  $EI = 12.62 \text{ lb.in}^2$ .  $EI$  was also measured directly from bending tests giving an average value of  $12.76 \text{ lb.in}^2$ . Taking  $EI = 12.7 \text{ lb.in}^2$ , the predicted buckling load is, by equation (3.78)

$$W_{cr} = 2.08 \text{ lbs.}$$

which is in good agreement with the measured value of 2.14 lbs.

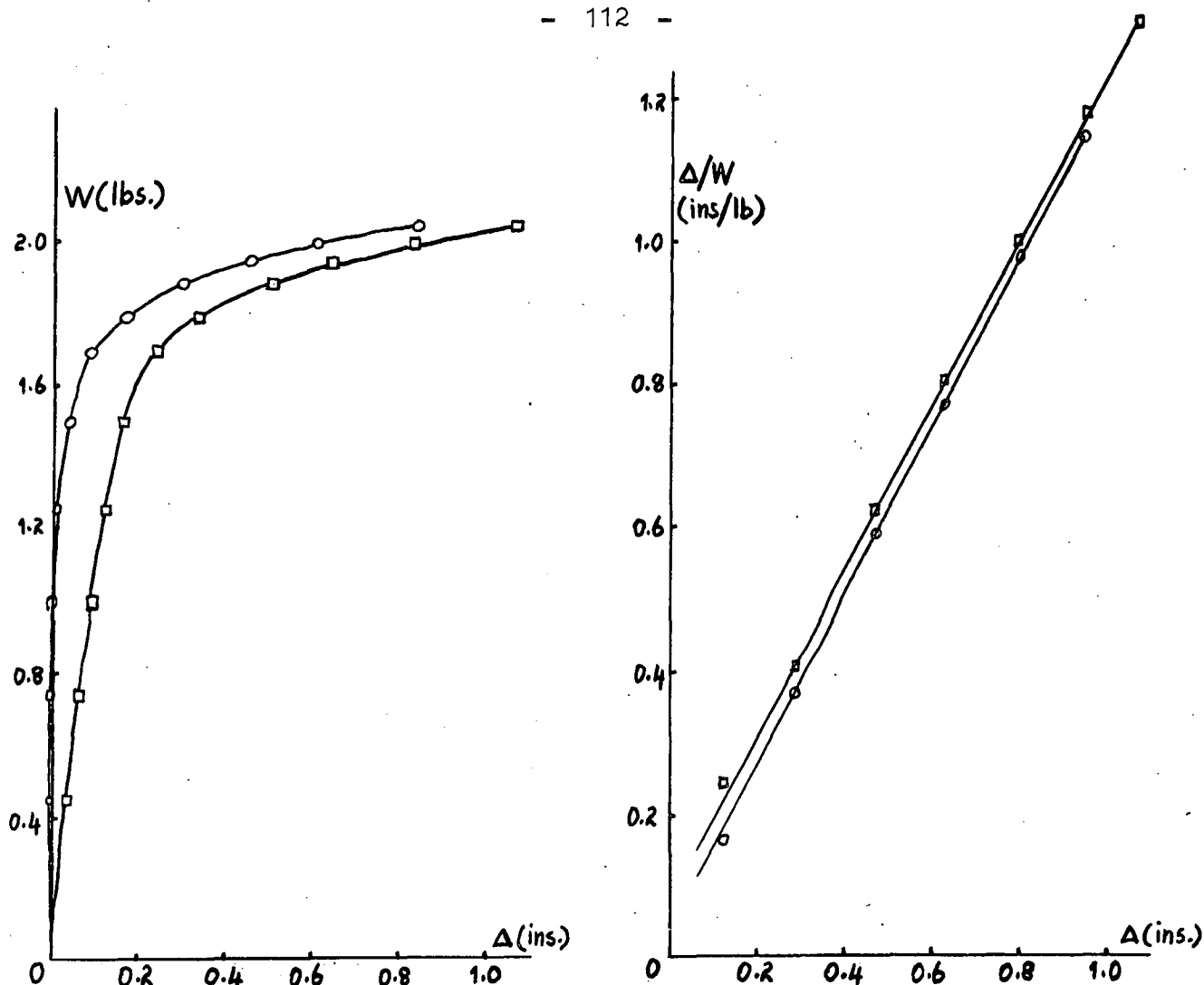


figure 3.14 - Measured sways

(c) Computer programs

In a discussion on a publication relating to the work in this chapter (reference 16), it was pointed out to the author that the calculated buckling load of the two bay Warren truss bridge is in error by some 12%. After subsequent private communication it was decided to check the calculations in this section by means of the electronic digital computing facility. Firstly a program was written to determine the buckling modes and loads of the bridge model by extracting all the latent roots and vectors of the matrix  $(\tilde{A}^{-1} \cdot \tilde{B})$ , where  $\tilde{A}$  and  $\tilde{B}$  are the matrices of equations (3.76). The program used was a standard library procedure which required these matrices to be read in as data. The results obtained were identical to those calculated on a slide rule; this meant that the matrices themselves were in error. A second program was then developed in which the matrix elements were generated in the machine and produced as output. Surprisingly these matrices agreed fairly closely to those set up by hand as can be seen in the following "matrix", in which the differences are expressed as

percentages of the exact values; the upper figures are the percentage errors in matrix  $\tilde{A}$ , while the lower figures are the percentage errors

$$\begin{array}{cccccc}
 \begin{pmatrix} 0.00 \\ 0.21 \end{pmatrix} & & & & & \\
 \begin{pmatrix} 0.31 \\ 0.06 \end{pmatrix} & \begin{pmatrix} 0.07 \\ 0.12 \end{pmatrix} & & & & \\
 \begin{pmatrix} 0.16 \\ 0.02 \end{pmatrix} & \begin{pmatrix} 0.07 \\ 0.08 \end{pmatrix} & \begin{pmatrix} 0.04 \\ 0.06 \end{pmatrix} & & & \\
 \begin{pmatrix} 0.07 \\ 0.08 \end{pmatrix} & \begin{pmatrix} 0.03 \\ 0.06 \end{pmatrix} & \begin{pmatrix} 6.34 \\ 0.18 \end{pmatrix} & \begin{pmatrix} 0.07 \\ 2.29 \end{pmatrix} & & \\
 \begin{pmatrix} 0.09 \\ 1.93 \end{pmatrix} & \begin{pmatrix} 0.00 \\ 0.00 \end{pmatrix} & \begin{pmatrix} 0.28 \\ 0.54 \end{pmatrix} & \begin{pmatrix} 0.91 \\ 0.50 \end{pmatrix} & \begin{pmatrix} 0.03 \\ 0.38 \end{pmatrix} & \\
 \begin{pmatrix} 0.05 \\ 0.04 \end{pmatrix} & \begin{pmatrix} 0.06 \\ 0.03 \end{pmatrix} & \begin{pmatrix} 4.46 \\ 0.01 \end{pmatrix} & \begin{pmatrix} 0.12 \\ 0.31 \end{pmatrix} & \begin{pmatrix} 0.37 \\ 0.11 \end{pmatrix} & \begin{pmatrix} 0.003 \\ 0.014 \end{pmatrix}
 \end{array}
 \quad \text{symmetric} \quad (3.80)$$

in the matrix  $\tilde{B}$ . The correct matrices were then re-used as data for the first program to calculate the fundamental buckling mode and load. The results obtained were

$$\phi_1 : \omega_1 : \phi_2 : \omega_2 : \phi_3 : \Delta_2 = 0.020 : -0.128 : -0.177 : -0.110 : -0.051 : 1 (3.8)$$

$$\rho_{cr} = 0.689 \quad (3.82)$$

As can be seen the mode differs little from the one calculated by hand, while the buckling load is 12% larger, as was indicated in the discussion cited above.

From these calculations we may conclude that the buckling load of this particular frame is very sensitive to small changes in individual member stiffnesses, since the incorrect matrices of equations (3.79) could be regarded as correct matrices for a similar frame with slightly changed member properties. On the other hand these changes have little effect on the buckling mode.

A third computer program was written to investigate in more detail the properties of the latent roots and vectors, and at the same time to check the accuracy of the linearization technique. The complete (24 x 24) stiffness matrix was generated in the machine using the exact stability functions. All its latent roots and vectors were extracted for a number of load values using a standard procedure, and the six smallest roots were printed as output. These are plotted against the

load parameter  $\rho$  in figure (3.15). It is interesting to note the multiple intersection points between the curves. Also, the latent vectors associated with the two least latent roots at low loads do not represent the

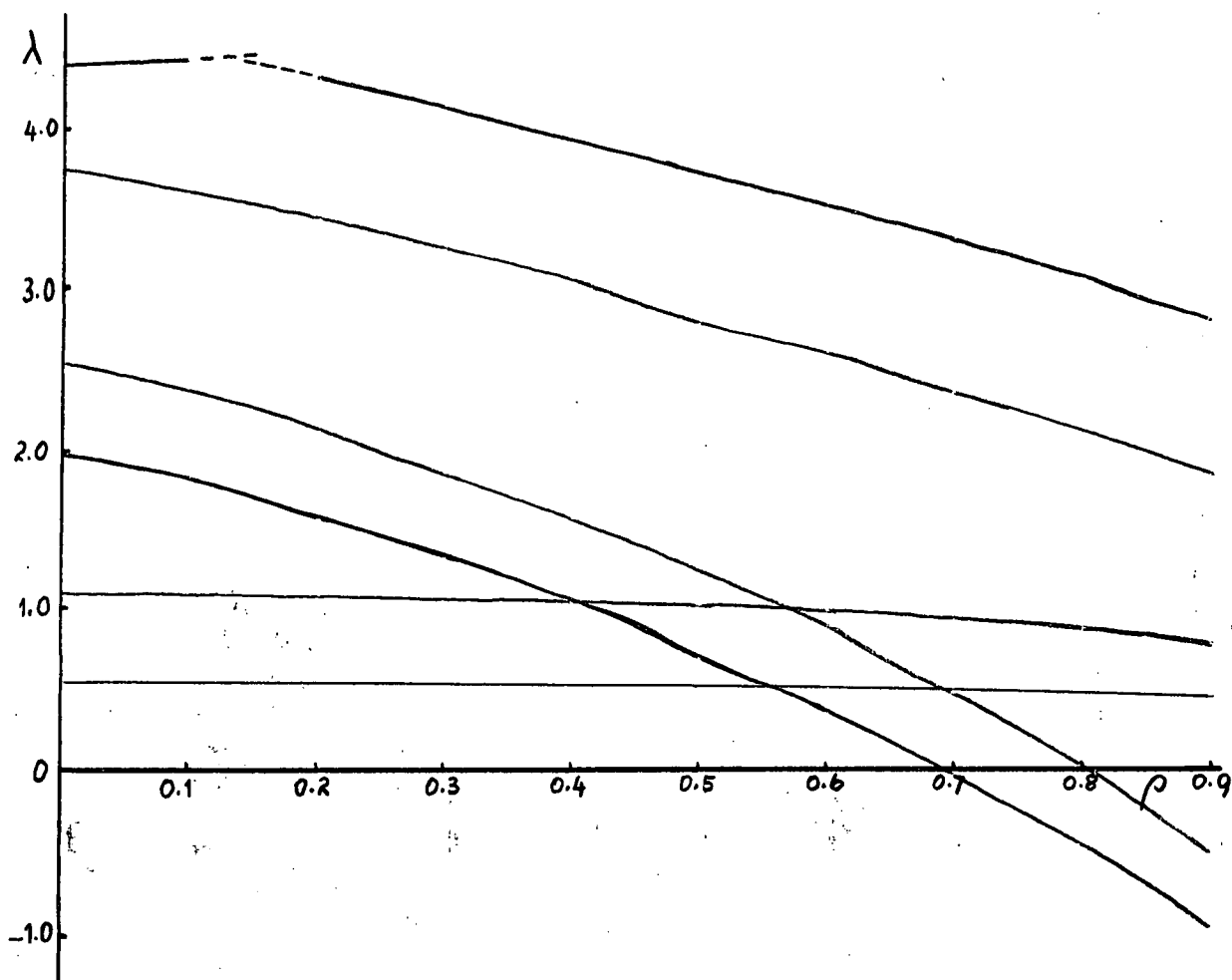


figure 3.15 - Latent roots of (24 x 24) exact stiffness matrix

fundamental or second buckling mode. That is, at low loads there are deformation patterns to which the frame offers a low stiffness, but these stiffnesses decrease only slowly with increasing load and are therefore not responsible for buckling. The deformation pattern of the first and second buckling modes have relatively higher stiffnesses at low loads, but deteriorate much more quickly and vanish earlier.

From the intersection of the latent root plots on the load axis the first and second buckling loads are obtained as

$$(\rho_{cr})_1 = 0.688 \quad ; \quad (\rho_{cr})_2 = 0.800 \quad (3.83)$$

The buckling modes are the latent vectors corresponding to the associated latent roots at these loads respectively. By interpolation between plotted points these are obtained as

$$\begin{aligned} (\phi_1 : \omega_1 : \phi_2 : \omega_2 : \phi_3 : \Delta_2)_{\text{mode } 1} &= 0.020 : -0.128 : -0.177 : -0.110 : -0.051 : 1 \\ (\phi_1 : \omega_1 : \phi_2 : \omega_2 : \phi_3 : \Delta_2)_{\text{mode } 2} &= 0.015 : -0.074 : -0.166 : -0.121 : -0.039 : 1 \end{aligned} \quad (3.84)$$



In both modes the trusses deform antisymmetrically, so that

$$\phi_5 = \phi_1 ; \phi_4 = \phi_2 ; \omega_5 = -\omega_1 ; \omega_4 = -\omega_2 ; \omega_3 = 0$$

The first mode is symmetrical about the bridge centreline while the second mode is antisymmetrical; this checks the simplifying statements made in part (a) of this section in order to reduce the number of unknowns to six. To the accuracy shown, the first mode calculated from the exact (24 x 24) stiffness matrix is identical to the approximate mode obtained from the linearized stiffness matrices. The second mode differs little from the first, the main change being a reduction in the tension chord deformations  $\phi_1, \omega_1, \phi_3$ . This is so because in the antisymmetric mode the floor beams have a reversal of curvature in the centre, and therefore offer more restraint to the truss. In the test model the floor beams were made of the same material as the truss members, but one and a quarter times as long. Consequently the resistance offered to the truss deformations at the deck level is small. Thus, although the stiffness of the floorbeams is trebled in the antisymmetric case, the overall buckling modes do not differ much. By the same token the two buckling loads are close together.

(d) Additional tests

From the extensive analytical treatment it is evident that the buckling load is sensitive to small changes in member properties, so that, in order to predict the buckling load reliably, the flexural and torsional stiffness of every member need to be known accurately. Four members were cut from the model and subjected to tension, bending, torsion and vibration tests to determine their EI and GJ values. The results were sufficiently close to warrant the use of the same values for each member. The average values obtained were

$$EI = 12.20 \text{ lb.in}^2 ; GJ = 7.16 \text{ lbsin}^2.$$

This gives the ratio  $GJ/EI = 0.587$ , whereas a value of 0.835 was used in previous calculations. Repeating the analysis with this value, the buckling load is obtained as

$$\rho_{cr} = 0.630$$

or

$$W_{cr} = 2.05 \text{ lbs.}$$

which is close to the measured value of 2.14 lb. It is perhaps disturbing to note that the measured value is higher than the calculated value; however taking into account the sensitivity of the calculated value, the difference cannot be regarded as significant.

### 3.13 EIGHT BAY THROUGH TRUSS BRIDGE

To conclude this chapter, a more realistic frame such as that in figure (3.16) is analyzed for stability; the buckling mode and load are estimated using linearized stability functions and simple polynomial functions to describe approximately the buckled shape. The results are compared with experimental work, and the merits of the alternative analytical approaches are briefly discussed.

#### (a) Description of model

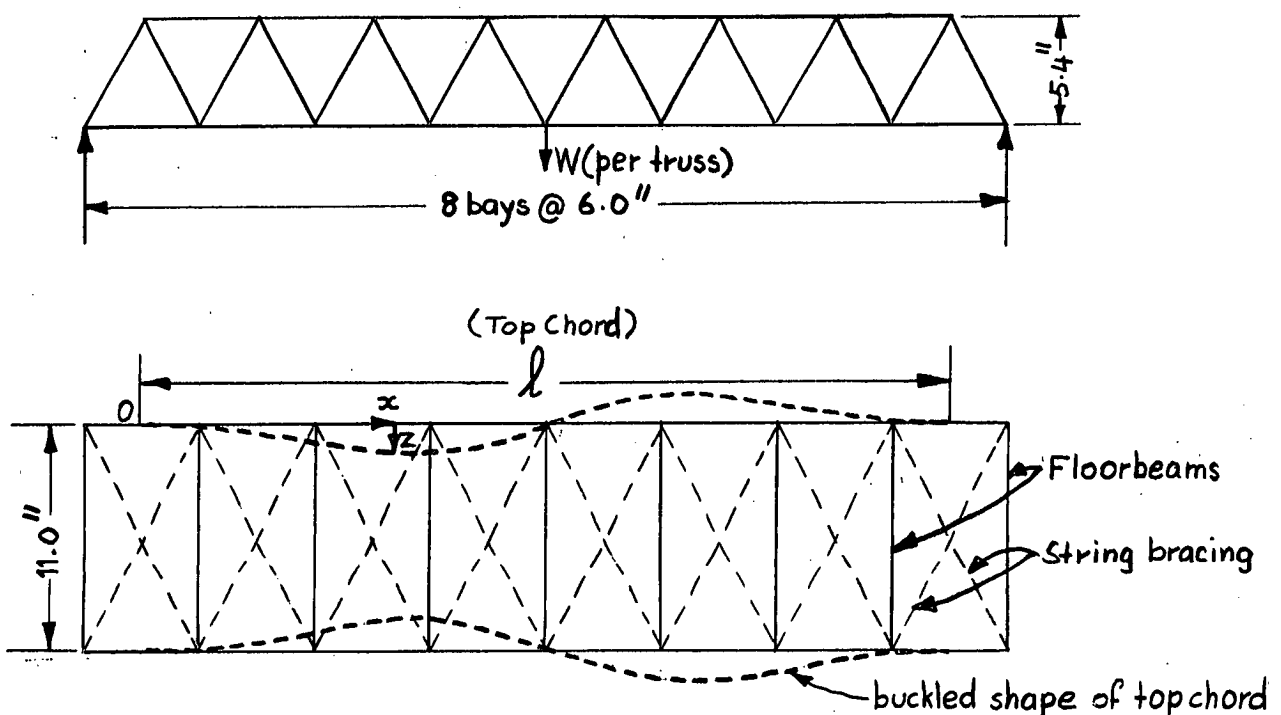


figure 3.16 - Through truss bridge

The tension and compression chords of the model were uniform and continuous, each  $3/16$  in. diameter bronze welding rod. The web was made by bending  $1/8$  in. diameter bronze welding rod to about  $1/8$  in. radius, so that, when assembled, the centrelines of the members intersected. Connecting the two trusses were floor beams made of  $3/16$  in. diameter bronze welding rods; these were connected below the tension chord so that some small eccentricity existed, but this was not deemed serious. All joints were silver soldered, and the finished model had a maximum initial crookedness of approximately  $1/16$  inch in the compression chords, the pattern being roughly in a half-wave form in each truss, and the two trusses were crooked in opposite senses. The whole bridge also exhibited a substantial amount of overall sidesway, but this was almost wholly eliminated by the diagonal bracing which was used to prevent swaying of the bridge during loading. The bridge was supported by resting it on the end floorbeams; knife edges were placed at one end, and rollers at the other end, so that the ends could approach each other fairly free of restraint

during the deformation of the bridge. Load, in the form of deadweights, was applied through wire hooks looped around the central floor beam in the planes of the trusses.

(b) Analysis

In both Engesser's and Timoshenko's treatments, an estimate of the equivalent spring stiffness is required. This can be obtained by considering a typical panel as in figure (3.17). The stiffness  $k$  is the force  $H$  required to produce unit lateral deflection  $\delta$  at the top chord joint. Clearly the panel shown deforms symmetrically about both the bridge centreline and about the panel centreline. Thus neither the floorbeams nor the tension chords twist. As a first approximation assume that the top chord joint is of the ball-type; this simplification means that the opposing diagonals and the floorbeam connecting them each

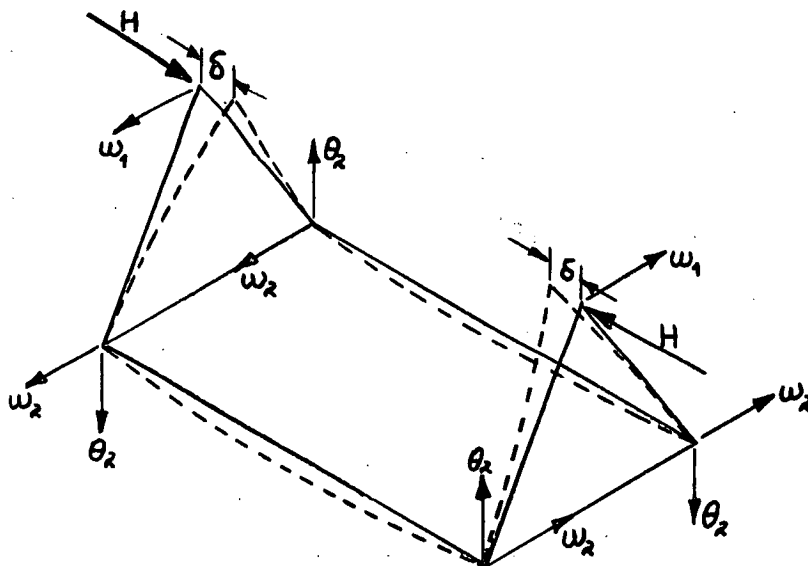


figure 3.17 - Isolated panel

behave as a rectangular portal frame as shown in figure (3.18), each carrying half of the force  $H$ . From an analysis of this frame, the stiffness  $k$  is readily obtained as

$$k = H/\delta = 2/l^2 [1/3EI_1 + b/2EI_2] \quad (3.85)$$

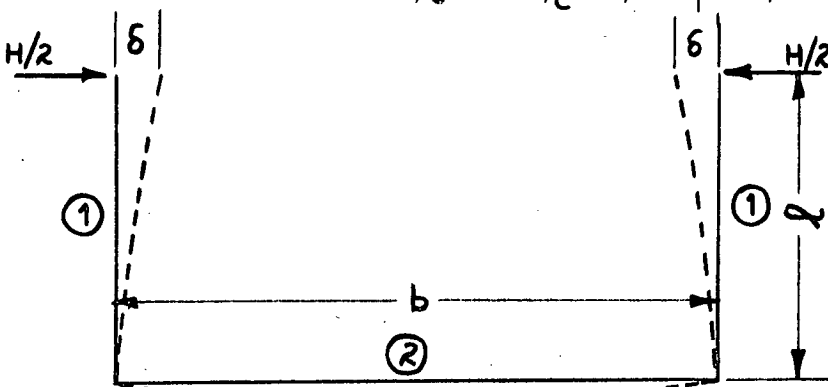


figure 3.18

where  $EI_1$ ,  $EI_2$  are the flexural rigidities of the diagonal and floorbeam respectively. Inserting the numerical values for this truss (see appendix), we find

$$k = 3.40 \text{ lb/inch} \quad (3.86)$$

This estimate can be improved somewhat by treating the panel as a unit. The joint rotations are shown in figure (3.17), in which the double symmetry has been taken into account. Analysing the frame by the usual deformation method, we obtain the equations of equilibrium, in terms of the rotations  $\omega_2, \theta_2, \omega_1$  and the sway  $\delta$ . Solution of these equations gives the stiffness as

$$k = H/\delta = 4.16 \text{ lb/inch} \quad (3.87)$$

which is about 20% larger than the first estimate.

Neither of the above two mathematical models takes into account the variation in stiffness of the members due to their axial loads. However this should not be a serious defect because the decrease in stiffness of the compression diagonal would be largely balanced by the increase in stiffness of the tension diagonal, and the tension chord itself does not deform.

The calculations also assume that the panel deforms freely on its own, that is the restraint from neighbouring panels is neglected. Another estimate for the spring stiffness can be determined by assuming an infinite restraint from the neighbouring panels, so that the deformations at the tension chord joints would be zero. Using this information in the equilibrium equations it is found that the spring stiffness is

$$k = 6.28 \text{ lb/inch} \quad (3.88)$$

It is clear from the above analysis that a considerable range of values for  $k$  can be calculated, depending on the simplifying assumptions made in setting up appropriate mathematical models. Nevertheless equations (3.87) and (3.88) can be taken as lower and upper limits respectively.

Engesser's model:- the buckling mode is assumed to be a series of equal half-sine waves of length  $v$ , given by

$$v = \pi(EI_s/k)^{\frac{1}{4}} \quad (3.89)$$

where  $s$  is the "spring" spacing. Using the numerical values for this truss, and the lower value,  $k = 4.16 \text{ lb/inch}$ , we find

$$v = 18.9 \text{ ins. (17.1)} \quad (3.90)$$

This is about three times the spring spacing, so that in fact Engesser's model predicts that the compression chord as a whole buckles approximately into two half waves, which is the antisymmetric mode as observed during tests on the model (see figure 3.16). However, this predicted mode is a poor fit to the observed mode in that slope and curvature at the ends ought to be close to zero. The buckling load predicted by Engesser's model is

$$P_{cr} = 2 \sqrt{EI k/s} = 50.4 \text{ lbs. (61.8)} \quad (3.91)$$

where  $P_{cr}$  is the axial load in the compression chord and which is assumed to be constant. The central loading actually used produces an axial compression which increases towards the centre; using the above value as an average, the buckling load is given by

$$W_{cr} = P_{cr}/1.26 = 40.0 \text{ lbs. (49.0)} \quad (3.92)$$

The buckling mode and load may be recalculated using the upper limit of the spring stiffness,  $k = 6.28 \text{ lb/inch}$ . These values are shown enclosed in parentheses alongside those determined for the lower limit of the spring stiffness.

Timoshenko's model: in this model the change in axial load along the compression chord is taken into account, and the springs are replaced by an equivalent elastic foundation of modulus  $\beta = k/s$  (see figure 3.19). The axial load is assumed to vary continuously, and for the loading in

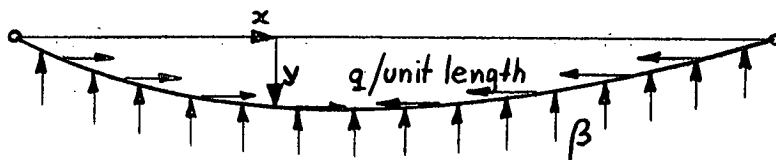


figure 3.19 - Column under uniformly distributed axial load on an elastic foundation

figure (3.16) this is seen to be a uniformly distributed axial load of intensity  $q$  per unit length. Denoting the deformed shape of the compression chord by the function  $y = y(x)$ , the total strain energy is evaluated from the expression

$$U = U_B + U_F - U_W \quad (3.93)$$

in which

$$\begin{aligned} U_B &= \text{strain energy of bending} = \frac{1}{2} \int_0^l EI (d^2y/dx^2)^2 dx \\ U_F &= \text{strain energy of foundation} = \frac{1}{2} \int_0^l \beta y^2 dx \\ U_W &= \text{work done by the load} = \frac{1}{2} \int_0^l q x (dy/dx)^2 dx + \frac{1}{2} \int_{l/2}^l q (1-x) (dy/dx)^2 dx \\ l &= \text{length of column} \end{aligned}$$

The function  $y$  is approximated by a Fourier series, and the coefficients are determined from the conditions of minimum total strain energy. Assuming an antisymmetrical buckling mode, the simplest approximate function is the one parameter Fourier term

$$y = a_2 \sin(2\pi x/l) \quad (3.94)$$

Using the value  $k = 4.16$  lb/inch, we find that the minimum total strain energy condition gives a buckling load of

$$q_{cr} = 40.2 \pi^2 EI/l^3 = 0.092 W_{cr} \quad (3.95)$$

whence  $W_{cr} = 53.4$  lbs.

The use of an additional term  $a_4 \sin(4\pi x/l)$  to describe the buckling mode, gives a value  $W_{cr} = 51.0$  lbs., which is only 5% smaller than the previous value, so that it is not necessary to extend the Fourier series further.

The buckling mode is given by the ratio

$$a_2 : a_4 = 1 : 0.13 \quad (3.96)$$

When the higher value of  $k$  is used we find

$$W_{cr} = 63.3 \text{ lbs.} \quad (3.97)$$

$$a_2 : a_4 = 1 : 0.21$$

From this analysis it is reasonably supposed that the buckling load lies somewhere between 51.0 and 63.3 lbs. Unfortunately the predicted buckling mode still does not satisfy the observed end conditions.

Horne's analysis:- Following the calculations for the general solution proposed by Horne, the buckling mode is found to be antisymmetric, as in the previous models, and the buckling load is calculated as

$$P_{cr} = 79.1 \text{ lbs.} \quad (3.98)$$

Here again the axial load is constant over the entire length and using it as an average value we have

$$W_{cr} = 79.1/1.26 = 62.7 \text{ lbs.} \quad (3.99)$$

Deformation method:- The complete stiffness matrix for the bridge model is of order  $(84 \times 84)$ , taking into account the sway bracing of the deck, the support conditions, and the fact that the in-plane deformations are separable. A manual method of solution of such a large number of equations

is out of question, even if the double symmetry conditions were used to reduce the number of unknowns to 21. However, with the aim of the technique developed in chapter two, the number of unknowns is reduced to as few as can be managed, and calculations are speeded up by using linearized approximations for the stability functions.

Obviously the buckling mode is dominated by the lateral deflections of the compression chord, that is by the sways of the joints, so that it is best to leave these as separate parameters in the equations of equilibrium. The remaining generalized joint displacements, for one truss, are conveniently grouped as follows:

- (i) all compression chord rotations in terms of the parameter  $r_1$ ,
- (ii) all compression chord twists in terms of the parameter  $r_2$ ,
- (iii) all tension chord rotations in terms of the parameter  $r_3$ ,
- (iv) all tension chord twists in terms of the parameter  $r_4$ .

Thus without the use of the symmetry conditions we would be left with 24 unknowns; however, using the symmetry conditions this number is reduced to 8, and solution by manual methods is possible.

During model tests it was observed that the tension chord rotations were negligible, so that as a further simplification these are made zero. For the purpose of defining the ratios of the generalized displacements in the above groups, it is convenient to fit a simple function to the buckled shape of the compression chord. From the sketch in figure (3.16) it is seen that as a first approximation the following boundary conditions apply:-

- (i) at  $x = 0$ ,  $z = 0$ ,  $dz/dx = 0$ ,  $d^2z/dx^2 = 0$
- (ii) at  $x = l/2$ ,  $z = 0$ ,  $d^2z/dx^2 = 0$

where  $z = z(x)$  is the lateral deflection of the compression chord. A fifth order polynomial satisfies these conditions, and by differentiation we obtain the approximate function for the compression chord joint rotations

$$\phi = dz/dx = r_1(x/l)^2[3-14(x/l) + 15(x/l)^2] \quad (3.101)$$

from which the ratios are determined as

$$\phi_0 : \phi_1 : \phi_2 : \phi_3 = r_1(0 : 0.593 : 0.407 : -1.00) \quad (3.102)$$

It was also observed that the compression chord twist varied almost proportionally to the lateral deflection, so that

$$\omega = r_2(x/l)^3[2- 7(x/l) + 6(x/l)^2] \quad (3.103)$$

whence we obtain the ratios

$$\omega_0 : \omega_1 : \omega_2 : \omega_3 = r_2(0 : 0.286 : 1.00 : 0.703) \quad (3.104)$$

Assuming a similar expression for the tension chord twists, we find

$$\omega_4 : \omega_5 : \omega_6 : \omega_7 = r_4(0 : 0.206 : 0.846 : 1.00) \quad (3.105)$$

At this stage the buckled shape of the bridge has been specified in terms of the six generalized displacements  $\Delta_1, \Delta_2, \Delta_3, r_1, r_2, r_4$ .

The corresponding generalized forces are denoted by  $F_1, F_2, F_3, R_1, R_2, R_4$  respectively. The first three of these are obtained directly as the sum of the shear forces at joints 1, 2 and 3, whereas the last three are determined as the weighted sums of the moments at all the joints, the weighting factors being the relative joint rotations as defined by the ratios in equations (3.102), (3.104), and (3.105). The member shears and end moments are a function of their P/Q ratios, and for convenience these functions are linearized. The load at which to linearize the stability functions should preferably be close to the buckling load, and the simple Engesser formula provides a quick estimate; in this example  $W_0$  is chosen as 45 lbs., which is about midway between the values obtained above. The stiffness matrix is set up by applying each generalized joint displacement in turn, computing the end moments and shears, from which the generalized joint forces are obtained by summation, taking due account of the weighting factors. The final equations are

$$\begin{bmatrix} \begin{pmatrix} 4440 \\ -12100w \end{pmatrix} \begin{pmatrix} -1830 \\ +8010w \end{pmatrix} \begin{pmatrix} 0 \end{pmatrix} \begin{pmatrix} 372 \\ -278w \end{pmatrix} \begin{pmatrix} 96.2 \\ -11.2w \end{pmatrix} \begin{pmatrix} 177 \\ +170w \end{pmatrix} \\ \begin{pmatrix} -1830 \\ +8010w \end{pmatrix} \begin{pmatrix} 4440 \\ -20150w \end{pmatrix} \begin{pmatrix} -1831 \\ +12050w \end{pmatrix} \begin{pmatrix} -1458 \\ +1440w \end{pmatrix} \begin{pmatrix} 337 \\ -39.2w \end{pmatrix} \begin{pmatrix} 311 \\ +9.8w \end{pmatrix} \\ \begin{pmatrix} 0 \end{pmatrix} \begin{pmatrix} -1831 \\ +12050w \end{pmatrix} \begin{pmatrix} 6280 \\ -47400w \end{pmatrix} \begin{pmatrix} -1289 \\ +1859w \end{pmatrix} \begin{pmatrix} 237 \\ -27.5w \end{pmatrix} \begin{pmatrix} 168 \\ -317w \end{pmatrix} \\ \begin{pmatrix} 372 \\ -278w \end{pmatrix} \begin{pmatrix} -1458 \\ +1440w \end{pmatrix} \begin{pmatrix} -1289 \\ +1859w \end{pmatrix} \begin{pmatrix} 2200 \\ -3980w \end{pmatrix} \begin{pmatrix} 0 \\ -50.8w \end{pmatrix} \begin{pmatrix} 52.8 \\ +2.5w \end{pmatrix} \\ \begin{pmatrix} 96.2 \\ -11.2w \end{pmatrix} \begin{pmatrix} 337 \\ -39.2w \end{pmatrix} \begin{pmatrix} 237 \\ -27.5w \end{pmatrix} \begin{pmatrix} 0 \\ -50.8w \end{pmatrix} \begin{pmatrix} 473 \\ -140w \end{pmatrix} \begin{pmatrix} 122 \\ +108w \end{pmatrix} \\ \begin{pmatrix} 177 \\ +170w \end{pmatrix} \begin{pmatrix} 311 \\ +9.8w \end{pmatrix} \begin{pmatrix} 168 \\ -317w \end{pmatrix} \begin{pmatrix} 52.8 \\ +2.5w \end{pmatrix} \begin{pmatrix} 122 \\ +108w \end{pmatrix} \begin{pmatrix} 786 \\ -156w \end{pmatrix} \end{bmatrix} \begin{bmatrix} \Delta_1/1 \\ \Delta_2/1 \\ \Delta_3/1 \\ r_1 \\ r_2 \\ r_4 \end{bmatrix} = \begin{bmatrix} F_1/1 \\ F_2/1 \\ F_3/1 \\ R_1 \\ R_2 \\ R_4 \end{bmatrix} \quad (3.106)$$



in which  $w = W \times 10^{-3}$ , and  $l$  is the panel length. The parameters, sway divided by panel length, are used rather than sway by itself, so that all unknowns have the dimension of rotation.

The buckling mode and load are determined from the condition that the right hand side of equations (3.106) vanishes. Denoting by  $\tilde{A}$  the matrix of constants on the left hand side of the equations, and by  $(-\tilde{B})$  the matrix of coefficients of  $w$ , the equations are written in the form

$$(1/w)\tilde{A} \cdot \tilde{x} = \tilde{B} \cdot \tilde{x} \quad (3.107)$$

where  $\tilde{x}$  is the solution vector. The solution of equations (3.107), as obtained by Gaussian elimination, is

$$\begin{bmatrix} 1.810 & 1.894 & 3.39 & 0.294 & -0.0019 & 0.0235 \\ 1.049 & 9.63 & 9.84 & 1.311 & 0.0415 & 0.1120 \\ -1.131 & 2.70 & 13.25 & 0.781 & 0.0484 & 0.1226 \\ -2.52 & 7.00 & 12.91 & 3.05 & 0.1039 & 0.1400 \\ 2.13 & -7.45 & -12.74 & -1.093 & 0.200 & -0.417 \\ 0.455 & -4.13 & -5.99 & -0.815 & -0.263 & 0.1831 \end{bmatrix} \begin{bmatrix} \Delta_1/l \\ \Delta_2/l \\ \Delta_3/l \\ r_1 \\ r_2 \\ r_4 \end{bmatrix} = (1/w) \begin{bmatrix} \Delta_1/l \\ \Delta_2/l \\ \Delta_3/l \\ r_1 \\ r_2 \\ r_4 \end{bmatrix} \quad (3.108)$$

In this form it follows that the fundamental buckling load is the reciprocal of the largest latent root of the above matrix, and the buckling mode is the associated latent vector. From rough measurements on the loaded model the mode is approximately given by the vector

$$(0.3 : 1.0 : 0.7 : 1.0 : -1.0 : -0.5)$$

Using this as a starting vector in the standard iteration process we obtain in succession the vectors

$$\begin{array}{l} (0.280 : 0.994 : 0.679 : 1.000 : -0.930 : -0.486) \quad 18.16 \\ (0.278 : 0.993 : 0.674 : 1.000 : -0.925 : -0.486) \quad 17.89 \\ (0.277 : 0.992 : 0.670 : 1.000 : -0.924 : -0.486) \quad 17.84 \\ (0.278 : 0.993 : 0.670 : 1.000 : -0.922 : -0.486) \quad 17.76 \end{array} \quad (3.109)$$

As can be seen the process has converged rapidly; this is because a good starting vector was used. The last vector is thus the buckling mode, and an estimate of the buckling load is

$$W_{cr} = 1000/17.76 = 56.3 \text{ lbs.}$$

A check on this value is obtained from the conservation of energy equation, that is

$$W_{cr} = 1000 (\tilde{A} \cdot \tilde{x}) \cdot \tilde{x} / (\tilde{B} \cdot \tilde{x}) \cdot \tilde{x}$$

where  $\tilde{A}$  and  $\tilde{B}$  are the matrices of equations (3.106), and  $\tilde{x}$  is the vector representing the buckling mode. This gives

$$W_{cr} = 1000 (1092/20,190) = 54.1 \text{ lbs.} \quad (3.111)$$

This value is known to be an upper bound but it should be close to the exact solution of equations (3.106). It must be remembered that these equations are approximate in two senses. Firstly there is the approximation arising from the linearization of the stability functions; however, since the calculated value of 54.1 lbs. is close to the trial load of 45 lbs., these errors may be neglected. Secondly there are errors in the assumed shape of the buckled bridge, as expressed by the ratios of rotations (equations 3.102, 3.104, 3.105). These ratios could be improved in a manner similar to that suggested in chapter two but in this case it is not warranted because the ratios fit the observed mode.

(c) Experimental verification

This particular model is sufficiently stiff to allow the use of Huggenberger tensometers for measuring strains. Three opposing pairs were used, and located approximately at points of maximum curvature, as judged by eye, which occurred about midway between joints two and three (see figure 3.16). Figure (3.20) shows the measured strains and their Southwell plots. The Southwell plots are seen to be almost linear, exhibiting a slight tendency to a higher

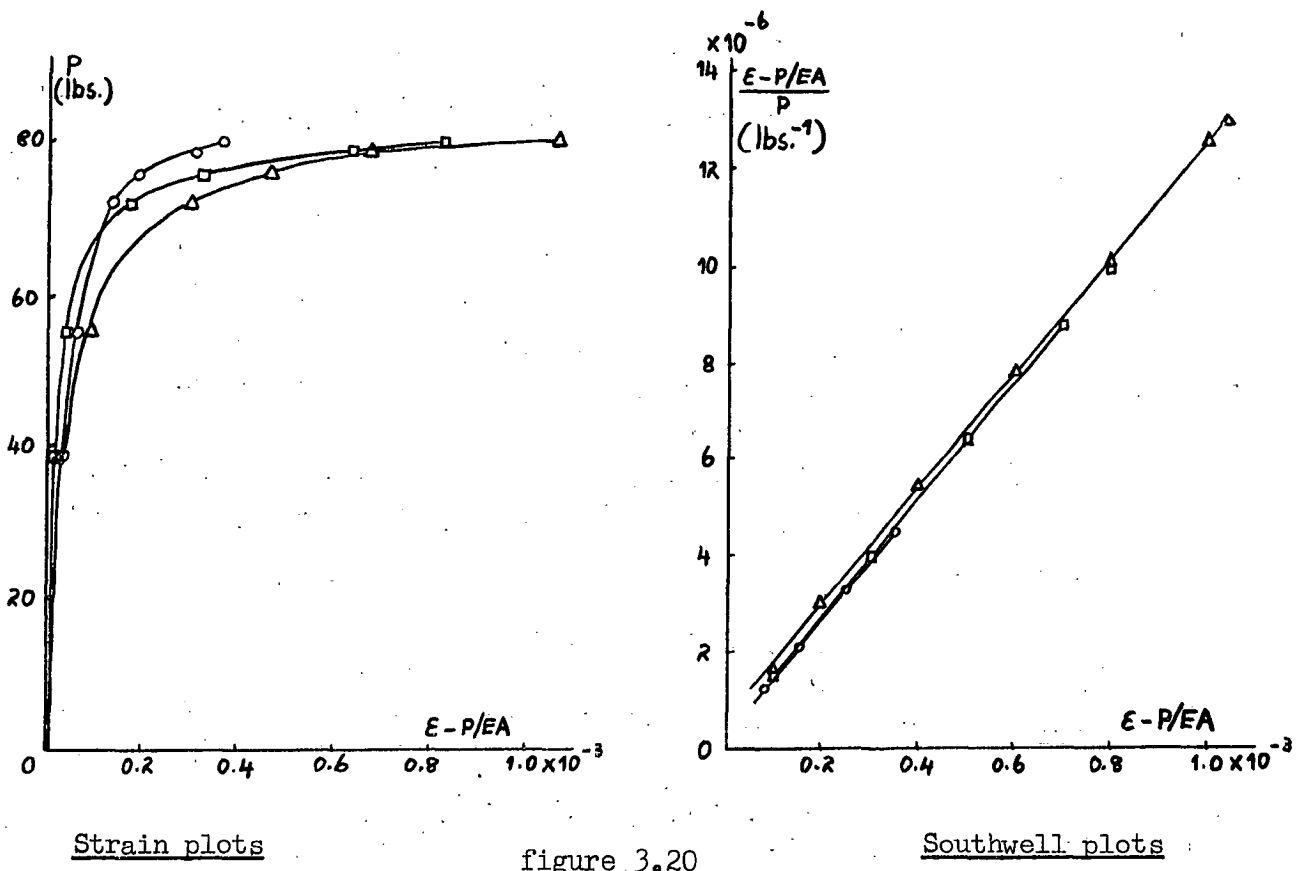


figure 3.20

mode component at low loads. From the average inverse slope we obtain

$$P_{cr} = 84.4 \text{ lbs.} \quad (3.112)$$

whence

$$W_{cr} = 51.0 \text{ lbs.}$$

This agrees very well with the calculated value of 54.1 lbs. which is known to be somewhat high. The predicted buckling mode is also close to the measured mode as can be judged from the relatively few iterations which were necessary to extract the largest latent root. The differences range from about five to ten percent.

(d) Comparison of Results

The following table summarizes the results of this section, from which it is seen that, as far as the buckling load is concerned,

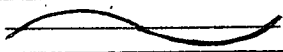
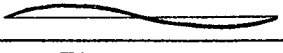

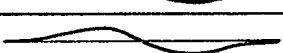

	Buckling Load (lbs.)	Buckling Mode
Engesser	40.0 — 49.0	
Timoshenko	51.0 — 63.3	
Horne	62.7	
Deformation method	54.1	
Measured	51.0	

Table 3.4

there is little difference between the methods. It is rather surprising that Engesser's formula predicts a low value for the buckling load. This could be ~~due~~ to the fact that the formula applies to the constant axial load problem which is then used as an average.

In all cases an antisymmetric mode is predicted for the compression chord deflections but the ~~first~~ three do not satisfy the end conditions. Since the first three mathematical models are based on these assumed functions for the buckling mode, one would expect the calculated buckling loads to be high. This is indeed the case in Horne's analysis, but some compensation must occur in Engesser and Timoshenko's models, since these neglect the rotational restraint of the diagonals on the compression chord.

### 3.14 CONCLUDING REMARKS

The most important feature of the new method presented in this chapter is the linearization of the stiffness matrix, the advantages of which have been clearly demonstrated. Attention is focussed on the buckling mode, and this is determined iteratively, using information from simple models (often a cardboard model is sufficient) to speed up the calculations. Once the buckling mode is known, the buckling load is readily calculated as some property associated with the mode, such as a latent root of the stiffness matrix for example.

The accuracy of the linearization method depends on the trial load used to set up the approximate stiffness matrix, and usually this can be estimated fairly closely beforehand. Should it be necessary, a second linearization can be carried out using the previously calculated buckling load as a guide in selecting a new trial load. Alternatively, more accuracy is achieved by using more terms in the Taylor's series expansion for the stability functions. This has been done by Firt (reference 17), but the resulting matrix equation leads to considerably more complicated manipulations, and it seems that there is little advantage over the simple linearization.

It has been shown that the deformation method of analyzing elastic instability also lends itself well to three-dimensional buckling problems. In the examples chosen the members were of circular sections for which every cross-sectional axis is a principal axis. This means that joint rotations can be resolved into any convenient direction. The only complication for non-circular members is that the rotations must be resolved into the principal axes of the members. Also, for some sections, it may be necessary to take into account the effect of axial load on the torsional stiffness. However, these modifications present no difficulties, and the basic principles remain otherwise unchanged.

Most of the emphasis in this chapter has been on manual methods of computation, but it should be pointed out that electronic digital computers are a powerful aid in this type of work; a glimpse of their use was given in the extensive analysis of the two-bay Warren truss through-bridge.



## APPENDIX - Properties of 8-bay through bridge

Flexural rigidities: top and bottom chords,  $EI = 915 \text{ lb.in}^2$   
                                 diagonals,          $EI = 194 \text{ lb.in}^2$   
                                 floorbeams,         $EI = 915 \text{ lb.in}^2$

torsional rigidities: top and bottom chords,  $GJ = 530 \text{ lb.in}^2$   
                                 diagonals,          $GJ = 124 \text{ lb.in}^2$   
                                 floorbeams,         $GJ = 530 \text{ lb.in}^2$

## REFERENCES

- (1) W. Merchant, "A Connection between Rayleigh's Principle and Stiffness Methods for determining Critical Loads", Proc. 9th Int. Cong. App. Mech., Brussels (1957).
- (2) G. Temple and S.W. Bickley, "Rayleigh's Principle", p 29f., O.U.P., (1933)
- (3) M.S. Gregory, "Framed Structures: the Instability Problem", Proc. I.C.E. (London), Vol 35, pp 451-473 (Nov. 1966).
- (4) see reference 2
- (5) N.H. Wittrick, "Rate of Change of Eigenvalues", Jnl. Roy. Aer. Soc., vol 66. p 590, (Sept. 1962)
- (6) D.N. deG. Allen, "Relaxation Methods in Engineering & Science", p 158f., McGraw-Hill (1954).
- (7) R.K. Livesley and D.B. Chandler, "Stability Functions for Structural Frameworks", Manchester University Press, (1956).
- (8) see reference (7), p 5ff.
- (9) S.J. McMin, "The Determination of the Critical Loads of Plane Frames", The Struct. Eng., (July, 1961).
- (10) S.J. McMin, "Matrices for Structural Analysis", p. 182f, Spon (1962).
- (11) F. Bleich, "Buckling Strength of Metal Structures", p 274-274, McGraw-Hill, (1952)
- (12) S.P. Timoshenko and J.M. Gere, "Theory of Elastic Stability", p 108f. McGraw-Hill, (2nd ed. 1961).
- (13) M.R. Horne, "The Elastic Lateral Stability of Trusses", The Struct. Eng., (May 1960).
- (14) R.K. Livesley, "The Application of an Electronic Digital Computer to some Problems of Structural Analysis", The Struct. Eng., (Jan. 1956).

- (15) L.C. Schmidt and L.K. Stevens, "Elastic Critical Loads of Laterally Braced Trusses", Trans. I.E. Aust., vol. CE7, No. 2, (Oct. 1965).
  
- (16) F. van der Woude, "The Elastic Instability of Frames", Int. Jnl. Mech. Sci., vol 7, No. 11, p 747-757, (Dec. 1965) [see also discussion: Int. Jnl. Mech. Sci., vol., 8 No 6, p. 465 (June, 1966) ].
  
- (17) V. Firt, "Eigenvibration and Stability of Bridges and Structures", Publ. Int. Assoc. Bridge Struct. Eng., Vol 23, p 127f., (1963).

## CHAPTER FOUR - THE BEHAVIOUR OF OVERBRACED FRAMES

### 4.1 INTRODUCTION

The previous chapter dealt with the behaviour of so called statically determinate frames. 'Statically determinate' in this context means that the axial forces in the members can be determined from a statical analysis alone. This definition implies two major simplifications; firstly, the deformations of the frame are assumed negligible in comparison with the overall frame dimensions, and secondly the effects of bending are neglected in setting up those equations of statics used to calculate the axial forces. The first simplification means that we can use the original frame geometry to resolve forces at the joints for the purpose of setting up the equations of equilibrium of the joints. Another implication is that member lengths may be changed, by small amounts of course, without altering the axial force distribution. The second simplification is seen to be equivalent to the assumption of pinned connections between members.

In practice the joints of a frame are usually welded and are therefore more nearly rigid, so that the members carry bending moments and shear forces in addition to axial loads. These bending actions cannot be determined from statics alone so that most 'statically determinate' frames are in fact statically indeterminate. A better description for such frames is 'statically determinate with respect to its axial force distribution'.

In the present chapter it is proposed to study the behaviour of frames for which the axial forces in the members cannot be calculated from statical considerations alone. Such frames are called 'statically indeterminate', 'redundant' or 'hyperstatic', but for reasons explained above the term 'overbraced' is preferable (see reference 1). Broadly speaking, this condition arises when the frame has redundant members or supports.

In order to calculate the axial forces in the members of an overbraced frame additional information is required, and it is evident that this is in the form of a compatibility condition relating the member lengths. That is, it is the changes in member lengths, however small these may be, which govern the axial force distribution. When bending of the members is neglected, the changes in length can be expressed in terms of the joint translations alone, and the axial

forces are computed using ordinary linear elastic theory. This is called the linearly elastic force distribution, and it is a reasonable description of the behaviour of overbraced frames provided bending deformations are small enough to be neglected. However, as for statically determinate frames, there exists a possibility of buckling and then the bending deformations certainly cannot be neglected. Also, any frame possesses initial crookedness so that bending occurs right from the start, and as loading progresses the bending deformations grow at an increasing rate. Due to bending the chord lengths of the members change by amounts which are often comparable in magnitude to those produced by the direct axial strains; in fact for slender frames the latter is usually much smaller. The total changes in lengths must meet the compatibility requirement, and to achieve this the axial forces in the members change. Thus, whereas in statically determinate frames these forces remain substantially in constant proportion, the axial force distribution in overbraced frames varies continually. This means that the designer's task becomes considerably more difficult since he must now also estimate the axial force distribution before he can determine member stiffnesses which he needs in order to assess bending effects. Furthermore there is the problem of prestrain within the frame. Undoubtedly this exists in all overbraced frames, and the question is whether or not it can be controlled, with a view to improving the frame behaviour under load.

#### 4.2 REVIEW

In comparison with the bulk of literature on buckling of statically determinate frames, little has been written about the behaviour of redundant or overbraced frames. To the author's knowledge the earliest contribution is that of Masur (reference 2), who concludes that when the non-linearity of the axial force distribution is taken into account, the ultimate buckling load is usually greater and never less than the value obtained by using the linearly elastic axial force distribution. The latter value he calls the buckling load, and the increase in load is referred to as the post-buckling strength. Masur shows that the ultimate load, if it exists and if no yielding occurs, is characterized by the equations

$$\begin{aligned} f &= 0 \\ \partial f / \partial \lambda_i &= 0 \end{aligned} \tag{4.1}$$

in which  $f$  is the determinant associated with the usual stiffness matrix, and  $\lambda_i$  ( $i = 1, 2, \dots, m$ ) are the parameters defining the  $m$  redundant



axial forces. The first of these equations is the familiar zero stiffness criterion, while the second equation is a modification of the compatibility relations involving the changes in member chord lengths, including the member shortenings due to bending. Masur also shows that the elastic ultimate load is independent of prestrain, although he does mention that prestraining affects the behaviour up to the ultimate load, especially if yielding occurs.

Giudici (reference 3) also considers the non-linearity of the axial force distribution, and he introduces the concept of an interaction curve, applicable to singly-redundant frames but which can be extended to multi-redundant frames. The interaction curve for singly-redundant frames is the locus of points in the W-R plane for which the determinant of the stiffness matrix is zero; that is, it gives the buckling load corresponding to any given value of the redundant force. A method for predicting the loading path is proposed, and by superimposing this on the interaction curve Giudici finds an estimate for the buckling load. This load is an improvement to the value calculated on the basis of a linear force distribution, but it provides no measure of the ultimate load. Giudici stresses the fact that the behaviour of redundant frames is highly dependent on initial crookedness and prestrain, and he concludes that the difficulty in predicting the behaviour is a lack of knowledge about member shortenings due to bending.

More recently, Murray (reference 1) developed an alternative mathematical criterion for the determination of the ultimate load. He shows that at the ultimate load both the frame stiffness and its derivative with respect to the distribution of axial forces in the members are zero. This criterion was derived experimentally, but was justified mathematically by Schmidt (reference 4) in a subsequent discussion on Murray's work. In order to calculate the ultimate load from this criterion Murray plots curves of joint stiffness against redundant force for different load values, the ultimate load being the value at which the stiffness curve just touches the line of zero stiffness. Basically this technique is similar to Giudici's interaction curve; the only difference is a variation in the presentation. It is evident that Murray's criterion is satisfied by a maximum on Giudici's interaction curve.

So far the discussion has been confined to elastic buckling behaviour, which occurs only in very slender frames. Investigations by Stevens and Lay (reference 5) have shown that for overbraced frames with low nominal slenderness ratios ( $l/r$  of the order of 100), the behaviour

can be satisfactorily predicted using simple "elastic-fully plastic" type curves to describe the axial load-axial shortening behaviour of the individual members. This is so because the shortenings due to bending can be neglected in the elastic ranges of such comparatively stiff members. Similar investigations have been reported by Neal and Griffiths (reference 6) who tested frames with nominal slenderness ratios in the range 104-225. They followed a method due to Ziegler to predict the behaviour, using axial load-axial deformation relations measured in previous tests on similar members.

\* \* \* \* \*

The above brief review is included for completeness' sake. Together with some of the remarks made in the introduction it provides a reasonable picture of the problem and the present state of knowledge.

In this chapter some aspects of the problem are investigated, mainly from a qualitative point of view, and a quantitative analysis is introduced for some relatively slender frames in which buckling effects become appreciable before yielding occurs.

#### 4.3 STATICAL INDETERMINACY OF FRAMES

It is perhaps well, at the outset, to clarify the meaning of the term 'statical indeterminacy' when used within the context of the present chapter. In simple terms, the degree of statical indeterminacy of any structure is the number of unknown generalized forces, (that is, force, moment, torque, etc.) both internal and external, minus the number of independent equations of statical equilibrium relating these unknowns. A general method for calculating the degree of indeterminacy has been developed by Henderson and Bickley, an outline of which is given in reference 7, but the following approach is believed to be simpler. Consider a single member, not necessarily straight, as in figure (4.1). In general there are six <sup>a</sup>actions at each end of the member; these consist of three forces (one axial force and two shear forces) and three moments (two bending moments and one torque). Apart from the external loads, which are presumed to be known, the foundations exert unknown forces on the frame. The number of these support reactions (including moments) are readily counted, so that the total

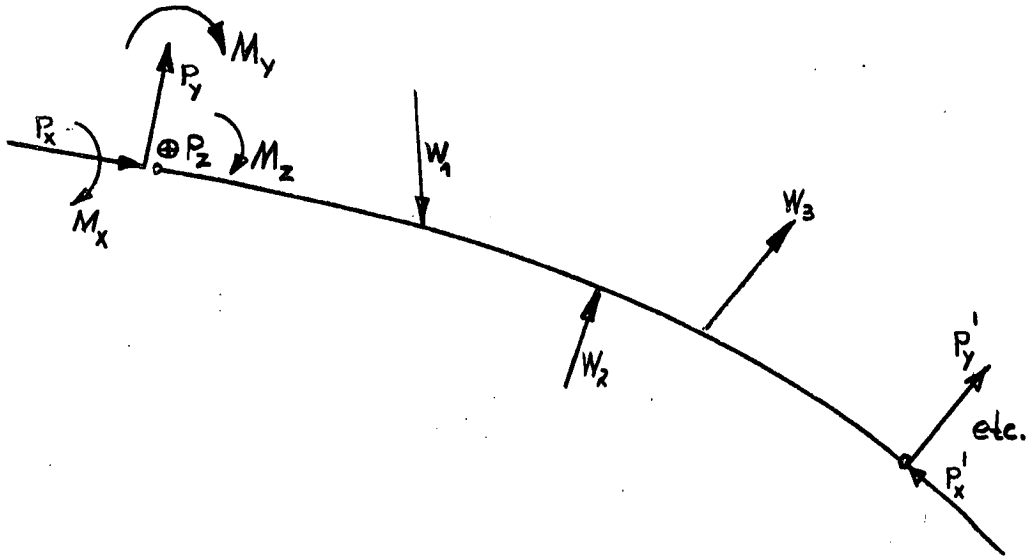


figure 4.1 - Forces on a single member

number of unknown forces,  $U$  is given by

$$U = 12m + S \quad (4.2)$$

where  $m$  is the number of members, and  $S$  is the number of support reactions.

The number of equations of equilibrium is derived in a similar manner. Firstly, for the equilibrium of each member six equations apply, namely

$$\begin{aligned} \sum X &= \sum Y = \sum Z = 0 \\ \sum M_x &= \sum M_y = \sum M_z = 0 \end{aligned} \quad (4.3)$$

where the symbols have their usual meaning. Thus effectively the number of unknowns per member is reduced to six. Secondly, treating the joints as rigid bodies, a further six equations of equilibrium are written for each joint. Thirdly, somewhere in the frame certain actions may be released; for example a ball and socket connection releases all three moments. Each release provides an additional equation, so that the total number of equations,  $E$  is given by

$$E = 6m + 6j + r \quad (4.4)$$

where  $j$  is the number of joints, and  $r$  is the number of releases. The degree of statical indeterminacy is therefore found from the equation

$$n = U - E = (6m + S) - (6j + r) \quad (4.5)$$

This general equation applies to space frames. In the case of a plane frame we find

$$n = (3m + S) - (3j + r) \quad (4.6)$$

When the frame is pinjointed, there is a further simplification in that there is only one unknown per member, that is an axial force, and only the first three of equations (4.3) apply. We are then left with the familiar equations for the degree of statical indeterminacy with respect to the axial force distribution

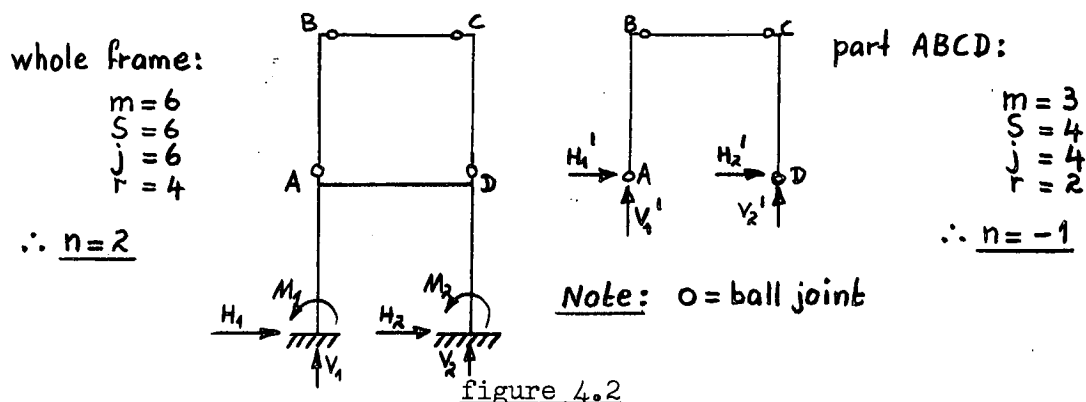
$$\begin{aligned} n &= m + S - 3j \text{ (for space frames)} \\ n &= m + S - 2j \text{ (for plane frames)} \end{aligned} \quad (4.7)$$

In the above equations we must have in general

$$\begin{aligned} S &\geq 6 \text{ (for space frames)} \\ \text{or} \quad S &\geq 3 \text{ (for plane frames)} \end{aligned} \quad (4.8)$$

since otherwise the frame is unstable, that is it can translate or rotate as a rigid body. When  $S = 6$  (or  $3$ ) the support reactions can be determined separately from the equations of equilibrium of the frame as a whole, and the frame is said to be supported in a statically determinate, or simply supported manner;  $S - 6$  (or  $3$ ) is called the degree of external indeterminacy.

In this analysis a joint is defined as a point where two or more members meet, or where a member runs into a foundation. Care must be taken in performing the analysis that no part of the frame is in itself a mechanism; this may occur, and if the remainder of the frame is sufficiently indeterminate the general formula for calculating the degree of indeterminacy leads to erroneous results. An example of this is shown in figure (4.2), in which it is seen that the degree of statical indeterminacy for the entire frame is



two, whereas part ABCD on its own has an indeterminacy of -1 and is therefore a mechanism of one degree of freedom.

#### 4.4 THE USE OF COMPLEMENTARY ENERGY IN THE ANALYSIS OF OVERBRACED FRAMES

Since the axial forces in the members of an overbraced frame cannot be determined from a statical analysis alone, additional information must be sought. It is fairly obvious that the required information is in the form of compatibility relations, and complementary energy methods provide a convenient means of deriving this type of equation. For example, consider the frame shown in figure (4.3), which is singly-redundant with respect to its axial force distribution. Let BD be the redundant member, and let  $R$  be its axial force. Imagine this member to be cut and treat  $R$  as an external

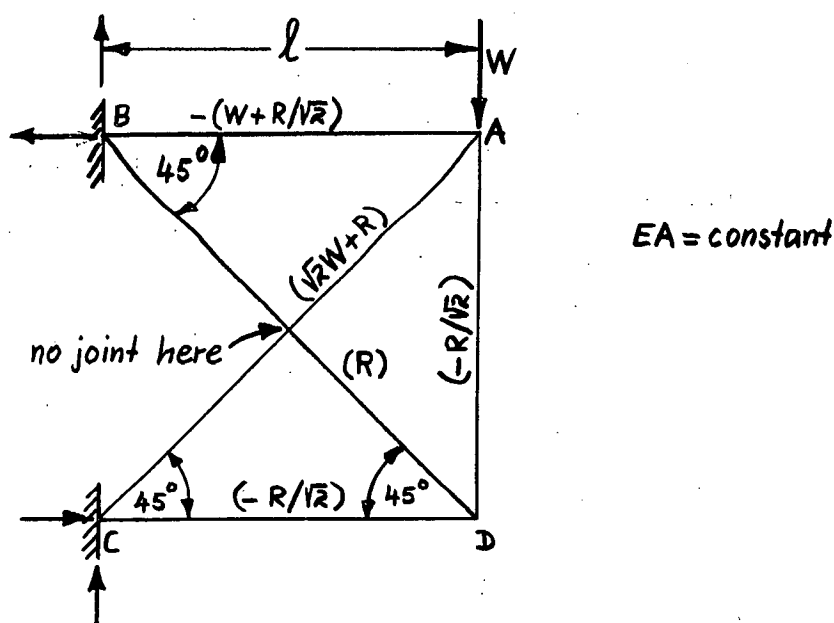


figure 4.3 - Singly-redundant frame

force acting across the cut. A primary force analysis then gives the axial forces in all the members in terms of the applied load  $W$  and the redundant force  $R$ ; these are shown in the figure, compression being taken as positive. This neglects bending but even when bending deformations are quite large it is still reasonable to ignore the effects of the resulting shear forces in the axial force analysis.

The complementary energy of the simplified system,  $C$  is defined as

$$C = \sum_i \int_0^{P_i} \delta_i dP_i - \int_0^W \delta_W dW - \int_0^R \delta_R dR \quad (4.9)$$

where the summation applies over all the members of the frame.  $\delta_i$  is the amount by which the ends of member  $i$  approach each other, and  $P_i$  is the compressive axial force in the member;  $\delta_W$  is the displacement of the applied load  $W$ , and  $\delta_R$  is opening of the cut in the redundant member. According to the rules enunciated in chapter two, the

complementary energy may be differentiated with respect to the independent force parameters, in this case  $W$  and  $R$ , provided that the differentiation is carried out subject to the restrictions imposed by the equations of equilibrium. In this problem the equations of equilibrium are of the form

$$P_i = a_i W + b_i R \quad (4.10)$$

where  $a_i$  and  $b_i$  are constants determined from the primary force analysis, as in figure (4.3); they depend only on the frame geometry. Differentiating  $C$ , we have

$$\begin{aligned} \partial C / \partial R &= \sum_i [\delta_i (\partial P_i / \partial R)] - \delta_R = 0 \\ \partial C / \partial W &= \sum_i [\delta_i (\partial P_i / \partial W)] - \delta_W = 0 \end{aligned} \quad (4.11)$$

Using the information in figure (4.3) to evaluate the terms  $\partial P_i / \partial R$  and  $\partial P_i / \partial W$  we get

$$\begin{aligned} -\delta_{AB}/\sqrt{2} - \delta_{AD}/\sqrt{2} - \delta_{CD}/\sqrt{2} + \delta_{BD} + \delta_{AC} - \delta_R &= 0 \\ -\delta_{AB} + \sqrt{2} \delta_{AC} - \delta_W &= 0 \end{aligned} \quad (4.12)$$

A word of explanation is required here to distinguish between  $\delta_{BD}$  and  $\delta_R$ ; the former represents the shortening of member BD and this is made up of the shortenings of the two halves separated by the cut. The opening of the cut,  $\delta_R$  is an independent quantity. Thus the first of equations (4.12) may be thought of as giving the gap across the cut, and solution of the problem is achieved by equating  $\delta_R$  to zero which signifies the fact that the member shortenings are compatible.

Equations (4.12) can of course be derived from an entirely geometric argument. Denoting by  $(u_A, v_A)$  and  $(u_D, v_D)$  the horizontal and vertical displacements of joints A and D respectively, we have for small displacements

$$\begin{aligned} \delta_{AB} &= u_A \\ \delta_{AC} &= u_A/\sqrt{2} + v_A/\sqrt{2} \\ \delta_{AD} &= v_A - v_D \\ \delta_{CD} &= u_D \\ \delta_{BD} &= u_D/\sqrt{2} - v_D/\sqrt{2} + \delta_R \end{aligned} \quad (4.13)$$

where  $v_A = \delta_W$ . Elimination of  $u_A, u_D, v_D$  from these relations gives equations (4.12).

In order to use the compatibility equations to find the axial force distribution, we must define a relation between member shortening and axial load  $P$ . If bending deformations are small enough to be neglected

is a function of  $P$  only and we write

$$\delta = f(P) \quad (4.14)$$

where the function  $f$  can be obtained from direct tension and compression tests. The usual simplification at this stage is to use the linear function

$$\delta = Pl/EA \quad (4.15)$$

where  $l$  is the member length,  $A$  its cross-sectional area (assumed uniform), and  $E$  is Young's modulus of the material. Also it is customary to use the same relation for both tension and compression. Substitution of the relevant information for the frame in figure (4.3), yields linear equations in  $R$  and  $\delta_W$ , whose solution is

$$\begin{aligned} R &= -0.626W \\ \delta_W &= 2.14 Wl/EA \end{aligned} \quad (4.16)$$

The final force distribution is given in figure (4.4).

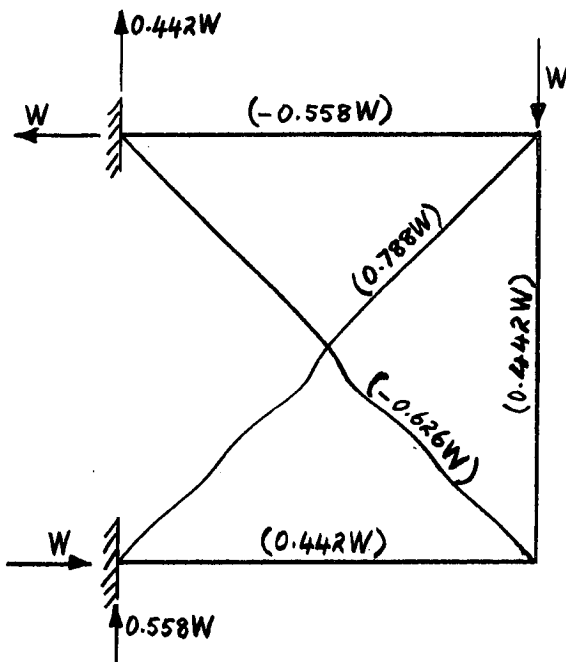


figure (4.4) - Linearly elastic axial force distribution

Any overbraced frame can be handled in a similar manner. There are always as many equations of compatibility as there are redundant members, and complementary energy principles can be used to derive these equations. Final solution is achieved by specifying a  $P$ - $\delta$  relation for each member. When the  $P$ - $\delta$  relations are linear, the final equations are also linear and therefore easy to solve. When the  $P$ - $\delta$  relations are non-linear, the final equations are usually too complex to solve analytically, and one needs to use approximate or iterative techniques to obtain a solution. A useful device is to fit a piecewise linear function to the  $P$ - $\delta$  relation. In some cases the final non-linear equations may have extraneous solutions, but these can usually be detected from a physical point of view, and discarded.

\* \* \* \* \*

When bending deformations are important, as in slender frames, the total shortening of a member may be written in the form

$$\delta = f(P) + \Delta \quad (4.17)$$

where  $f(P)$  is the shortening due to the axial load effect (see equation 4.14 above), and  $\Delta$  is the shortening due to bending. Denoting by  $y_0$  and  $y$  respectively the unloaded and loaded bent shapes, then we have, for small deflections

$$\Delta = \frac{1}{2} \int_0^l (dy/dx)^2 dx - \frac{1}{2} \int_0^l (dy_0/dx)^2 dx \quad (4.18)$$

Thus it is seen that in order to calculate this term we need to know both the initial crookedness,  $y_0$  and the deflected shape under load,  $y$ . When the frame has pinned joints, bending in any member can take place independently of other members, provided the resulting shortenings are compatible. In **such** instances it is reasonable to use isolated pin-ended column relations as is shown in the following sections. In a rigidly jointed frame however, bending in any one member is distributed throughout the frame, and the deflected shape under load depends on the restraints of neighbouring members, which in turn depend on their deflections and axial load, and so on. In other words the axial force distribution is a function of the deflected shapes of all the members which themselves are functions of initial crookedness and of the axial force distribution which we want to calculate. It is precisely this interdependence which makes an analytical solution to the problem of the behaviour of overbraced frames so intractable.

#### 4.5 THE BENDING SHORTENING OF PIN-ENDED MEMBERS

Before extending the analysis of frame behaviour by taking into account initial crookedness, a simple mathematical model is developed for the determination of the bending shortening of isolated pin-ended members. Suppose that the initial crookedness pattern of a pin-ended column can be expressed in terms of the infinite Fourier series

$$y_0 = \sum_{n=1}^{\infty} a_n \sin(n\pi x/l) \quad (4.19)$$

In chapter one it was shown that under load  $P$  the deflected shape,  $y$  is given by the series

$$y = \sum_{n=1}^{\infty} a_n \sin(n\pi x/l) / (1 - P/n^2 Q) \quad (4.20)$$



where  $Q = \pi^2 EI/l^2$  is the Euler load of the column. From these expressions the shortening due to bending is obtained as

$$\begin{aligned}\Delta &= \frac{1}{2} \int_0^l (dy/dx)^2 dx - \frac{1}{2} \int_0^l (dy_0/dx)^2 dx \\ &= \sum_{n=1}^{\infty} (\pi^2 a_n^2 / 4l) [(1 - P/n^2 Q)^2 - 1]^{-1}\end{aligned}\quad (4.21)$$

Usually we find  $a_1 > a_2 > a_3 > \dots$ , and as  $P$  reaches a reasonable proportion of  $Q$  the first term in this series dominates, so that as a first approximation the bending shortening is given by

$$\Delta \approx (\pi^2 a_1^2 / 4l) [1/(1 - P/Q)^2 - 1] \quad (4.22)$$

Also, as a further simplification, the same expression, with  $P$  replaced by  $-P$ , may be used to calculate the bending shortening of a tension member. In frames the bending shortening of tension members is usually small, so that this simplification, although crude, introduces no great errors.

An estimate of the order of magnitude of the bending shortening is obtained by expanding the term in brackets and replacing  $Q$  by

$\pi^2 EI/l^2 = \pi^2 EA/(l/r)^2$ ; this gives

$$\Delta = \frac{1}{4} (a_1/l)^2 (l/r)^2 [(2 - P/Q)/(1 - P/Q)^2] (Pl/EA) \quad (4.23)$$

where  $r$  is the radius of gyration of the cross section. For most columns the initial crookedness is some fraction of its length, a figure of  $l/400$  being in frequent use for design purposes. Thus for common engineering structures, with  $l/r$  ratios in the vicinity of 100, we have

$$\Delta \approx [(2 - P/Q)/64(1 - P/Q)^2] (Pl/EA) \quad (4.24)$$

whence it is seen that for  $P/Q$  ratios less than about 0.5 the above term amounts to no more than about 10% of the elastic axial load shortening  $Pl/EA$ . On the other hand, for very slender frames  $l/r$  may be of the order of 400 or more, in which case at a  $P/Q$  ratio of about  $1/3$  the bending shortening becomes of the same order as the axial load shortening.

The above analysis is of course restricted to linearly elastic material behaviour. After yielding occurs the shortening expression will be quite different. However, in this thesis only elastic effects are examined.

\*

\*

\*

\*

\*

When analysing a pin-jointed frame with initially crooked members, use is made of the mathematics developed above. For this purpose equation (4.23) presents the most convenient form for the bending shortening, since the total shortening is then given by

$$\delta = Pl/EA + \Delta = (Pl/EA)(1 + kc) \quad (4.25)$$

where  $k = \frac{1}{4}(a_1/l)^2(1/r)^2$   
and  $c = (2-P/Q)/(1-P/Q)^2$ .

In this form the total shortening is made pseudo-linear by treating  $c$  as a constant. The complementary energy of the member then becomes

$$C = \int_0^P \delta dP = (1 + kc)(P^2/2EA) \quad (4.26)$$

and when this is differentiated with respect to some unknown force parameter  $X$ , we get

$$\partial C / \partial X = (1 + kc)(Pl/EA)(\partial P / \partial X) \quad (4.27)$$

The term  $(Pl/EA)(\partial P / \partial X)$  arises in the usual straight member analysis, so that the term  $(1 + kc)$  may be regarded as a correction factor, that is

$$\partial C / \partial X = (\text{correction factor}) \times (\partial C / \partial X)_{\text{linear}} \quad (4.28)$$

An example of the use of this relation is given in the next section.

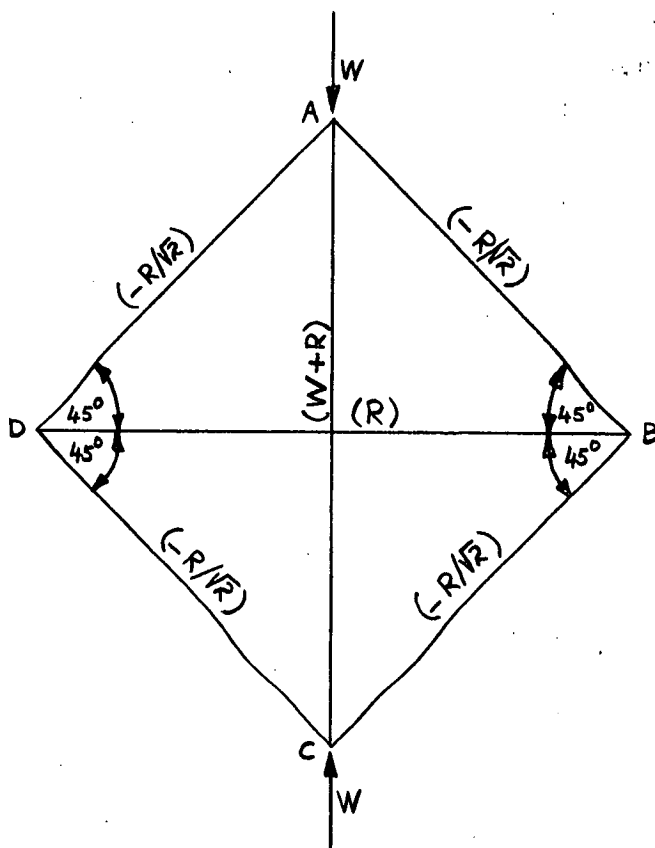
#### 4.6 THE BEHAVIOUR OF PIN-JOINTED OVERBRACED FRAMES

Although pin-jointed frames rarely exist in practice, it is enlightening to study their behaviour, firstly because it helps to formulate and understand the problem of rigidly jointed overbraced frames, and secondly the mathematics involved is sufficiently simple to handle by manual methods of computation. Consider the pin-jointed frame shown in figure (4.5); it is seen to be statically indeterminate to the first degree with respect to the axial forces in its members. For simplicity all members are uniform and of the same cross-section.

##### (a) Initially straight members

In the first instance bending is neglected, that is the members are assumed to be perfectly straight initially. The axial forces in the members are indicated in the figure in terms of  $W$  and  $R$ ,  $BD$  being treated as the redundant member whose axial force is  $R$ . A complementary energy analysis is carried out in table (4.1) below. Summation of the partial derivatives of the complementary energy (sixth column), gives the opening across the cut as

$$\delta_R = (1/AE)[\sqrt{2} W + (2 + \sqrt{2}) R] \quad (4.29)$$



axial stiffness =  $EA$   
flexural rigidity =  $EI$

member lengths:

AB, BC, CD, DA: 1  
AC, BD:  $\sqrt{2}l$

$Q$  = euler load of side members  
 $= \pi^2 EI / l^2$

figure (4.5) - A pin-jointed overbraced frame

Member	axial stiffness	length	Axial force	Comp. ener. $C = P^2 l / 2AE$	$\partial C / \partial R$	$P$	$P'$
AB	$AE$	1	$-R/\sqrt{2}$	$R^2 l / 4AE$	$Rl / 2AE$	$0.207W$	$W/\sqrt{2} - Q/2\sqrt{2}$
BC	"	1	$-R/\sqrt{2}$	"	"	"	"
CD	"	1	$-R/\sqrt{2}$	"	"	"	"
DA	"	1	$-R/\sqrt{2}$	"	"	"	"
BD	"	$2l$	$R$	$R^2 l / \sqrt{2} AE$	$\sqrt{2} Rl / AE$	$-0.293W$	$Q/2 - W$
AC	"	$2l$	$W+R$	$(W+R)^2 l / \sqrt{2} AE$	$\sqrt{2} (W+R) l / AE$	$0.707W$	$Q/2$

Table 4.1- Complementary energy analysis

For compatibility to be satisfied, this quantity must vanish; the redundant force is calculated from this condition as

$$R = - 0.293 W \quad (4.30)$$

The above value of  $R$  is used to determine the axial forces in the members; these are given in the next to last column of the table.

Let us now examine the possible behaviour of this frame as it is loaded. Since the members are initially straight, they remain straight, and all deformations and axial forces increase linearly with the applied load  $W$ ; this could continue until yielding occurs. However, during this process one or more members may reach its Euler load, that is the load at which it would buckle if it were an isolated pin-ended column. In this

problem member AC first reaches its Euler load,  $Q/2$  ( $Q$  = Euler load of side members), when the applied load has a value  $Q/\sqrt{2}$ . But the deflections of member AC cannot run away in the usual sense because this involves a large shortening of the distance AC, and the other members of the frame do not permit it to do so. Nevertheless member AC cannot be expected to take a further increase in load, so that the remainder of the frame subsequently behaves as a statically determinate frame carrying a load  $W$  together with a constant force of  $Q/2$  in member AC. The new axial force distribution is now independent of member shortenings and can thus be calculated from statics alone; the member forces after the redistribution are given in the last column, headed  $P'$ , in table (4.1).

When one more member reaches its Euler load (in this case members AB, BC, CD and DA do so simultaneously), it can deflect under constant load because its shortening is independent of other members. That is, deflections in all side members, and in member AC, can now increase freely, and compatibility of member shortenings is maintained while the deflections progress. In other words, the frame as a whole has reached its buckling load at which it will ultimately collapse. For this frame the buckling load,  $W_{ult}$  is given by

$$Q = P'_{AB} = W_{ult}/\sqrt{2} - Q/2\sqrt{2} \quad (4.31)$$

$$\text{whence} \quad W_{ult} = 1.91 Q \quad (4.32)$$

which is seen to be about 2.7 times the load at which member AC on its own would buckle if the remaining members did not restrain its shortening.

The complete behaviour of the frame is pictured in figure (4.6) in which the lateral deflection of member AC at loads above  $W = Q/\sqrt{2}$  is indicated by a broken curve, because in this region it tries to buckle but its shortening is restrained by the other members whose shortenings continue to increase linearly with load. Since the shortening due to bending is proportional to the square of lateral deflections, it can be argued that the curve is parabolic. This also satisfies the "buckling criterion" for member AC, that is

$$\partial W / \partial \Delta = 0 \quad (4.33)$$

with the restriction that  $\Delta$  must be zero. In other words the lateral deflection curve of member AC exhibits an instantaneous bifurcation point but it continues to rise until the frame as a whole buckles.

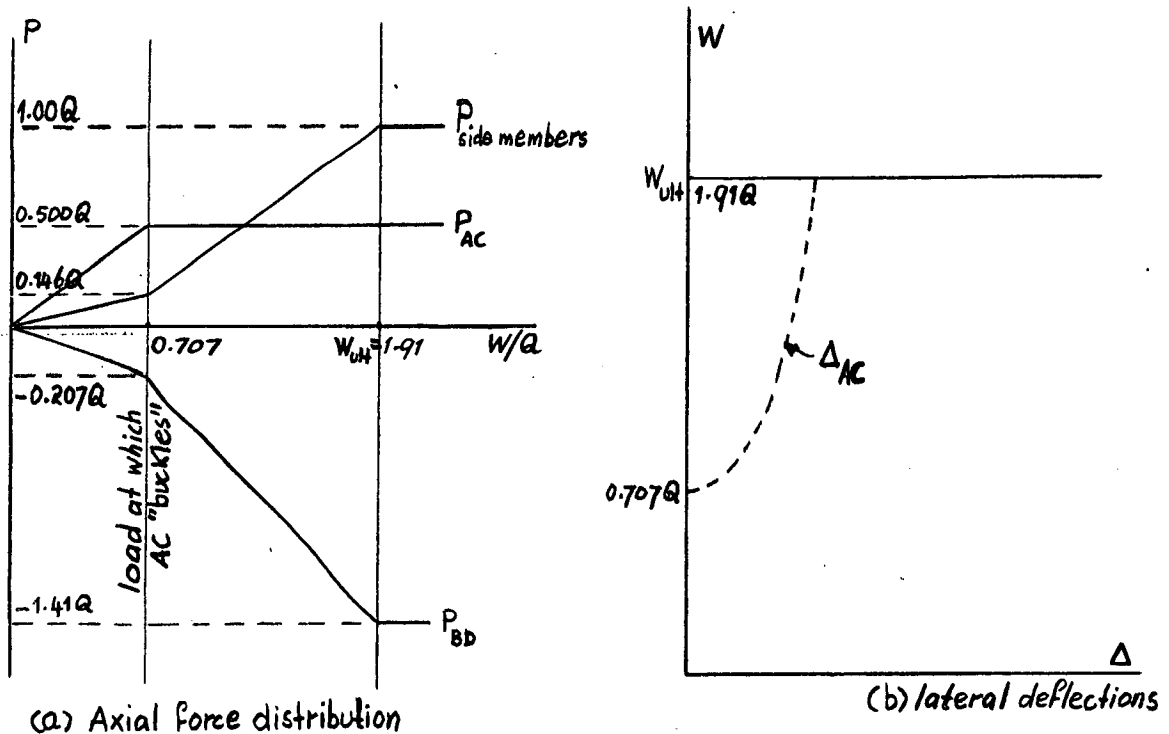


figure 4.6

Summing up, a pin-jointed overbraced frame with initially straight members behaves similarly to a statically determinate frame. The members of such a frame act independently of each other except with regard to the axial shortenings. When an individual member reaches its Euler load, the load-lateral deflection characteristic exhibits a zero slope tangent, but immediately curves upwards again because the shortening is restrained by other members. Large deflections, and hence shortenings, can occur only once a sufficient number of members have attained their buckling loads. The necessary number is one more than the degree of statical indeterminacy with respect to the axial force distribution, since the remainder of the frame is then in effect a mechanism in which the joints can approach or move away from each other compatibly, without upsetting statical equilibrium in axial forces.

In conclusion it should not be forgotten that the above argument is restricted to small deflections in the usual meaning of the phrase. Large deflections introduce other non-linearities into the mathematical model, even if the material remains elastic, but any more refined mathematics which takes this into account becomes too involved for practical use. For example, large deflection theory applied to a pin-ended column leads to elliptic integrals, and the load deflection characteristic can be shown to curve slightly upwards. A similar behaviour is to be expected for frames. However, practical frames are usually so stiff that yielding occurs before deflections become large, so

that for practical purposes the use of small deflection theory should be adequate.

(b) Initially crooked members

The simple mathematical model developed above is of course inadequate to describe the behaviour of a real pin-jointed overbraced frame. Initial crookedness of the members, eccentric connections, and many other factors result in a behaviour which is markedly different from the straight-line representation depicted in figure (4.6b). The members of the real frame begin to deflect as soon as load is applied, but whereas in statically determinate pin-jointed frames this is possible without changing the axial forces in the members, a redundant frame's behaviour is determined to a large extent by the axial shortenings of the member, and these in turn are governed by the magnitude and pattern of initial crookedness. Thus a foreknowledge of crookedness in redundant frames is of even more importance than in statically determinate frames. It has been shown (see chapter one) that the behaviour of statically determinate frames is reasonably well described by hyperbolic load-deflection curves, and this is a valuable experimental tool, the linear Southwell plot. An important question at this stage is, can the behaviour of a redundant frame be described by a linear Southwell plot? It is shown in this chapter that the answer to this question is, in general, in the negative, although it is suspected that in certain cases a near linear Southwell plot is obtained.

\* \* \* \* \*

In order to examine quantitatively the effect of initial crookedness on the elastic behaviour of the pin-jointed frame in figure (4.5), assume a half-sine wave initial crookedness pattern of magnitude  $a_1 = l/400$  for all members, where  $l$  is the respective member length. Also, make the  $l/r$  ratio of the side members equal to 200; the ratio for the diagonal members is then  $200\sqrt{2}$ . Having assigned numerical values to these quantities, the total shortening of the members can be calculated from equation (4.25) if the axial force is known. The total shortenings are then substituted in the equation of compatibility, which results in a non-linear equation for the unknown force  $R$  in terms of the applied load  $W$ . In general this equation must be solved by trial and error for various values of  $W$ . However, the compatibility equation can be linearized by using

equation (4.28) for the total shortening as follows: for any value of  $W$  guess a value of  $R$  (for example using linear theory), so that correction factors for all the members can be calculated; if these are temporarily treated as constant then the resulting equation of compatibility is pseudo-linear and the solution for  $R$  is used as a new trial value, and so on until agreement is obtained. A sample calculation, for  $W = 0.4Q$ , is given in table (4.2), in which  $R = -0.117Q$  is used as a first guess. Summation of the  $\partial C/\partial R$  terms

Member	k	$\frac{AE}{L}(\partial C/\partial R)_{lin.}$	P/Q	P/Q	c	1+kc	$(\partial C/\partial R)'$
AB,BC,CD,DA	0.0625	0.500R	-0.707R/Q	0.083	2.28	1.142	0.571R
BD	0.125	1.414R	2.00 R/Q	-0.234	1.47	1.184	1.676R
AC	0.125	1.414(W +R)	2.00(W+R)/Q	0.566	7.62	1.953	2.76R + 1.11Q

Table 4.2

for all the members gives the linear equation

$$(1/EA)[6.72R + 1.11Q] = 0$$

whence

$$R = -0.164Q$$

Using this as a new trial value, and so on we obtain in succession the values

$$R = -0.150Q, -0.154Q, -0.153Q$$

which is seen to have converged reasonably well after only three cycles. However, at higher applied loads  $W$ , the correction factors are much higher and it is quicker to use the average value of  $R$  as a new guess; the first guess can of course be obtained by extrapolation of the  $R-W$  graph.

The complete curve up to  $W = 1.8Q$  is shown in figure (4.7), together with that obtained by using an initial crookedness of  $1/1000$  in all the members. As can be seen, the latter adheres more closely to the straight lines  $OX, XY$  obtained when the members are initially straight. Ultimately both curves approach the intersection of these two straight lines, which is the ultimate buckling load. A third curve is calculated for which the side members have a much larger initial crookedness ( $1/100$ ) than the diagonal members ( $1/400$ ).

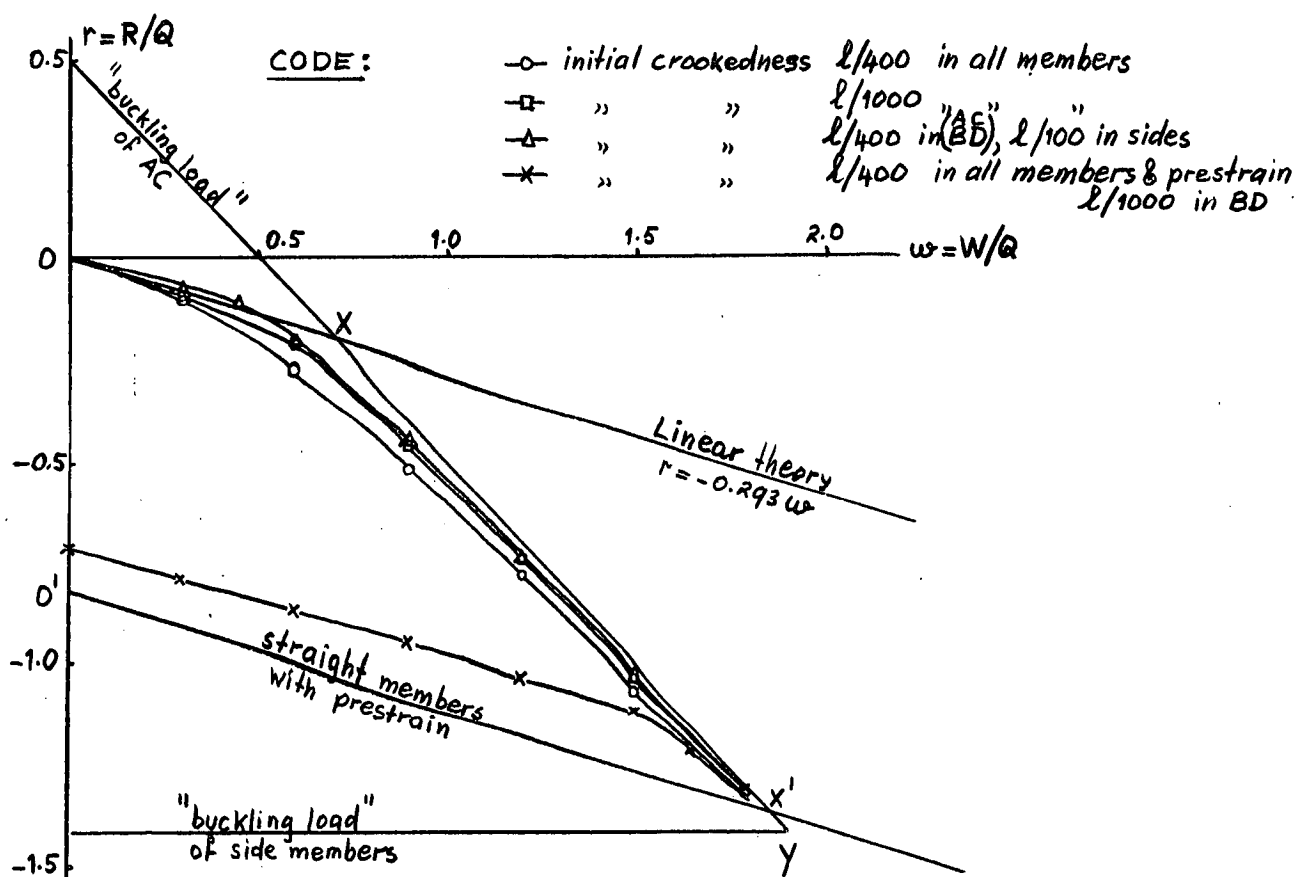


figure 4.7 - Loading paths for various initial imperfections.

In this case the non-linear loading path is seen to vary first on one side and then on the other side of the straight lines obtained when bending is neglected.

Lastly, the effect of prestrain is examined; broadly speaking this is another kind of initial imperfection, and it is most easily pictured as an initial lack of fit of the members. For example, suppose member BD is initially too short by an amount  $\epsilon$ ; then it must be tensioned with a force  $R_0$  say, before it can be connected, and this will strain the other members. The resulting axial forces can be computed from the equation of compatibility by putting  $\delta_R$  equal to  $-\epsilon$ , and  $W$  equal to zero. When the members are initially straight, this gives

$$(1/EA)(2 + 2\sqrt{2}) R_0 = -\epsilon \quad (4.34)$$

whence we obtain

$$R_0 = -0.207 EA\epsilon/l \quad (4.35)$$

In terms of the non-dimensional force  $r = R/Q$ , this becomes

$$r_0 = -0.207(1/\pi r)^2(\epsilon/l) = -838(\epsilon/l) \quad (4.36)$$



When  $\epsilon$  is taken as  $1/1000$ ,  $r_0 = -0.838$ . Similarly, when there is an applied load  $W$ , or non-dimensionally  $w = W/Q$ , we find

$$r = -0.838 - 0.293w \quad (4.37)$$

The loading path is therefore moved downwards by an amount  $-0.838$ ; this is indicated by the two straight lines  $O'X'Y$  in figure (4.7). The frame's ultimate buckling load remains the same.

When the members are initially crooked as well, the term  $\epsilon = 1/1000$  is again included in the final compatibility equation, and the usual terms are multiplied by their respective correction factors, successively iterating towards a solution as before. The loading path thus obtained is also shown in figure (4.7), in which it is seen to be close to linear in the early stages having a slope slightly less than  $0.293$ . After a load  $w = 1.2$  is reached, the curve drops rapidly and curves towards the point  $Y$  at which the side members and member  $AC$  have a  $P/Q$  ratio of unity.

Knowing the axial loads in the members for all values of applied load  $W$ , the central lateral deflections of the members are calculated from

$$a = a_1 / (1 - P/Q) \quad (4.38)$$

When these are plotted against the axial load  $P$  in the member, the Southwell plot is linear and gives the Euler load of the member, which,

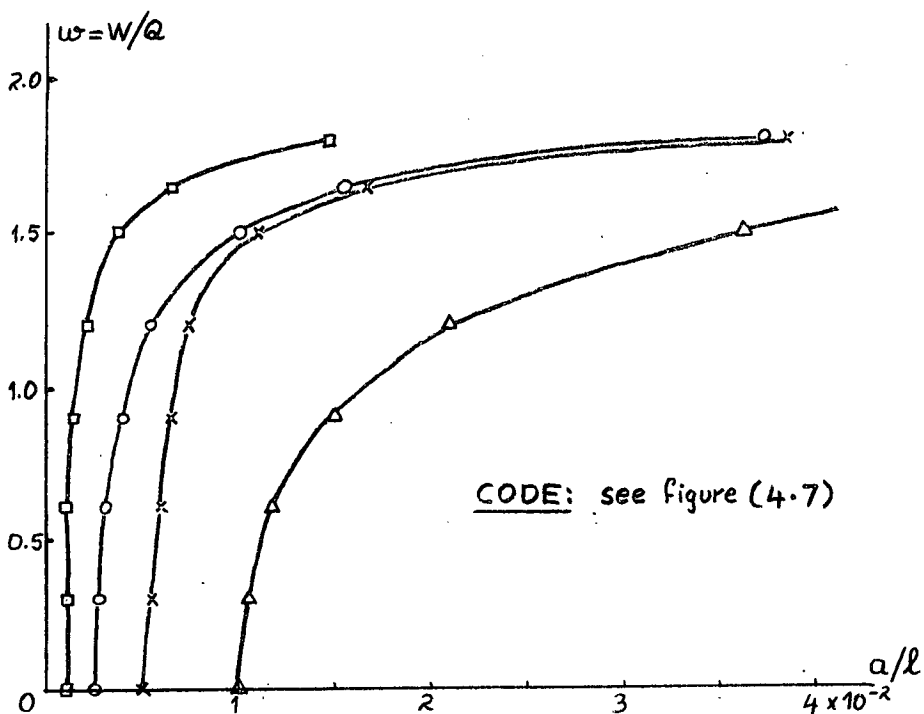


figure 4.8 - Central deflection of members AB, BC, CD, DA

on its own, is of little use. It could be used to determine the frame buckling load by extrapolating the P-W curve to  $P = Q$ , but as an experimental tool this is obviously not very satisfactory. For this reason the deflections calculated above are plotted against applied load. The results are given in non-dimensional form in figures (4.8) and (4.9) for the various cases of initial crookedness and prestrain dealt with above. Clearly these curves all approach some asymptote. It is interesting

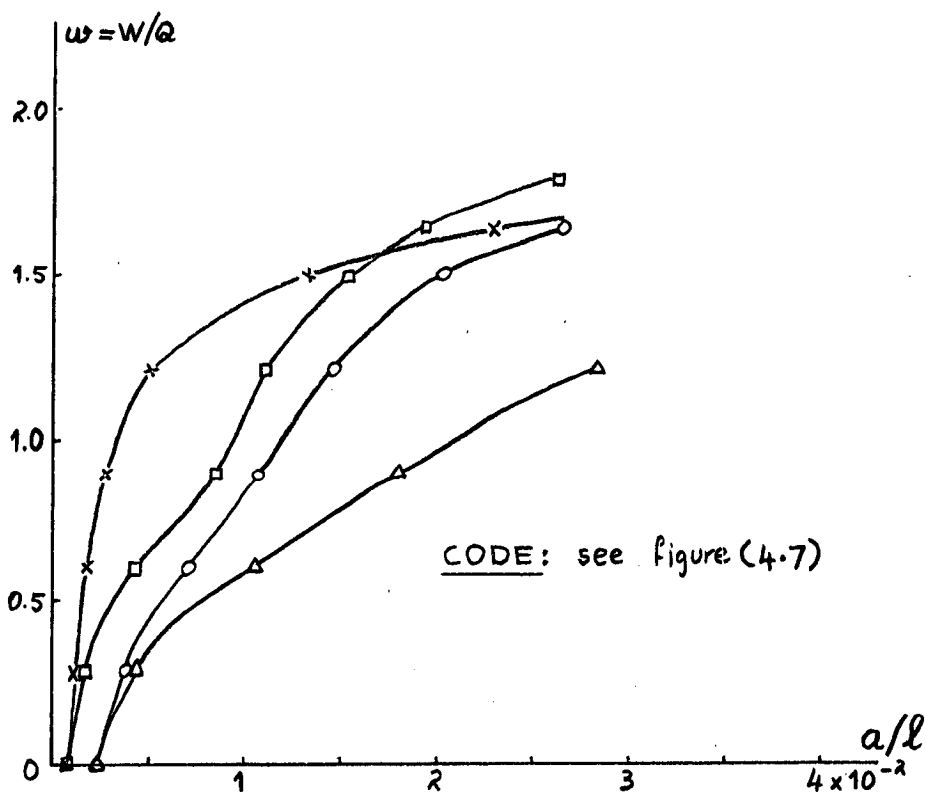


figure 4.9 - Central deflection of member AC

to note that the deflections of member AC at first appear to run away at some low value of applied load but then the curves start to rise again. This type of behaviour is to be expected, and is explained by returning to figure (4.6b) which indicates the behaviour if all the members are initially straight. The tendency is not evident when the frame is prestrained; possibly because both AB and AC now "buckle" almost simultaneously when the members have no crookedness (see figure 4.7). Figures (4.10) and (4.11) show the Southwell plots on the central deflections of the compression members. Those for members AB, BC, CD, DA are slightly convex upwards when the deflections are small, the greater the initial crookedness the more pronounced is the curve. However, after the deflections reach a magnitude of about  $1/100$ , the plots are close to linear. Using the average slope of the linear portions of the graphs, the buckling load is estimated as

$$w_{cr} = 1.88$$

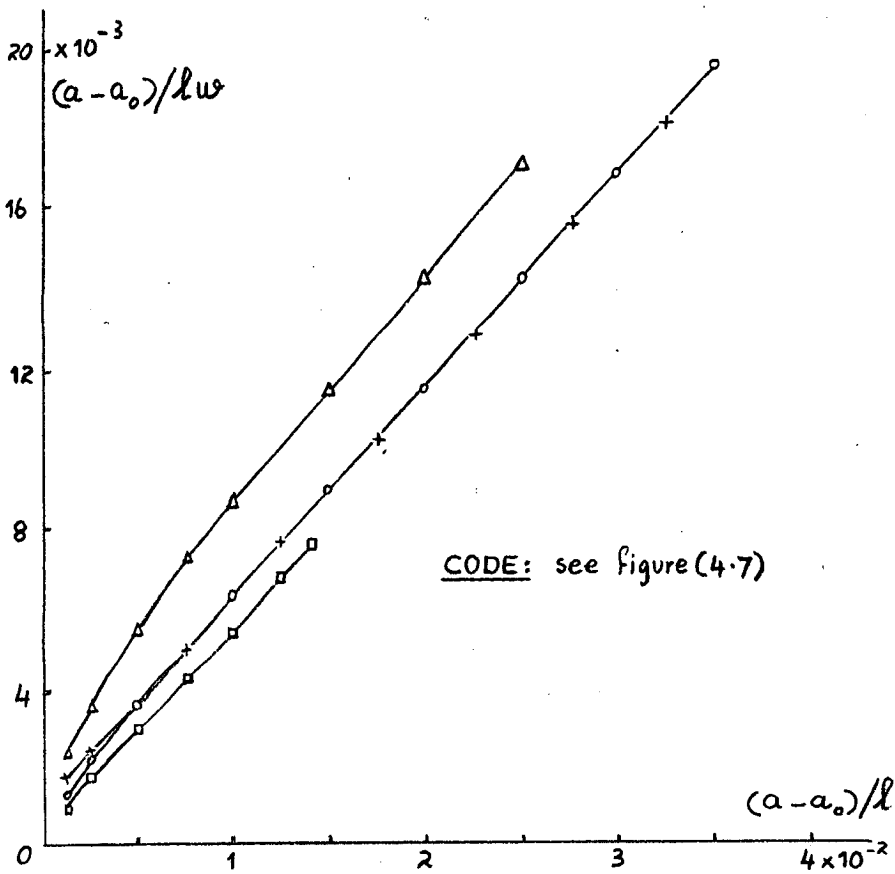


figure 4.10 - Southwell plots for members AB, BC, CD, DA

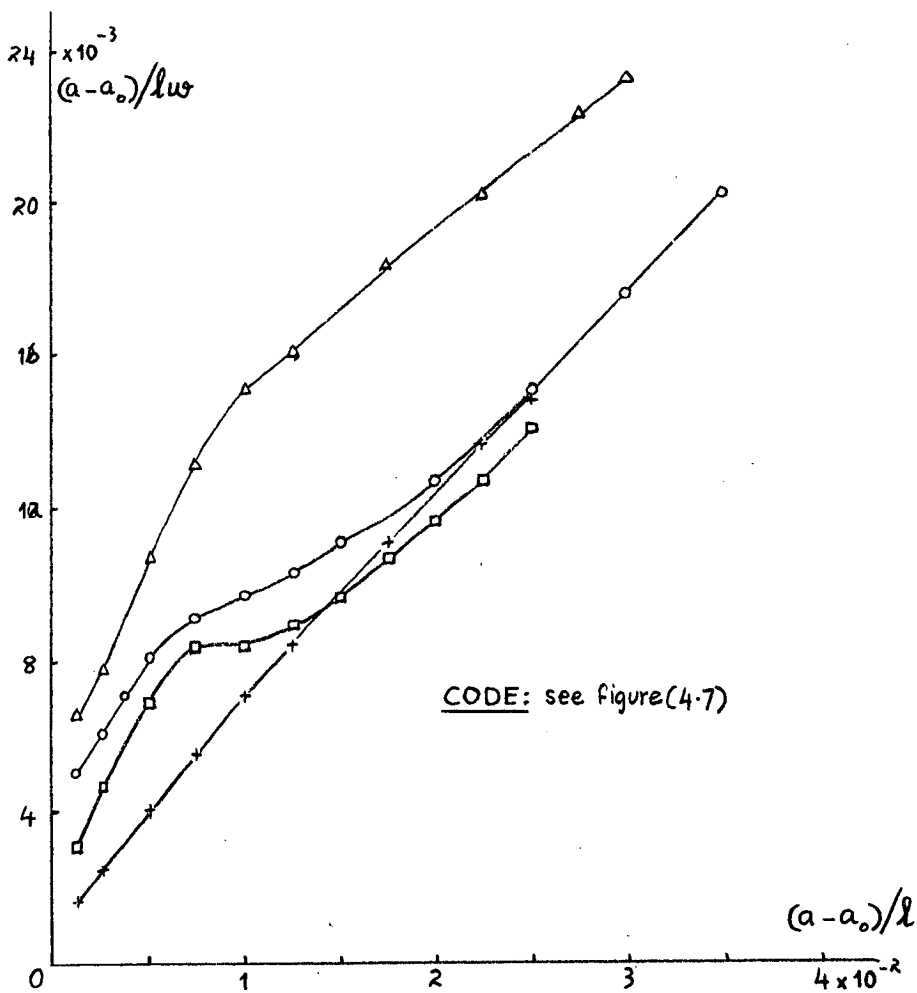


figure 4.11 - Southwell plots for member AC

the largest variation being -0.08. It is worthwhile noting that the behaviour of the frame with initial prestrain gives a Southwell plot which is almost wholly linear. Its inverse slope is 1.90, which agrees with the buckling load predicted when the members are assumed to be initially straight.

The Southwell plots on the central deflections of member AC, the critical member, are extremely curved but they seem to flatten out towards a straight line. The inverse slopes of the latter portions give an average value for the buckling load

$$w_{cr} = 1.91$$

with the largest variation being +0.09. It also appears that the very early portions of the graphs are reasonably well described by straight lines. Of these, the case with a small initial crookedness of  $1/1000$  in all members, has an inverse slope of about 0.74, which is close to the value at which the linear axial force distribution first intersects the interaction diagram, OXY in figure (4.7). The remaining cases without prestrain have inverse slopes of 0.87 and 1.04 respectively. The prestrain case is again interesting in that its Southwell plot for member AC consists of two almost linear portions. When the deflections are less than about  $1/100$ , the inverse slope has a value of 1.60, whereas the remainder has an inverse slope of 1.85. Inspection of the loading path for this case (see figure 4.7), shows that up to about  $w = 1.2$  the path is almost linear. Extending this it is found to intersect the interaction diagram at  $w = 1.50$ , which is close to the value of 1.60 obtained above.

### (c) Load carrying capacity

Although this chapter is primarily concerned with the elastic behaviour of overbraced frames, the above analyses provide sufficient information to comment on the load carrying capacity of this particular frame. Since the frame is relatively slender, the limit of the elastic range, that is the load to cause first yield, ought to provide a close estimate of the ultimate load which the frame can support. For each member the axial load to cause first yield is readily calculated, and the corresponding applied load  $W_Y$  is inferred from the plotted loading paths. In these computations the frame members are taken to be of 1 in. x  $\frac{1}{2}$  in. cross section, with a Young's modulus  $E$  of  $30 \times 10^6$  p.s.i. and the length of the sides of the frame is taken to be 28.8 in. so that the  $l/r$  ratio

is 200, as used in the analysis. Table (4.3) below summarizes the results for the four cases of initial crookedness and prestrain; the yield strain is taken as 0.0012. As can be seen, there is

Case	$(a_1)_{AB}$ (ins.)	$(a_1)_{AC}$ (ins.)	prestrain	(lbs) $(P_y)_{AB}$	(lbs) $(P_y)_{AC}$	(lbs) $W_y$	axial forces at yield	
							$P_{AB}$	$P_{AC}$
I	0.0720	0.1020	none	3050	1630	5640	2830	1630
II	0.0288	0.0407	none	3410	1755	6120	3410	1755
III	0.288	0.102	none	2050	1630	3640	1440	1630
IV	0.0720	0.102	yes	3050	1630	5950	3050	1615

Table 4.3 - Loads to cause first yield of 36,000 psi.

comparatively little difference in load to cause first yield in the various cases, except that when the initial crookedness in members AB, BC, CD and DA is very large (1/100). This is explained by the fact that the loading paths beyond  $W = 5500$  lbs. all lie very close to one another. For comparison, the elastic ultimate buckling load of this frame is

$$W_{ult} = 7090 \text{ lbs.}$$

(4.39)

which is about 25% in excess of the load to cause first yield in case I, which is appropriately regarded as the design.

It is also interesting to compare the above loads with the working load obtained by designing the frame on an individual member basis, and, as is almost universal practice, on the assumption of a linear loading path. Using a factor of safety of 2.0 against first yield in individual members, the safe working load is 1150 lb. when there is no prestrain. Member AC governs the design in this case. On the other hand, in the case of prestrain (see figure 4.7), member AB would be overloaded without any applied load, so that this particular amount of prestrain would not be considered practical when designing the frame on an individual member basis and on a linear loading path. The best that can be done on this basis is to choose a prestrain so that all compression members reach their allowable axial forces. If  $R_0$  is the prestraining force then we want

$$P_{AB} = P_{BC} = P_{CD} = P_{DA} = 1525 \text{ lbs.} = -0.707 R_o + 0.293 W_W \quad (4.40)$$

and 
$$P_{AC} = 815 \text{ lbs.} = R_o + 0.707 W_W$$

where  $W_W$  is the safe working load, based on a factor of safety of 2.0 in individual members. Solving these equations we find

$$R_o = -1285 \text{ lbs.} ; W_W = 2970 \text{ lbs.} \quad (4.41)$$

In case IV, table 4.3, the prestraining force  $R_o$  is -2600 lbs., and this is close to optimum because it is seen that all compression members yield nearly simultaneously. Thus it follows that the non-linearity of the loading path may have a considerable influence on the 'most favourable' pattern of prestrain.

#### 4.7 THE MEASURED BEHAVIOUR OF RIGIDLY JOINTED OVERBRACED FRAMES

The previous section was aimed at the establishment of a simple mathematical model to describe the behaviour of pin-jointed overbraced frames. Due to the difficulty of making truly pinned connections in practice, an experimental verification was not attempted. Practical frames have rigid or nearly rigid joints, and any analysis for the corresponding pin-jointed frames provides little indication of their behaviour.

This section presents the results of the measurement of the behaviour of some simple overbraced frames with rigid joints. Only simple measurements are taken, the main aim being to establish whether or not buckling in the usual sense does occur, and if so whether or not the Southwell plot can be used to measure the buckling load.

##### (a) Three bar frame

One of the simplest redundant frames is the three bar frame shown in figure (4.12). This particular frame was made from clockspring steel members measuring 0.500 in. x 0.0275 in. in cross section. The frame was loaded vertically with deadweights, and the central deflections of the members were measured to 0.01 in. with a rule. No attempt was made to measure the axial forces in the members. In the first test the members were rigidly clamped to a stiff supporting base, while in the second test the base connections were pinned.

Figure (4.13) shows the central deflection of member AD plotted against the applied load  $W$ , with the Southwell plot superimposed on it.

measured  $EI = 26.0 \text{ lb}\cdot\text{in}^2$   
all members are of equal  
length  
member AC is vertical

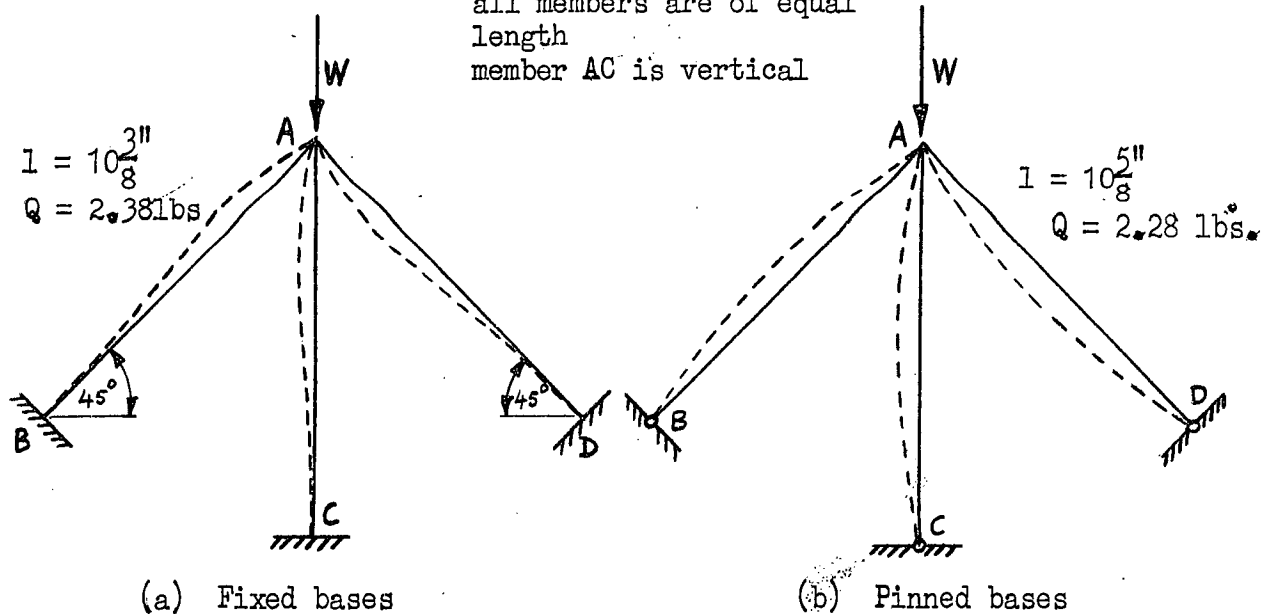


figure 4.12 - Three bar frame

For both the fixed base and pinned base tests the Southwell plots are very nearly linear over the whole range, indicating the existence of elastic buckling loads. From the inverse slopes the ultimate buckling loads are estimated as

$W_{ult} = 12.2 \text{ lbs.}$  for the fixed base case

and

$W_{ult} = 5.8 \text{ lbs.}$  for the pinned base case.

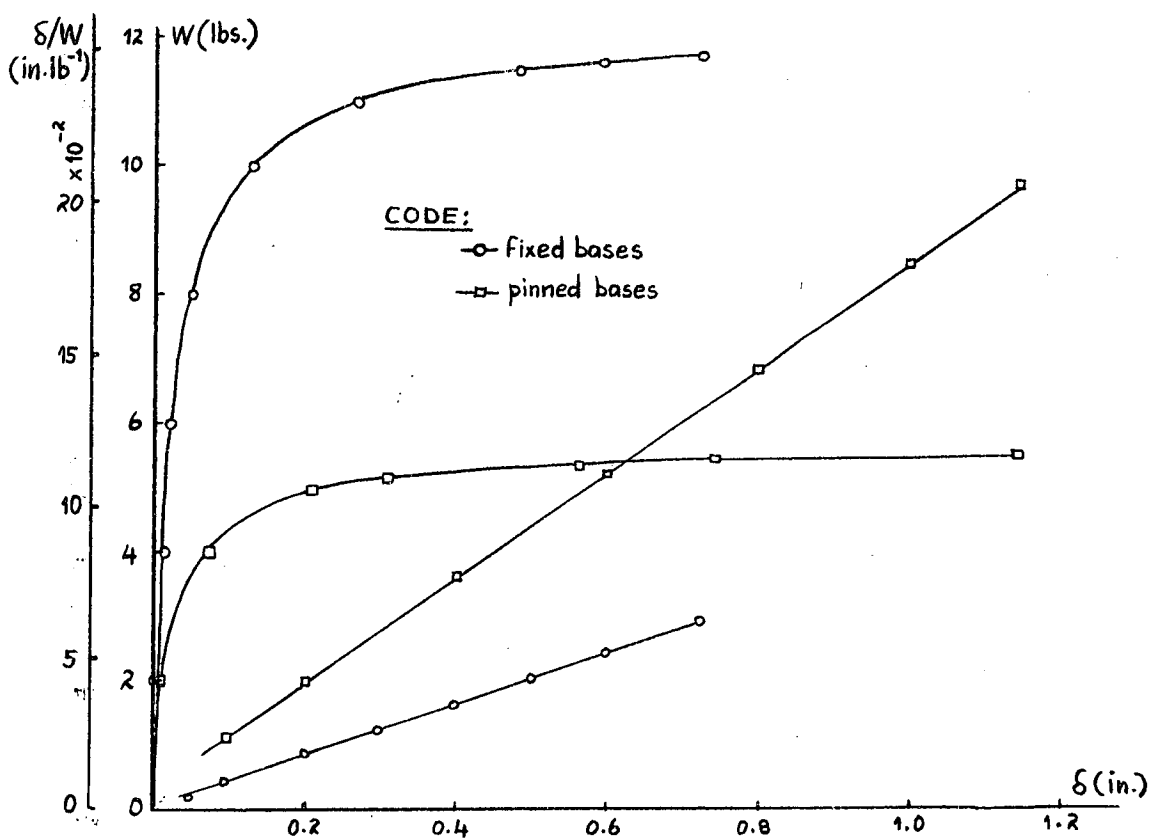
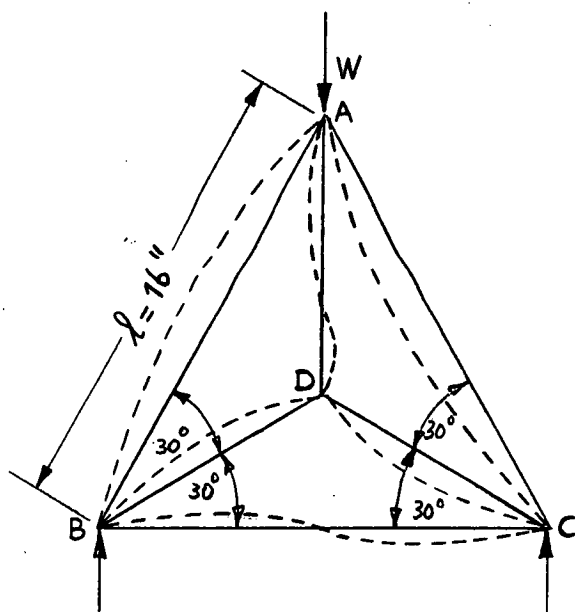


figure 4.13 - Southwell plots on lateral deflections

Since the Southwell plot for this particular frame behaviour is almost wholly linear, it is suspected that there is little redistribution of axial forces in the members as the frame is loaded. This is verified mathematically in section (4.10).

(b) Triangulated Frame

This frame, whose geometry is shown in figure (4.14), was made of  $\frac{1}{2}$  in. x  $\frac{1}{8}$  in. mild steel members, the major axes lying in the plane of the frame to ensure planar buckling. The leading dimension  $l$  was 16 inches, giving a nominal slenderness ratio  $l/r$  of about 450. Due to



measured  $EI = 2350 \text{ lb.in}^2$ .

Euler load of side members  $Q = 90.7 \text{ lbs.}$

figure 4.14

space limitations only two pairs of Huggenberger tensometers could be attached to the frame; these were located approximately at the centres of members AB and AC.

Figure (4.15) shows the measured bending strains plotted against applied load  $W$ . It is seen from these graphs that at low loads the curvatures appear to be asymptotic to some load, but subsequently the curves rise again and run away at a much higher load. This behaviour is very similar to that predicted for the pinjointed frame in figure (4.9). It suggests that the initial portion of the loading path is approximately linear, and the first apparent asymptote is some measure of where this portion of the loading path, when extrapolated, intersects the interaction curve.

Obviously the above behaviour cannot be described by a linear Southwell plot over the entire range of measurements, but the two asymptotes may be estimated by assuming the above curves to be made up of two hyperbolic portions separated by a transition region, as shown



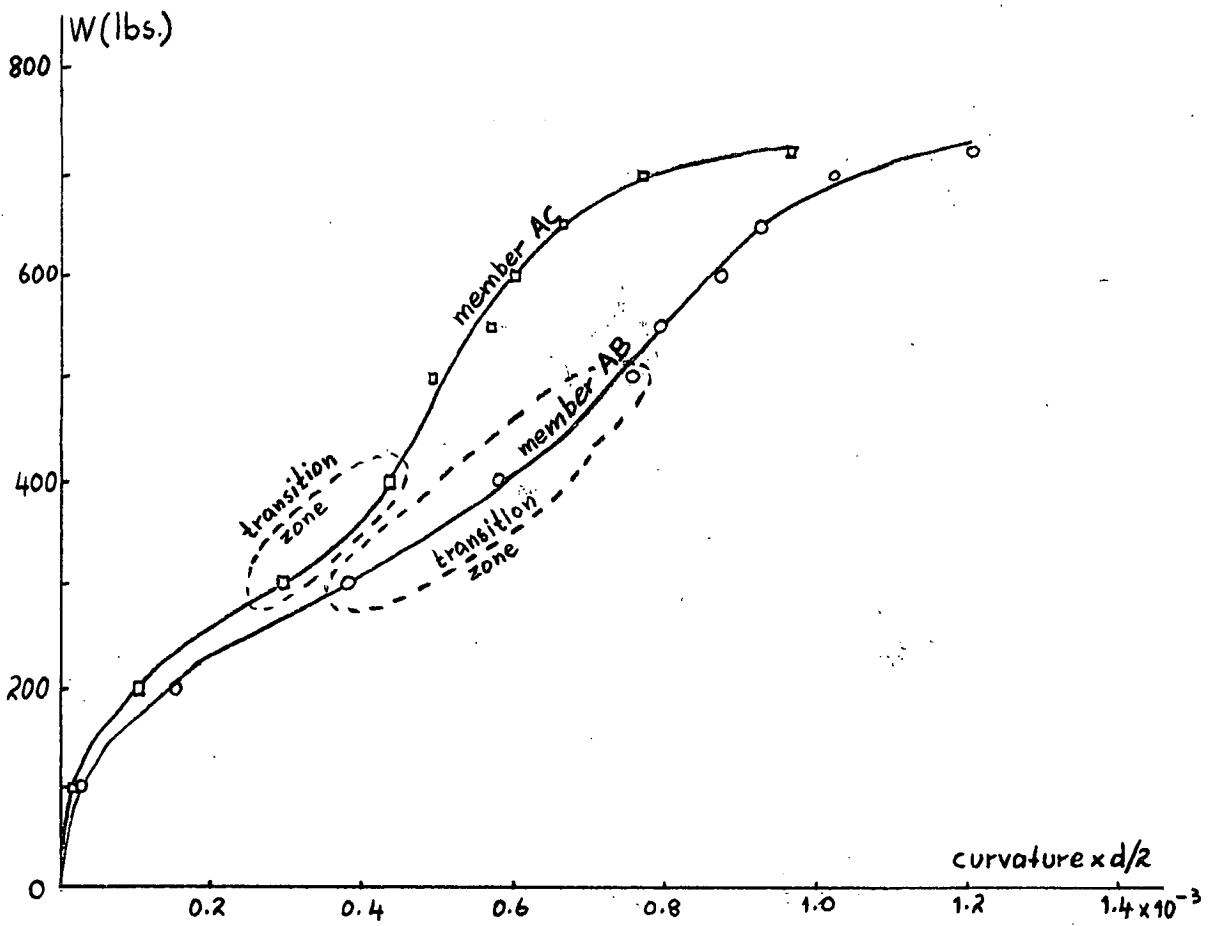


figure 4.15 - Measured curvatures

in figure (4.15). The Southwell plots for the low load regions are

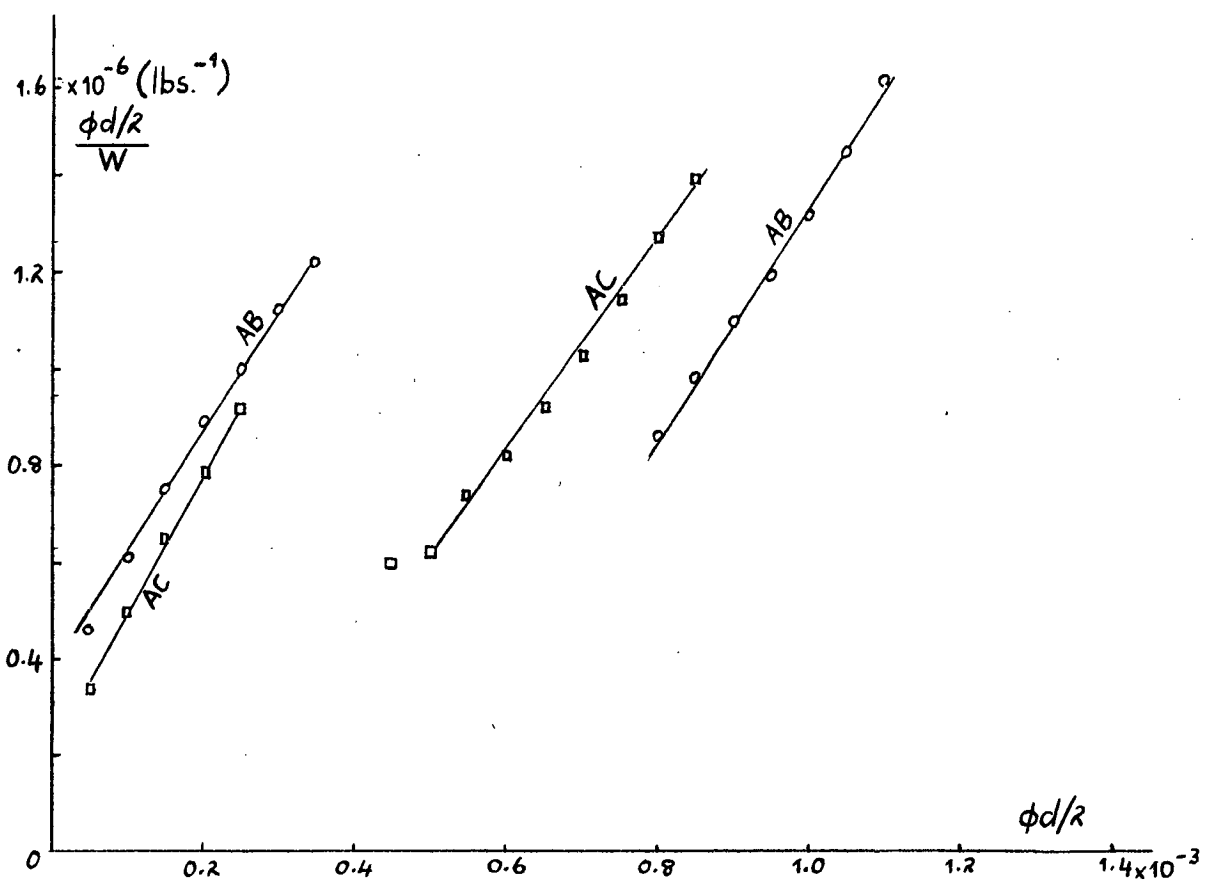


figure 4.16 - Southwell plots on curvatures

constructed in the usual way, and are seen to be reasonably linear, the average inverse slope giving an apparent buckling load of 380 lbs. Beyond the transition regions a Southwell-type plot is constructed by graphing  $(\epsilon - \epsilon_0)/(W - W_0)$  against  $\epsilon$ , where  $(\epsilon_0, W_0)$  is the point defining the start of the final hyperbola. For member AB this was taken as 500 lbs., and for member AC as 400 lbs. These two plots are also close to linear, having inverse slopes of 430 lbs. and 460 lbs. respectively. Adding to these the respective  $W_0$  values, we get 930 lbs. and 860 lbs. or an average of 900 lbs. for the elastic ultimate load of the frame. The observed buckling mode is superimposed in figure (4.14.)

In this particular test the graphs of curvature against load exhibited fairly well defined transition regions, and the curves were reasonably described by two separate linear Southwell plot equations. However, in general the transition from the initial apparent buckling condition to the ultimate elastic buckling behaviour is likely to be much more gradual, in which case it would be difficult to fit a linear Southwell plot type equation. It is impossible at this stage to establish definite behaviour patterns for redundant frames; a large variety of frames would need to be tested and the results correlated. At the same time, mathematical models predicting the behaviour need to be formulated, and it seems that a Southwell plot type of equation, which has proved to be extremely powerful for statically determinate frames, may often be a poor fit. The main factor responsible for this is the non-linearity of the loading path, which in turn depends on the magnitude and form of the initial crookedness, the slenderness of the members, and on the amount of prestrain existing in the unloaded frame. Practical frames usually have fairly stocky members, and the non-linearity is probably not so pronounced. For this type of frame the behaviour would be governed primarily by the initial buckling load and mode, for which the methods described in earlier chapters of this thesis are quite adequate. However, for more slender frames the ultimate elastic buckling load and mode control the behaviour. Since the ultimate elastic buckling load, if it exists, may be very much higher than the initial buckling load, an interesting question arises as to whether to design a given frame using slender or stocky members.

#### 4.8 THE ELASTIC BUCKLING LOADS OF RIGIDLY JOINTED OVERBRACED FRAMES

In this section it is proposed to examine a method for the prediction of the elastic buckling loads and modes for overbraced frames with rigid joints. The basic definition of instability is identical to that adopted in chapter one, that is

$$\partial X / \partial x = 0 \quad (4.42)$$

where  $X$  is a generalized force acting on the frame, and  $x$  is the generalized displacement corresponding to  $X$ . For clarity in what follows this definition requires careful interpretation. According to customary instability studies, the frame is assumed to be "perfect" initially, so that an equilibrium state with all members remaining straight is always possible. There are, however, certain discrete loading systems at which the straight form is not stable. At these loads any infinitesimal disturbance can excite large deformations, and the frame is said to buckle. The usual mathematical treatment assumes that the buckling deflections are small compared with the overall frame dimensions so that equation (4.42) should, more properly, be written as

$$(\partial X / \partial x)_{x \rightarrow 0} = 0 \quad (4.43)$$

This equation states that the load-lateral deflection graph exhibits a horizontal bifurcation, but it does not define the complete curve. The above small deflection theory works well even if the deflections are quite large, and certainly so in the working range of practical engineering structures. Hence the restriction  $x \rightarrow 0$  can, for all practical purposes, be removed and the load-deflection graph is in fact closely approximated to a horizontal straight line over the range of deflections commonly encountered.

For statically determinate frames the above condition is fulfilled when the frame stiffness is zero, since there are no other restrictions on the magnitudes of the deflections. However, for overbraced frames, the deflections must also satisfy the compatibility equations relating the changes in member lengths. While the members remain approximately straight, these changes in length are practically independent of the bending deflections, and by complementary energy methods it can be shown that the loading path is linear. Under these conditions the overbraced frame's behaviour is identical to that of a statically determinate

frame, and the critical load and its associated mode can be computed by methods described in earlier chapters of this thesis.

The subsequent behaviour is quite different because the deformations of the overbraced frame cannot, in general, run away at the critical load unless, by chance, the compatibility equations are also satisfied for large deflections, in which case the member shortenings are dominated by the portions due to bending. In general the compatibility equations are not satisfied at the critical load and mode. To achieve compatibility, the axial forces in the members redistribute themselves, and this redistribution alters the critical load and mode, and so on. The complete behaviour is difficult to trace, but it appears that some kind of ultimate load at which the frame buckles elastically still exists. As Masur (reference 2) has shown, the ultimate load is usually greater and never less than the critical load, so that the behaviour of an overbraced frame is of the form shown in figure (4.17).

From this figure it is seen that a possible definition for ultimate buckling is

$$(\partial X / \partial x)_{x \rightarrow \infty} = 0 \quad (4.44)$$

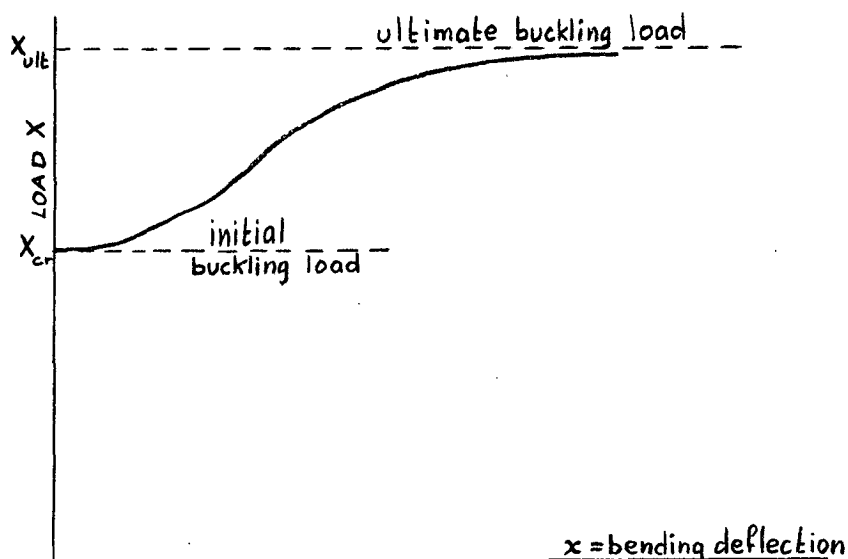


figure 4.17 - The behaviour of an overbraced frame

This definition is adopted in the work to follow. It is assumed that the members are initially straight and behave elastically all the way, and that, although bending deflections are tending to the infinite, small deflection theory is still applicable. For simplicity the argument is confined to plane frames buckling in their plane. As a further simplification it is assumed that the bending moments arising from the changes in member lengths are negligible, and that the shears have no effect on the axial forces in the members.

Consider any general plane frame having  $m$  redundant members (or supports), and let  $R_1, R_2, \dots, R_m$  be the axial forces in these members. The magnitudes of these forces are determined by cutting these members and equating to zero the total incompatibilities across the cuts. As shown in section (4.4), complementary energy provides an elegant method of deriving the compatibility equations. The complementary energy of the frame,  $C$  is defined as

$$C = \sum_{\text{members}}^{\text{all}} \left\{ \int_0^{P_i} \delta_i dP_i \right\} - \int_0^W \delta_W dW - \sum_{j=1}^m \int_0^{R_j} \delta_j dR_j \quad (4.45)$$

where  $\delta_i$  = shortening of the  $i$ th frame member

$P_i$  = axial force in the  $i$ th member (compression positive)

$\delta_W$  = displacement of  $W$

$W$  = applied load

$\delta_j$  = opening across the cut in the  $j$ th redundant member.

The first summation is applied over all the members of the frame, including the redundant members; as mentioned in section (4.4), the shortening of a cut redundant member is the sum of the shortenings of the two halves. The above complementary energy integral may be differentiated with respect to the independent forces  $W, R_1, R_2, \dots, R_m$ , whence we obtain the compatibility conditions

$$\partial C / \partial W = \sum_i \left\{ \delta_i (\partial P_i / \partial W) \right\} - \delta_W = 0 \quad (4.46)$$

$$\partial C / \partial R_j = \sum_i \left\{ \delta_i (\partial P_i / \partial R_j) \right\} - \delta_j = 0 ; (j = 1, 2, \dots, m)$$

In order to obtain the coefficients  $\partial P_i / \partial W$  and  $\partial P_i / \partial R_j$ , we need to express the axial forces in the members as functions of  $W$  and of the redundant forces  $R_1, R_2, \dots, R_m$ . These are readily deduced from a primary force analysis. Neglecting the change on frame geometry due to the deformations, the force in the  $i$ th member can be written as

$$P_i = a_i W + \sum_j b_{ij} R_j \quad (4.47)$$

where the coefficients  $a_i, b_{ij}$ , depend only on the overall frame geometry. From equation (4.47) we obtain

$$\partial P_i / \partial W = a_i \quad (4.48)$$

$$\partial P_i / \partial R_j = b_{ij}$$

so that the compatibility equations become

$$\delta_W = \sum_i a_i \delta_i \quad (4.49)$$

$$\delta_j = \sum_i b_{ij} \delta_i ; (j = 1, 2, \dots, m)$$

The first of these equations gives the deflection of the load in terms of the individual member shortenings, while the second set of equations gives the openings across the cuts in the redundant members. The latter set is used to evaluate the redundant forces, but in order to do so it is necessary to specify a relation between the axial force and shortening for each member. When the members are elastic and when there is no bending, we can write

$$\delta_i = (Pl/EA)_i \quad (4.50)$$

which, on substitution into the compatibility equations, leads to linear algebraic equations to solve for each  $R_j$  in terms of  $W$ . If there is no initial prestrain, each  $\delta_j$  is zero, otherwise it will have some value (see section 4.6b).

Having determined the redundant forces, equations (4.47) are used to express the axial forces in the members in terms of  $W$  only, and it is seen that the axial forces are in constant proportion. Hence it follows that the frame with all its members remaining straight is in equilibrium for all values of  $W$ , and it remains to investigate its stability. As in chapter one, this is most conveniently done by applying small disturbances, in the form of infinitesimal moments at the joints, exciting lateral deflections. In the limit, as deflections tend to zero, equations (4.50) remain approximately valid, so that the axial forces may be calculated as above. The usual equations of equilibrium in terms of the joint rotations are then set up by the stiffness method giving, in the usual matrix notation,

$$\tilde{\delta M} = \tilde{K} \cdot \tilde{\theta} \quad (4.51)$$

where  $\tilde{\theta}$  is the vector defining the joint rotations,  $\tilde{K}$  is the stiffness matrix, and  $\tilde{\delta M}$  is the vector defining the infinitesimal disturbing moments. In the limit as  $\tilde{\delta M}$  becomes the null vector, this analysis leads to the familiar zero determinant criterion

$$|\tilde{K}| = 0 \quad (4.52)$$

or the zero latent root criterion

$$\lambda = 0 \quad (4.53)$$

Either of these equations may be used to calculate the buckling modes and loads, that is the buckling loads for zero deformations ( $W_{cr}$  in figure (4.17)).

In order to determine the ultimate load, or buckling load for "large" deformations, that is  $W_{ult}$  in figure (4.12), the above analysis must be modified to include the effect of the member shortenings due to the bending deflections. Under these conditions it seems reasonable to neglect the axial shortening  $Pl/AE$  and the initial prestrain (if any), so that the shortening of the  $i$ th member becomes

$$\delta_i = \frac{1}{2} \int_0^l (dy_i/dx)^2 dx \quad (4.54)$$

where  $y_i$  is the deflected shape. In chapter one it was shown that the deflected shape is

$$y = A \sin(\sqrt{\rho} \pi x/l) + B \cos(\sqrt{\rho} \pi x/l) + Cx + D \quad (4.55)$$

where  $\rho = P/Q$ , and  $A, B, C, D$  are constants to be determined from the boundary conditions; the subscript  $i$  has been dropped for convenience. The boundary conditions are

$$(y)_{x=0} = (y)_{x=l} = 0 ; (dy/dx)_{x=0} = \theta_0 ; (dy/dx)_{x=l} = \theta_1 \quad (4.56)$$

which gives the shortening as

$$= (-1/\pi^2) [\frac{1}{2} F_1(\theta_0^2 + \theta_1^2) F_2 \theta_0 \theta_1] \quad (4.57)$$

where  $F_1$  and  $F_2$  are functions of  $\rho$ , and can be shown to be the derivatives of the stability functions  $s$  and  $sc$  respectively, that is

$$F_1 = ds/d\rho ; F_2 = d(sc)/d\rho \quad (4.58)$$

$$\text{where } s = \pi^2 \rho / 4(1-w) + w ; sc = \pi^2 \rho / 4(1-w) - w \quad (4.59)$$

$$w = \alpha \cot \alpha ; \alpha = (\pi/2) \sqrt{\rho} ; \rho = P/Q \quad (4.60)$$

Thus the shortening for "infinite" deflections is seen to be a non-linear function of the axial load in the member, and, as well as this, the expression contains the quadratic terms of the member end slopes  $\theta_0$  and  $\theta_1$ .

Using the expression (4.57), the compatibility equations for "infinite" deflections become

$$\sum_i \left\{ (-1/\pi^2) [\frac{1}{2} F_{1i}(\theta_{oi}^2 + \theta_{li}^2) + F_{2i} \theta_{oi} \theta_{li}] (b_{ij}) \right\} = 0 ; (j = 1, 2, \dots, m) \quad (4.61)$$

By virtue of joint rigidity, the member end slopes

$\theta_{oi}$  and  $\theta_{li}$  are equal to the relevant joint rotations, and these in turn satisfy the stiffness equations at the ultimate load, that is

$$\tilde{K} \cdot \tilde{\theta} = \tilde{O} \quad (4.62)$$

The problem then is to solve equations (4.61), (4.62), simultaneously, for the lowest value of  $W$  and the corresponding values of the redundant forces, for then the frame has buckled, or can buckle, because the frame stiffness is zero so that large deflections are possible, and the large deflections satisfy the compatibility equations.

As can be seen, the compatibility equations cannot be solved independently for the redundant forces since the expressions contain also the joint rotations, that is the redundant forces depend on the buckling mode. Once the mode has been determined, the compatibility equations can be solved for the redundant forces. In general some iterative scheme must be adopted, and except for very simple frames, the computations are usually too numerous to be performed by manual methods.

The above compatibility equations may be changed into a slightly simpler form, similar to that proposed by Masur (see equations 4.1) by substitution of the member's moment-slope relations.

$$\begin{aligned} M_0 &= (EI/l)(s \theta_0 + sc \theta_1) \\ M_1 &= (EI/l)(sc \theta_0 + s \theta_1) \end{aligned} \quad (4.63)$$

By definition,  $\theta_0$  and  $\theta_1$  are imposed rotations, so that at this stage they are independent of the axial loads in the members, that is independent of  $W$ ,  $R_1$ ,  $R_2$ , ...,  $R_m$ , and therefore we have

$$\begin{aligned} \partial M_0 / \partial R_j &= (EI/l)(\theta_0 \partial s / \partial R_j + \theta_1 \partial sc / \partial R_j) \\ \partial M_1 / \partial R_j &= (EI/l)(\theta_0 \partial sc / \partial R_j + \theta_1 \partial s / \partial R_j) \end{aligned} \quad (4.64)$$

But  $s$  and  $sc$  are explicit functions of  $\rho$  so that

$$\begin{aligned} \partial s / \partial R_j &= (ds/d\rho)(\partial \rho / \partial R_j) = F_1(1/\rho Q)(\partial P / \partial R_j) \\ \partial sc / \partial R_j &= \text{etc.} \end{aligned} \quad (4.65)$$

Substituting  $Q = \pi^2 EI / l^2$ , we get

$$\begin{aligned} \partial M_0 / \partial R_j &= (1/\pi^2)(\theta_0 F_1 + \theta_1 F_2)(\partial P / \partial R_j) \\ \partial M_1 / \partial R_j &= (1/\pi^2)(\theta_0 F_2 + \theta_1 F_1)(\partial P / \partial R_j) \end{aligned} \quad (4.66)$$

where  $F_1$  and  $F_2$  are defined by equations (4.58). Comparing these equations with the expression for the bending shortening, it follows that

$$\delta(\partial P / \partial R_j) = -\frac{1}{2}[\theta_0(\partial M_0 / \partial R_j) + \theta_1(\partial M_1 / \partial R_j)] \quad (4.67)$$



This is in fact the contribution of any member towards the opening of the  $j$ th cut. Summation over all the members of the frame gives the total opening which, for compatibility of member shortenings, is zero. Using the fact that the sum of the end members connected at a joint equals the applied joint moment, this summation reduces to

$$-\frac{1}{2}\theta_1(\partial M_1/\partial R_j) - \frac{1}{2}\theta_2(\partial M_2/\partial R_j) - \dots - \frac{1}{2}\theta_n(\partial M_n/\partial R_j) = 0 \quad (4.68)$$

where  $\theta_1, \theta_2, \dots, \theta_n$  are the joint rotations, and  $M_1, M_2, \dots, M_n$  are the joint moments which must be applied to maintain these rotations. The generalized frame stiffness is defined as the latent root of the stiffness matrix, that is

$$\lambda = M_1/\theta_1 = M_2/\theta_2 = \dots = M_n/\theta_n \quad (4.69)$$

whence we obtain

$$\partial M_1/\partial R_j = \theta_1(\partial \lambda/\partial R_j) ; \partial M_2/\partial R_j = \theta_2(\partial \lambda/\partial R_j) ; \text{etc.} \quad (4.70)$$

Hence the compatibility equations reduce to

$$-\frac{1}{2}(\partial \lambda/\partial R_j) \sum_{\text{joints}} \theta^2 = 0 \quad (4.71)$$

or simply

$$\partial \lambda/\partial R_j = 0$$

That is, the member shortenings for "infinite" deflections are compatible when the derivatives of the generalized frame stiffness with respect to the redundant forces are zero. This criterion is a generalization of that developed by Murray (reference 1). The argument is valid only if the shortening due to axial strain,  $Pl/AE$ , is negligible compared with the bending shortening. This is a reasonable simplification when the frame has buckled at its ultimate load. Thus finally, the ultimate elastic buckling mode and load are characterized by the equations

$$\lambda = 0 \quad (4.72)$$

$$\partial \lambda/\partial R_j = 0 ; (j = 1, 2, \dots, m)$$

where  $\lambda$  is a latent root of the stiffness matrix which is associated with a latent vector or buckling mode. In general there may be several modes which satisfy the above equations or there may not be any. Furthermore it seems possible that the ultimate buckling mode is not necessarily the one which has the lowest stiffness over the entire range of applied loads, since the latent root plots can cross (see for example figure 3.15). Obviously these considerations give rise to computational difficulties. A large number of frames needs to be analyzed and the results checked by model tests to assess the reliability of the above equations. Although the equations in their

present form are not used in this thesis, the following iterative scheme, backed by a reasonable picture of the mode from observations of simple inexpensive models, appears to be an attractive method of finding a solution:

- (a) take a trial value for the ultimate load  $W$
- (b) guess values of the redundant forces  $R_1, R_2, \dots, R_m$
- (c) calculate the axial forces in the members
- (d) set up the stiffness matrix  $\tilde{K}$
- (e) extract the latent roots and vectors of the stiffness matrix
- (f) for each mode in turn set up the compatibility equations. This is most easily done by Wittrick's method (reference 5 chapter 3), that is

$$\partial \lambda / \partial R_j = \tilde{\theta}^T \cdot \tilde{K}_j \cdot \tilde{\theta}$$

where  $\tilde{\theta}$  is the normalized latent vector,  $\tilde{\theta}^T$  its transpose, and  $\tilde{K}_j$  is the matrix whose elements are the derivatives with respect to  $R_j$  of the elements of  $\tilde{K}$ . In general the compatibility equations are not satisfied.

- (g) linearize the compatibility equations by using the first two terms in Taylor's series for the derivatives of the elements of  $\tilde{K}_j$ ; this involves the use of second derivatives of  $s$  and  $sc$ .
- (h) assuming the modes remain constant, solve the linearized equations for the increments  $\delta R_1, \delta R_2, \dots, \delta R_m$  in the redundant forces.
- (i) repeat steps (c) to (h) until reasonable agreement is obtained. The sign of the smallest latent root at this stage indicates whether or not the ultimate load has been reached. Once the buckling mode has been established it is not necessary to calculate all the latent roots and vectors, but only that corresponding to the correct mode. It should also be kept in mind that a compatibility solution need not exist for every latent vector; an example of this is seen in the following section.

#### 4.9 FRAMES WITH ONE DEGREE OF STATICAL INDETERMINACY

In the case of a frame which has only one degree of statical indeterminacy with respect to the axial forces in its members, the solution for the ultimate elastic buckling loads and modes is relatively straightforward, and can be performed graphically. Denoting by  $R$  the single redundant force, then the latent root of the stiffness matrix corresponding to any particular latent vector or mode can be represented by a function of the two variables  $W$  and  $R$ , that is

$$\lambda = \lambda(W, R) \quad (4.73)$$

This function can be visualized as a surface in space. For convenience  $W$  and  $R$  are measured in a horizontal plane and  $\lambda$  is measured as the height of the surface above or below this plane. When the frame buckles in any mode, the latent root corresponding to the mode under investigation vanishes, and this condition is satisfied by the intersection of the surface with the  $W$ - $R$  plane. The curve so defined in the  $W$ - $R$  plane is readily calculated, and this is what Giudici (reference 3) calls the interaction curve. It is the locus of simultaneous values of  $W$  and  $R$  for which the frame stiffness is zero. Simple examples of interaction curves have already been given in section (4.6). The interaction curve in general may be of any shape, and there is of course a curve associated with each buckling mode of the frame. Figure (4.18) depicts a typical example. Since the frame stiffness is zero on the interaction curve, the initial buckling load  $W_{cr}$  is obtained as the intersection of the linear loading path  $R = kW$  (assuming the members do not bend) on the interaction curve, as in the figure. The ultimate elastic buckling load must, in addition to lying on the interaction curve, satisfy the compatibility equation for "large" deflections, that is

$$\partial \lambda / \partial R = 0$$

Along the interaction curve, from any point to a neighbouring point, we have

$$d\lambda = 0 = (\partial \lambda / \partial W) dW + (\partial \lambda / \partial R) dR \quad (4.74)$$

whence we obtain

$$\partial \lambda / \partial R = -(\partial \lambda / \partial W) (dW/dR) \quad (4.75)$$

and since  $(\partial \lambda / \partial W) = (\text{deflection of } W) \neq 0$ , we find that  $\partial \lambda / \partial R$  is zero when

$$(dW/dR)_{W=W_{ult}} = 0 \quad (4.76)$$

That is the ultimate elastic buckling load is the peak of the interaction curve.

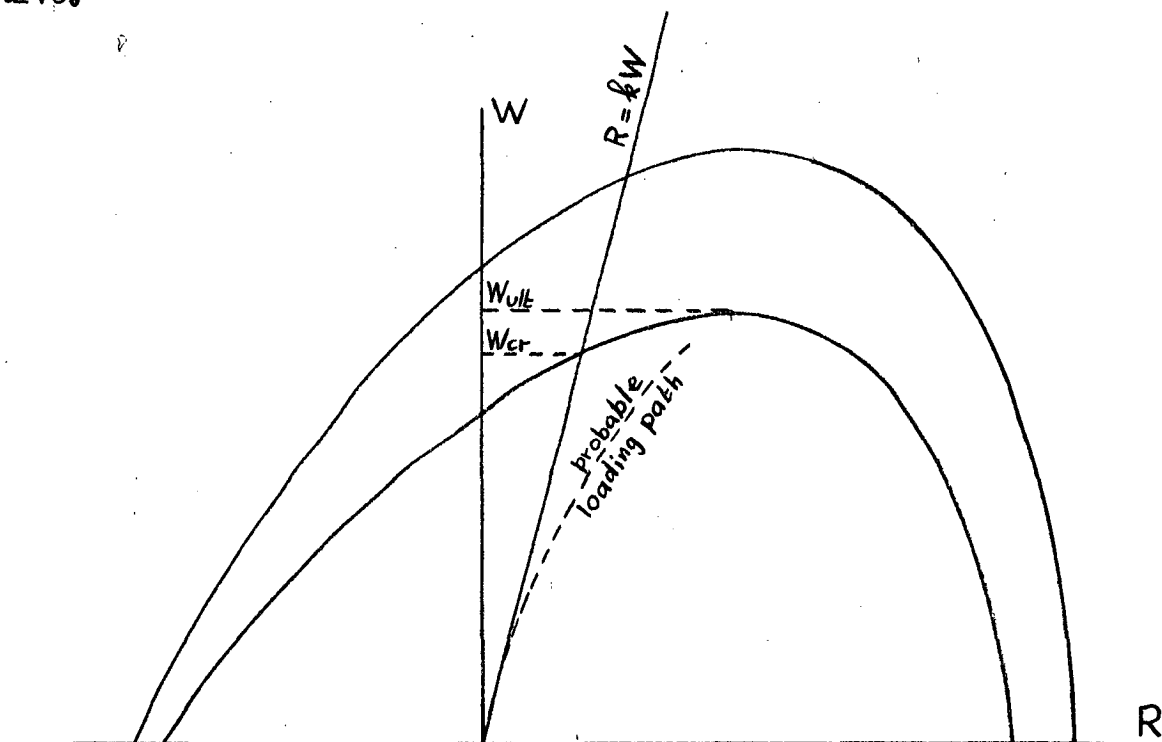


figure 4.18 - Typical interaction curve

The interaction curve thus provides a useful means of determining both the initial and ultimate elastic buckling loads. The associated modes are also readily obtained by interpolating between two calculated points one on either side of the respective load. At the same time the curve gives an indication as to which way the axial forces are most likely to redistribute themselves in a test.

#### 4.10 EXAMPLES OF INTERACTION CURVES

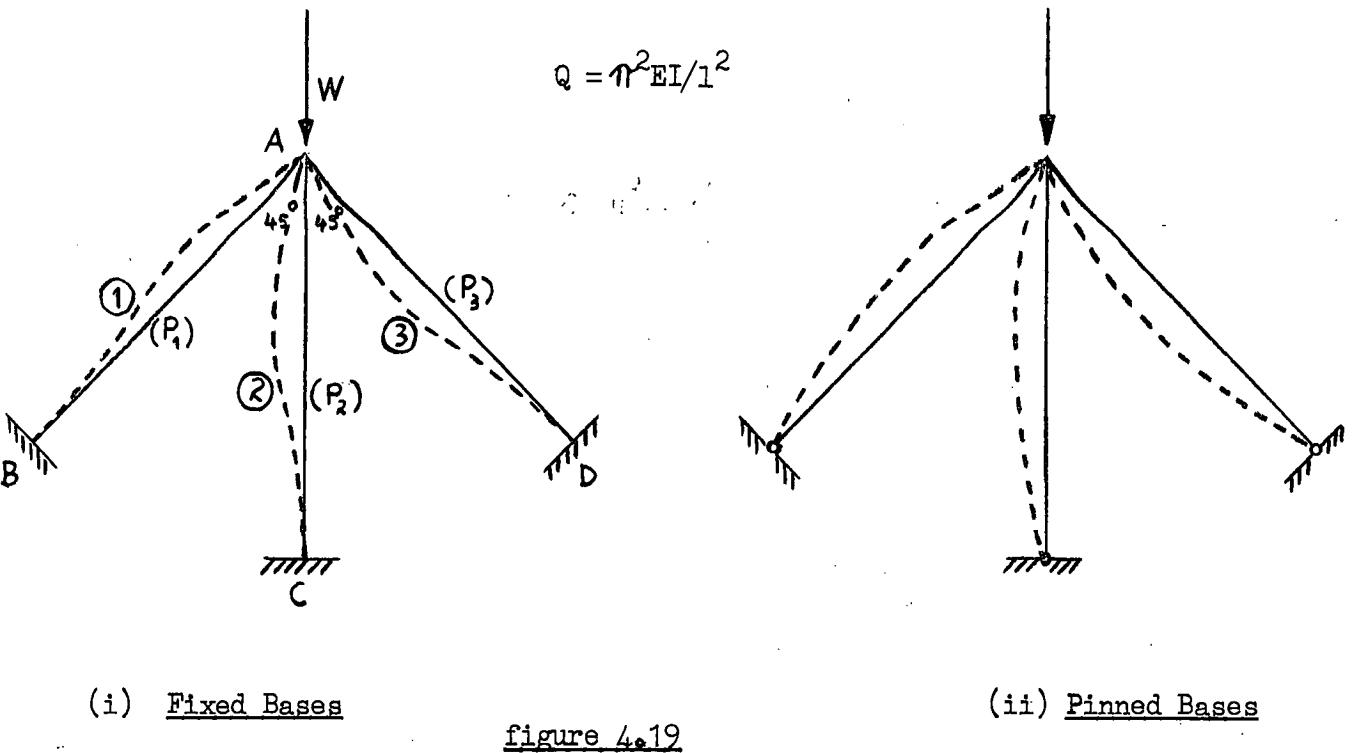
##### (a) Three bar frame

As a simple example consider the frames shown in figure (4.19), which have the same overall dimensions but different base connections. All members are of the same length, material and cross section, and buckling is confined to the plane. Member AC is vertical and load is applied vertically. The measured behaviour of these frames was given in section (4.7).

Member AC is arbitrarily designated as the redundant member and  $R$  is the axial force in it. From a primary force analysis we obtain the axial forces in the members as

$$P_3 = P_1 = (W-R)/\sqrt{2} \quad ; \quad P_2 = R \quad (4.77)$$

compression being taken as positive.



(1) Fixed bases

In this case joint A only can rotate, and if  $\theta$  is the angle of rotation then the moment required to produce  $\theta$  is

$$M = (EI/l)(s_1 + s_2 + s_3) \quad (4.78)$$

where  $s_1$ ,  $s_2$ ,  $s_3$  are the stiffness coefficients of the respective members. The frame stiffness, or latent root, in this case is therefore simply

$$\lambda = M/\theta = (EI/l)(s_1 + s_2 + s_3) \quad (4.79)$$

Since  $P_3 = P_1$ , we have  $s_3 = s_1$ , and the interaction curve is defined by  $\lambda = 0$  which then becomes

$$2s_1 + s_2 = 0 \quad (4.80)$$

This equation can be solved by inspection of the tabulated stability functions. Working non-dimensionally, we put

$$\rho_1 = P_1/Q \quad ; \quad w = W/Q \quad ; \quad r = R/Q = \rho_2 \quad (4.81)$$

By fixing  $r$ , that is  $\rho_2$ , the value of  $s_2$  is read from tables; equation (4.80) gives  $s_1 = -0.5s_2$ , and the tables are entered again to determine the corresponding  $\rho_1$  value; the value of  $w$  is calculated from equation (4.77) as

$$w = \sqrt{2} \rho_1 + r \quad (4.82)$$

Figure (4.20) shows the interaction curve for positive values of  $w$  only.

(ii) Pinned bases

In this case all joints can rotate, but since the bases are pinned we have

$$\theta_B = -c_1\theta ; \theta_C = -c_2\theta ; \theta_D = -c_3\theta \quad (4.83)$$

where  $\theta$  is the rotation of joint A, and  $c_1, c_2, c_3$  are the carry-over factors of the respective members. The moment required at A to produce these rotations then becomes

$$\begin{aligned} M &= (EI/l)[s_1(1-c_1^2) + s_2(1-c_2^2) + s_3(1-c_3^2)] \\ &= (EI/l)(s_1'' + s_2'' + s_3'') \end{aligned} \quad (4.84)$$

where  $s''$  is a function which is also tabulated directly. Again  $s_3'' = s_1''$ , and the interaction curve for the frame with pinned base connections is therefore given by

$$2s_1'' + s_2'' = 0 \quad (4.85)$$

which is solved in the same manner as before.

(iii) Completely pin-jointed

When the members meeting at A are also free to rotate relatively, the interaction curve degenerates to two straight lines given by

$$\rho_3 = \rho_1 = 1 ; \rho_2 = 1 \quad (4.86)$$

that is

$$w - r = \sqrt{2} ; r = 1$$

These are also shown in figure (4.20).

It is interesting to note that all three interaction curves are

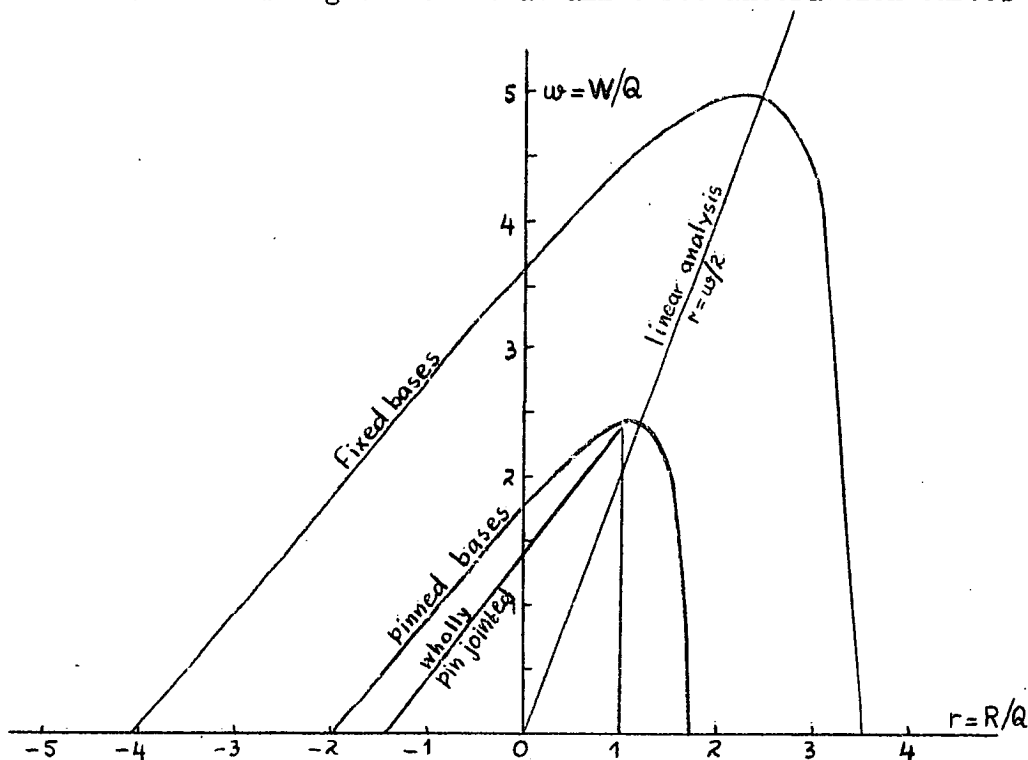


figure 4.20 - Interaction curves for three bar frame

similar in shape, but that there is a decrease in size as more pinned joints are introduced. On the basis of a linearly elastic analysis with no bending, the compatibility equations are satisfied by the relation

$$R = W/2 \quad (4.87)$$

Superimposing this linear loading path on the interaction curves, we see that it very nearly passes through the peaks of the curves. This suggests that the actual loading path in a measured test might also be close to linear, which explains why a good linear Southwell<sup>plot</sup> was obtained in the model tests (see section 4.7).

From the peaks of the interaction curves the predicted ultimate elastic buckling loads for these frames are

$$W_{ult} = 4.98Q \text{ for the fixed-base frame,}$$

and

$$W_{ult} = 2.43Q \text{ for the pinned-base frame.}$$

Inserting the numerical values of  $Q$  given in figure (4.12), the predicted values are respectively 11.85 lbs. and 5.55 lbs. These are in good agreement with the measured values 12.2 lbs. and 5.8 lbs.

(b) Triangulated frame

As a second example, the frame shown below is analysed and its interaction curve drawn. Treating member AD as redundant, and denoting by  $R$  its axial force, the axial forces in the remaining members are found to be as given in the figure. The stiffness matrix for this frame is

$$\begin{bmatrix} M_A \\ M_B \\ M_C \\ M_D \end{bmatrix} = (EI/l) \begin{bmatrix} (2s_1 + \sqrt{3}s_2) & s_1c_1 & s_1c_1 & \sqrt{3}s_2c_2 \\ s_1c_1 & (s_1 + \sqrt{3}s_2 + s_3) & s_3c_3 & \sqrt{3}s_2c_2 \\ s_1c_1 & s_3c_3 & (s_1 + \sqrt{3}s_2 + s_3) & \sqrt{3}s_2c_2 \\ \sqrt{3}s_2c_2 & \sqrt{3}s_2c_2 & \sqrt{3}s_2c_2 & 3\sqrt{3}s_2 \end{bmatrix} \begin{bmatrix} \theta_A \\ \theta_B \\ \theta_C \\ \theta_D \end{bmatrix} = \begin{bmatrix} 0 \\ 0 \\ 0 \\ 0 \end{bmatrix} \quad (4.88)$$

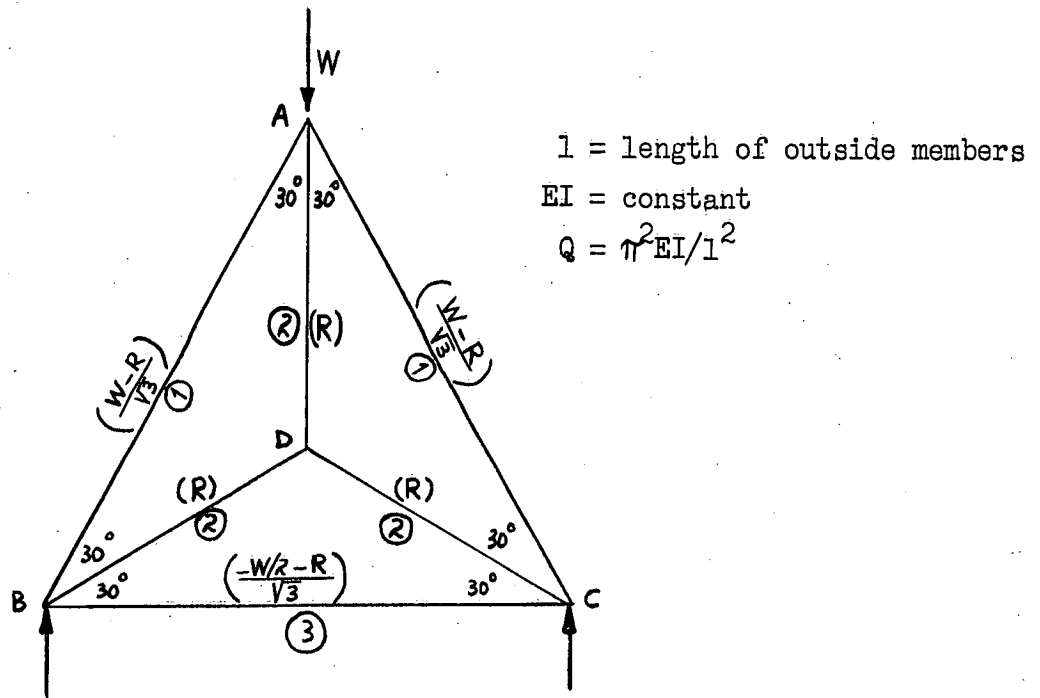


figure 4.21 - Triangulated frame

where  $s$  and  $sc$  are stability functions, the subscripts of which denote the respective members as shown in the figure by encircled numerals. For this  $(4 \times 4)$  stiffness matrix there exist in general four latent roots corresponding to four latent vectors, each of which represents a possible mode of buckling. The interaction curves are loci of points in the  $W$ - $R$  plane for which the respective latent roots are zero. In order to plot these, a digital computer program was written. The procedure adopted was to select various  $W$  values and extract the latent roots and vectors at several values of  $R$ , the limits being chosen so that the  $P/Q$  ratio in any member was always less than 4. From these results graphs of latent roots against  $R$  were plotted with  $W$  as a parameter. These graphs are of similar form; a typical set is shown in figure (4.22). The modes corresponding to the latent roots are sketched in figure (4.23). From the graphs in figure (4.22) we can locate the points at which the latent roots are zero, and hence the interaction curves can be drawn. These are shown in figure (4.24). The interaction curves for modes 1 and 2 are seen to intersect at  $w = 0$ . In fact at  $w = 0$  two latent root plots shown in figure (4.22) coincide for all values of  $r$ . The interaction curve for mode 3 intersects both the other two, and within the range of calculated points it does not exhibit a peak. Mode 4 does not have any zero stiffness in the range covered. For comparison, the interaction curve for the frame with all joints pinned is also shown.



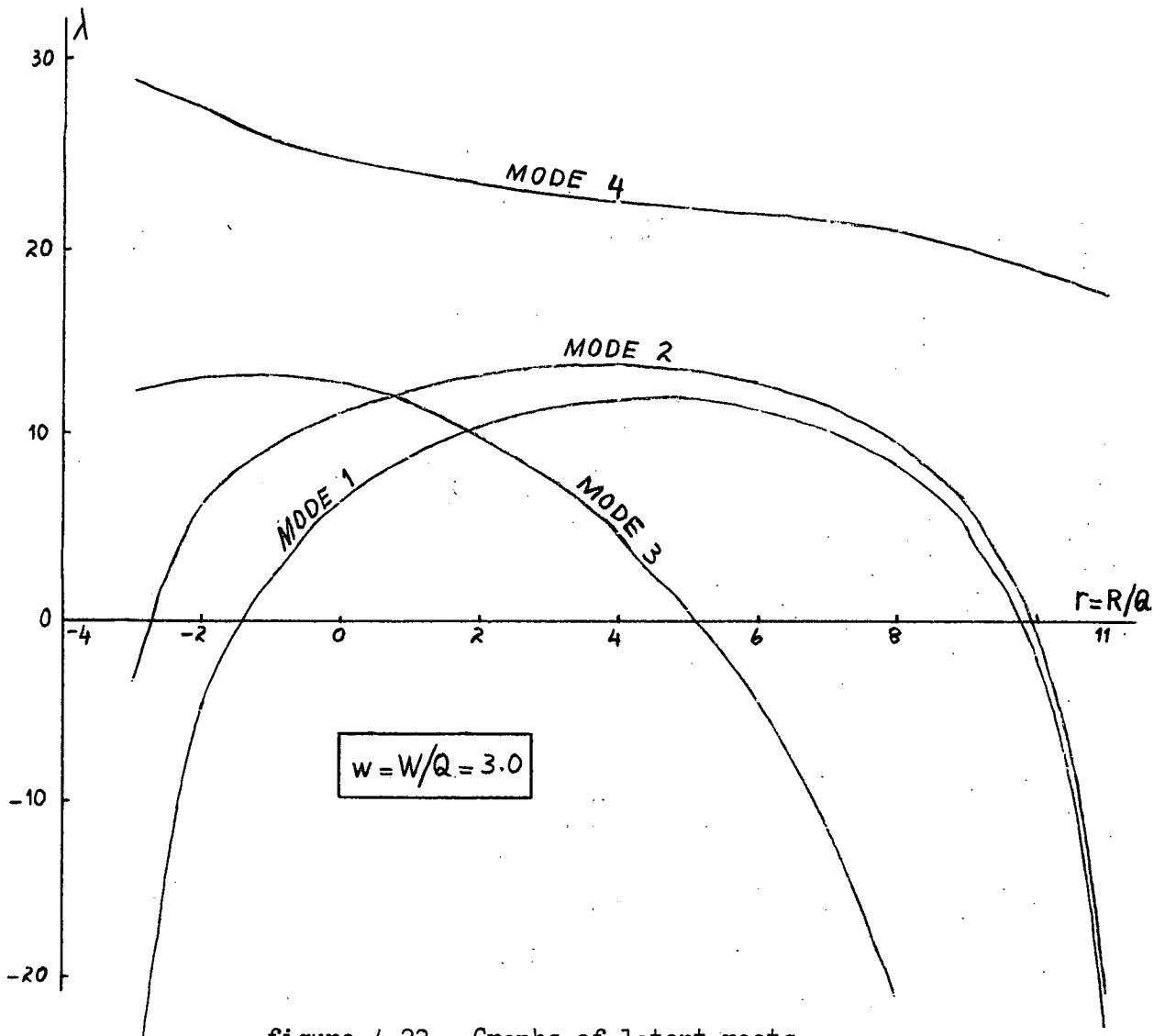


figure 4.22 - Graphs of latent roots

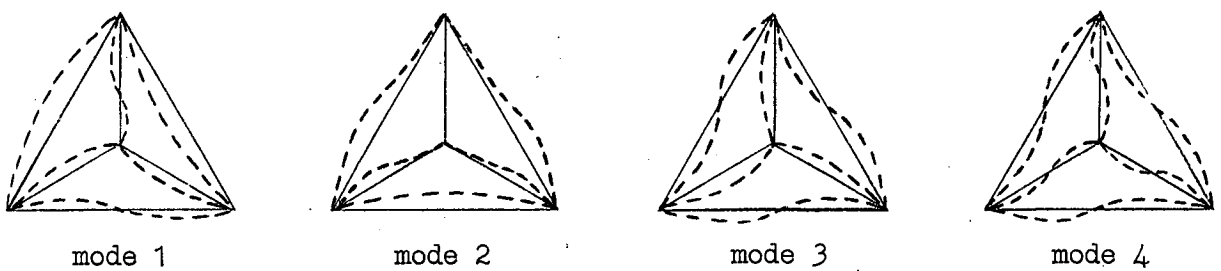


figure 4.23 - Modes associated with latent roots of figure 4.22

From the curves drawn it is seen that the ultimate buckling deformations are in mode 1, which agrees with that observed in model tests. The ultimate elastic buckling load, as given by the peak of the interaction curve is

$$W_{ult} = 9.75Q$$

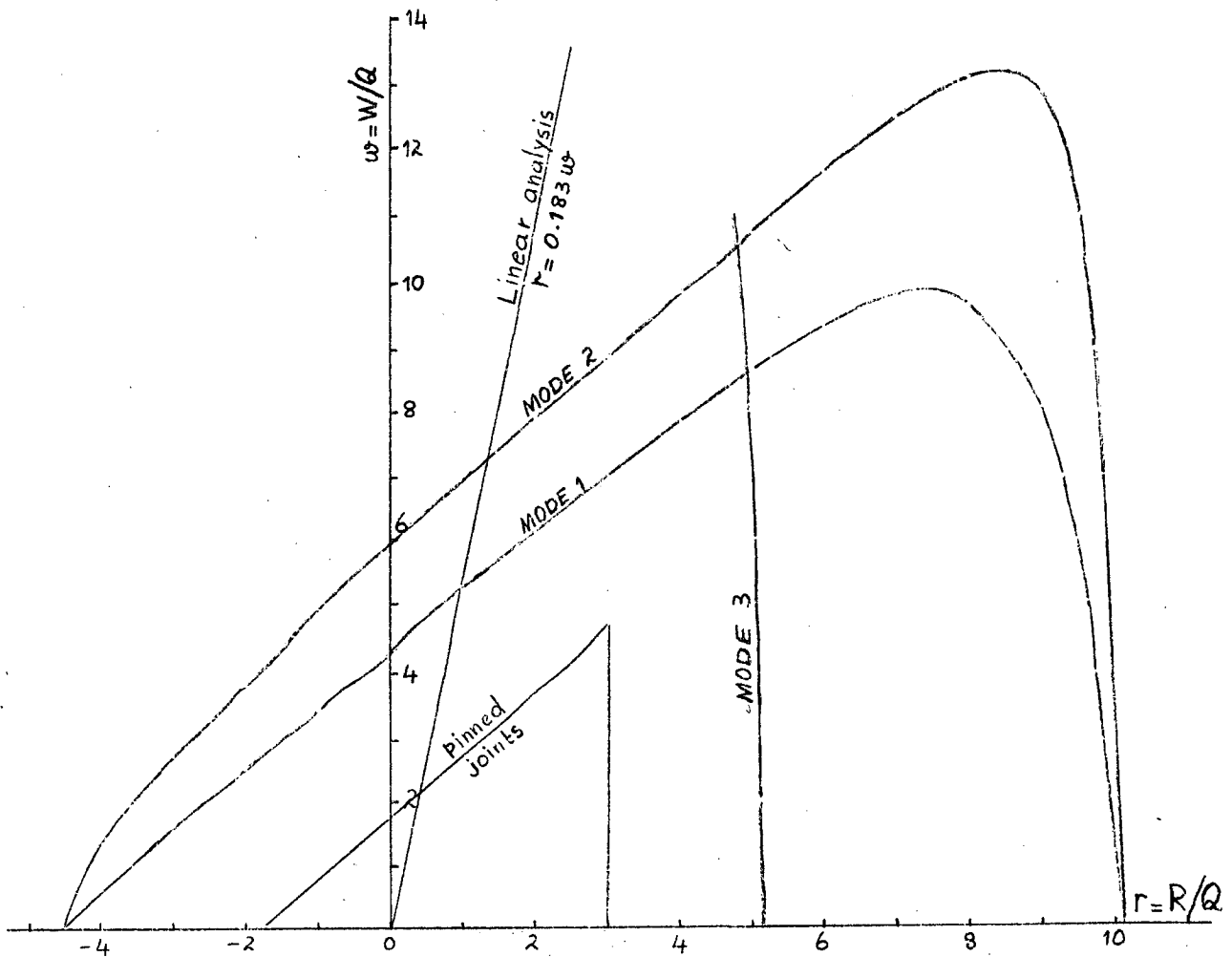


figure 4.24 - Interaction curves

Inserting the numerical value for  $Q$  given in figure (4.14), we get

$$W_{ult} = 885 \text{ lbs.}$$

which is in good agreement with the measured value of 900 lbs. The agreement is perhaps not as good as it looks, because the measured value is accurate to only about 5%.

The predicted initial buckling load is found from the intersection of the linear loading path on the interaction curve, that is

$$W_{cr} = 5.10Q = 463 \text{ lbs.}$$

which is to be compared with a measured value of 380 lbs. However the predicted value does not allow for prestrain, which has the effect of shifting the loading path either to the left or to the right, and hence a different point of intersection results. Also the loading path in a real test is non-linear, which again influences the initial behaviour. These aspects are discussed in the following sections.

Another point of interest arising from the above interaction curves is the question of how the actual loading path passes through the interaction curve for mode 3. At this point the frame stiffness is zero but only against deformations of the type mode 3, whereas the stiffness against mode 1 type deformations is still positive. Also, the frame first begins to deform into mode 1 so that it is more likely to continue to do so, unless there is some influence strong enough to make it change to mode 3. This might have occurred for example if mode 3 had a lower peak than mode 1.

#### 4.11 THE BEHAVIOUR OF INITIALLY CROOKED OVERBRACED FRAMES

As for statically determinate frames, or indeed any structure, a knowledge of the buckling loads and modes alone is not sufficient for design. Such knowledge provides only a picture of the behaviour of an oversimplified mathematical model of the real frame, one which is initially perfect. The ideal behaviour of the "perfect" model is pictured in figure (4.25). At low loads the frame is in stable equilibrium with all the members remaining straight. At some

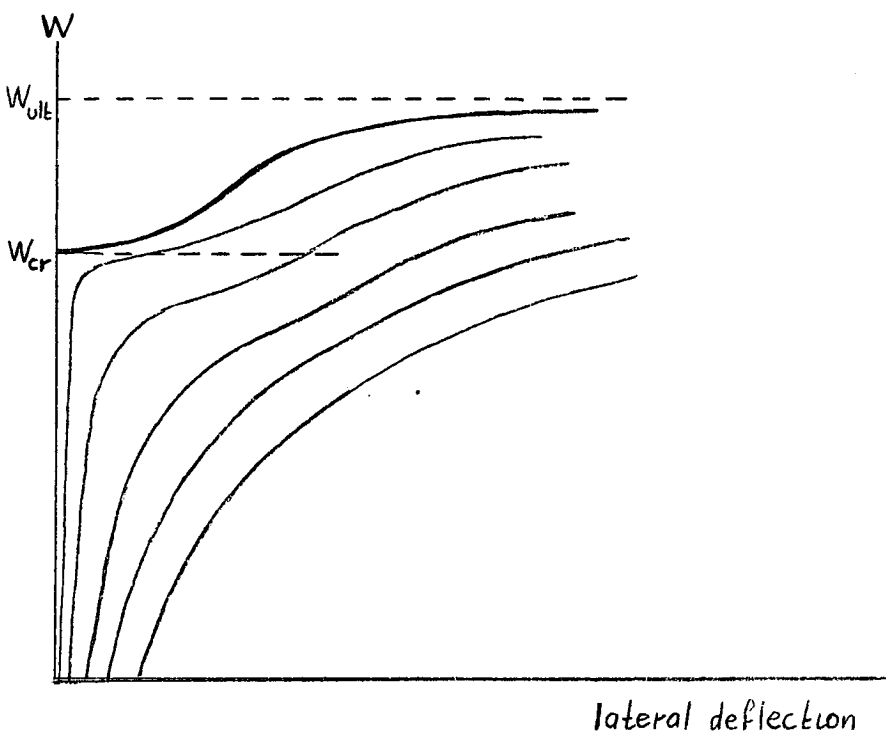


figure 4.25

load,  $W_{cr}$ , the straight form first becomes unstable but only against small deflections. As load is increased the deflections increase, rapidly at first, but the rate of increase gradually decreases. At a still later stage the rate of increase in deflections begins to rise again, and eventually becomes infinite at the ultimate load,  $W_{ult}$ , at which the frame must collapse.

The real frame possesses initial crookedness so that it begins to deform as soon as load is applied. If the magnitude of the imperfections is small, its behaviour follows closely that of the perfect frame, but in general, the larger the crookedness the more it departs from the latter, somewhat as given by the curves in the figure. Also the material of the real frame behaves elastically only for a limited range, up to a yield point say, and in most designs one tries to keep well within the range. Ultimately the designer is interested in the factor of safety against total collapse, that is the ratio of collapse load to working load.

In chapter one it was shown that the behaviour of a statically determinate frame is reasonably well described by a linear Southwell plot equation. This provides a convenient design method; assuming an initial crookedness pattern similar to the buckling mode, the deflections under load are obtained as the initial deflections multiplied by the ratio  $1/(1-W/W_{cr})$ . It is therefore relatively simple to trace the frame behaviour, and hence to estimate the load to cause first yield. For statically determinate frames the collapse load is usually only slightly higher than the load to cause first yield, and this criterion thus provides a useful design tool.

However, for overbraced frames the situation is more complicated. In general, the behaviour of an overbraced frame cannot be described by a linear Southwell plot, and the simple design method is lost. The reason for this is that the loading path for an overbraced frame is non-linear, that is the axial forces in the members do not remain in constant proportion to one another. As mentioned earlier, the main factors affecting the severity of the non-linearity are (a) the mode and magnitude of initial imperfections (including prestrain), (b) the ratio  $W_{ult}/W_{cr}$ , and (c) the slenderness of the frame members. If these factors are favourable then the departure from the linear loading path can be neglected.

Most practical frames have relatively low slenderness ratios, and for these frames the member shortenings are dominated by the axial strain rather than by bending effects, so that the analysis of section (4.8) breaks down. For these frames the compatibility conditions are approximately satisfied by a linear loading path, and yielding occurs before the departure from linearity becomes appreciable. Hence these frames are likely to behave similarly to statically determinate frames, and the design method described in chapter one, with  $W_{cr}$  as in figure (4.25) as the buckling load, can be used up to

first yield. As soon as a member yields it is reasonable to assume that its axial load subsequently remains constant. A new axial force distribution can then be calculated from modified compatibility equations, and the analysis is continued, and so on until a sufficient number of members has yielded so that the frame can collapse as a mechanism. Obviously  $(m + 1)$  members need to yield for the frame to become a mechanism.

A design based on the above simplifications, although conservative, is undoubtedly crude, but a detailed technique taking into account more of the important factors is likely to be too complicated for routine design office work. In the following section an attempt is made to formulate a mathematical model for a more detailed prediction of the behaviour of initially crooked overbraced frames.

#### 4.12 THE ANALYSIS OF INITIALLY CROOKED OVERBRACED FRAMES

The main difficulty in the analysis of overbraced frames lies in the treatment of the compatibility equations, from which the loading path is determined. A knowledge of the axial force distribution is necessary for the calculation of frame stiffness and hence the deformations. Unfortunately the compatibility equations contain quadratic terms in the deformations as well as non-linear force terms (see equation 4.61), so that neither can be determined independently of the other. However, this type of situation is very common to engineering problems, and frequently a solution can be obtained by trial and error, iterative or graphical methods, or other such powerful techniques.

In this section it is proposed to set up the necessary equations for general analysis, and a graphical solution is presented for a very simple singly-redundant system. Parts of the argument are repetitions of ideas presented already in chapter one, but are again included in order to stress the limitations of the mathematical model.

Consider first a single member isolated from the frame. At zero load the member is bent into a shape  $y_0$  say, which is assumed to be expressible as the infinite Fourier series

$$y_0 = (1/\pi) \sum_{n=1}^{\infty} \theta_n \sin(n\pi x/l) \quad (4.89)$$

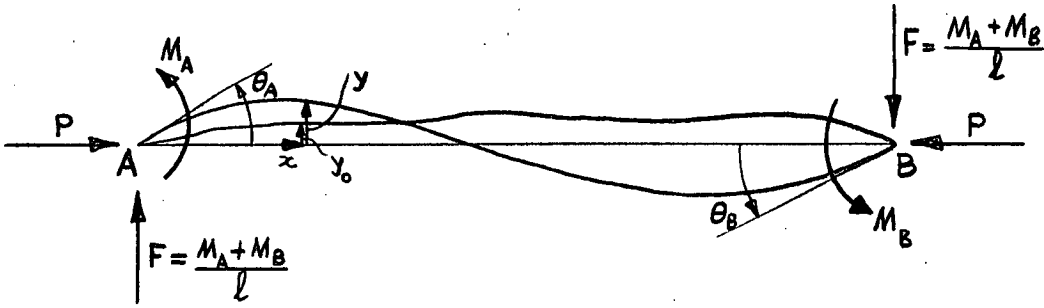


figure 4.26

where the choice of the parameters  $\theta_n$  (end slopes) will become apparent later. When the frame is loaded, the compressive axial force in the isolated member is  $P$ , the end slopes are  $\theta_A$ ,  $\theta_B$ , and the end moments are  $M_A$ ,  $M_B$  whence the end shears are obtained as  $(M_A + M_B)/l$ . The deflected shape  $y$  is to be determined. At any point  $(x, y)$  on the centreline of the deflected member, the bending moment is given by

$$M = -M_A(1-x/l) + M_B(x/l) - Py \quad (4.90)$$

and if linearly elastic material behaviour is assumed, we can write

$$\begin{aligned} M &= EI \times (\text{change in curvature}) \\ &= EI (d^2y/dx^2 - d^2y_0/dx^2) \end{aligned} \quad (4.91)$$

These two equations combine into a single linear differential equation, whose solution is

$$\begin{aligned} y &= A \sin(\sqrt{\rho} \pi x/l) + B \cos(\sqrt{\rho} \pi x/l) - (M_A/P)(1-x/l) + (M_B/P)(x/l) \\ &\quad + (1/\pi) \sum_{n=1}^{\infty} [\theta_n \sin(n\pi x/l)/(1-\rho/n^2)] \end{aligned} \quad (4.92)$$

where  $\rho = P/Q$  ;  $Q = \pi^2 EI/l^2$

The constants  $A$  and  $B$  are determined from the boundary conditions of zero deflection at the ends. When the end slopes are also introduced we find that the end moments are given by the equations

$$M_A = (EI/l)[(s\theta_A + sc\theta_B) - (s-sc)\phi_0 - (s+sc)\phi_e] \quad (4.93)$$

$$M_B = (EI/l)[(sc\theta_A + s\theta_B) + (s-sc)\phi_0 - (s+sc)\phi_e]$$

where

$$\begin{aligned} \phi_0 &= \sum_{n=1,3,5,\dots}^{\infty} [n\theta_n/(1-\rho/n^2)] \\ \phi_e &= \sum_{n=2,4,6,\dots}^{\infty} [n\theta_n/(1-\rho/n^2)] \end{aligned} \quad (4.94)$$

These expressions for the end moments contain the usual terms in the final end slopes  $\theta_A$ ,  $\theta_B$ , together with the terms  $\phi_0$ ,  $\phi_e$  which are the initial end slopes corresponding to the Fourier terms, magnified by the ratios  $n/(1-\rho/n^2)$ .

The axial shortening due to bending,  $\Delta$  is given by

$$\Delta = \frac{1}{2} \int_0^l (dy/dx)^2 dx - \frac{1}{2} \int_0^l (dy_0/dx)^2 dx \quad (4.95)$$

Using equations (4.89) and (4.92) this gives, after a lengthy manipulation

$$\Delta = -(1/\pi^2) \left\{ \frac{1}{2} F_1 (\theta_A'^2 + \theta_B'^2) + F_2 \theta_A' \theta_B' - (s-sc) \sigma_0 (\theta_A' - \theta_B') - (s+sc) \sigma_e (\theta_A' + \theta_B') - (\pi^2/4) \sigma_1 \right\} \quad (4.96)$$

where  $F_1$  and  $F_2$  are the derivatives of the stability functions  $s$  and  $sc$  respectively (see equations 4.58), and

$$\begin{aligned} \sigma_0 &= \sum_{n=1,3,5,\dots}^{\infty} [\theta_n / n(1-\rho/n^2)^2] \\ \sigma_e &= \sum_{n=2,4,6,\dots}^{\infty} [\theta_n / n(1-\rho/n^2)^2] \\ \sigma_1 &= \sum_{n=1}^{\infty} n^2 \theta_n^2 [1/(1-\rho/n^2)^2 - 1] \\ \theta_A' &= \theta_A - \sum_{n=1}^{\infty} [n \theta_n / (1-\rho/n^2)] \\ \theta_B' &= \theta_B - \sum_{n=1}^{\infty} [(-1)^n n \theta_n / (1-\rho/n^2)] \end{aligned} \quad (4.97)$$

The total shortening,  $\delta$  is obtained by adding to the above the term  $Pl/EA$ , that is

$$\delta = Pl/EA + \Delta \quad (4.98)$$

\* \* \* \* \*

When the above equations are to be used in frame analysis, the first step is to decide on the overall crookedness of the frame. Since there is little, if any, information regarding the type and pattern of crookedness to be expected, this task is not easy. Consequently, whatever is done, one must try to make conservative estimates. As in chapter one, it seems reasonable to focus attention on joint rotations, and to assume that the initial crookedness can be expressed in terms of the initial joint rotations. The relative magnitudes of these rotations are chosen to resemble the ultimate buckling mode. This leaves the overall magnitude of the frame crookedness as a free parameter which, if desired, can be expressed as a fraction of representative member lengths and related to the initial rotations.

Once the magnitudes of the initial joint rotations have been fixed, there remains the question of the deflected shapes of individual members. However, it is thought that this is rather less important than the assigning of a pattern and magnitude of crookedness, so that any reasonable shape, having end slopes corresponding to the relevant joint rotations, will suffice. This can be achieved by using the first two Fourier terms in equation (4.89) for any member, and the two coefficients are readily calculated from the boundary conditions.

Under load, the members of the frame deflect further and strain longitudinally. The final joint rotations and axial force distribution are calculated from the equations of equilibrium and of compatibility. As before, let there be  $m$  redundant members and assume that the shear forces arising from bending are negligible compared with the axial forces. Then the axial force in each member is expressed in terms of the applied load  $W$  and the redundant forces  $R_1, R_2, \dots, R_m$  from a simple primary force analysis. We can then set up the joint equilibrium equations using the single member relations of the type (4.93). These equations are of the form

$$\tilde{K} \cdot \tilde{\theta} = \tilde{\theta}_0 \quad (4.99)$$

where  $\tilde{K}$  is the usual  $(n \times n)$  stiffness matrix whose elements are functions of  $W$  and  $R_1, \dots, R_m$ ;  $\tilde{\theta}$  is the vector whose elements are the final joint rotations, and  $\tilde{\theta}_0$  is a vector whose elements are the initial joint rotations modified according to the factors appearing in equations (4.93).

The compatibility equations are most easily derived by complementary energy methods as described earlier, and when equations such as (4.98) are introduced, they become of the form

$$A_j \tilde{\theta}^2 + B_j \tilde{\theta} \cdot \tilde{\theta}_0 + C_j \tilde{\theta}_0^2 + D_j = 0 \quad ; (j = 1, 2, \dots, m) \quad (4.100)$$

where  $A_j, B_j, C_j, D_j$  are functions of  $W$  and  $R_1, \dots, R_m$ ;  $D_j$  represents the linear term corresponding to the axial shortenings of the members. Equations (4.99) and (4.100) together provide a solution for the  $n$  unknown joint rotations and the  $m$  unknown redundant forces.

Clearly a direct solution of either set of unknowns is not possible. To obtain a solution one must iterate. If an axial force distribution is assumed, the joint equilibrium equations (4.99) reduce to an ordinary linear set which may be solved by classical methods.



These rotations, together with the assumed axial forces, do not in general satisfy compatibility. The force terms in the compatibility equations can be linearized, and by holding the rotations constant, the resulting linear equations are solved for improved values of the forces. This process is continued until satisfactory agreement is reached. It is not known whether this process converges.

#### 4.13 A WORKED EXAMPLE

In order to demonstrate the technique developed above, the simple "frame" shown in figure (4.27) is analyzed. In this case there is only one joint rotation, that of joint A, and one

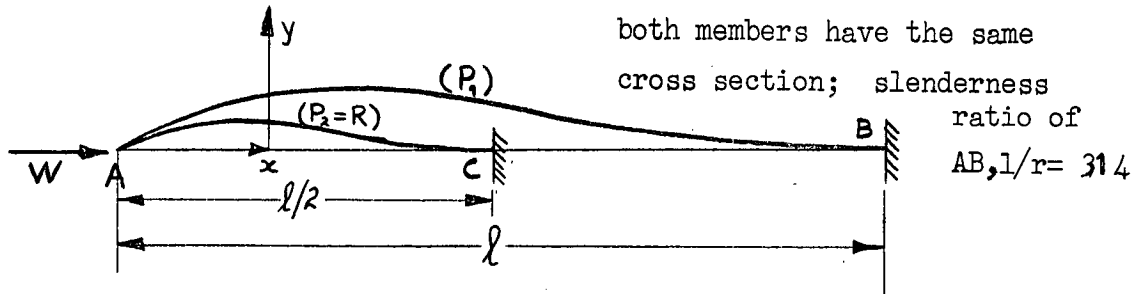


figure 4.27

redundant member. The buckled shape is as shown in the figure, and the initially crooked shape is taken to be similar, with  $\theta_0$  as the initial misalignment of joint A. Using the first two terms of a Fourier series to represent the initial crookedness of the members, we find

$$(y_0)_1 = (1/\pi) [\frac{1}{2} \theta_0 \sin(\pi x/l) + \frac{1}{4} \theta_0 \sin(2\pi x/l)] \quad (4.101)$$

$$(y_0)_2 = (1/\pi) [\frac{1}{4} \theta_0 \sin(2\pi x/l) + 1/8 \theta_0 \sin(4\pi x/l)]$$

Under load the rotation of joint A increases to  $\theta$ , and the member axial forces are  $P_1$  and  $P_2$ , where

$$P_1 = W - R \quad (4.102)$$

$$P_2 = R$$

Working non-dimensionally, we put  $w = W/Q$ ;  $r = R/Q_1$ ;  $\rho_1 = P_1/Q_1$ ;  $\rho_2 = P_2/Q_2$ , where  $Q_1 = \pi^2 EI/l^2$  = Euler load of member AB;  $Q_2 = 4\pi^2 EI/l^2$  = Euler load of member AC.

Thus we obtain

$$\begin{aligned} \rho_1 &= w - r \\ \rho_2 &= r/4 \end{aligned} \quad (4.103)$$

The member end moments are obtained from equations (4.93) and summation

at joint A gives

$$(s_1 + 2s_2)\theta = \theta_0 [2(s_1 - s_1 c_1)/(1 - \rho_1) + 2(s_1 + s_1 c_1)/(1 - \rho_1/4) + (s_2 - s_2 c_2)/(1 - \rho_2) + (s_2 + s_2 c_2)/(1 - \rho_2/4)] \quad (4.104)$$

where  $s$  and  $sc$  are the stability functions, the subscripts denoting the respective members.

The compatibility equation for this frame is

$$P_1 l / EA + \Delta_1 = P_2 l / 2EA + \Delta_2 \quad (4.105)$$

where  $\Delta_1$  and  $\Delta_2$  are the bending shortenings, which are calculated from equation (4.96).

In this simple problem a graphical solution is most convenient. For any value of  $w$  select various  $r$  values, calculate  $\rho_1$  and  $\rho_2$  from (4.103), from tables read off the values of  $s_1$ ,  $c_1$ ,  $s_2$ ,  $c_2$  and hence calculate the rotation  $\theta$  from (4.104). The bending shortenings are then calculated from (4.96), and the discontinuity across the cut is given by

$$\mathcal{E} = (P_1 l / EA + \Delta_1) - (P_2 l / 2EA + \Delta_2) \quad (4.106)$$

The solution is thus obtained by graphing  $\mathcal{E}$  against  $r$  and locating the zero. In the numerical work,  $r$  values are chosen to lie within the limits of the interaction curve. Figure (4.28) shows the form of the curve obtained. The graph runs away rapidly near the interaction curve limits, and there is

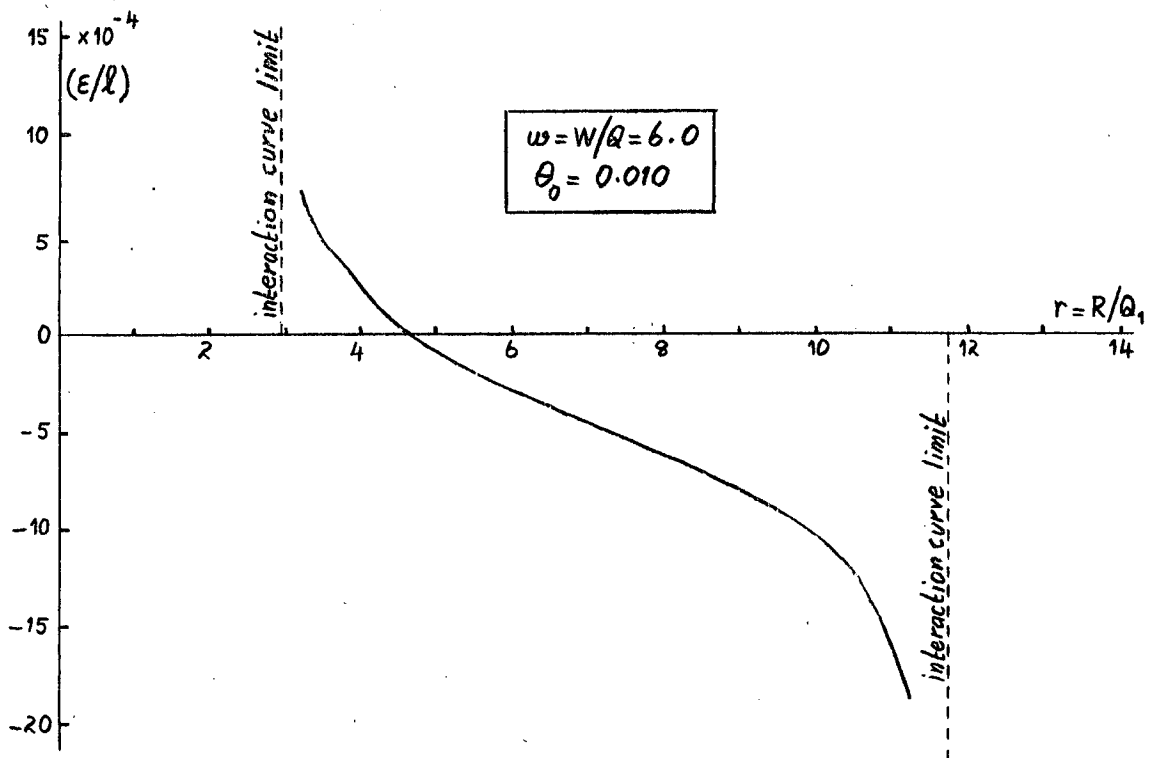


figure 4.28 - Discontinuity graph

an intermediate point of inflection. The form of the graphs remains substantially similar at other values of  $w$  and  $\theta_0$ .

From a set of the above graphs the zeros are located, and hence the loading path can be plotted. This is shown in figure (4.29) for various values of initial crookedness. The interaction curve is also shown. The loading paths for this frame do not curve greatly.

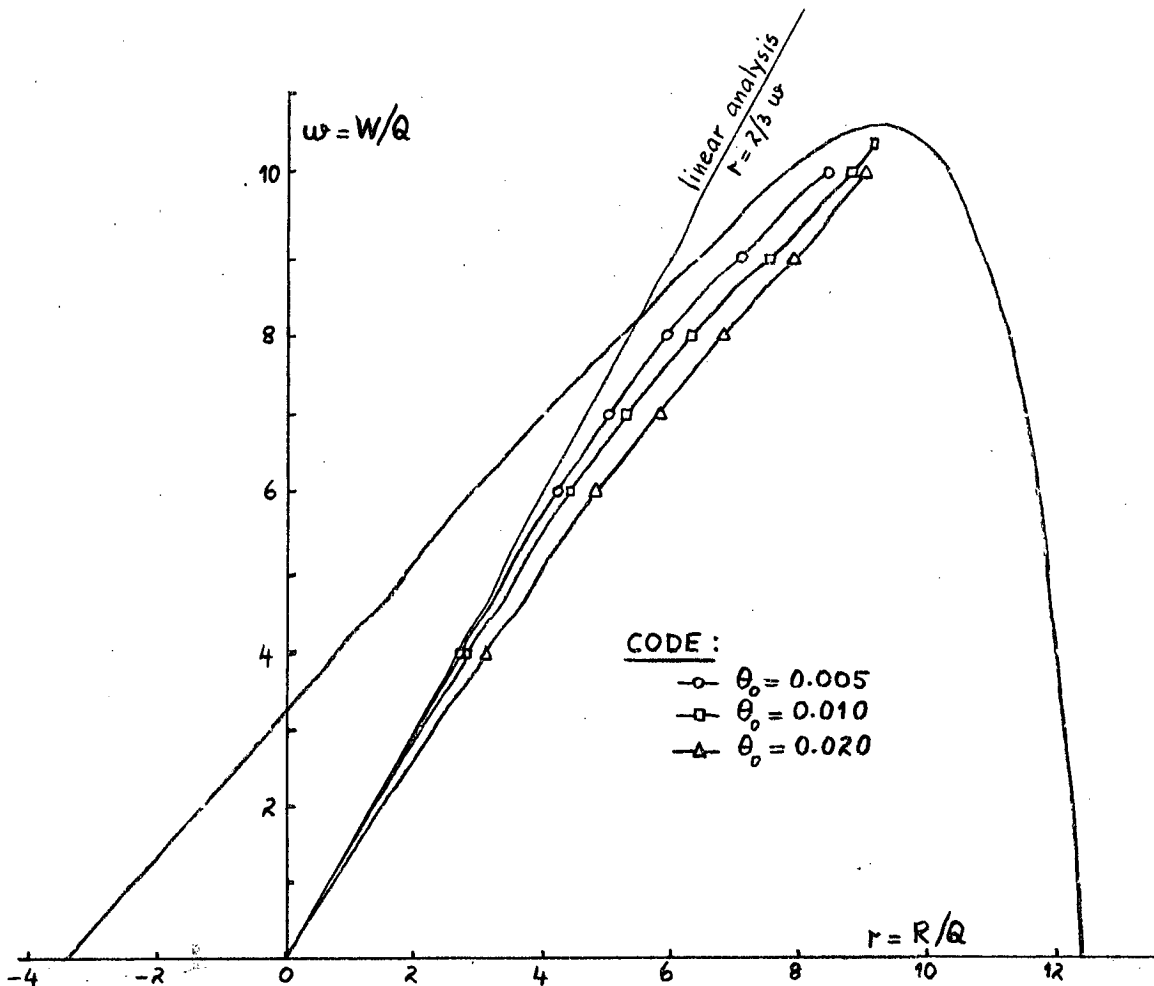


figure 4.29 - Loading paths

Initially the curves are very close to the linear path  $r = 0.667w$ , and as the load increases they head towards the peak of the interaction curve which represents the ultimate buckling condition. It is interesting to note that some of the curves show a point of inflection just before reaching the peak.

Inspection of the form of the incompatibility graph suggests that the iterative technique outlined in the previous section should converge. The method was programmed for the electronic computer so that the results obtained manually could be checked. The iterative procedure for handling the compatibility equation was based on the straightforward Newton method of linearisation, using a straight line through the origin and the peak of the interaction curve as a first guess. This method did not work at high loads; failure resulted

because the points of inflection on the incompatibility graphs gradually move below the axis so that after a while the first step in the iterative scheme gives an  $r$ -value which lies outside the limits of the interaction curve. Once outside these limits, the iterative scheme diverges or oscillates indefinitely. This eventuality was subsequently prevented by the inclusion of a subroutine into the computer program to modify the first guess of  $r$  if an iterated value fell outside the interaction curve. Difficulties of this kind or another are bound to arise in most analyses of overbraced frames; the above notes are included as a typical example. However, it should usually be possible to overcome them by a suitable re-arrangement of the computations.

Knowing the loading path which satisfies the compatibility equation, it is an easy matter to calculate the rotation of joint A. Figure (4.30) shows the rotation plotted against load for the various values of initial crookedness. The Southwell plots calculated from these curves are shown in figure (4.31). As is to be expected, because the loading paths are reasonably close to linear, the Southwell plots do not exhibit transition regions of the type encountered earlier, but are, to the accuracy of calculations, almost straight lines and parallel. The ultimate buckling load, as obtained from the inverse slope, is  $w_{ult} = 10.65$ , which agrees with the value given by the peak of the interaction curve.

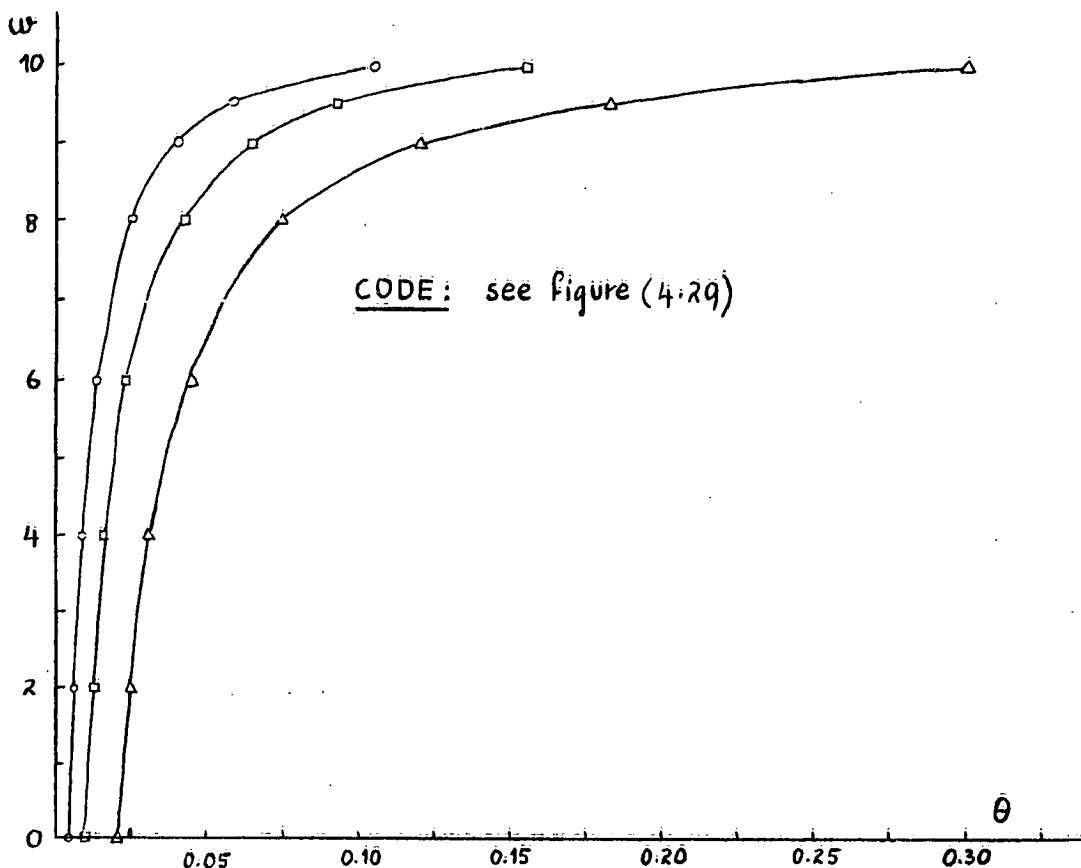


figure 4.30 - Calculated rotation vs. load

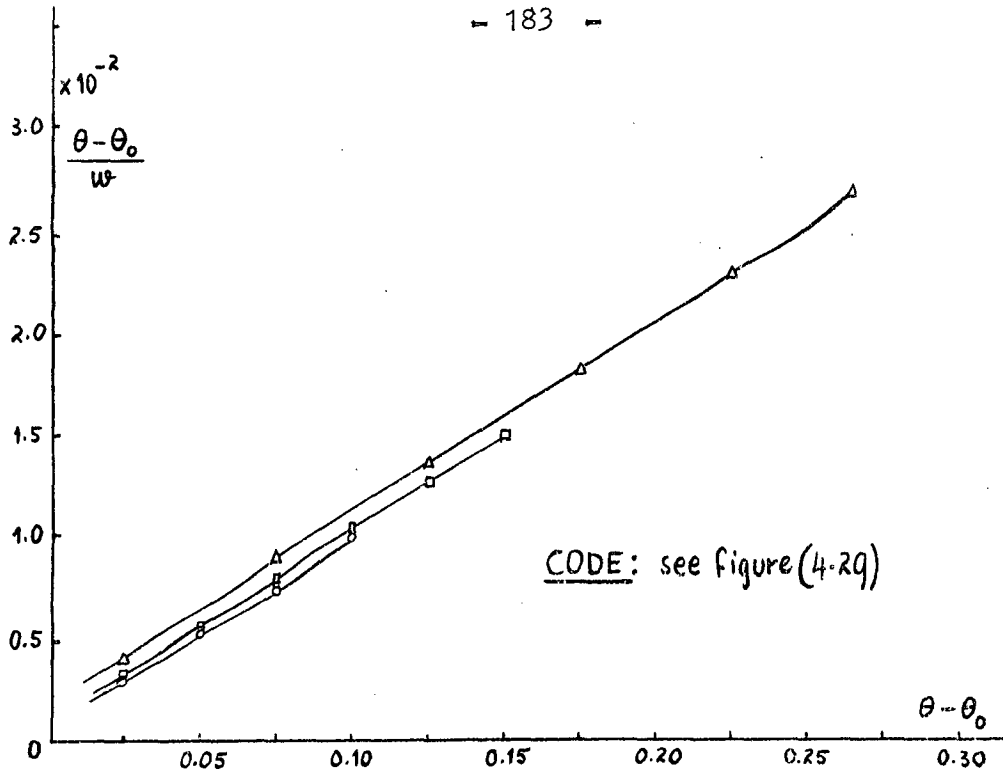


figure 4.31 - Calculated Southwell plots

#### 4.14 THE EFFECT OF PRESTRAIN

As mentioned earlier, prestrain can be regarded as a kind of imperfection which, like initial crookedness, has a considerable effect on the frame's behaviour. Prestrain arises whenever the initial member lengths are incompatible. This is caused by errors in cutting to length, bending during handling, temperature expansion and other factors. Most of these factors are uncontrollable but need to be taken into account in design, or some provision must be made for their control, for example by building into the frame a number of turnbuckles.

It was shown in section (4.6) that the main effect of prestrain on the loading path is a shift of origin. For this reason it is obvious that the ultimate buckling modes and loads are independent of prestrain. However, the initial buckling modes and loads are affected by prestrain, as can be seen from figure (4.18), and it should be possible to arrange a prestraining pattern to increase  $W_{cr}$  or, in some cases, make it the same as the ultimate buckling load. Referring to figure (4.25), such a system is clearly advantageous in practice because it helps to delay the onset of large deformations, which ultimately cause yield, and hence govern the load carrying capacity of the frame.

The analysis of initially crooked overbraced frames with prestrain is in essence no more difficult than that outlined in section (4.12). All that needs to be done is to modify the compatibility

equations by the inclusion of terms representing the initial lack of fit [for comparison see section (4.6b)]. The difficult part is the assessment of the magnitudes and directions of the initial discontinuities. When there is no provision to control prestrain, such as in the usual construction, the initial lack of fit is random, and it is quite likely to produce an unfavourable strain pattern which may considerably reduce the useful working range of the structure. On the other hand when control is provided, one can devise a prestrain pattern to optimize the working range. Also, in contrast with statically determinate frames, it should be possible to suppress first and perhaps higher modes, thereby forcing the frame to deflect into a mode associated with much higher buckling loads, both initially and ultimately. The deformations then grow less rapidly resulting in an increased load carrying capacity.

#### 4.15 CONCLUDING REMARKS

Although the work presented in this chapter merely touches the surface of a wide and challenging field in structural instability studies, it has brought to light certain aspects of sufficient importance to warrant a brief recapitulation. Firstly, the loading path of an overbraced frame, that is the variation of axial forces in its members, is non-linear even though the material behaviour is linearly elastic. The extent and form of the non-linearity depends on both the magnitude and pattern of the initial crookedness. The loading path is predictable when the axial force-shortening relations for the members are known, and this in turn requires a knowledge of the initially crooked shape and of the deflected shape under load. The pressing need is for a simple but adequate mathematical model to describe the shortening behaviour, and the relations used in this chapter are but a short step in that direction.

As a result of the non-linear loading path the behaviour of an overbraced frame cannot, in general, be described by a linear Southwell plot. Nevertheless the deformations grow at an ever increasing rate with load, and it has been shown that some kind of limiting asymptote exists. As the asymptote is approached, the Southwell plot tends to straighten, and the inverse slope of this portion provides an estimate of the frame's elastic ultimate buckling load. It is suspected that in some cases more nearly linear Southwell type plots can be obtained by graphing deformation divided by some function of load against deformation.

This function is probably related to the non-linear loading path, but due to the latter's variability it is not possible to lay down general rules. Some simple functions have been tried in an attempt to straighten the non-linear Southwell plots obtained in experiments, but these met with very restricted success. In other cases certain parts of the loading path are approximately linear. Under these circumstances the Southwell plots over these regions are also substantially linear. However, the equations describing such linear portions appear at this stage to be of questionable value.

Prestrain is another kind of imperfection which alters the loading path, predominantly by a shift of origin but also in form. The ultimate buckling load is unaffected, but the initial buckling load may change appreciably. Since the latter governs the frame behaviour initially, it follows that by increasing it, the deformations can be kept low, which is exactly what the designer wants.

As far as design of overbraced frames is concerned, the author is of the opinion that the 'individual member design' method is generally overconservative. This method uses the linear loading path obtained by neglecting the bending shortenings, and hence the initial buckling load and a linear Southwell plot are its basis. The next step in design is to take into account overall frame deformations, as in chapter one, but ultimately the only satisfactory method is to include the non-linear loading path, and incorporate prestrain as a means of optimizing the frame behaviour. However, until simpler computational procedures are developed such a detailed method is beyond the facilities of the average design office. Perhaps after analyzing many and varied types of frame it will be possible to gather the information into concise semi-empirical rules.

#### REFERENCES

1. N.W. Murray, "On the Instability of Plane Overbraced Frameworks", Civil Eng. Trans. I.E. Aust., vol. CE6, No 1 (March 1964)
2. E.F. Masur, "Post-Buckling Strength of Redundant Trusses", Paper No. 2692, Trans. A.S.C.E., vol. 119 (1954).
3. S. Giudici, "An Investigation into Some Problems of Elastic Stability", Ph.D. Thesis, Univ. of Oxford (1963).

4. L.C. Schmidt, Discussion on ref. 1 above, Civil Eng. Trans. I.E. Aust., vol. CE6, No. 2 (Sept. 1964).
5. L.K. Stevens and M.G. Lay, "Behaviour of Indeterminate Triangulated Steel Frameworks", Civil Eng. Trans. I.E. Aust., vol. CE3, No. 2 (Sept. 1961).
6. B.G. Neal and D.M. Griffiths, "The Collapse of Rigidly Jointed Singly Redundant Light Alloy Trusses", The Struct. Eng., vol. 41, no 12 (Dec. 1963).
7. P.B. Morice, "Linear Structural Analysis", p 48f. Thames and Hudson (1959).



# APPENDIX - Stability functions series

The following series, for which the author is indebted to Professor J.J. Koch, are useful for the calculation of the stability functions  $s$  and  $sc$  and its derivatives. Consider a uniform column, carrying an axial load  $P$ , deformed by endmoments  $M_A$  and  $M_B$ .

Neglecting initial crookedness we obtain the deflected shape as (see chapter one)

$$y = c_1 \sin(\sqrt{\rho}\pi x/l) + c_2 \cos(\sqrt{\rho}\pi x/l) - (M_A/P)(1-x/l) + M_B(x/l) \quad (A1)$$

where  $\rho = P/Q$ ;  $Q = \pi^2 EI/l^2$ ;  $EI$  = flexural rigidity; and  $c_1$  and  $c_2$  are constants determined by the boundary conditions of zero deflection at both ends. Introducing the end slopes  $\theta_A$  and  $\theta_B$ , we obtain the moment-slope relations

$$\begin{aligned} M_A &= (EI/l)(s \theta_A + sc \theta_B) \\ M_B &= (EI/l)(sc \theta_A + s \theta_B) \end{aligned} \quad (A2)$$

where  $s$  and  $sc$  are given by the expressions

$$s = [\pi^2 \rho / 4(1-\omega)] + \omega ; \quad sc = [\pi^2 \rho / 4(1-\omega)] - \omega \quad (A3)$$

in which  $\omega = \alpha \cot \alpha$ ;  $\alpha = \pi \sqrt{\rho}/2$

An alternative approach is to guess the deflected shape in terms of floating parameters and minimize the strain energy to evaluate the parameters. The strain energy is defined as

$$U = \int_0^l \int_0^\phi M d\phi dx - \int_0^\Delta P d\Delta - \int_0^{\theta_A} M_A d\theta_A - \int_0^{\theta_B} M_B d\theta_B \quad (A4)$$

where  $\phi$  and  $M$  are the curvature and bending moment respectively at any point along the column and  $\Delta$  is the total shortening. Assume that the deflected shape, as given by equation A1, can be expressed as the infinite Fourier series

$$y = \sum_{n=1}^{\infty} a_n \sin(n\pi x/l) \quad (A5)$$

where the parameters  $a_n$  ( $n=1, 2, \dots$ ) are to be determined from the condition that the strain energy is a minimum. The above series already satisfies the boundary conditions of zero and deflections.

From equation A4 the minimum energy conditions are

$$\partial U / \partial a_n = \int_0^l M (\partial \phi / \partial a_n) dx - P (\partial \Delta / \partial a_n) - M_A (\partial \theta_A / \partial a_n) - M_B (\partial \theta_B / \partial a_n) = 0 \quad (A6)$$

For small deflections and linearly elastic material behaviour we can put

$$\Delta = \frac{1}{2} \int_0^l (dy/dx)^2 dx ; \quad \phi = d^2 y / dx^2 ; \quad M = EI \phi \quad (A7)$$

and from equation A5 the end slopes are obtained as

$$\theta_A = (dy/dx)_{x=0} = (\pi/l) \sum_{n=1}^{\infty} n a_n ; \quad \theta_B = (dy/dx)_{x=l} = (\pi/l) \sum_{n=1}^{\infty} (-1)^n n a_n \quad (A8)$$

From equations A6, A7 and A8  $a_n$  is obtained as

$$a_n = (2l^2/\pi^3 EI) [M_A + (-1)^n M_B] / n(n^2 - \rho) \quad (A9)$$

Using this expression in equations A8 to determine the end slopes and inverting the result, equations similar to A2 are obtained and hence the following series for the stability functions  $s$  and  $sc$ :

$$s = \frac{1}{2} \pi^2 A / (A^2 - B^2) ; \quad sc = -\frac{1}{2} \pi^2 E / (A^2 - B^2) \quad (A10)$$

$$\text{where } A = \sum_{n=1}^{\infty} 1/(n^2 - \rho) ; \quad B = \sum_{n=1}^{\infty} (-1)^n / (n^2 - \rho) \quad (A11)$$

More rapidly convergent series are obtained by using the facts that

$$\begin{aligned} 1/(n^2 - \rho) &= 1/n^2 + \rho/n^2(n^2 - \rho) \\ \sum_{n=1}^{\infty} 1/n^2 &= \pi^2/6 ; \quad \sum_{n=1}^{\infty} (-1)^n / n^2 = -\pi^2/12 \end{aligned} \quad (A12)$$

This process may be continued but it is not considered worthwhile. A slight rearrangement of equations A10 gives the following expressions from which  $s$  and  $sc$  are obtained by addition and subtraction

$$s + sc = 1/[1/6 + (4\rho s_{\text{even}}/\pi^2)] ; \quad s - sc = 1/[1/2 + (4\rho s_{\text{odd}}/\pi^2)] \quad (A13)$$

$$\text{where } s_{\text{even}} = \sum_{n=2,4,6,\dots}^{\infty} 1/n^2(n^2 - \rho) ; \quad s_{\text{odd}} = \sum_{n=1,3,5,\dots}^{\infty} 1/n^2(n^2 - \rho) \quad (A14)$$

The derivatives of the stability functions are obtained as

$$ds/d\rho + d(sc)/d\rho = -4(s+sc)^2 s'_{\text{even}}/\pi^2 ; \quad ds/d\rho - d(sc)/d\rho = -4(s-sc)^2 s'_{\text{odd}}/\pi^2 \quad (A15)$$

$$\text{where } s'_{\text{even}} = \sum_{n=2,4,6,\dots}^{\infty} 1/(n^2 - \rho)^2 ; \quad s'_{\text{odd}} = \sum_{n=1,3,5,\dots}^{\infty} 1/(n^2 - \rho)^2 \quad (A16)$$

and the second derivatives are given by the expressions

$$\begin{aligned} d^2s/d\rho^2 + d^2(sc)/d\rho^2 &= \frac{2[ds/d\rho + d(sc)/d\rho]^2}{(s+sc)} - 8(s+sc)^2 s''_{\text{even}}/\pi^2 ; \\ d^2s/d\rho^2 - d^2(sc)/d\rho^2 &= \frac{2[ds/d\rho - d(sc)/d\rho]^2}{(s-sc)} - 8(s-sc)^2 s''_{\text{odd}}/\pi^2 \end{aligned} \quad (A17)$$

$$\text{where } s''_{\text{even}} = \sum_{n=2,4,6,\dots}^{\infty} 1/(n^2 - \rho)^3 ; \quad s''_{\text{odd}} = \sum_{\text{odd } n=1,3,5,\dots}^{\infty} 1/(n^2 - \rho)^3 \quad (A18)$$

